Predicting the Wind Resource Available to Roof-Mounted Wind Turbines in Urban Areas

Joel Millward-Hopkins

Submitted in accordance with the requirements for the degree of

Doctor of Philosophy

The University of Leeds

Energy Research Institute (ERI) and Energy Technology and Innovation Initiative (ETII)

School of Process, Environmental and Materials Engineering

April, 2013

Declaration

I confirm that the work herein is my own and that appropriate credit has been given where reference has been made to the work of others.

Joel Millward-Hopkins

Acknowledgements

Completing this research project has been an immense challenge, with periods of stress, fatigue, and frustration contrasting with phases of fulfilment, exhilaration, and relief. In addition to the research skills I have gained, it has been a character-building experience, and there are numerous people I must thank for both the success of the project and my own personal development.

Firstly I must thank my supervisors, Alison Tomlin and Lin Ma, for providing me with the invaluable guidance and support. Both have fostered my development into a competent research student, and without their assistance this project would not have been possible. I also wish to thank Derek Ingham for his support, which, to all intents and purposes, has felt like that of a third supervisor. In addition, I must thank Mohamed Pourkashanian for the financial backing that was instrumental in offering me the opportunity of the previous three years.

There are also other academics with whom, through their generous sharing of experimental data and helpfulness throughout the exchange process, I have been lucky to collaborate. These include Professor Ian Castro, Dr Zhengtong Xie, Professor Aya Hagishima, Dr Sheikh Ahmad Zaki (for data used in Chapters 2 and 3), and Dr Michael Flynn (for data used in Chapters 5 and 6). Data from the Warwick Wind Trials was also indispensible in Chapters 5 and 6.

Finally, I must, and indeed wish to thank the various friends and family members that have been a valuable part of my life over the past three years (Shemaiah Weekes, Sam Pickard, Phillipa Hardy, Ed Causton, and particularly my partner Rosie Goodman, to name but a few), for listening to my complaining when work has been tough, my enthusiastic outpourings of results in times of productive research, and of course distracting me from all things urban wind for well needed periods of rest.

Abstract

Anthropogenic climate change is one of the most difficult challenges currently faced by society, and in order to prevent the most dangerous scenarios from occurring it is essential that human activities and behaviour in the industrialised world are made environmentally sustainable. A large part of these changes must involve reducing the amount of energy that we use, and changing the way in which it is produced, and here renewable energy technologies will play a vital role.

The research reported in this Thesis focuses upon one such technology, namely that of wind energy in the urban environment. A major barrier to the deployment of this technology reaching its full potential is the lack of accurate and affordable methods of estimating wind speeds in urban areas. Thus, improving these methods is what this research aims to address.

Firstly, by analysing a number of experimental datasets, an evaluation of currently available methods of predicting urban wind resource is undertaken in order to establish the feasibility of developing more accurate methods. Subsequently, new models are developed that allow the mapping of predicted mean wind speeds over urban areas. The accuracy of the predictions is then evaluated using measured meteorological data from various locations. An evaluation of the cumulative potential for generating wind energy in the major UK city of Leeds is then made.

The models that are developed are found to improve the accuracy of estimations of surface aerodynamic parameters and mean wind speeds in urban areas, with respect to currently available models. The results highlight the importance of including the influence of building height variation and changes in wind direction in such models, and also the value of utilising detailed building geometric data as model input. Finally, the investigation of the cumulative potential for generating wind energy in Leeds indicates a largely untapped wind resource available that could allow for a significant expansion of urban wind energy.

The estimates of the deployment potential of urban wind energy have practical value for turbine manufactures and urban planners alike. In addition, the wind maps presented offer a valuable means for pinpointing locations where a significant wind resource may be available, and hence where useful carbon savings can be made. Therefore, in order to

maximise the impact of this research, it would be valuable for these maps to be made available and easily accessible to interested parties and individuals, and hence this is a major objective of future work.

Contents

List of Tables

List of Figures

Glossary of Terms and Notation

Wind Turbine Index:

A	Turbine swept area (m^2)
C_p	Turbine power coefficient
C_{pmax}	Maximum power coefficient
'HAWT'	Horizontal axis wind turbine
'LCA'	Lifecycle assessment
P	Power extractable from the wind (W)
R	Turbine radius (m)
'VAWT'	Vertical axis wind turbine
ρ	Air density (1.225 kgm^{-3})
λ	Tip speed ratio (TSR)
λ_{max}	Optimum tip speed ratio (required to obtain C_{pmax})
ω	Angular velocity ($rad.s^{-1}$)

Meteorological Index:

'ABL'	'Atmospheric Boundary Layer'
d	Zero-plane displacement height (m)
d_C	Height of the drag profile centroid (m)
d_{fetch}	Zero-plane displacement height of the upwind fetch (m)
d_{local}	Zero-plane displacement height of the local area (m)
C_D	The depth integrated drag coefficient (for bluff bodies)
'CL'	'Canopy Layer'
'CFD'	'Computational Fluid Dynamics' modelling

F_D	The drag force of a surface (N)
$h_{m\text{-}eff}$	The 'effective' mean building height (m; the derivation can be found in Chapter 3)
$h_{m\text{-}eff\text{-}fetch}$	The 'effective' mean building height of the upwind fetch (m)
$h_{m\text{-}eff\text{-}local}$	The 'effective' mean building height of the local area (m)
'IBL'	'Internal Boundary Layer'
'ISL'	'Inertial Sublayer'
l_m	Prandtl 'mixing length' (m)
'NCIC'	'National Climate Information Centre' wind climatology
'NOABL'	'Numerical Objective Analysis of Boundary Layer' wind climatology
'RSL'	'Roughness Sublayer'
'TL'	'Transition Layer'
$U = (u, v, w)$	Temporally averaged, 3D wind speed, and its orthogonal components (ms^{-1})
$\hat{U}$	Temporally and spatially averaged, 3D wind speed (ms^{-1})
$U` = (u`, v`, w`)$	Instantaneous 3D wind speed, and its decomposition into streamwise, lateral and vertical components (ms^{-1})
$U_{rms} = (u_{rms}\ v_{rms}\ w_{rms})$	Root mean square of the fluctuations of instantaneous 3D wind speed and its orthogonal components (ms^{-1})
U_{UBL}, U_{bl} and U_{hub}	Temporally averaged, 3D wind speed at the urban boundary layer height, blending height, and turbine hub height, respectively (ms^{-1})
U_{pre}	Predicted time averaged, 3D wind speeds (for real-life sites; ms^{-1})
U_{msr}	Measured time averaged, 3D wind speeds (for real-life sites; ms^{-1})
U_N	Wind speed obtained from a regional wind climatology (ms^{-1})
U_{5yr}	Measured time averaged, 3D wind speeds, representative of a 5 year period (for real-life sites; ms^{-1})

u_*	Friction velocity (ms^{-1})
'UBL'	'Urban Boundary Layer'
V_{Dc}	Viscous drag force due to building roofs (N)
V_{Dg}	Viscous drag force due to the ground surface (N)
z	Above-ground height (m)
z_{UBL}, z_{bl} and z_{hub}	Above-ground height of the urban boundary layer, blending height, and turbine hub height, respectively (m)
z_0	Surface roughness length (m)
$z_{0\text{-fetch}}$	Surface roughness length of the upwind fetch (m)
$z_{0\text{-local}}$	Surface roughness length of the local area (m)
$z_{0\text{-ref}}$	Reference surface roughness length for open terrain (m)
κ	Von Karman constant (= 0.4)
τ	Shear stress ($kgm^{-1}s^{-2}$)

Geometric Index:

A_p	Roof area of surface elements (m^2)
A_f	Frontal area of surface elements (m^2)
A_f^*	*Unsheltered* frontal area of surface elements (m^2)
A_T	Ground area associated with the surface elements contributing to $A_p/A_f/A_f^*$ (m^2)
b	Building width (m)
h_m	Average building height (m)
$h_{m\text{-local}}$	Average local building height (m)
H	Individual building height (m)
H_{mast}	Turbine mast height (m)
l	Building length (m)

L_R	Wake recirculation length (m)
L_W	Wake lateral width (m)
X	Distance from the upwind edge of the city (m)
λ_p	Plan area density (= A_p/A_T)
λ_f	Frontal area density (= A_f/A_T)
$\lambda_p(z)$	Vertical profile of plan area density
$\lambda_f(z)$	Vertical profile of frontal area density
σ_h	Standard deviation of building height (m)

1 An Introduction to Urban Wind Energy

1.1 Research Overview

1.1.1 The big picture and where small wind fits in

For many decades the role of humans in climate change has been the subject of fierce debate. However, the on-going and extensive research into the global climate has built an overwhelming body of evidence implicating human activities in the unnatural warming of the planet, and hence a solid scientific consensus has finally been reached (IPCC, 2007). Furthermore, the dangerous environmental impacts of a rapidly warming planet are no longer simply uncertain future predictions; rather they are now underway (Hansen et al., 2012, Rahmstorf and Coumou, 2011). Already there are less developed populations, living in areas of the world experiencing higher levels of warming, who are struggling to adapt (Malla, 2008). Consequently, it is essential that human activities and behaviour –particularly in the industrialised world– undergo extensive change in order to become sustainable, and hence minimise the future impacts of global warming.

A large part of this change must involve the way in which we produce energy, as well as reducing the quantities that we use, as it is well known that the greenhouse gas emissions arising from energy production make a substantial contribution to climate change. Consequently, renewable, low carbon sources of energy are undergoing rapid development around the world. In the UK, legally binding targets have been set by the government to encourage this development, the most notable being that of the Climate Change Act (2008), which requires that a reduction in CO_2e (CO_2 equivalent) emissions of 80% by 2050 (compared to a 1990 baseline) is achieved. Furthermore, due to the abundant wind resource available in the UK, which is the most intense in Europe (Petersen and Troen, 1990), the expansion of wind energy is expected to play a significant role in reaching this target (DECC, 2009).

The variation in scale of wind energy generation technologies is enormous, ranging from multi-megawatt offshore machines to sub-kilowatt battery charging applications. Although small-scale wind turbines produce much less energy than those used in large wind farms, they have a number of unique advantages. Their smaller size means that planning objections are less common, but more notably, as a distributed energy source they reduce

dependence upon energy imports, decrease transmission losses, and allow individuals to take more responsibility for their energy use. In addition, small wind turbines can be located upon building roofs in urban areas, and hence they can support cities in their transition to low carbon and energy efficient operation.

The urban-wind industry, however, is currently still in its infancy, and in its early stages it has suffered some setbacks. Inadequate assessment of the available wind resource at urban locations, often owing to misuse of the UK's most widely used regional wind climatology (i.e. the NOABL database) to estimate mean wind speeds, has led to some turbines being installed at unsuitable sites resulting in their underperformance (Marsh, 2008). Nonetheless, as with other forms of wind energy, building-mounted wind turbines can produce significant amounts of electricity and make useful carbon savings when installed at locations with a sufficient wind resource.

1.1.2 Helping the urban wind industry grow

In order for the technology to become more widely deployed and reach its full potential, it is vital that accurate and affordable methods of estimating wind speeds in urban areas are developed, and that the information is made available to turbine customers. This would reduce the likelihood of customers purchasing turbines expecting unrealistically high energy yields, or companies installing turbines at unsuitable locations for 'greenwashing' purposes (Stankovic et al., 2009), both of which can be detrimental to the reputation of the wind energy industry as a whole.

The most notable example of a simple, free, user friendly tool accessible for potential wind turbine customers to assess the viability of a specific site is the Carbon Trust Online Wind Estimator (www.carbontrust.com). The methodology underlying the tool was developed by the UK Meteorological Office (Best et al., 2008). It is based upon a standard 'wind atlas methodology' (Landberg et al., 2003), which involves scaling wind speeds from a regional wind climate up to a height at which the frictional effect of the land surface is negligible, then scaling back down accounting for the effect of the surface roughness upon the wind profile. However, mean wind speed estimations using these types of methodologies currently contain significant uncertainties (Energy Savings Trust, 2009; Weekes and Tomlin, 2013), and hence to obtain an accurate wind resource assessment at a potential site it is normally necessary to make long-term measurements, at multiple heights (Walker, 2011).

Although this is a sensible approach for wind farm developers, for small-scale urban installations this is normally neither convenient nor financially viable.

1.1.3 The need for research

This discussion highlights the urgent need to develop accurate models that can be used to quickly assess wind resource, which are easily accessible for potential turbine customers. Thus, the principal objective of this Thesis is to develop analytically based methods to advance the accuracy of wind speed predictions in urban areas, and to use the results to explore the extent of untapped wind energy potential in UK cities. This is achieved via the development of a novel, geometrically based model for estimating wind profiles above urban surfaces, in conjunction with other modelling methods obtained from the increasing body of research into urban meteorology. More specific objectives will be discussed in Section 1.5 after a review of the relevant literature.

1.2 Wind Energy Fundamentals

1.2.1 Extracting energy from the wind

The basic concept behind wind energy generation is to extract any kinetic energy that is available in the wind and convert this into useful power. Using basic physical principles, it is straightforward to calculate the total available wind power passing through an area (A), which lies perpendicular to the wind direction. This can be expressed in terms of the wind speed (U) and the density of the air (ρ) (Gipe, 2004):

$$Wind\ power = \tfrac{1}{2}\rho A U^3. \qquad \text{Equation 1-1}$$

Here, a fundamentally important observation can be made: Equation 1-1 shows that the power in the wind is proportional to the cube of the wind speed. This relationship arises due to the fact that the kinetic energy in a particular mass (m) of air is $\frac{1}{2}mU^2$, while the mass of air passing through a turbines swept area in one second is ρAU. Therefore, when estimating the wind resource at a potential turbine site, minor inaccuracies in predicting wind speeds can result in significant errors in estimated energy yields. Furthermore, it dictates that the wind speed distribution at a site must be known, rather than just the mean wind speed, if

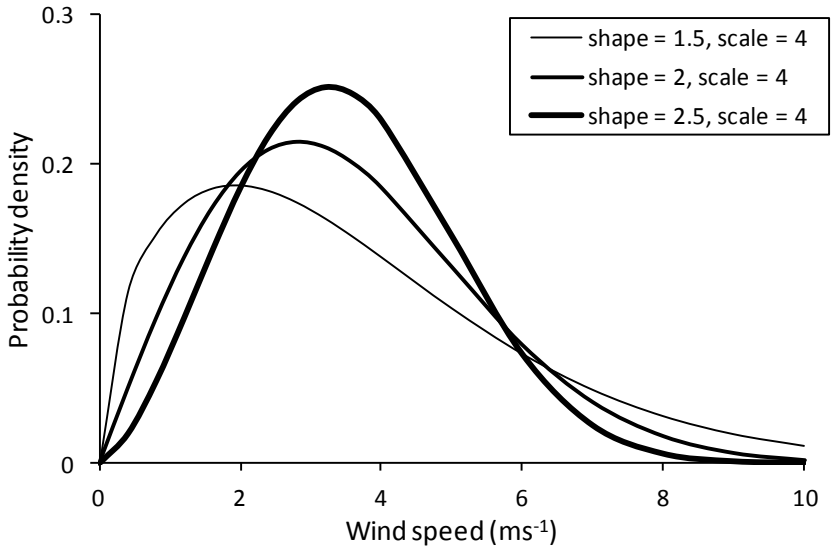

Figure 1-1: Examples of Weibull distribution typically used to represent wind speed distributions

the available wind power is to be estimated. This is typically estimated using a Weibull distribution (Burton, 2001), which is controlled by two parameters referred to as the 'shape' (β) and 'scale' (η) factors. The probability density function (PDF) of this distribution is given by:

$$\mathrm{PDF} = \frac{\beta}{\eta}\left(\frac{U}{\eta}\right)^{\beta-1} e^{-\left(\frac{U}{\eta}\right)^{\beta}}.$$

Equation 1-2

Specific values of these parameters can be chosen to best represent the available wind speed distribution at a particular site, as illustrated in Figure 1-1.

In urban areas this cubic relationship of wind power with wind speed is particularly significant, as winds speeds near roof level where turbines are normally sited are highly spatially variable. This variation occurs in both horizontal and vertical directions, due to the complex influence of building aerodynamics and the high roughness of urban surfaces. An important consequence of this is that even a small increase in a turbines mast height can result in a large increase in power output (Gipe, 2004).

Although Equation 1-1 describes the total available power in the wind, not all of this power can be harnessed by a wind turbine. It is in fact theoretically impossible to extract 100% of the kinetic energy in the wind, as this would require the wind to instantaneously stop on

encountering the turbines swept area. The fraction of the power in the wind that a turbine can capture is expressed through its power coefficient, C_p (Burton, 2001), and hence the power that can be extracted from the wind (P) becomes:

$$P = \tfrac{1}{2} C_p \rho A U^3$$

Equation 1-2

It can be shown that there is a theoretical limit on C_p of 0.593, which is referred to as the Betz limit (Burton, 2001), and typically wind turbines maximum power coefficients (C_{pmax}) lie in the range of 0.35-0.5 (Eriksson et al., 2008).

Values of turbine power coefficients vary not only between different turbines but they also depend upon the turbines operating conditions, most notably the tip speed ratio (TSR, or λ; as shown in Figure 1-2, left). This ratio is that of the velocity of the turbine blades tips relative to the incoming wind speed:

$$\lambda = R\omega/U,$$

Equation 1-3

where, R is the radius of the turbine and ω is the angular velocity. In order for a particular turbine to operate at maximum efficiency (C_{pmax}) it must also operate at the required TSR

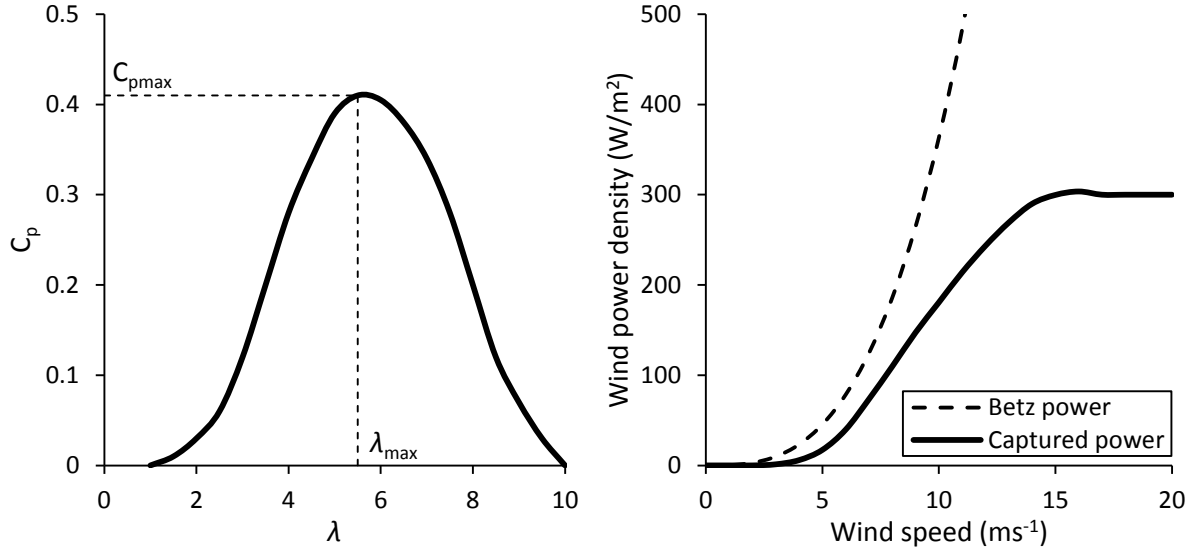

Figure 1-2: Left: illustration of the relationship between a generic wind turbine power coefficient (C_p) and tip speed ratio (λ_{max}). Right: illustration of the maximum extractable power in the wind (the Betz power) alongside a generic wind turbine power curve. Each curve is normalised by turbine swept area to give the wind power density (W/m^2).

(λ_{max}; as shown in Figure 1-2, left). Consequently, a number of advanced turbine control mechanisms have been developed which modify the rotational speed of a turbine in response to changes in the incoming wind speed in order to track λ_{max} (Johnson et al., 2004). However, these systems are not always present on small-scale turbines.

The resulting outcome of all these factors (the cubic relationship between power and wind speed, the Betz limit, and the interplay between turbine efficiency and TSR) is the power curve of the wind turbine. This curve indicates the expected power output of the turbine as a function of the incoming wind speed, as shown in the example in Figure 1-2 right. By multiplying this power curve together with the wind speed distribution at a potential site, the expected energy yield of the installation can be obtained, and hence the environmental and financial viability of the site can be assessed.

1.2.2 Environmental and financial viability

When considering the viability of a potential turbine installation the primary considerations are the environmental and financial payback periods. There are various factors influencing the length of these periods, such as the particular turbine model, the financial subsidies that are available, and the carbon intensity of the electricity which is offset by that produced by the turbine. However, potentially the most important determining factor is the wind resource that is present at the site (Rankine et al., 2006, Bahaj et al., 2007, Allen et al., 2008).

To determine the environmental viability of a turbine, it is necessary to first carry out an audit of the environmental impacts due to its production, transport and maintenance (a life cycle analysis; LCA). A comparison can then be made with the emissions that will potentially be avoided through generating renewable energy rather than importing electricity from the grid. An estimate of the amount of electricity that will be generated can be made using the on-site wind speed distribution and the turbine's power curve (Rankine et al., 2006, Allen et al., 2008). However, the accuracy of this estimate depends upon how accurately the onsite wind conditions are predicted for the future. In addition, estimates of the environmental impacts embedded in a turbine are inherently uncertain due to the difficulties in tracing the 'cradle to grave' impacts of any complex goods when carrying out an LCA (Allen et al., 2008).

In general, however, studies investigating the viability of small wind turbines from an environmental perspective have found payback times to be well within the expected turbine lifetime, even for sites with relatively low mean wind speeds (Allen et al., 2008, Rankine et al., 2006, Celik et al., 2007, Allen and Hammond, 2010). It has been suggested from modelling studies that at sites with low mean wind speeds and high levels of turbulence (< 5ms^{-1} and ≈ 50%, respectively), the installation of a turbine may prove detrimental from an environmental perspective. However, the balance is changed back in favour of installation when more complex environmental impacts are considered (such as heavy metal pollution, production of smog related chemicals, etc.; Allen et al. 2008). Furthermore, other authors have shown that environmental payback times can be reduced significantly through the use of recycled materials in turbine production (Rankine et al., 2006).

Generally, financial payback times are found to be significantly longer than environmental payback times (Allen et al., 2008, Peacock et al., 2008), although the subsidies available in the UK through the feed in tariff can substantially reduce financial payback times (Energy Savings Trust, 2006). This means that for most customers the purchase of a turbine is made based upon purely financial considerations. In this respect, in order for a site to be worthy of further investigation (via onsite measurements) the Energy Saving Trust (2006) suggest that the estimated mean wind speed at a site obtained with the Carbon Trust online wind estimator should be at least 5 ms^{-1}. However, this proposed wind speed does not take into account the fact that some models of turbine are designed specifically to operate in lower, more turbulent winds (see for example www.hi-vawt.com.tw), and hence these designs may be suitable for installation at sites with low mean wind speeds (< 5 ms^{-1}).

In summary, previous studies into the environmental and financial benefits of small-wind energy have shown that the technology can be viable when used at appropriate locations with a sufficient wind resource. However, it is clear that the tools currently available to estimate this resource are inadequate, particularly in urban areas. A fundamental, underlying issue is the lack of sufficiently accurate methods to estimate mean wind speeds at potential sites, and it is these estimates that make the starting point of any viability study.

Also of significance, although to a lesser extent, is the lack of a reliable method for choosing the most appropriate model of turbine for a particular site, given the characteristics of the

available wind resource. To explain why this is the case, various different turbines designs that are available will now be discussed.

1.2.3 Which turbine is best for which site?

The expansion of the small wind industry has brought with it a vast array of unique, original, and occasionally elegant turbine designs (www.urbanwind.net). In general however, they can all be divided into two distinct categories: propeller type horizontal axis wind turbines (HAWT's) or vertical axis wind turbines (VAWT's), as illustrated in Figure 1-3. These two designs can be categorised further into those with drag based aerodynamics and those with aerofoils utilising lift, the latter being generally more efficient. Each of these types of turbines has its own benefits and drawbacks, all of which need to be considered when in the process of choosing the optimum design for a particular site.

Figure 1-3: Illustrations of the main two wind turbine designs: the HAWT (www.kingspanwind.com) and the VAWT (www.quietrevolution.com).

1.2.3.1 Vertical Vs. horizontal axis wind turbines

Despite the fact that the original design of wind turbine was the VAWT, which was developed by the Persians over a thousand years ago (Manwell et al., 2002), HAWT's are currently the more developed of the two turbine designs. Consequently, their efficiencies are typically slightly higher than that of VAWT's (Eriksson et al., 2008). However, it has been suggested that the aerodynamic principles that lead to the Betz limit may not be relevant to VAWT's, and hence the theoretical limit on efficiency may in fact be significantly higher than

59% (Agren et al., 2005). This implies that in the future the efficiencies of VAWT's might eventually exceed that of HAWT's.

For wind energy applications in urban areas VAWT's also have a number of unique advantages over HAWT's. The most significant of these relate to turbulence, high levels of which are typically present in urban areas. These turbulent wind conditions, in which the frequency and intensity of wind directional change is normally high, have a relatively small impact upon VAWT's as they accept wind from any incoming direct. In contrast, HAWT's efficiencies are greatly reduced as they must attempt to track the incoming wind direction with a yawing mechanism. In addition to this, the wind flow experienced by roof-top turbines often contains a significant vertical component, as a result of building aerodynamics (Mertens, 2003). Under these conditions it has been suggested that the energy yield of a VAWT may be increased slightly, while the efficiency of a HAWT would suffer (Mertens et al., 2003).

In contrast, however, the balance is tipped back in favour of the HAWT when the issue of turbine start up is considered, as these designs have the ability to self-start at low wind speeds (Eriksson et al., 2008). Although it has been shown that some lift based VAWT's are also capable of self-starting (Hill et al., 2009), it can be more problematic for these designs. Considering the prevalence of gusts in urban areas and the significant energy they contain (McIntosh et al., 2007), the ability of a turbine to efficiently self-start may prove valuable.

1.2.3.2 Drag Vs. lift based wind turbines

One final important consideration, from a design perspective, is the potentially higher efficiency of drag based turbines at low wind speeds with respect to lift based aerofoil designs, and also their greater self-starting capacity.

Lift based aerofoils are designed in such a way that their shape generates a difference in flow velocity around (and hence the pressure upon) each side of the blade. This leads to a lift force acting in a direction perpendicular to the flow (Burton, 2001). At low wind speeds, however, the drag of the aerofoils are high and this results in poor turbine efficiencies and difficulties self-starting (Hill et al., 2009). This may reduce the gap in efficiency between drag and lift based turbine designs at low wind speed. Moreover, drag based designs (either HAWT's or VAWT's) may prove to be the more sensible choice of technology at sites with

low wind speeds and high turbulence. In fact, the ideal choice of turbine for such sites may be hybrid turbines that utilise both drag and lift based technologies (www.hi-vawt.com.tw).

It is clear from this discussion that there is no definitive recommendation that can be made of an optimum turbine design, either with respect to the orientation of the turbine axis or the aerodynamic design of the blades. Instead there are a number of different, independent factors that must be considered, with respect to the character of the potential turbine location and the nature of the available wind resource. Furthermore, as different technologies develop, more suitable designs of turbine may emerge.

1.3 Predicting the Wind Resource in Cities

There are a number of different approaches that can be used to estimate the available wind resource and evaluate the suitability of a potential wind turbine site. The complexity of these ranges from 'folklore', which relies simply upon the subjective knowledge of local residents, to detailed computational methods that utilise large-scale (≈ 5-10 km) mesoscale modelling in combination with micro-scale (≈ 1 m) flow models, such as computational fluid dynamics, i.e. CFD (Landberg et al., 2003). With respect to urban sites, the methods appropriate for predicting wind resource normally involve taking direct wind speed measurements, using analytical models, or utilising a hybrid approach.

1.3.1 Three different approaches

1.3.1.1 Measurement based approaches

In general, undertaking measurements over long periods of time (1- 3 years, as is typically done during wind farm site assessments) is impractical for small-scale installations. Alternatively, measurements over shorter time periods can be made, which can then be extrapolated to estimate the future wind resource with the use of long-term measurements from a local reference site, which is referred to as a 'measure-correlate-predict' approach (Landberg et al., 2003). However, this approach can still incur a significant financial cost. The availability of accurate, cheap analytical models is thus of particular benefit for small-scale wind energy applications (Weekes and Tomlin, 2013).

1.3.1.2 Analytical models

Analytical models for predicting the wind resource available to small-scale wind turbines typically follow a 'wind atlas methodology' (Landberg et al., 2003). Two prominent examples of such models are the software package 'WASP' (Mortensen et al., 2003) and that developed by the UK Meteorological Office (Best et al., 2008; first introduced in Section 1.1). The recently published model of Drew et al. (2013) is another notable example, and, although it has similar underlying methodology to that of the Met Office, it was developed specifically for urban areas. This model will be discussed further in Chapters 5 and 6.

The starting point of the WASP methodology is a dataset of long-term wind measurements from a local reference site. These are then modified to remove any influence of sheltering and local surface roughness, in order to give the 'regional wind climate'(Landberg et al., 2003). Subsequently, by considering the local topography, the surround surface roughness, and the sheltering of nearby obstructions at the potential turbine location, the regional wind climate is corrected to estimate the available wind resource.

The methodology of the Met Office is broadly similar to that of WASP, although its starting point is the NCIC database (Best et al., 2008). This database gives wind speeds over the whole of the UK (at a resolution of 1 km) that are valid at a height of 10 m above a smooth surface, and which also takes into account the influence of the local topography (on scales greater than 1 km.) Consequently, the Met Office methodology only follows the latter half of the methods employed by WASP.

1.3.1.3 Computational Fluid Dynamics

An issue with the analytical approaches described above is that they do not take account of the complex flow patterns that occur due to the local buildings and other nearby obstructions. For these complexities to be modelled accurately, CFD simulations must be performed. These techniques involve simulating the flow field around a specified arrangement of surface obstructions, within a bounded domain, by solving the fundamental equations of motion that govern fluid flow, i.e. the Navier-Stokes equations (Davidson, 2004). As no exact solution to the equations exists, it is necessary to use numerical methods to resolve the flow field, after first designing a mesh to divide the domain into discrete grid cells.

A highly important factor influencing both the accuracy of CFD simulations and the required computational resources is the turbulence model that is employed. For wind resource prediction and urban meteorology, either Reynolds Averaged models (RANS) or large eddy simulations (LES) are generally used. LES is a transient modelling approach that fully resolves all scales of turbulence greater than the mesh resolution, and calculates sub-grid scale turbulence with a sub-grid turbulence model. In contrast, RANS techniques calculate all the various scales of turbulence with parameterised, time-averaged models. As a consequence of this, LES simulations are typically more accurate than RANS (Cheng et al., 2003; Xie et al., 2008; Tominag et al., 2008). However, this potentially higher accuracy comes at a cost, as more computational resources, processing time and modelling expertise are required.

In practice, the computational resources and expertise required even for simpler RANS approaches are usually prohibitive for small-scale wind site assessments, particularly for domestic purposes. Furthermore, the substantial computational resources required for CFD make it impractical to apply such methods to full cities (Hang et al., 2009). City-scale simulations that have been undertaken in the past have either drastically simplified the surface geometry (Hang et al., 2009; Yang and Li, 2011), or parameterised building-scale flow rather than fully resolving it (Ashie and Kono, 2011). More commonly, CFD is used to study relatively small local areas, less than about 10 km^2 in size (Xie and Castro, 2009; Bou-Zeid et al., 2009; Neophytou et al., 2011, Liu et al., 2011). Consequently, when predicting urban wind resource using CFD it is usually necessary to use a simpler model (such as a wind atlas methodology) to estimate the boundary conditions for a smaller scale CFD model (Landberg et al., 2003).

Nonetheless, CFD has proven useful for understanding the wind resource in cities. Various researchers have used CFD to explore above-roof wind resource over simplified urban geometries, and these studies will be discussed further in Section 1.4.5. In addition, CFD continues to be highly valuable for evaluating simpler, spatially-averaged flow models for use in urban areas. These simpler models are very often integrated into wind atlas methodologies, and hence they are discussed comprehensively in Section 1.4.3.2.

1.3.2 The UK Met Office approach

The steps that are executed in the wind atlas methodology of the Met Office to predict the mean wind speed for a given height are indicated in Figure 1-4. Each step relies upon

describing the vertical variation of the horizontal wind speed with the standard logarithmic wind profile:

$$U = \frac{u_*}{\kappa} \ln\left(\frac{z-d}{z_0}\right).$$

Equation 1-4

Here, z_0 and d are the surface aerodynamic parameters of roughness length and displacement height, u_* is the friction velocity, κ is the Von Karman constant (≈ 0.4), and z is the height above the ground. Physically, z_0 offers a measure of the frictional drag exerted by a surface, while d accounts for the fact that for rough surfaces (such as cities) the surface drag force is elevated above the actual ground level due to the drag from the surface obstructions (Wieringa, 1993). A derivation of Equation 1-4 is given in Section 1.4.2, along with a description of the physical meaning of u_* and κ.

The first stage of the method illustrated in Figure 1-4 involves obtaining the mean wind speed (U_N) from the NCIC database (which represents the regional wind climate) and scaling this up to the top of the urban boundary layer. This height (z_{UBL}) is assumed to be high enough for the influence of the urban surface upon the flow to be negligible. In the Met Office methodology it is fixed to a constant value of 200 m. The standard logarithmic wind profile is used here with a reference, 'open country' roughness length of 0.14 m ($z_{0\text{-ref}}$), and hence the wind speed at z_{UBL} is:

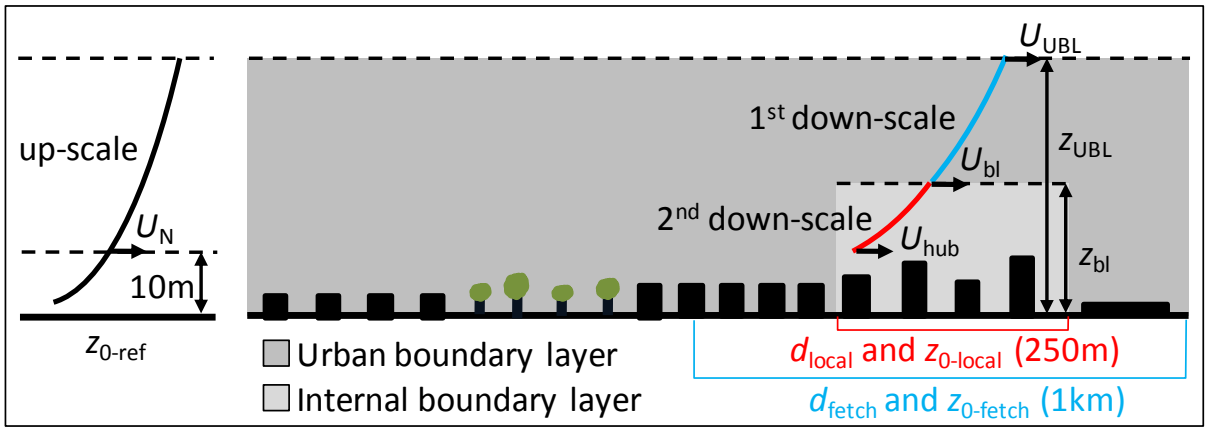

Figure 1-4: Illustration of the small-scale wind prediction model developed by the UK Met Office (Best et al., 2008).

$$U_{UBL} = U_N \frac{\ln(z_{UBL} / z_{0-ref})}{\ln(10 / z_{0-ref})}.$$

Equation 1-5

In the second stage of the method U_{UBL} is scaled down through the urban boundary layer (UBL) to the 'blending height' (z_{bl}; see Section 1.4.1). At this height the flow is considered to be horizontally homogeneous (Grimmond and Oke, 1999). Again, the logarithmic profile is used, and hence the wind speed at z_{bl} is:

$$U_{bl} = U_{UBL} \frac{\ln\left[\left(z_{bl} - d_{fetch}\right) / z_{0-fetch}\right]}{\ln\left[\left(z_{UBL} - d_{fetch}\right) / z_{0-fetch}\right]}.$$

Equation 1-6

Here, the aerodynamic parameters $z_{0\text{-fetch}}$ and d_{fetch}, as well as the blending height, are calculated on a regional scale, which the Met Office chose to be 1 km square. The calculation process and potential alternatives will be discussed in the next section.

Finally, in order to estimate the wind speed at z_{hub}, U_{bl} is scaled down to the turbine hub height (z_{hub}) through the lowest region of the UBL:

$$U_{hub} = U_{bl} \frac{\ln\left[\left(z_{hub} - d_{local}\right) / z_{0-local}\right]}{\ln\left[\left(z_{bl} - d_{local}\right) / z_{0-local}\right]}.$$

Equation 1-7

This layer of flow is considered to be adapted to the local area in the surrounding 100 to 200 m, and hence aerodynamic parameters $z_{0\text{-local}}$ and d_{local} are chosen to be appropriate to the land cover in this area.

When assessing energy yields the Met Office assume a Weibull distribution, using the predicted mean wind speed along with a shape factor of 1.8. This value was found to represent reasonably well the shapes of the wind speed distributions measured at a wide variety of UK sites.

1.3.3 The total small-wind energy resource in the UK

With the use of this model, the Met Office was able to make a first assessment of the total energy resource of small-scale wind turbines in the UK (Best et al., 2008). This was achieved

by first using the wind speed distributions predicted by the wind atlas methodology (at a 1 km resolution) to map the expected energy yields of various different turbines over the UK. Subsequently, by combining these estimated energy yields for different turbines with census data (indicating the number of households in each 1 km cell), estimates of the potential cumulative energy generation of small-wind turbines were obtained, assuming a turbine is installed at every UK property.

These calculations were carried out separately for rural, suburban, and urban areas, and for a number of different turbines that would be suitable for each of these local area types. The turbines considered ranged from 1 to 15 kW in rated power, had generic power curves, and were assumed to be installed on masts from 2 to 15 m tall. These turbine types and the associated local area type are included in Table 1-1, along with the cumulative energy yield results.

Rating (kW)	Local Area Type	Mounting	Above roof height	Max energy generated (TWh/yr)	Energy generated with 1% random penetration (TWh/yr)	Energy generated with 1% optimal penetration (TWh/yr)
15	Rural	Pole	15	70.73	0.707	1.879
6	Rural	Pole	15	27.10	0.271	0.678
2.5	Rural	Pole	11	8.61	0.086	0.266
0.08	Rural	Pole	6	0.30	0.003	0.011
2.4	Suburban	Pole	10	17.16	0.172	0.859
1.5	Suburban	Roof	1.95	6.37	0.064	0.289
1.5	Suburban	Roof	2.95	8.31	0.083	0.359
1.5	Suburban	Roof	8.95	17.83	0.178	0.643
1	Suburban	Roof	2.125	2.35	0.024	0.169
1	Suburban	Roof	3.125	3.35	0.034	0.216
1	Suburban	Roof	9.125	8.99	0.090	0.385
2.4	Urban	Pole	10	0.12	0.001	0.031
1.5	Urban	Roof	1.95	1.41	0.014	0.104
1.5	Urban	Roof	2.95	1.81	0.018	0.123
1.5	Urban	Roof	8.95	3.99	0.040	0.197
1	Urban	Roof	2.125	0.51	0.005	0.060
1	Urban	Roof	3.125	0.71	0.007	0.070
1	Urban	Roof	9.125	1.96	0.020	0.104
Total Rural				26.684	0.267	0.709
Total Suburban				9.194	0.092	0.417
Total Urban				1.501	0.015	0.098
Total				**37.38**	**0.37**	**1.22**

Table 1-1: The estimates of the Met Office (Best et al., 2008) for the cumulative energy potential of small-wind turbines in the UK, categorised by the local area type and the turbine size and elevation. Total cumulative energy yields are calculated based upon an equal proportion of each size of turbine being installed in each local area type (i.e. in rural areas, each of the sizes of turbine are assumed to make up 25% of the total number of rural turbines)

The final numbers of the Met Office calculations suggested that the total energy that could be generated in the UK via large-scale deployment of small-wind turbines is just less than 40 TWh/year, assuming an equal weighting of each turbine type within each local environment. For example, in rural areas, each of the four sizes of turbine is assumed to be installed at 25% of UK rural households. This total is similar to the estimate made by the Carbon Trust (2008b), which also used the Met Office's wind speed predictions. In comparison, a total of 15 TWh of electricity was generated from wind energy in the UK in 2011 (Digest of UK Energy Statistics; www.gov.uk).

Clearly, however, it is unrealistic to expect a small-wind turbine to be installed at every property, partially due to various financial and social barriers, but also the unavoidable fact that a large proportion of properties receive an insufficient wind resource. More realistically

therefore, the Met Office offer estimates of the potential cumulative energy generation for scenarios in which turbines are installed at the most suitable 1% of all properties, or at a randomly selected 1% sample of properties. These more realistic figures suggest that small-wind turbines could supply around 1.2 TWh of electricity if the optimum properties could be identified, but that this yield would be reduced by about 70% if properties were randomly selected (Table 1-1). This indicates the necessity of developing quick, accurate methods of estimating wind resource, as these are invaluable in pinpointing viable turbine sites.

There are of course a number of assumptions and simplifications that had to be made to obtain these estimated energy yields, given the extensive task of estimating the available wind resource and potential energy yield of a turbine at each UK property. Some of these simplifications have particularly important implications for the urban wind resource.

Firstly, because real, geometric building data wasn't used (this would be highly expensive and computationally demanding to carry out at a national level), it was assumed that properties were all of the same height in suburban and urban areas. Specifically, these heights were set to 6 m and 12 m, respectively. Secondly, commercial properties were not specifically considered, which is a significant issue as in urban areas it is likely that tall commercial buildings will be the most valuable turbine locations. Furthermore, upon these types of properties it is possible that larger roof-top turbines than those considered suitable for urban and suburban areas (only up to 1.5 kW, as in Table 1-1) could be installed, and in addition multiple turbines may be sited upon a single roof. For example, the Greenhouse

sustainable living project in Leeds houses two 6 kW turbines, each achieving capacity factors of 15 to 25% (www.greenhouseleeds.co.uk).

Due to these limitations, it would be useful to assess the available wind resource in cities using a more detailed approach that considered potential turbine installations in a site-specific manner. This will be undertaken in Chapters 5 and 6 of this Thesis.

1.3.4 Reducing uncertainty in the models

The accuracy of the Met Office model for estimating wind speeds has been tested over a large number of sites by Weekes and Tomlin (2013). Also, it is tested specifically at various urban sites in Chapter 5 of this Thesis. For locations in built-up areas, it has been found that average uncertainties in the model predictions lie within the region of 20-35% for mean wind speed, with maximum errors of over 80% also observed. When converted to errors in power prediction, these errors are amplified significantly so that even on average they may be as high as 90% (Weekes and Tomlin, 2013).

Although little investigation has been made into the accuracy of the more sophisticated WASP software for resource prediction in urban areas, it is likely to suffer from a similar level of uncertainty. This is due to the fact that much of the model uncertainty arises from the difficulties in quantifying the influence of complex, heterogeneous surfaces upon wind flow. It is invaluable therefore, that the uncertainties in these methodologies are decreased, and the process by which this can potentially be achieved is by integrating novel modelling techniques from the advancing field of urban meteorology.

1.4 Urban Meteorology

1.4.1 The structure of the urban boundary layer

When wind flow encounters an abrupt change in surface roughness, such as at the rural-to-urban transition found at a city's edge, a new boundary layer begins to grow within the atmospheric boundary layer (ABL), as the flow adapts to the underlying surface (Garratt, 1990). When this process takes place above urban surfaces, the developing layer is referred to as the urban boundary layer (UBL), and this layer eventually grows to extend throughout the ABL, as illustrated in Figure 1-5. Typically, the depth of the UBL is about 500 to 1000 m

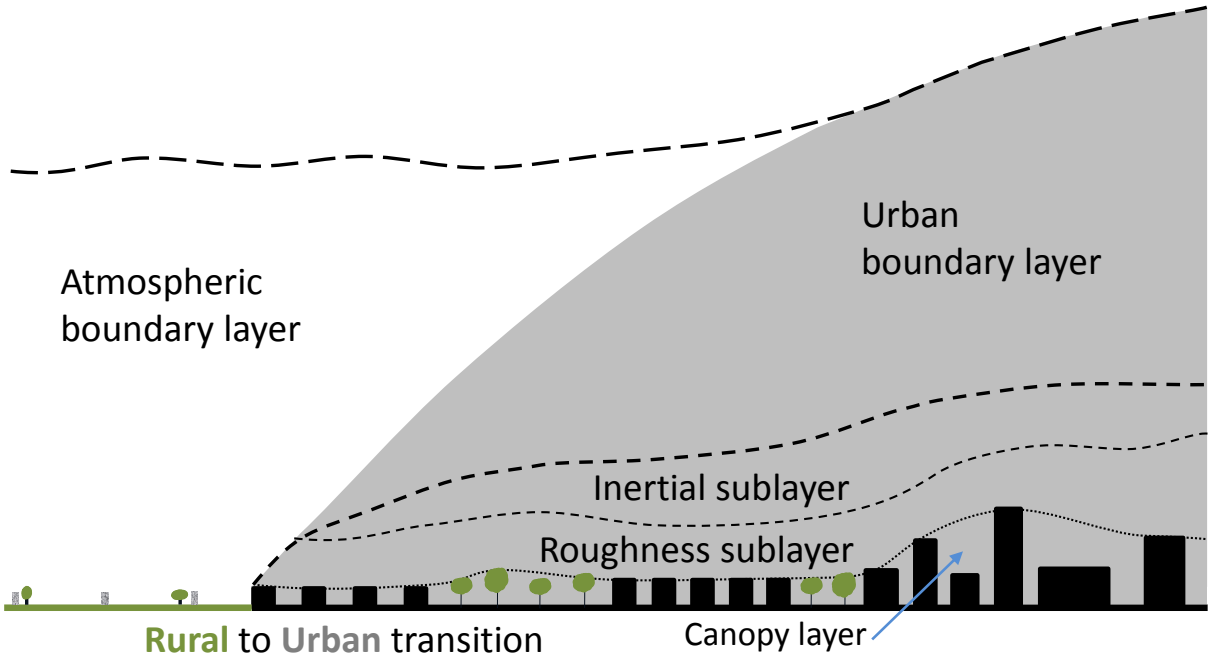

Figure 1-5: Illustration of the development of the urban boundary layer and various sublayers

(Britter and Hanna, 2003), and contained within it are a number of sublayers whose locations are determined based upon the characteristics of the flow.

The uppermost of these layers is the inertial sublayer (ISL), which is characterised by horizontally homogeneous flow and a constant magnitude of shear stress (τ; which is properly defined in the next subsection). Typically, the ISL extends to a height of about 100 to 200 m (Britter and Hanna, 2003). Below the ISL lies the roughness sublayer (RSL), within which there is a high level of spatial variation in the wind speeds due to the influence of the wakes produced by the buildings (Grimmond and Oke, 1999). In urban areas, the RSL normally extends to about 2 to 5 times the average height of the local buildings, a height which is referred to as the 'blending height' (Grimmond and Oke, 1999). The lowest and final layer lying with the UBL is the canopy layer (CL), which lies within the buildings and surface obstructions. Here, the flow is a highly complex combination of recirculating vortices and channelled flows (Dobre et al., 2005), and is generally too disrupted to be of value for wind energy generation.

1.4.2 Theoretical mean wind profiles

1.4.2.1 The inertial sublayer

As a consequence of the constant shear stress in the ISL, the wind profile here follows the standard logarithmic profile of Equation 1-4 (in conditions of neutral atmospheric stability). When atmospheric stability deviates from neutral, it is necessary to modify Equation 1-4 to account for thermal effects. However, as medium to high wind speeds events typically occur during neutral conditions, wind energy methodologies often confine their analysis to these conditions (Best et al., 2008).

Equation 1-4 can be derived by considering Prandtl's 'mixing length' hypothesis applied to a two-dimensional boundary layer flow. Prandtl hypothesised that in a simple shear flow (such as a boundary layer) the turbulent fluctuations in the streamwise ($u`$) and vertical directions ($w`$) are proportional to the vertical wind speed gradient ($\partial u/\partial z$). The constant of proportionality is the mixing length (l_m), which is suggested to represent the average length-scale of the turbulent eddies, thus:

$$u` = w` = l_m \frac{\partial u}{\partial z}.$$

Equation 1-8

This allows the shear stress (or Reynolds stress, τ) to be defined as:

$$\tau = -\rho \overline{u`w`} = \rho l_m{}^2 \frac{\partial u}{\partial z}\left|\frac{\partial u}{\partial z}\right|.$$

Equation 1-9

In wall bounded flows, it is assumed that the average length-scale of the turbulent eddies is restricted by the presence of the wall, and hence the mixing length becomes proportional to the above ground height, i.e. $l_m = \kappa z$. This constant of proportionality is the Von Karman constant (κ) that was introduced in Section 1.3.3, which, empirically, is found to be approximately 0.4. The shear stress can be converted to a scaling velocity, namely the friction velocity $u_* = (\tau/\rho)^{0.5}$, and hence by substituting the mixing length relationship into Equation 1-9 and rearranging:

$$\frac{u*}{\kappa} = z \frac{\partial u}{\partial z}.$$

Equation 1-10

This is easily integrated to obtain:

$$u = \frac{u^*}{\kappa} \ln z + \mathrm{C},$$

Equation 1-11

where C is a constant of integration. This can be rewritten with a constant, namely the roughness length z_0, inside the logarithmic term, such that $u = 0$ at $z = z_0$:

$$u = \frac{u^*}{\kappa} \ln \frac{z}{z_0}.$$

Equation 1-12

Finally, by correcting the ground level for rough wall boundary layers with a displacement height (i.e. substituting '*z*' with '*z* - *d*') and assuming the flow has only a horizontal, streamwise component (i.e. $U = u$), Equation 1-12 becomes the standard logarithmic profile of Equation 1-4.

1.4.2.2 The roughness sublayer

Within the RSL, due to the shear stress gradient and the horizontal variability of the flow, Equation 1-4 is not theoretically valid for describing *U*. Nonetheless, for urban-like surfaces, observations have suggested that throughout both the RSL and the ISL, the horizontally average wind speed ($\hat{U}$) may be estimated using a single logarithmic profile down to the mean building height (Cheng and Castro, 2002b, Rooney, 2001, Britter and Hanna, 2003).

When estimating wind speeds, however, it is important to remember that the heterogeneity of the RSL flow can cause above-roof wind speeds to deviate significantly from the spatially-

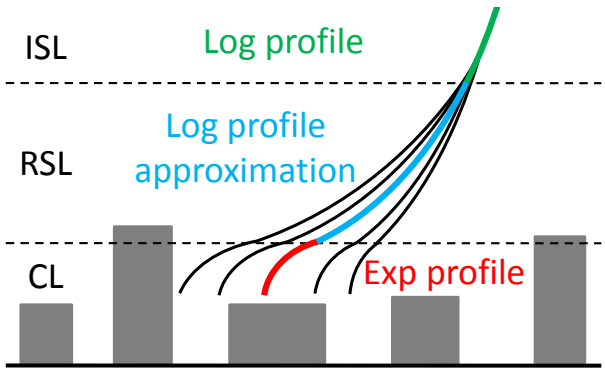

Figure 1-6: Illustration of the sublayers in the lower urban boundary layer and their mean wind speed profiles. Coloured lines indicate the horizontally-averaged wind profile in each of the layers, and the black lines indicate potential variations in the wind profile at different horizontal locations.

averaged profile, as is illustrated in Figure 1-6. Thus, this spatial variation is of particular interest in regards to wind atlas methodologies, such as that of the Met Office, as these methods typically use a logarithmic profile to estimate above-roof wind speeds. An open question therefore, is whether or not the uncertainties that arise from overlooking the spatial variability in the RSL when estimating above-roof wind resource are acceptable, given the resulting uncertainties in assessing energy yields. This question is investigated in detail in Chapter 2.

1.4.2.3 The canopy layer

Within the canopy layer, the flow is substantially modified by street and building geometry and distribution, and it is difficult to predict even the spatially-averaged characteristics (Best et al., 2008). Nevertheless, simple models have been developed which suggest that the spatially-averaged wind profile here is approximately exponential (Macdonald, 2000, Coceal and Belcher, 2004), as illustrated in Figure 1-6. Wind resource prediction methods are fortunate enough to not often be influenced by these uncertainties, as the disruption to the flow within this layer makes it generally unsuitable for the installation of a turbine to be worth consideration.

1.4.3 Predicting mean wind profiles

For the inherently complex and highly rough surfaces found in urban areas, accurately estimating the aerodynamic parameters (z_0 and d) that govern the logarithmic profile can be a challenging task. These parameters can be derived from meteorological measurements via a number of different methods (with the method chosen depending upon the type of anemometry used, and the number of vertical measurements available), and some of these are discussed in Section 1.4.3.3. However, data for urban areas is generally quite sparse, and there may still be significant uncertainties in the estimations (Grimmond et al., 1998). Furthermore, this type of data is rarely available for wind resource prediction methodologies, and if measurements were available they could most likely be used to directly assess the available wind resource at a site, negating the need for a methodology such as that of the Met Office (described in Section 1.3.3).

Consequently, for wind resource prediction methodologies, z_0 and d must typically be estimated without the use of meteorological measurements, and instead by considering the

geometrical characteristics of the urban surface via the use of 'morphometric models' (Grimmond and Oke, 1999). Before these models are introduced, it is valuable to consider the flow patterns that may occur within the canopy layer, as this offers a physical insight into the relationship between aerodynamic parameters and a city's geometrical form.

1.4.3.1 Canopy layer flow patterns

The flow patterns that occur within the canopy layer can broadly be categorised into the three flow regimes which were described by Oke (1988) after the wind tunnel studies of Hussain and Lee (1980). The occurrence of each regime is primarily dependent upon the density of the buildings covering the surface, which can be measured via the parameter λ_p (the ratio of building plan area to ground area). For the special case of arrays of uniform height, these relationships are estimated by the curves sketched in Figure 1-7, where z_0 and d are normalised by the mean building height, h_m.

The first of these regimes, 'isolated roughness flow', occurs at low area densities where the wakes of the individual buildings have negligible interference with the buildings downstream. Associated with this regime are low magnitudes of z_0 and d, which increase

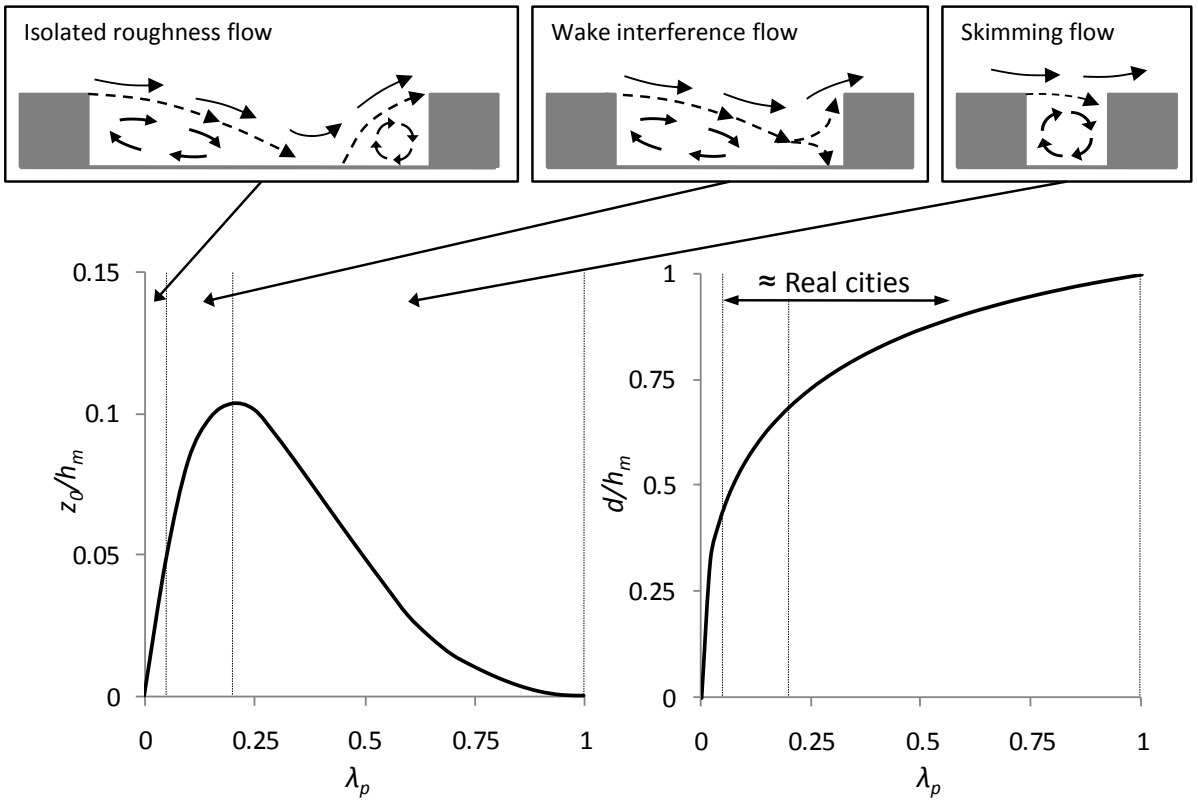

Figure 1-7: Curves illustrating, qualitatively, the dependence of the surface aerodynamic parameters (z_0 and d) upon λ_p and the three flow regimes described by Oke (1988).

with increasing density. Eventually, when the surface becomes sufficiently dense, the building wakes begin to interfere with the downstream buildings, and the flow regime is now referred to as 'wake interference flow'. In this regime there is also an increase in z_0 and d as the density of the surface increases, until at a certain density, z_0 reaches a characteristic peak. As the surface density increases further the flow undergoes transition to the 'skimming flow' regime, in which the main flow effectively skims over the top of the surface elements. The mutual sheltering of the obstacles that occurs under skimming flow increases with the surface density, leading to a reduction in the drag and a decrease in z_0. In this regime, d continues to increase with density, but the rate of increase gradually slows. Eventually, as λ_p reaches its theoretical limit of 1, a new surface is formed of height h_m, and hence it follows that d is now equal to h_m.

For real building arrays however, which have many additional levels of geometrical complexity, these simple relationships can quickly break down. Nevertheless, morphometric models are widely used to estimate aerodynamic parameters of complex urban areas, even though in theory their derivation makes them appropriate to be used only for highly idealised geometries. More specifically, the models that have previously been developed were generally derived and validated for arrays of buildings that are all of a uniform height and shape, and are laid out in an evenly spaced, square or staggered grid.

1.4.3.2 Morphometric models

The majority of morphometric models that have been developed aim to capture the influence of the three flow regimes upon z_0/h_m and d/h_m, by relating them to two geometrical parameters describing the underlying urban surface; the plan (λ_p) and frontal (λ_f) area densities (Raupach, 1992, Raupach, 1994, Raupach, 1995, MacDonald et al., 1998, Kastner-Klein and Rotach, 2004). As illustrated in Figure 1-8, λ_p is defined to be the ratio of building plan area to ground surface area ($\lambda_p = A_p/A_T$) and λ_f is defined to be the ratio of building frontal area to ground surface area ($\lambda_f = A_f/A_T$). Few models use more detailed surface geometry descriptors than these as an input, one example being that of Bottema (1996, 1997) that uses additional parameters specifying the spacing and aspect ratios of the buildings.

In general, the approach taken by these models involves quantifying the mutual sheltering that occurs as the density of buildings increases, and then estimating the associated change

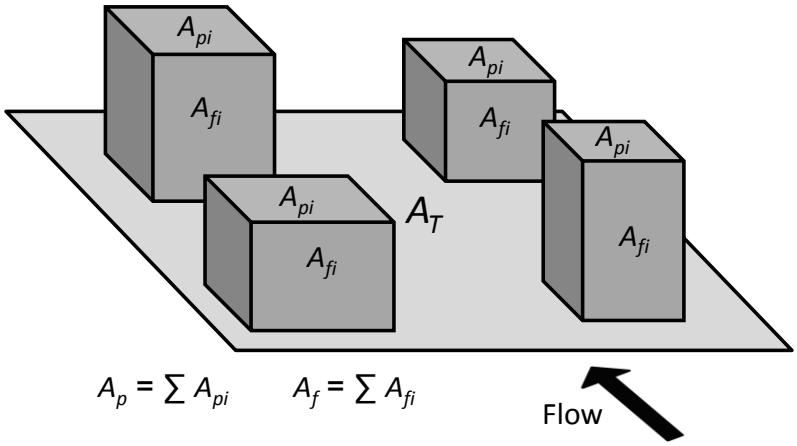

Figure 1-8: Illustration of the basic geometric measures: A_p, A_f and A_T.

in the surface drag. The surface drag can then be balanced with the shear stress in the inertial sublayer and an equation for z_0 can then be obtained, given in terms of d and the building density (λ_p and/or λ_f).

A problem that now arises is the question of finding a reliable method of estimating the relationship between d and the building density. The exact physical meaning of d is still debated, and although a theoretical investigation has proposed that d is the height of the centroid of the drag acting upon a surface (Jackson, 1981), in the derivation of morphometric models various other methods have been implemented to estimate d. Bottema (1996, 1997), for example, assumes that d is equal to the total volume of buildings and their wakes divided by the total ground area. Alternatively, Macdonald et al. (1998) suggest an empirical expression for d (based upon either λ_p or λ_f) that best represented d values experimentally derived from wind tunnel data over arrays of cubes. In Section 3.3.3, previous methods of estimating d are discussed further, and a new method is proposed.

A crucial observation is that model estimates of z_0 are highly sensitive to the expression that is used to estimate d (MacDonald et al., 1998). Largely as a consequence of this, the various morphometric models that have been developed offer wide-ranging estimates of surface aerodynamic parameters, even for idealised arrays of cubes, as shown in Figure 1-9. Furthermore, when these models are applied to real urban areas with complex geometries, the level of uncertainty can be high (Grimmond and Oke, 1999).

There is, therefore, much scope for improving these models, via both the development of more accurate methods of estimating d, and the inclusion of more detailed geometric

parameters to represent the complexities of real urban areas. Furthermore, by feeding more accurate estimates of aerodynamic parameters into wind atlas methodologies, there is the potential to significantly increase the accuracy of mean wind speed predictions.

With this in mind, in Chapter 3 a new morphometric model is developed by reconsidering the physical meaning of *d* and capturing a higher degree of geometric complexity with respect to currently available models.

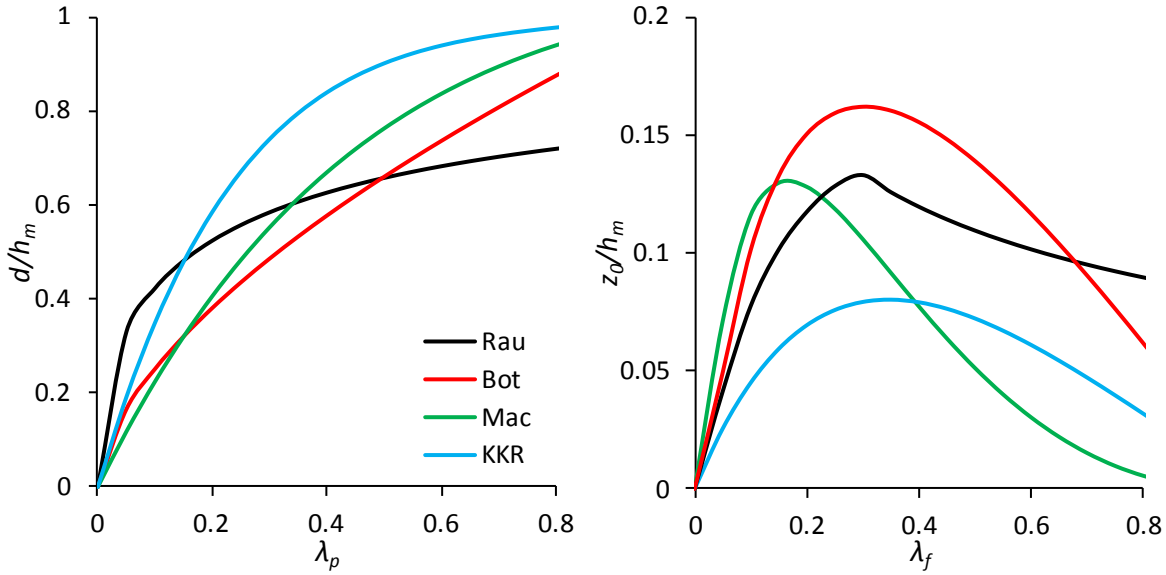

Figure 1-9: A comparison of four of the most commonly used morphometric models for estimating the aerodynamic parameters of staggered arrays of cubes. Shown are the models of Raupach (1992, 1994, 1995), Bottema (1996, 1997), Macdonald (1998), and Kastner-Klein and Rotach (2004), referred to as Rau, Bot, Mac, and KKR, respectively. The equations used to plot these curves are available in each of the author's papers.

1.4.3.3 Validating and calibrating morphometric models

An important difficulty with developing accurate morphometric models arises due to the experimental data that must be used both to validate the predictions, and often calibrate model parameters that cannot be defined by theoretical principles. This was alluded to in Section 1.4.3.1, where it was pointed out how previous models have generally been developed for highly idealised arrays. Some important geometric complexities that are omitted from the analysis of morphometric models are discussed in the next Section. A further issue, however, that is discussed in this section, is that aerodynamic parameters can be derived from experimental data (usually measured in wind tunnel studies, or more recently using CFD simulations) via methods that differ in accuracy.

Generally, the methods of deriving z_0 and d from wind tunnel data (or CFD results) have the same overall structure, although they differ in two important ways. Firstly, wind profiles are measured above the particular idealised array being studied, often at multiple locations so that the horizontal, spatially-averaged profile (i.e. the profile of $\hat{U}$) can be estimated. Subsequently, u_* is obtained from the measurements so that Equation 1-4 can be best fitted to the measured $\hat{U}$ profile to estimate z_0 and d (Cheng and Castro, 2002). The methods differ firstly in the way that u_* is obtained, and secondly in the chosen height range within which the best fitting of Equation 1-4 is performed. Specifically, u_* can be obtained either from measuring the vertical profile of the Reynolds stress, or by directly measuring the drag force exerted by the surface obstructions (Cheng and Castro, 2002, Hagishima et al., 2009, Zaki et al., 2011). The latter is suggested to be potentially the more accurate method (Cheng and Castro, 2002). The significance of the height range chosen for the best fitting procedure is explored further in Chapter 2. A final point to make is that, whichever of these methods is employed, it is crucial that any measurements used to derive z_0 and d are taken after a length of fetch that is sufficient for the flow to be fully adapted to the surface being studied (see Section 1.4.4 for further discussion of this subject).

The outcome of these complexities is that, even for identical experimental arrays, significantly different aerodynamic parameters can be derived via different methods. This has important implications for morphometric models that use such experimental data in their development. These considerations will become important throughout Chapter 3.

1.4.3.4 Geometric complexities

There is a substantial disparity between the idealised, uniform arrays that morphometric models are generally derived for, and the geometries of real urban landscapes. However, wind tunnel studies and computational fluid dynamics simulations have begun to investigate types of building arrays that bridge this gap (Rafailidas, 1997, Cheng and Castro, 2002b, Hagishima et al., 2009, Bou-Zeid et al., 2009, Zaki et al., 2011). These studies have accomplished this by considering less simplified arrays, which incorporate geometrical complexities such as obliquely angled buildings, realistic roof shapes, and heterogeneous building heights, as illustrated in Figure 1-10.

The influence of these geometric parameters upon wind profiles, and hence z_0 and d, has proven in some cases to be substantial. For example, the roughness of uniform height arrays with blocks aligned at 45° to the flow has been found to be up to a factor of two higher than that of arrays aligned normally to the flow (Zaki et al., 2011), although values of d were less affected. The addition of pitched roofs has also been found to have a similarly significant effect upon the magnitude of aerodynamic parameters (Rafailidas, 1997). However, the most considerable changes in aerodynamic parameters have been observed under the presence of building height variability.

Some investigations have shown height variability to increase z_0 by almost a factor of four (Zaki et al., 2011), and it has consistently been found that d can exceed the mean building height significantly for arrays of heterogeneous height. These results are examined in detail during the model development of Chapter 3 (see Figure 3-7 and Figure 3-9). The reason that this behaviour arises is the disproportionately large influence of tall buildings upon the flow in arrays of variable height (Xie et al., 2008). As a consequence of this, in dense urban arrays where a skimming flow regime (with low z_0) would normally be expected to occur, tall buildings can remain unsheltered and exert a significant magnitude of drag. Unfortunately however, height variability is generally still omitted from morphometric models that aim to predict z_0 and d.

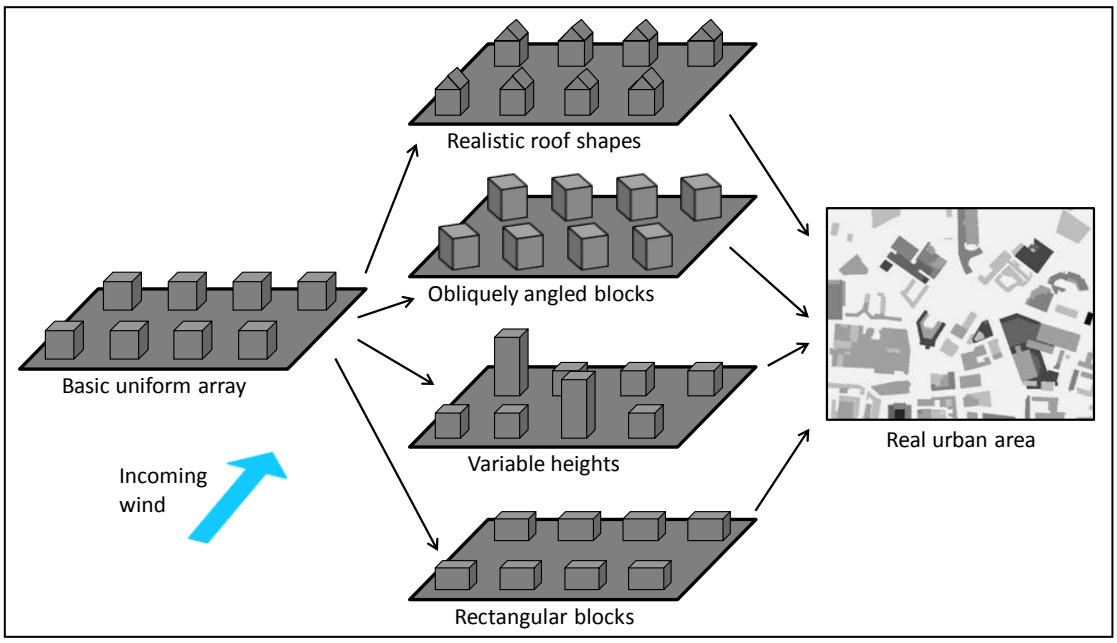

Figure 1-10: Illustration of the basic uniform arrays traditionally used to represent urban geometries (left), some more complex arrays that have begun to be investigated, (middle) and an example of a real urban area (right; shading here represents building heights).

An additional implication of the large values of z_0 and d that are inherent to arrays of heterogeneous height, which is of particular relevance to wind resource prediction, is that the wind profile can no longer be considered to be logarithmic down to the mean building height. This brings into question what wind profile should be used in the RSL to estimate above-roof wind resource, as buildings within real urban areas are almost always of heterogeneous heights.

1.4.3.5 The influence of building height variability

If accurate estimates of wind profiles in urban areas are to be made, it appears to be crucial to account for the influence of building height variability. However, incorporating this parameter into morphometric models is a non-trivial task.

An initial question concerns how the height variability of an array can be measured using a simple geometric parameter. The most straightforward choice is the standard deviation of the building heights (σ_h), which has often been used as a measure of height variability in wind tunnel studies. Some investigators have suggested that aerodynamic parameters increase linearly with σ_h, relative to those of a uniform height array (Jiang et al., 2008, Zaki et al., 2011), however the exact relationships reported vary and appear also to be a function of building density (Kanda, 2006, Zaki et al., 2011). Specifically, these authors have found that the impact of a set level of height variability upon surface roughness increases in magnitude with increasing building density.

In real urban areas this matter is complicated further by the fact that building footprints are of differing sizes, which means there are multiple ways in which σ_h can be calculated (for example, it could be weighted by building roof area). Furthermore, it is clear that σ_h gives no

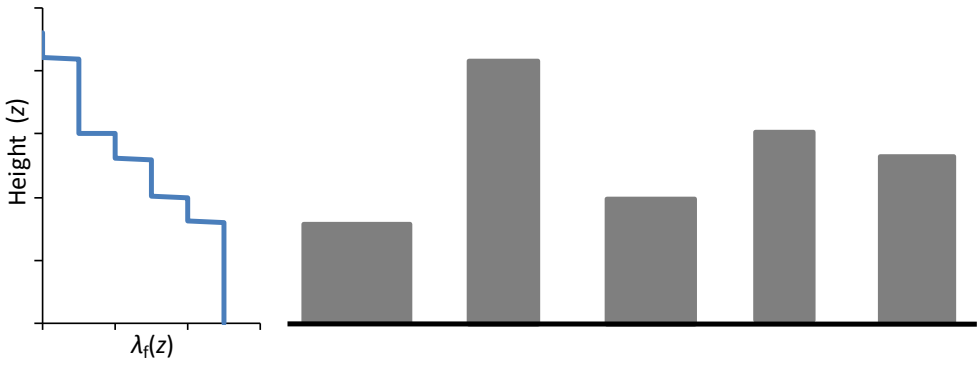

Figure 1-11: An illustration of the parameter $\lambda_f(z)$ for a simple variable height array.

description of building height distributions, and the shapes of these for real urban areas can vary dramatically (Hagishima and Tanimoto, 2005). Given the disproportionately large impact of tall buildings upon wind profiles (Xie et al., 2008) this is problematic, and hence it is desirable to use more complex descriptors of height variability than σ_h.

One more sophisticated parameter that has been used to quantify height variability is the vertical profile of the frontal area density, $\lambda_f(z)$, where z is the above ground height (see Figure 1-11). This parameter offers a complete description of the height distribution, although unavoidably it is relatively complex with respect to σ_h. In addition, when building footprints are not square, $\lambda_f(z)$ is a function of the incoming wind direction. Nevertheless, there is one morphometric model that has been developed to estimate wind profiles that utilises this parameter (Di Sabatino et al., 2008).

The model of Di Sabatino et al. (2008) is based upon a horizontally-averaged balance equation between the building drag force and the local shear stress. This balance is evaluated from the ground up to a reference height in the ISL, and the output is an estimate of the profile of U throughout this height range. A notable advantage of the model is that is does not assume the existence of logarithmic and exponential profiles in the RSL and CL, respectively. Therefore, for urban areas with height variability, the model presents a potential opportunity to improve the accuracy of the estimated wind profile throughout these sublayers. However, the model does not explicitly calculate the aerodynamic parameters of the standard logarithmic profile. In fact, the input parameters include d and dU/dz, the latter of which can be estimated with a knowledge of z_0. Thus, to implement this model, it is useful to first estimate z_0 and d by another method that is dependent upon λ_p or λ_f.

There remains therefore, a significant incentive to develop a morphometric model to estimate z_0 and d as a function of a set of geometric parameters that include a measure of height variability. Without such a model, the estimations of above-roof wind speeds made using wind atlas methodologies are likely to remain highly uncertain.

1.4.3.6 Applying morphometric models in cities

Finally, it is important to discuss the process via which morphometric models are applied to real city geometries, as there are a number of important considerations that must be made as well as some practical challenges.

Before a morphometric model is used to estimate the aerodynamic parameters of a city, it must be decided what area is appropriate for the application of such a model. There are two factors that determine the appropriate scale: (i) the area must be large enough to contain a sufficient number of buildings for the parameters z_0 and d to be meaningful, as these are intended to describe the bulk aerodynamic effect of groups of buildings, and (ii) the area should not be so large that it contains a mixture of land use types (such as suburbs, industrial areas, parklands, etc.), rather it should consist of relatively homogeneous surface cover.

The intermediate scale that is bounded by these criteria is referred to the neighbourhood scale (up to 1 - 2 km), and it lies between the street-scale (100 - 200 m) and the city-scale (Britter and Hanna, 2003). Although this scale is reasonably appropriate for applying morphometric models, the problem of choosing appropriate 'neighbourhood regions' which are of a homogeneous surface type still remains. It would be valuable if an intelligent, automated method could be developed to choose neighbourhood regions based upon the homogeneity of surface cover, although the complexity of city geometries makes this a challenging task. Currently therefore, researchers generally apply morphometric models to neighbourhood regions determined by simple uniform grids, using resolutions ranging from 150 m to 1 km (Bottema and Mestayer, 1998, Ratti et al., 2002, Holland et al., 2008, Di Sabatino et al., 2010).

The outputs of such processes are gridded maps of aerodynamic parameters over a city, or urban area. However, the wind profiles above the surface cannot necessarily be described by simply inputting these parameters directly into the standard logarithmic law. First, the heterogeneity of the land cover (and the hence the surface's aerodynamic characteristics) must also be considered.

1.4.4 Heterogeneous surface cover

When wind flows over an area of heterogeneous land cover, there is an interaction between the aerodynamic effects of each of the 'patches' of surface roughness (Mason, 1988, Mahrt, 1996). In this situation, the flow behaves in a manner analogous to that occurring in the RSL and ISL:

As was described earlier in this section, the flow in the RSL is characterised by a high level of spatial variability due to the influence of the wakes produced by the buildings on the surface, while in the ISL this spatial variation is eliminated via turbulent mixing, and hence the flow is determined by the bulk effect of the buildings. Similarly, above areas of heterogeneous land cover, below a particular height-scale the influence of the different patches of roughness upon the flow is discernible, while above this height the flow behaves in response to the surface as a whole.

Slightly confusingly, this height-scale is often also referred to as the 'blending height' (Mahrt, 1996), and above this height the wind profile still follows the standard logarithmic profile of Equation 1-4. However, the aerodynamic parameters that determine its shape are now dependent upon the aggregate effect of the patches of roughness forming the heterogeneous surface. These are referred to as the 'effective' aerodynamic parameters, and they can be calculated by considering the aerodynamic parameters of the individual patches (Taylor, 1987). (Note that in this section, blending height is used to refer to this height scale, as opposed to the top of the RSL.)

Below the blending height however, the wind profile becomes far more complex due to the development and interaction of the different 'internal boundary layers' forming above each patch of roughness.

1.4.4.1 Effective aerodynamic parameters

Various models have been developed to estimate the effective roughness length ($z_{0\text{-eff}}$) that determines the wind profile above the blending height (Taylor, 1987, Mason, 1988, Goode and Belcher, 1999, Bou-Zeid et al., 2004). Typically, the blending height itself is also output by these models. Earlier researchers derived $z_{0\text{-eff}}$ by ensuring that the correct, spatially-averaged wind speed was obtained at the blending height (Taylor, 1987). More recent investigations have argued that it is more appropriate to balance the average shear stress

above the blending height with the sum of the shear stresses due to each of the individual roughness patches (Mason, 1988, Goode and Belcher, 1999, Bou-Zeid et al., 2004).

The majority of these studies however, have used quite simple surfaces in their model development, with alternating strips of two different roughness lengths, normally each of a single characteristic length-scale. For real world applications, the single length-scale required as a model input, to characterise the horizontal dimensions of the surface roughness patches, presents a problem. Generally, real surfaces are far more complex than this, consisting of patches of different land cover on a wide variety of length-scales, particularly in urban areas (Roth, 2000).

Fortunately, a method of estimating the characteristic length-scale of a complex heterogeneous surface has been developed (Bou-Zeid et al., 2007) that relies upon the 'structure function' calculated for the surface. The structure function is a standard mathematical formula used to measure the variability scale of a particular surface characteristic. Using results from their CFD modelling studies, the developers of this model also highlighted the importance of considering the size and layout of roughness patches. Specifically, they found that when the various roughness patches of a heterogeneous surface were chopped up and randomly rearranged, there were significant increases and decreases in the effective roughness length and blending height, respectively. Recently, the model of Bou-Zeid et al. (2007) has been successfully applied to complex urban surfaces by other researchers (Barlow et al., 2008).

One potentially significant problem that remains when modelling the wind profile above heterogeneous urban surfaces is that there is as yet no model for estimating the 'effective' displacement height (d_{eff}) of such a surface (Best et al., 2008). However it is possible, that wind prediction models are not too sensitive to the exact value of the effective displacement height, as at reasonable above-ground heights the logarithmic profile is not too sensitive to d. Therefore, calculating d_{eff} as a simple arithmetic average of local d values may prove sufficient for wind resource prediction, and this approach is tested in Chapters 5 and 6.

1.4.4.2 Internal boundary layers

Just as the urban boundary layer grows when the wind flows from a rural to a built-up area, a new, internal boundary layer (IBL) grows when any significant change in roughness is encountered (Garratt, 1990). This consists of a transition layer (TL), which is affected by the new surface but not yet adapted to it, and an equilibrium layer, where the wind profile is determined entirely by this new surface (see Figure 1-12). If the surface cover remains homogeneous over a sufficiently long fetch (i.e. it doesn't vary between suburbs, industrial areas, parkland, etc.) then the equilibrium layer will develop to contain the normal sublayers: the CL, RSL and ISL (Cheng and Castro, 2002a).

Although a number of analytical formulae have been suggested to estimate the growth rate (with fetch) of the internal boundary layer (Elliot, 1958, Garratt, 1990), these may not be appropriate for rough urban surfaces (Cheng and Castro, 2002a). However, various researchers have investigated the growth of equilibrium layers over urban-like arrays using experimental methods, and some useful findings have been reported.

Typically, the flow in the CL adapts relatively quickly to a new surface, and may become fully adapted within a few hundred meters (about 3 – 6 rows of buildings), depending upon the nature of the roughness change (Coceal and Belcher, 2005). A similarly short fetch (about 5 – 10 rows of buildings) is normally required for the RSL to adapt to a new surface, and reach its full depth (Cheng and Castro, 2002a, Cheng and Castro, 2002b, Kurita and Kanda, 2009). The development of the ISL however, has been found to occur far more slowly (Cheng and Castro, 2002b, Cheng and Castro, 2002a). Consequently, due to the frequently varying

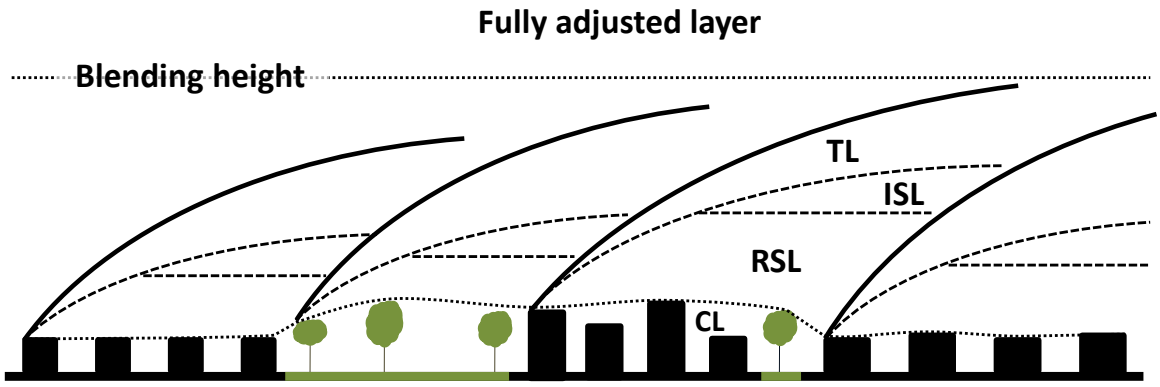

Figure 1-12: Illustration of the internal boundary layers which grow at changes in land cover, adapted from Goode and Belcher (1999) and Cheng and Castro (2002b). Their structure is also shown, including the CL, RSL and ISL (that make up the equilibrium layer), and the transition layer (TL).

surface cover, ISL's in equilibrium with the underlying surface may rarely be found in real urban areas (Cheng and Castro, 2002b).

In summary, this makes describing the wind profile below the blending height in real urban areas a complex task, as it may be difficult to estimate the extent to which the IBL and its sublayers (CL, RSL and ISL) have developed. It is likely therefore, that a number of assumptions will have to be made when describing these profiles in wind atlas methodologies.

1.4.4.3 Estimating wind profiles above heterogeneous surface cover

It can be gathered from this discussion that the wind profiles above urban surfaces are more complex than the simple illustration of the urban boundary layer in Figure 1-5 implies. Nevertheless, it can now be inferred how they may be described with the use of maps of aerodynamic parameters calculated over a city by using, for example, a morphometric model, and a methodology similar to that of the Met Office detailed in section 1.3.

As indicated in Figure 1-13, the uppermost layer of flow is that lying above the blending height, where the flow is fully adapted to the heterogeneous urban fetch. Within this layer, the wind profile can be considered logarithmic, with the effective roughness length calculated via a blending method from the aerodynamic parameters of the individual patches. Within the equilibrium layer, which lies closest to the ground, the wind profile can

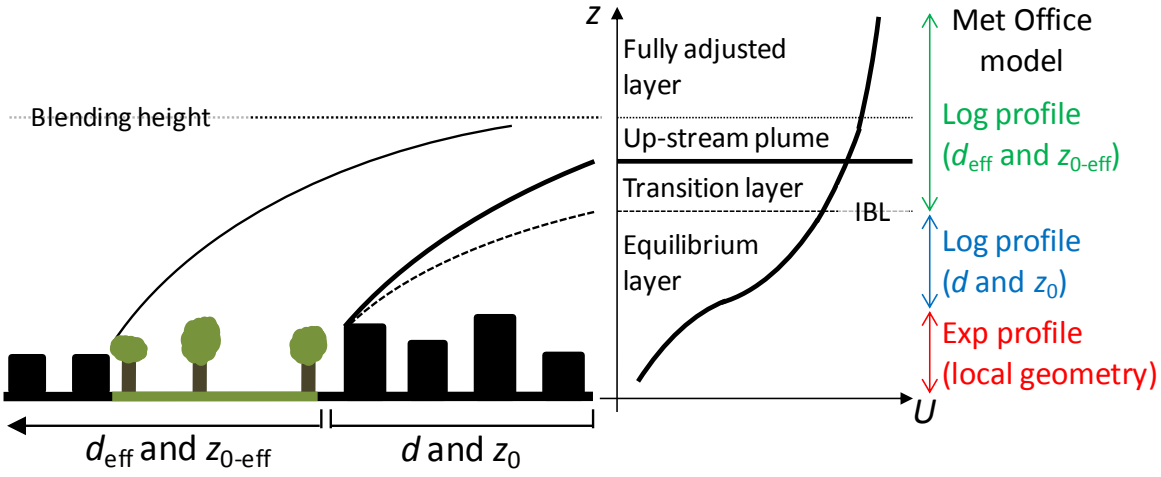

Figure 1-13: A breakdown of the different layers that exist above heterogeneous, urban surfaces. The approximated form of the wind profiles as used by the Met Office model (Best et al., 2008) is indicated on the right.

be described by considering only the directly underlying surface, although two different profiles must be used: (i) in the RSL (and the ISL, if it exists) the standard logarithmic profile can be used with the aerodynamic parameters calculated directly from a morphometric model, for the local neighbourhood region, and (ii) in the CL, an exponential profile may be used, again by considering the geometry of the local neighbourhood region.

In between these layers, the profile is more difficult to describe, as it is in equilibrium neither with the local neighbourhood nor the full heterogeneous urban surface. For

example, in the region below the blending height but above the IBL, it has been suggested that the flow will mainly be influenced by the 'upstream-plume' produced by the surface lying directly upstream (Bou-Zeid et al., 2007). Below here, in the transition layer forming the upper part of the IBL (see Figure 1-13), the wind profile will be influenced to a varying degree by both the underlying and upwind surfaces (Cheng and Castro, 2002a). Unfortunately however, there are no reliable methods of estimating the height range of these layers or the wind profiles present within them.

Consequently, in wind atlas methodologies such as that of the Met Office described in Section 1.3, it is necessary to make some simplifications to the wind profiles in these layers. In the Met Office methodology, the wind profile is simplified by assuming that above the blending height the flow is in equilibrium with the full, heterogeneous urban surface, and below the blending height it is adapted to the underlying surface, as indicated in Figure 1-13. In practical situations there is some evidence to suggest that these simplifications may be reasonable:

(i) It has been shown (Bou-Zeid et al., 2004, Bou-Zeid et al., 2007) that above surfaces with rapidly and frequently varying surface cover (with characteristic length-scales ≈ 500 m) the blending height may be relatively low (< 100 m).

(ii) For urban-like surfaces a roughness sublayer (of height 2 - 5 h_m) in equilibrium with the underlying surface may grow rapidly after a change in surface cover (Cheng and Castro, 2002a, Cheng and Castro, 2002b).

The consequence of this is that the thickness of the transition layer and the upstream-plume may be small relative to the equilibrium and fully adjusted layers. Thus, describing the wind profile in terms of two parts –a layer adapted to the underlying surface, and a layer

responding to the heterogeneous surface as a whole– may be a useful modelling approach. In contrast however, results from the field study of Barlow et al. (2008) show that the extent of this region can be significant (potentially about 100 m thick), and hence it should be borne in mind that neglecting these layers in wind atlas methodologies represents a potential source of error.

1.4.5 Building aerodynamics

When modelling the wind resource available to roof-mounted turbines using urban meteorological principles, as discussed above, an additional source of uncertainty arises due to the influence of individual building aerodynamics upon the flow. The complex flow patterns that occur around building roofs can cause the wind speed to deviate significantly from the spatially-averaged wind profile at the same height, which is an important consideration to make when using a spatially-averaged profile (logarithmic or exponential) to predict above-roof wind speeds.

In order to estimate with high accuracy the effect of building aerodynamics upon above-roof wind resource, it is necessary to use more complex techniques, such as computational fluid dynamic (CFD) modelling, or wind tunnels with a scaled-down model of the potential site. However, the financial costs of such methods are usually prohibitive for small-scale wind energy projects. Therefore, it is important to understand the main characteristics of rooftop flows so their effects can be approximately quantified, or at least qualitatively assessed.

1.4.5.1 Flow patterns around individual buildings

Flow patterns around individual buildings have been investigated for many decades (Castro and Robins, 1977, Hunt et al., 1978, Fackrell, 1984, Peterka et al., 1985), and the basic characteristics are well known. These are summarised in Figure 1-14 for a building lying normal to the flow. It can be seen here that the main characteristics are three separated regions of flow containing recirculating vortices, located upwind, upon the roof, and downwind of the building (i.e. within its wake). Separation zones are also present around the vertical, upwind edges of the building (although not visible in this two-dimensional figure).

With respect to roof-mounted turbines, the main concern is for the turbine to be mounted at a sufficient elevation above the roof to be clear of any separated flow, and also to be at a

sufficient distance from upstream buildings so as not to be affected by their wakes. Therefore, the dimensions of these separated regions of flow –which are strongly dependent upon a building's shape, its alignment with the flow, and the form of the incoming wind profile– must be estimated. To this end, the advantages of site specific modelling, such as CFD, are clear. If a turbine is mounted in one of these regions of flow, the energy output may suffer dramatically due to the minimal wind speeds. This is in fact a primary reason that field studies into roof-mounted turbines have reported disappointing energy yields, as in general only suburban installations are considered where turbines are elevated less than 2 m above the building roof (James et al., 2010, Glass and Levermore, 2011).

There are a number of simple formulae that have been developed to estimate the extent of the downwind recirculation region behind an isolated building based upon its shape (Hosker, 1984, Fackrell, 1984, Becker et al., 2002). These can be used to offer some guidelines for ensuring a turbine will not be sheltered by upwind obstructions (although it must be borne in mind that the sheltering effects behind a building will extend some way beyond the recirculation region, as shown in Figure 1-14). Examples of such guidelines are offered by the Met Office (Best et al., 2008), who suggest that the distance between a turbine and any upwind obstructions (of above-ground height *h*) should be 3 - 10*h*, or alternatively that the turbine must be located at an above-ground height of 1.5 - 2*h* or more. The American Wind Energy Association offer a stricter guideline, which is clearly difficult to satisfy in urban areas: the lowest part of the turbine rotor should be 30 ft higher than any obstruction contained within a 500 ft radius (www.awea.org/smallwind).

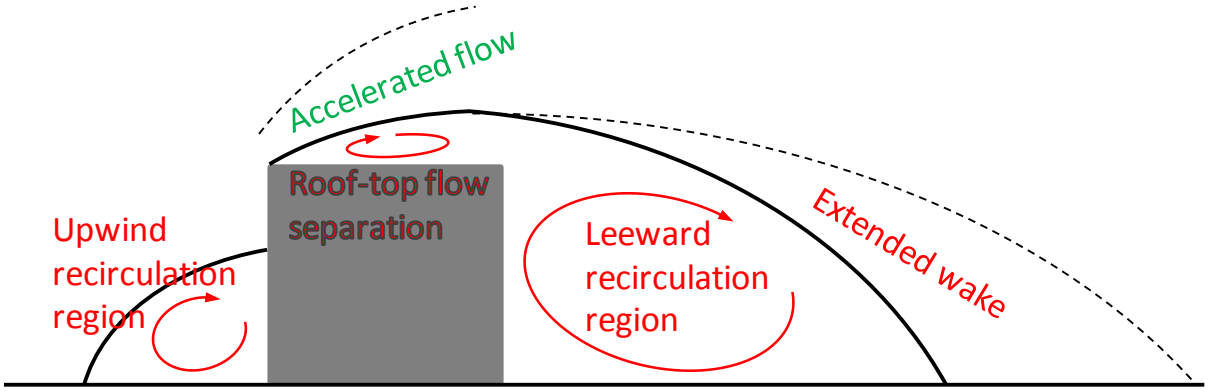

Figure 1-14: The basic characteristics of the flow pattern around an individual building aligned normally with the flow.

There are also a small number of studies that have investigated roof-top flow patterns (above individual buildings) with specific application to building-mounted turbines, most notably that of (Mertens, 2003). Mertens' results show that a region of accelerated flow with large vertical wind angles exists at a small distance above the leading edge of an isolated building, lying above the separated roof-top flow. The implication of this is that a well-placed roof-top turbine may receive a wind resource more favourable than the spatially-averaged wind profile at the same height. However, estimating the magnitude of this effect for different buildings is a difficult task, and there is the additional complication of varying incoming flow profiles and directions. For example, if a turbine is placed at the leading edge of a building (with respect to the prevailing wind direction) in order to access this accelerated flow, then when the wind direction changes the turbine may instead be in the separated roof-top flow. This means that, when micro-siting a roof-top turbine, it is necessary for roof-top flow patterns to be considered in conjunction with a local wind rose.

Another important factor to consider is that roof-top flow patterns are influenced dramatically by the presence of surrounding buildings. Consequently, in dense urban arrays they may differ substantially from those observed above the roof of an isolated building.

1.4.5.2 Roof-top flow patterns in building arrays

There are a number of researchers that have investigated roof-top flow patterns in building arrays for the purpose of building-mounted turbines. Mostly researchers have used CFD techniques (Heath et al., 2007, Lu and Ip, 2009, Ledo et al., 2010, Ayhan and Sağlam, 2012, Balduzzi et al., 2012), although some wind tunnels studies have also been undertaken (Anderson et al., 2007).

Many of these investigations have been carried out for building arrays representative of suburban areas, comprised of rows of residential properties of identical heights (Heath et al., 2007, Anderson et al., 2007, Ledo et al., 2010). These studies show that the accelerated flow found above the roof of isolated buildings is absent in suburban areas. Instead, above arrays of homogeneous height, a strong shear layer of flow develops at roof level where turbulence intensities can be as high as 50% (Coceal et al., 2006). Furthermore, turbulence intensities may be higher above arrays of buildings with pitched roofs, relative to buildings with flat roofs (Ledo et al., 2010). Some studies have gone on to estimate the potential

energy yield of turbines installed upon residential properties in suburban areas and have suggested that these will typically be quite low (Heath et al., 2007).

A number of other researchers have investigated the potential to generate wind energy upon taller buildings in more complex urban landscapes (Lu and Ip, 2009, Ayhan and Sağlam, 2012, Balduzzi et al., 2012), and these studies have shown promising results. Under some geometric situations, building aerodynamics have been shown to increase above roof wind speeds via the same flow patterns that occur around isolated buildings (Balduzzi et al., 2012). In addition, wind speed-up effects have been found to occur in-between pairs of tall buildings (Lu and Ip, 2009).

In particular, Balduzzi et al. (2012) have investigated in detail flow patterns above the roof of tall buildings, and their dependence upon the upwind buildings height and spacing. They found that the wind speeds at the leading edge of a tall building may be accelerated to be greater than the incoming wind speed at the same height. This effect was dependent upon the height of the potential 'installation' building and the height and spacing of the upwind

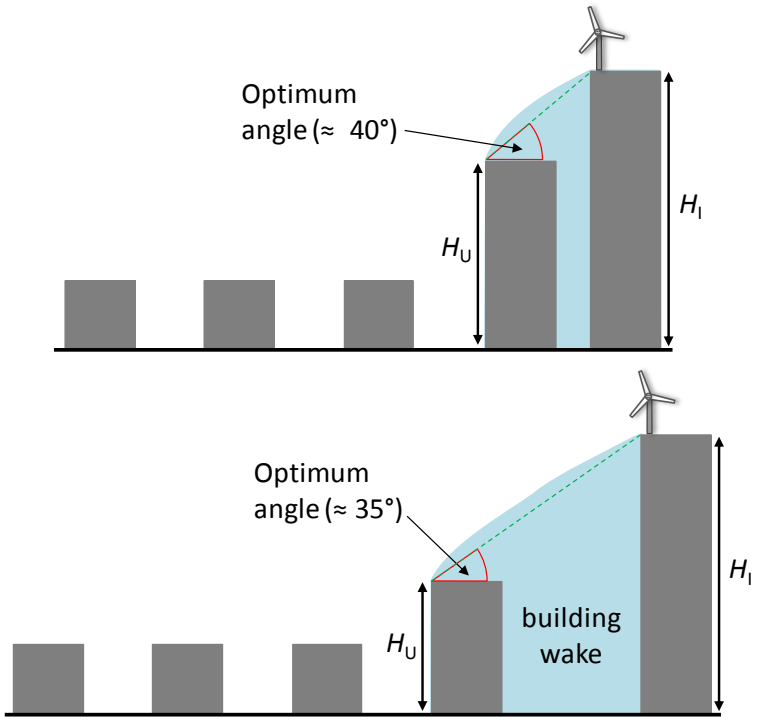

Figure 1-15: Illustration of the speed up effect that may occur above a tall (installation) building's roof, due to the upwind building (Balduzzi et al., 2012). For this effect to occur there is an optimum value for the ratio, H_U/H_I, and this value *decreases* as the building spacing *increases*.

building. Interestingly, they found that this flow acceleration could be due not only to flow acceleration over the installation building but also flow that is 'ramped up' and accelerated over the upwind building. For the latter effect to occur, they found that the angle between the horizontal and a line joining the leading edges of the upwind and installation buildings should be within about 30 - 40°, depending upon the building spacing, as illustrated in Figure 1-15. This physical reasons that give rise to this optimum angle are that if the upwind building is too tall then the installation site will lie within its wake and the above-roof wind resource will suffer, and conversely, if the upwind building is too small then any accelerated flow above its roof will not reach the roof of the installation building.

Overall, the investigations into generating wind energy on tall buildings in cities have suggested this is an underutilised form of wind energy generation. Potentially, wind turbines mounted upon tall buildings could access significant wind speeds that would otherwise require the erection of large towers. Importantly, these investigations have highlighted the unjustifiably negative perception that can be associated with urban wind energy when conclusions drawn from suburban wind energy investigations are applied too generally.

1.5 Research Objectives

Drawing upon the opportunities for research highlighted in this literature review, the primary objective of the work herein is to develop an analytical methodology for assessing the available wind resource over large urban areas, which reduces the need for onsite meteorological measurements. In developing this methodology, some of the most significant issues that occur when predicting urban wind resource will be rectified using novel modelling techniques. The research is divided into various separate stages, each with distinct intermediate goals:

(i) Initially, a detailed evaluation of currently available wind atlas methodologies is undertaken in order to investigate the various sources of model error, and quantify their relative contributions (see Chapter 2). This investigation guides the direction of the subsequent research so as to be focused on improving the most uncertain aspects of current models. An important finding of this investigation is that one of the most significant sources of error in urban wind atlas methodologies arises from the inadequate methods of estimating aerodynamic parameters of surfaces using morphometric models.

(ii) In Chapter 3, a new morphometric model is developed for simplified urban surfaces, which takes into account an important geometric complexity overlooked by other available models. The model predictions are also validated over a number of different urban-like arrays using a number of experimental datasets.

(iii) In Chapter 4, a technique is developed for applying this new morphometric model to complex urban environments, using the UK city of Leeds as a case study. Aerodynamic parameters predicted for the UK city of Leeds are compared to those previously reported in the literature for similar urban areas, and their relationship to the geometric form of the city is investigated.

(iv) Using the modelling techniques described in Chapters 3 and 4, in Chapter 5 a new wind atlas methodology is developed that is optimised for urban environments. The model is then used to map mean wind speeds over a number of UK cities, and the predictions are compared to measured data from a wide variety of urban locations. The accuracy of the model over these validation sites is also compared to that of the UK Met Office methodology.

(v) In Chapter 6, the wind atlas methodology of Chapter 5 is refined further, via the use of more complex input datasets. This allows for a more informed evaluation of the uncertainties in the method, and hence an increased level of confidence in the accuracy of the results. The suggested accuracy of the results allows for a preliminary evaluation of the cumulative, city-scale potential for generating wind energy in cities to be made, using the UK City of Leeds as a case study.

(vi) Finally, in Chapter 7, conclusions of the research are summarised and their implications and impacts are discussed.

1.5.1 Bibliography of published work:

As a result of the research performed in this PhD study, the following research papers have been produced:

Chapter 2:

J T Millward-Hopkins, A S Tomlin, L Ma, D Ingham, and M Pourkashanian, The predictability of above roof wind resource in the urban roughness sublayer (2011), *Wind Energy, volume 15 (issue 2) 225-243*

Chapter 3:

J T Millward-Hopkins, A S Tomlin, L Ma, D Ingham, and M Pourkashanian, Estimating Aerodynamic Parameters of Urban-Like Surfaces with Heterogeneous Building Heights (2011), *Boundary-Layer Meteorology,* volume 141**,** 443-465

Chapter 4:

J T Millward-Hopkins, A S Tomlin, L Ma, D Ingham, and M Pourkashanian, Aerodynamic Parameters of a UK City Derived from Morphological Data (2012), *Boundary-Layer Meteorology***,** volume 146, 447-468

Chapter 5:

J T Millward-Hopkins, A S Tomlin, L Ma, D Ingham, and M Pourkashanian, Mapping the Wind Resource over UK Cities (2013), *Renewable Energy*, volume 55, 202-211

Chapter 6:

J T Millward-Hopkins, A S Tomlin, L Ma, D Ingham, and M Pourkashanian, A Preliminary Investigation into the City-Scale Potential of Urban Wind Energy (2013), *Renewable Energy*, (accepted with minor revisions)

2 The Predictability of Above Roof Wind Resource in the Urban Roughness Sublayer

2.1 Introduction and Objectives

In this Chapter, using a typical wind atlas methodology, the predictability of above-roof wind resource in the urban roughness and inertial sublayers is evaluated (measured here as the 3D, mean wind speed). Essentially, the objective is to investigate sources of uncertainties in wind atlas methodologies when they are applied to urban areas. These uncertainties can be thought of as occurring at two scales:

(i) Firstly, wind atlas methodologies typically estimate the wind resource at the neighbourhood scale by using a logarithmic profile to estimate the wind resource at a particular above-ground height in a neighbourhood region. The process used to estimate this wind profile has a number of inherent uncertainties, which occur for a variety of reasons.

(ii) Secondly, within a neighbourhood region, there is spatial variability in the roughness sublayer flow at the building scale, which is unaccounted for in the logarithmic profile. Additionally, above each building, roof-top flow patterns can cause wind speeds to deviate further from the logarithmic profile. These complexities amplify the uncertainties of wind atlas methodologies.

The primary aim of this Chapter is to consider the latter uncertainties that arise due to building scale flow processes, as these questions have not yet been fully addressed in the literature. The focus is upon the roughness sublayer, as in the majority of cases roof-top turbines will be located within this region of flow. In order to evaluate these uncertainties, data from wind tunnel experiments and a large eddy simulation are used, which were obtained by previous researchers investigating flow above idealised urban arrays (Xie et al., 2008, Cheng and Castro, 2002b, Hagishima et al., 2009). The idealised arrays considered include an array of blocks of heterogeneous heights and also arrays of uniform cubes. These are representative of a relatively complex city array and simpler suburban areas, respectively.

The structure of analysis in this Chapter is as follows: Within the array of heterogeneous blocks, the spatial variation of the wind resource within the RSL (Section 2.4.1) and then more specifically around the individual building roofs (Section 2.4.2) is considered. The above-roof mounting positions likely to receive the most favourable wind resource are also discussed. In Section 2.4.3, by considering the results of both Sections 2.4.1 & 2.4.2, the representativeness of a spatially-averaged wind profile for estimating the wind resource in the RSL is first assessed. Subsequently, currently available methods of predicting spatially-averaged wind profiles above urban like surfaces are discussed, and their feasibility is considered based upon their accuracy and ease of use in real urban areas. Bearing in mind the conclusions of the previous two sections, in Section 2.4.4 a typical urban wind resource prediction methodology is followed, and the uncertainties arising at each stage are estimated. By comparing the magnitudes of these uncertainties, the stages of the methodology where improvements would be of most value to improving the overall accuracy of the method are highlighted.

Prior to this data analysis, details of the experimental procedures of the previous authors will be described in Section 2.2, and validation of the numerical results will be discussed in Section 2.3.

2.2 Experimental Details

In order to explore the above-roof flow patterns that may be found in a complex city array, data from the large eddy simulation (LES) of Xie et al. (2008) are analysed. As mentioned in Section 1.3.1.3, LES is a transient CFD modelling approach that fully resolves all scales of turbulence greater than the mesh resolution, and only employs a turbulence model for sub-grid scale turbulence. This is a more sophisticated approach than Reynolds Averaging (RANS) techniques. Consequently, LES can give more accurate predictions of separation and reattachment processes than the simpler RANS techniques (Cheng et al., 2003, Xie and Castro, 2006, Tominag et al., 2008). Therefore, it is expected that the LES data considered here will be well suited for predicting above-roof flow patterns, where these flow processes are crucial.

After analysis of this computational data, above-roof flows that may be found in suburban areas are also investigated, by considering wind tunnel data collected for arrays of cubes of various densities by Cheng and Castro (2002b) and Hagishima et al. (2009).

2.2.1 LES data

The LES data used in this work was produced by Xie et al. (2008), who developed numerical methodologies to investigate near surface flow processes within homogeneous and heterogeneous arrays of blocks designed to represent rough urban surfaces. Their previous work includes validation of the LES data (see Section 2.3) but with a slightly different focus than the work presented here. Since this work has a different aim, further validation of the data against wind tunnel data is carried out for above roof profiles in Section 2.3. A detailed description of the numerical methods used to produce the data was included in Xie et al. (2008) and Xie and Castro (2006), therefore only an overview of these methods is included here.

Their methods involve solving the filtered, incompressible continuity and Navier-Stokes equations:

$$\frac{\partial u_{\mathrm{i}}}{\partial x_{\mathrm{i}}} = 0$$

Equation 2-1

$$\frac{\partial u_{\mathrm{i}}}{\partial t} + \frac{\partial u_{\mathrm{i}} u_{\mathrm{j}}}{\partial x_{\mathrm{j}}} = -\frac{1}{\rho}\left(\frac{\partial p}{\partial x_{\mathrm{i}}} + \delta_{\mathrm{i1}}\frac{\partial P}{\partial x_{\mathrm{i}}}\right) + \frac{\partial}{\partial x_{\mathrm{j}}}\left(\tau_{\mathrm{ij}} + \nu\frac{\partial u_{\mathrm{i}}}{\partial x_{\mathrm{j}}}\right)$$

Equation 2-2

where u_{i} and p are the filtered velocity and pressure respectively, τ_{ij} is the residual stress (subgrid-scale Reynolds stress –see Equation 1-9– which is modelled using the Smagorinsky model), and ν is the kinematic viscosity. Finally, $\partial P/\partial x_1 = \rho u_\tau^2/10h_{\mathrm{m}}$ (where u_τ is the total wall friction velocity and $10h_{\mathrm{m}}$ is the domain height), was a constant streamwise pressure gradient applied as the driving force for the flow, shown in Xie and Castro (2006) to be an appropriate method for simulating this type of flow. In zero pressure gradient flows u_* in the standard logarithmic profile is equal to u_τ.

Periodic boundary conditions were used in both the streamwise and lateral directions to ensure the flow was fully developed, and the top of the domain was considered to be a free slip wall. On all other surfaces relatively simple wall functions were used, however, Xie and Castro (2006) discuss that due to the dominance of building scale turbulent motions and the relatively small influence of near wall dynamics in these types of geometries, these simple wall functions do not have a critical influence on the overall nature of the flow.

The computational domain used in the LES work consisted of four repeating units of an array of blocks of heterogeneous heights and 25% plan area density. The same array was previously studied by Cheng and Castro (2002b) who refer to it as RM10s (see Figure 2-1). The base of each block was of dimensions $h_m \times h_m$, where h_m was the mean height of the blocks. The dimensions of the domain in the streamwise, lateral and vertical directions were $16h_m$ x $16h_m$ x $10h_m$. A hexahedral mesh with 2.3 million cells was used in the calculations, where there were 16 cells per length, h_m, in the region near the surface elements. An image of this mesh is available as Figure 3 (a) in Xie et al. (2008).

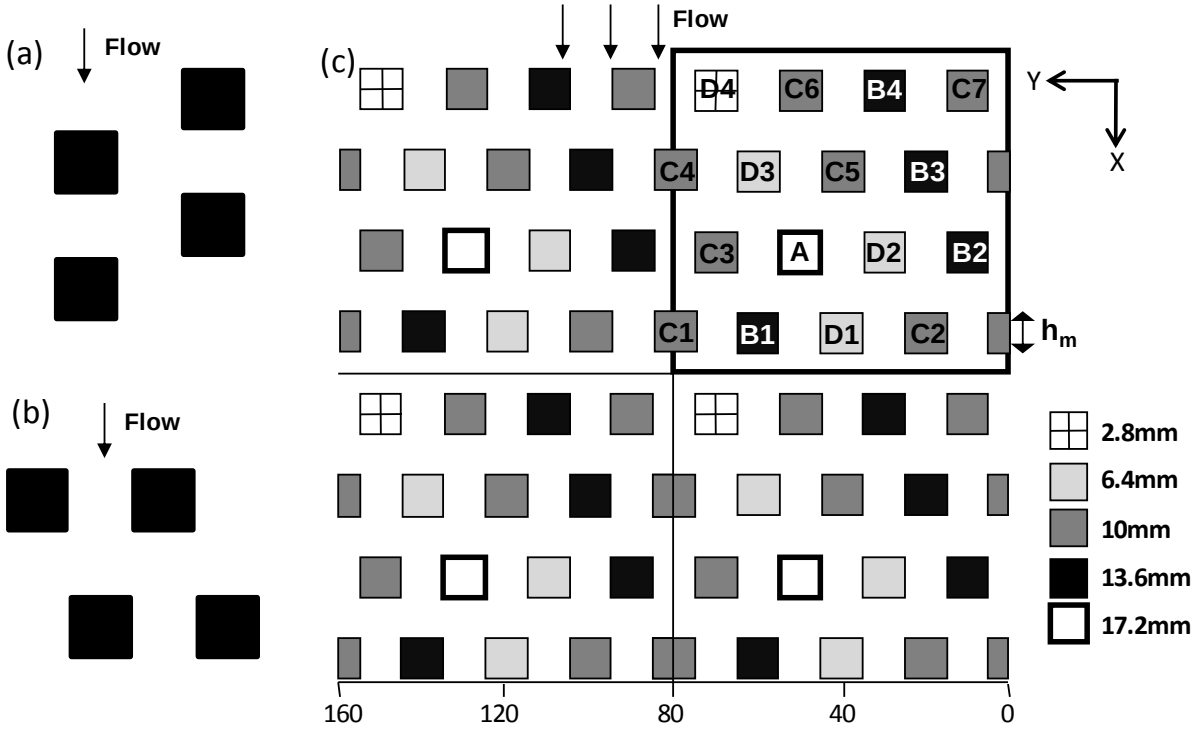

Figure 2-1: Schematics of the three idealised arrays to be considered from the wind tunnel study of Cheng and Castro (2002). (a) and (b) Arrays C20a and C20s, where the cube sides are of length 20mm. (c) The domain used in the numerical experiment of Xie et al. (2008) which represents the array RM10s. The mean block height, h_m is 10mm, and the block bases are h_m x h_m.

In this Chapter, *u*, *v* and *w* are the time averaged velocity components in the streamwise, lateral and vertical directions, and hence the 'mean wind speed' becomes $U = \sqrt{u^2 + v^2 + w^2}$. After an initial running time of 150*T* allowing the flow to develop (where $T = h_m/u_\tau$ and time steps are 0.002*T* seconds), each of these mean quantities is averaged over a model run of 300*T*. U_{rms}, u_{rms}, v_{rms} or w_{rms} refer to the root mean square of the fluctuations of the instantaneous velocity component (e.g. *U'*, *u'*, etc,) around the associated mean velocity component, or the mean turbulent fluctuations, e.g. $u_{rms} = \sqrt{(u' - u)^2}$.

2.2.2 Wind tunnel data

The wind tunnel data of Cheng and Castro (2002b), measured over the RM10s array, has previously been used to validate the LES data of Xie et al. (2008). In the current work this validation is extended to focus more closely upon the above roof profiles (see Section 2.3). Furthermore, these wind tunnel data includes measurements over uniform arrays which are analysed in the current work in Section 2.4.3. The experimental details of their wind tunnel studies are only briefly discussed here as they are explained thoroughly by Cheng and Castro (2002b), along with a discussion of the accuracy of the measurements.

The three roughness arrays studied are schematically shown in Figure 2-1, with (a) an inline array of uniform cubes, (b) a staggered array of uniform cubes, and (c) the array of heterogeneous blocks also studied by Xie et al. (2008). Measurements were made by Cheng and Castro using hot wire anemometry after a long fetch where the flow was fully developed, and the boundary layer thickness had ceased to grow significantly. The uniform geometries, C20a and C20s, were comprised of cubes with sides of length 20 mm, in aligned and staggered configurations respectively, and for the RM10s array the blocks, which were of varying heights around a mean of 10 mm, were again in a staggered configuration. All three geometries had plan and frontal area densities both equal to 25%.

For each array, a RSL and ISL were determined from the measurements. At a certain height above the surface, profiles of turbulence components and Reynolds stresses over the array were found to converge, and this height was considered to be the top of the RSL. Above this, the ISL was considered to be the region within which the converged profiles of Reynolds stress remained almost constant, and hence the wind profile here could be described by a logarithmic profile. For each surface C20a, C20s and RM10s, the RSL was

found to extend to a height of $1.85h_m$, $1.85h_m$ and $2.5h_m$, with the ISL above extending to heights of $2.4h_m$, $2.3h_m$ and $3.3h_m$, respectively.

For the C20a and C20s surfaces, pressure drag measurements were also taken via the inclusion of a single pressure tapped cube in each roughness array. These simply measured the pressure difference between the front and back face of the element, which could then be used to calculate the shear stress due to pressure drag, ignoring any viscous effects which were likely to be negligible. Shear stresses measured by this method were found to be significantly higher than those calculated from a spatial-average of the Reynolds stresses in the ISL. The likely reason for this was explained in a subsequent paper (Cheng et al., 2007), and it was suggested that direct surface drag measurements should be used to determine shear stress, and hence friction velocity, and this approach is taken in the current work.

2.3 Validation of the LES Data

Previous validation carried out by Xie et al. (2008) concluded that the accuracy of the LES data over RM10s was satisfactory for studying the flow within the RSL, capturing building scale turbulent motions (which turn out to be dominant) and calculating surface drag. Also, more detailed validation of the same LES model over the C20s array was performed in an earlier study by Xie and Castro (2006). Further details can be found within these papers.

One region in which single profiles were not considered in the previous validation of Xie et al. (2008) is within the RSL directly above the tops of the blocks. It is possible that in this region the simple wall functions employed by the model could give rise to significant errors. Since this is where the current study is almost exclusively focused, a comparison of the LES and experimental data in this region is now discussed.

Vertical profiles of U, u_{rms} and w_{rms} directly above the centre of a number of blocks were compared with those obtained from the wind tunnel study (Cheng and Castro, 2002b) over RM10s. These are shown in Figure 2-2 (a-c) for blocks A, B2 and C3, which are three unsheltered blocks of varying height. These are chosen in view of the typical locations where a turbine may be placed. It is important to mention that for each block, the lowest

available wind tunnel data point is at approximately 0.35-0.4h_m above its top, hence, below this point the accuracy of the LES cannot be assessed.

Figure 2-2 (a) shows that numerical and experimental data for U compare well, with only a very slight divergence between profiles beginning at the lowest wind tunnel data points. Figure 2-2 (b) shows three distinct peaks in the predicted u_{rms}, unfortunately occurring at a height just below the first experimental points. Above this height, agreement between the two datasets is good, although there is a slight underestimation by the LES in all cases. Vertical fluctuations shown in Figure 2-2 (c) are also underestimated by the LES. However the profiles of w_{rms} given by the LES appear to be following very much the same pattern as

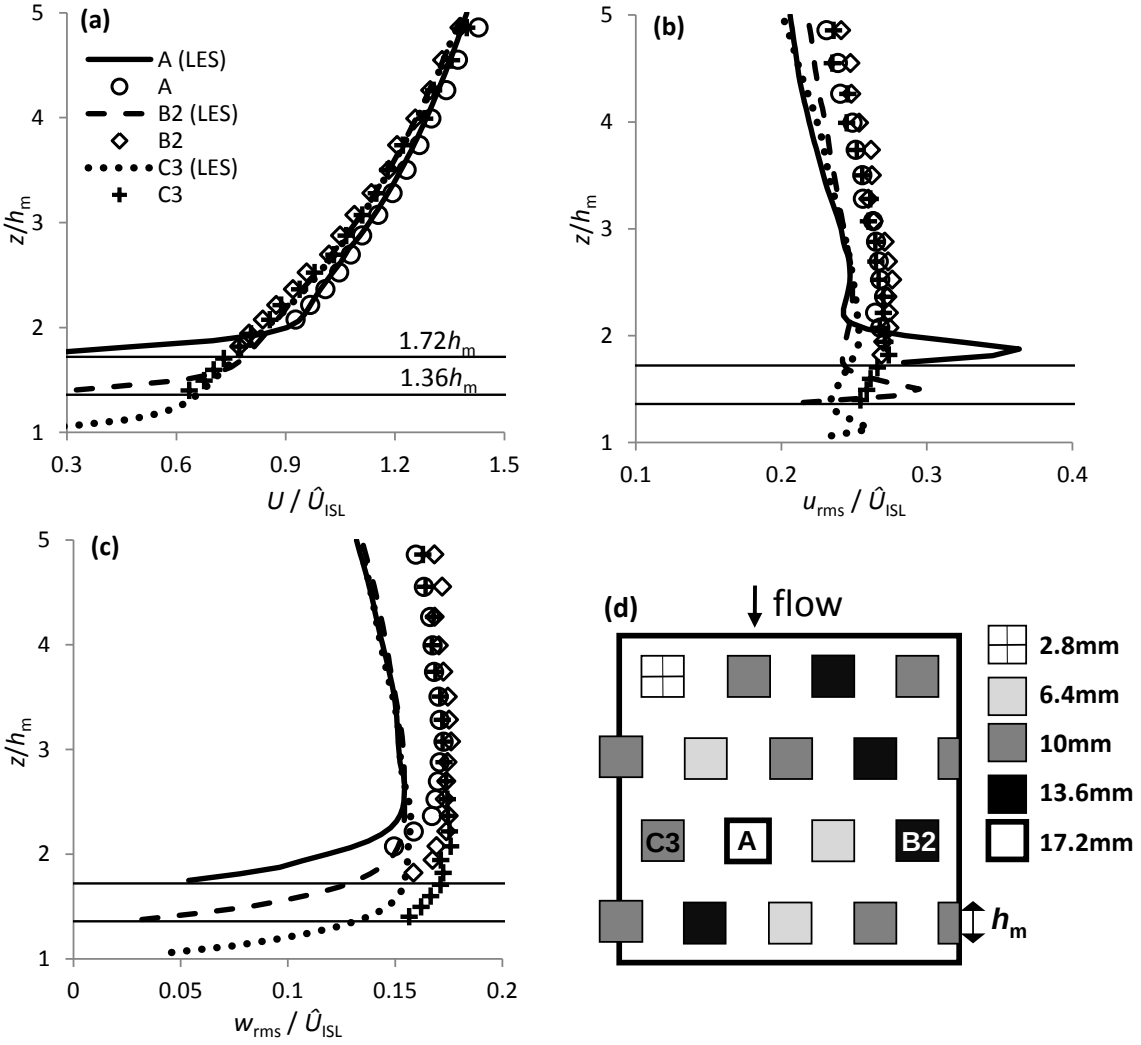

Figure 2-2: Vertical profiles above various blocks from both LES (lines) and wind tunnel data (symbols). (a) Mean wind speed, (b) Streamwise turbulence and (c) Vertical turbulence. Quantities are normalised by the spatially-averaged mean wind speed at 2.5h_m ($\hat{U}_{ISL}$), and horizontal lines indicate the block heights. (d) Schematic diagram indicating the locations of the blocks that are considered.

the experimental data at the lowest few data points. This is taken as an indication that the LES results are likely to continue to be accurate for at least a small distance below the lowest measurement points from the wind tunnel data, perhaps down to a height of about 0.15-0.2h_m above the block tops. This should be kept in mind when considering the results presented in the following sections.

2.4 Results

2.4.1 The spatial variation of the mean flow in the roughness sublayer

In this subsection, the horizontal, spatial variation of the wind resource in the RSL above the heterogeneous array (RM10s) is considered. The density of the RM10s surface is 25%, which is lower than many central city areas which can have densities of around 50%. However, RM10s can still be considered to be representative of a relatively complex urban area. Therefore, the spatial variation of wind speeds in the RSL above RM10s has important implications for the predictability of the urban wind resource.

To consider this spatial variation, a comparison of vertical profiles of U above the centres of different blocks is shown in Figure 2-3 (a). Each profile is normalised by the spatially-averaged wind speed at the top of the RSL ($\hat{U}_{ISL}$). Only the wind resource above blocks of mean height or greater are considered here, as within a dense geometry such as this, buildings less than the local mean building height are unlikely to receive a favourable wind resource at any realistic turbine mounting height. The profiles can be split into categories based upon the heights of the blocks, with those of height h_m split further into those that are sheltered by larger upstream blocks (C2, C6 and C7), and those that are not (C1, C3, C4 and C5). These latter two groups of blocks will now be referred to as C_s and C_{un}, respectively. For comparison, the spatially-averaged wind profile over the full domain is also shown ($\hat{U}$), calculated as the average of 64 equally spaced profiles over the domain as in Cheng and Castro (2002b) (see their figure 3).

When examining the profiles above the taller blocks and the unsheltered blocks of average height in Figure 2-3 (A, group B and group C_{un}), it can be seen that $\hat{U}$ acts as a lower bound for the wind resource at these potential turbine locations. This is provided the turbine is not located so close to the roof that it is within a region of separated flow (see Section 2.4.2).

There are two reasons for this:

(i) In the lower RSL the spatial-average is comprised of lower speed regions of flow in the wakes of the larger blocks, and higher velocities in unsheltered regions elsewhere. Thus, the wind resource above the unsheltered blocks in group C_{un} and B always exceeds the spatial-average.

(ii) Above the largest block, mean velocities again exceed the spatial-average significantly, but this time this is primarily due to the flow acceleration effect around the roof.

This second point deviates from the conclusion of Heath et al. (2007), namely that the accelerated above-roof flow highlighted by Mertens (2003) is absent in urban areas. The reason for this is simply that Heath et al. (2007) considered an array of blocks of uniform height, within which each block is well sheltered by those upwind. In contrast, within arrays of heterogeneous building height, the high pressures on the windward face of tall blocks appear to lead to a significant acceleration of the flow over the roof, similar to that observed over an isolated building.

The representativeness of this spatial-average for predicting the wind resource and how this spatial-average itself can be estimated is returned to in Section 2.4.3.

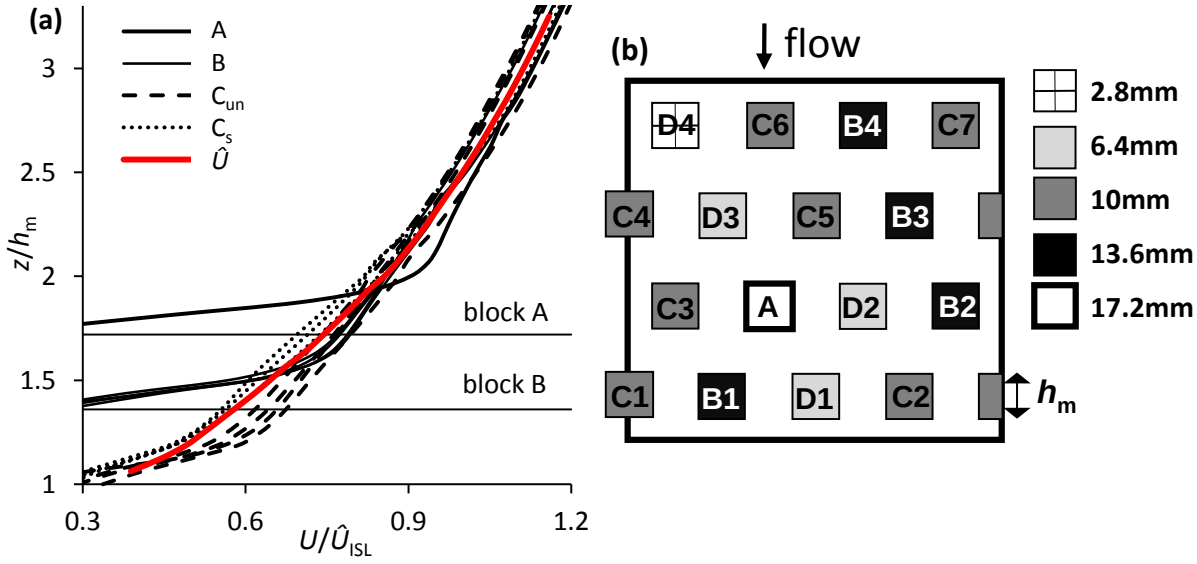

Figure 2-3: (a) Comparison of mean wind speed profiles from LES data above the centres of all blocks equal or greater than the mean building height, with $\hat{U}$ representing the spatially-averaged profile. (b) Schematic diagram indicating the blocks positions. C_{un} represents unsheltered blocks and C_s sheltered blocks.

2.4.2 The spatial variation of the flow around the individual building roofs

2.4.2.1 Roof-top flow patterns

In order to investigate regions above a roof where a turbine should ideally be placed to avoid any separated roof-top flow, this section focuses more closely upon these roof-top flow patterns. The focus of the analysis is upon blocks A, B4 and C3, as they are all unsheltered and of heights greater or equal to h_m, and hence represent buildings which receive the most favourable wind resource. The flow patterns above the other blocks in groups B and C_{un} are not shown here, however they were examined and found to be similar to those above blocks B4 and C3, respectively. In addition, to offer an insight into the flow conditions that may be found at a less desirable turbine location, the sheltered block C6 is included in Figure 2-4.

Contours of U over the centres of these blocks are shown in Figure 2-4, again normalised by $\hat{U}_{ISL}$. To indicate the vertical angle of the mean flow, 2D in plane velocity vectors are also shown. A qualitatively similar pattern can be observed over blocks A, B4 and C3. Above each of these blocks, a separated region of flow, containing minimal wind speeds, grows vertically with increasing horizontal distance from the leading edge, although at a decreasing rate. Above this separated flow lies a region of accelerated flow, which is at its most intense almost directly above the leading edge. In addition, these effects are more prominent for the highest block (block A).

The mean vertical wind angles (vertical angle in degrees of the 2D, in plane velocity vector, from the horizontal) shown above blocks A, B4 and C3 are relatively small, with the exception of the region just above their leading edges where they can be as high as 45°. Higher up (about $0.25h_m$ above block A and higher), mean vertical angles are at most around 10°, and for the lower blocks these are smaller still. It is worth reiterating here that for vertical axis turbines moderate vertical wind angles may increase the power output (Mertens et al., 2003).

Large deviations from the flow characteristics described above are only found when a heavily sheltered block, such as C6, is considered (Figure 2-4). As a result of this block being in the wake of the large upstream block, the acceleration over its leading edge is minimal. In fact, the highest velocities are found close to its downstream edge where the flow has recovered more from the disruption of the upstream block. However again, it is emphasised

that it is highly unlikely a similarly sheltered building in an urban area would receive a sufficient wind resource to justify turbine installation.

In order to visualise more clearly the regions above blocks A, B4 and C3 that receive the highest wind resource, the pattern of mean wind speeds above their tops from Figure 2-4 are re-plotted in Figure 2-5 using a different approach. The contours now shown represent the deviation of U from the maximum mean wind speed above the block at the same height (U_{max}). Effectively, the white filled contours in Figure 2-5 illustrate the region within which the local mean wind speed is at least 97% of the maximum wind speed found above the block at that height, and hence approximately encloses the region within which the highest wind resource is found. It is important to remember the following suggestions arise from

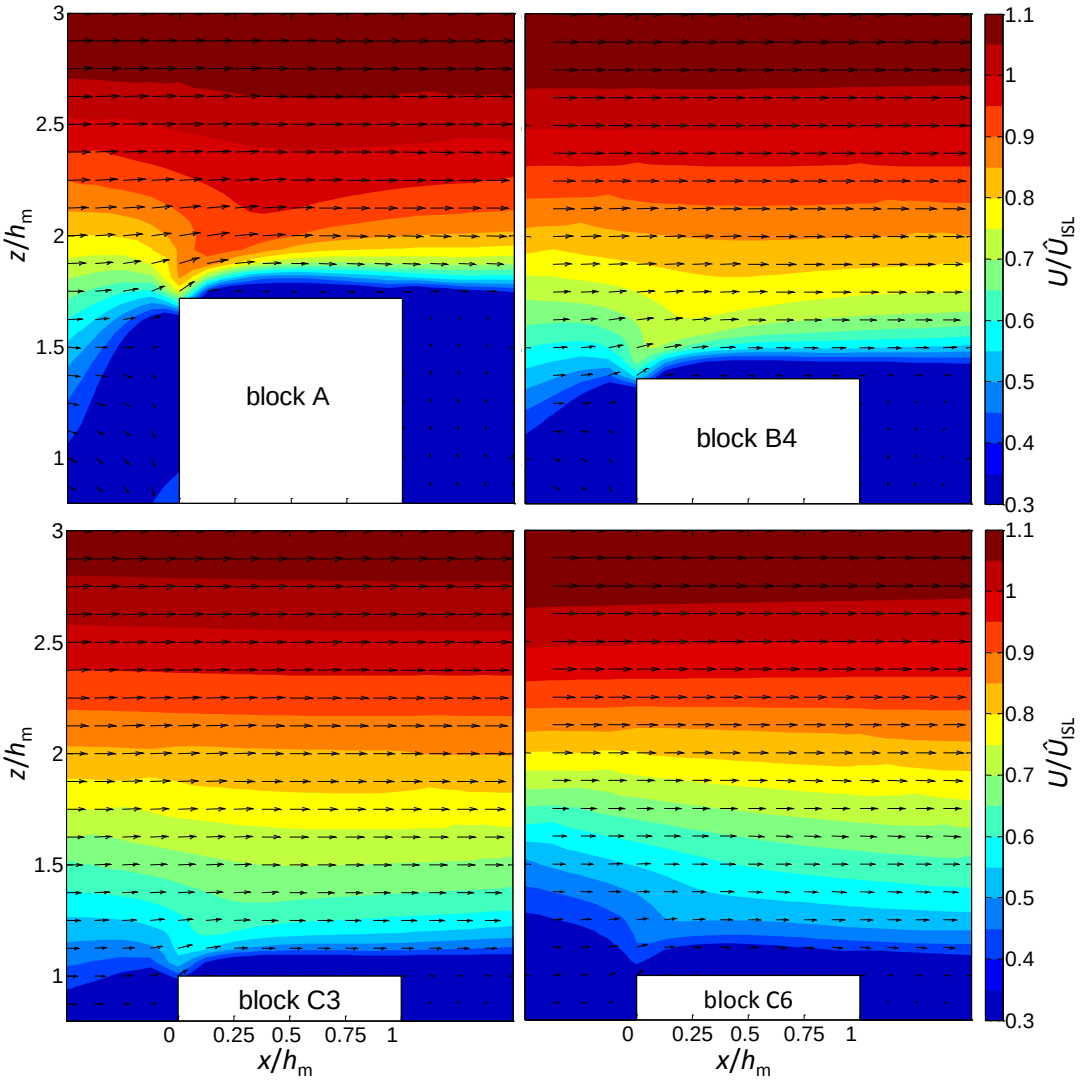

Figure 2-4: Contour plots of normalised mean wind speed above blocks of various heights. The vectors give a qualitative representation of vertical wind angles, and are shown at half resolution for clarity.

consideration of only a single wind direction, and ideal turbine placement will also be highly dependent upon the direction of the incoming wind.

As expected from Figure 2-4, the flow patterns above each of the blocks shown in Figure 2-5 are very similar. Above each block, the roof-top separation results in a region of low wind speeds that grows in thickness with increasing horizontal distance from the leading edge, and this is most significant above the highest block. Additionally, directly above the leading edge of all three blocks there lies a region of slightly reduced mean velocities, which is found between heights of about 0.2-0.5h_m. Again, this region is more prominent above the highest block.

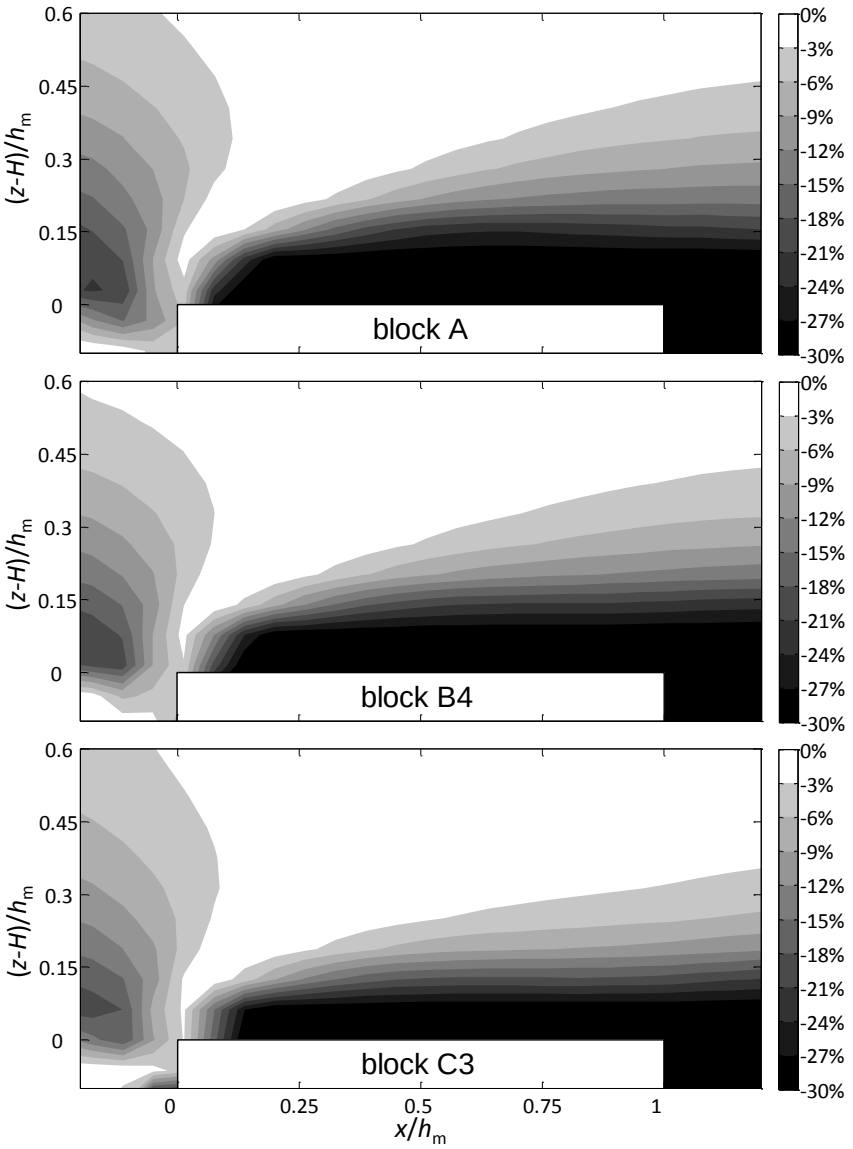

Figure 2-5: Contour plots showing the percentage deviation of the local mean wind speed from the maximum mean wind speed found above the block at the same height (U_{max}). Vertical profiles of U_{max} are shown in Figure 2-6 (b).

In Figure 2-6 (a), a single contour from Figure 2-5 representing a 3% deviation from U_{max} for block A, is overlaid onto a contour plot of turbulence intensities (U_{rms}/U), to consider both mean flow and turbulence together. As expected, it can be seen that turbulence intensity follows the opposite pattern to the mean velocities, and from $0.2h_m$ above the block levels of about 0.3-0.35 are found within the region of accelerated flow. Although not shown, turbulence intensities above the blocks in groups B and C_{un} reach magnitudes of approximately 0.35-0.45, and 0.4-0.5 respectively. Simple turbulence statistics such as this however, are not particularly informative as they give very little indication of the turbulence structure, and turbulence can result in an either an increase or a decrease in power output

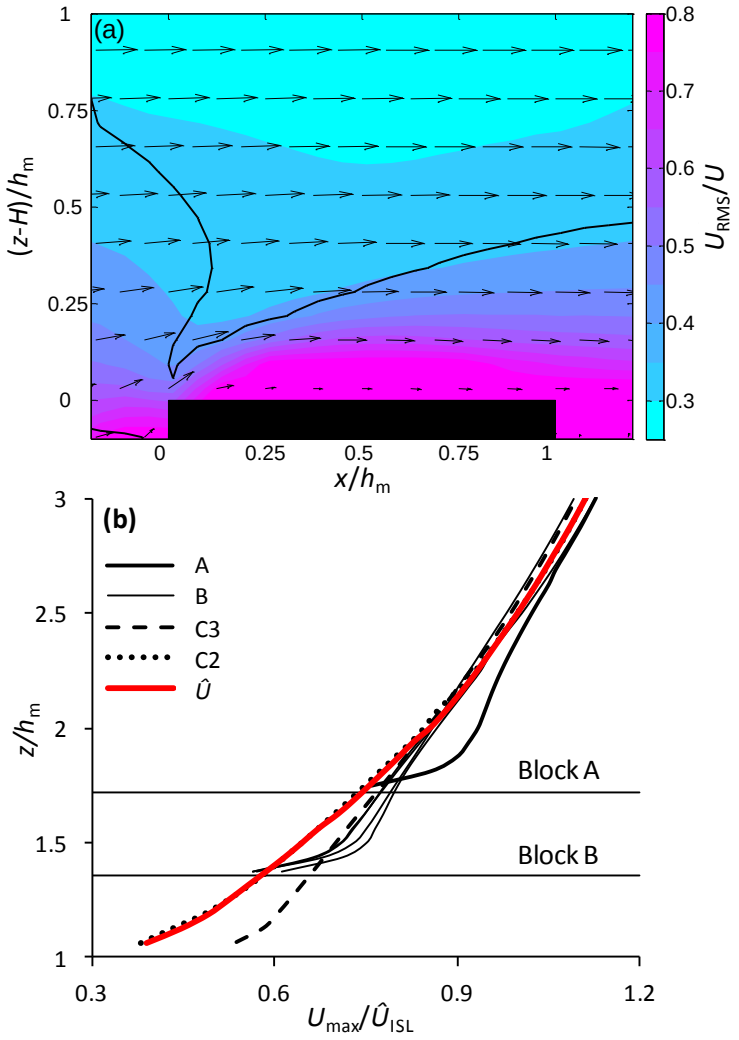

Figure 2-6: (a) Contour plot of turbulence intensity above block A normalised by the local mean wind speed. A single contour from Figure 2-5 (top) (—) is overlaid to indicate the region of highest speeds (those within 3% of U_{max}). (b) Profiles of the maximum mean wind speed found at each height in the region above various blocks. The horizontal lines indicate the heights of the blocks, and $\hat{U}$ is the spatially-averaged profile.

(Rosen and Sheinman, 1994). However, it is beyond the scope of the present Chapter to pursue these structures further.

Figure 2-6 (b) shows the profiles of the maximum mean wind speed found at each height above various blocks (U_{max}). Therefore for each block in Figure 2-5, the velocities within the white filled contours can be considered to follow the corresponding profile in Figure 2-6 (b) to within 3%. From this figure the significance of the accelerated flow over block A can again be seen: at about $2h_m$ ($\approx 0.3h_m$ above block A) while the profiles above the other blocks have collapsed onto $\hat{U}$, the maximum mean velocities found above block A exceed these by over 10%. Another useful observation is that the accelerated flow at the leading edge is not significant enough to prevent the mean velocities from being monotonically increasing with height. In other words, there is always an increase in wind resource with height, provided a turbine is appropriately placed in the regions suggested by Figure 2-5.

2.4.2.2 Implications for turbine siting

When the roof-top flow characteristics mentioned in the previous subsection are considered collectively, the implication is that the ideal location for a turbine to be placed in order to receive the most favourable wind resource will depend upon the height at which it is to be mounted. In general, to access a significant wind resource above any reasonably tall unsheltered building, and to avoid the effects of roof-top separation, it appears that a turbine with a low mounting height (0.1-0.15H, where H is the *individual* building's height) must be placed no more than about 0.1H from the leading edge with respect to the prevailing wind direction. However, due to the separated roof-top flow, this low height can result in a vastly decreased resource available to the turbine when the wind is approaching from other directions. The higher the turbine is elevated, the further from the leading edge it can be mounted without receiving a reduced wind resource, hence increasing the available resource from non-prevailing wind directions.

Although oblique wind directions have not been considered here, the results of Mertens (2003) indicate that the same general guidelines will apply; i.e. a turbine with a low mounting height should be mounted towards the front of the building (with respect to the prevailing wind direction), while it can be mounted further from the edge as its mounting height increases.

Ideally therefore, these results suggest that planning permission should allow roof-top turbines to be mounted at least high enough for their full swept area to extend no closer to the roof-top than about 0.2-0.25 times the individual building's height. Clearly however this recommended height becomes excessive for buildings much taller than about 20m, so for buildings above this height it seems reasonable to suggest that a minimum distance between the turbines swept area and the roof of about 5m should be permitted. As well as the advantage of the significant increase in wind speed that is found with a moderate increase in turbine height (and the even greater increase in available wind power), these suggested elevations will give a turbine the advantage of having the best chance of receiving the most abundant wind resource available from all directions.

2.4.3 The predictability of the roof-top wind resource in the roughness sublayer

2.4.3.1 Using spatial-averages to estimate above-roof wind resource

In this section attention is now returned to the predictability of the above roof wind resource in the RSL. As well as the surface of random blocks that has been the focus up until now (RM10s), mean wind profiles above both inline and staggered arrays of cubes are also considered (C20a and C20s respectively, shown in Figure 2-1). These cube arrays are of the same moderate density (λ_p = 0.25) as the heterogeneous surface RM10s that was previously considered. The uniformity of C20a and C20s makes them comparable mainly to suburban areas for example, while the heterogeneity of RM10s results in a more disrupted flow, representative of that found in more complex urban geometries (the height variability is comparable to the city of London for example; Ratti et al., 2002). To consider the influence of packing densities from 7.7 to 39.1%, wind profiles above staggered arrays of cubes (as in Figure 2-1 (b)) made available from the wind tunnel experiments of Hagishima et al. (2009) are also used.

The contour plots in Figure 2-7 (a-c) show the percentage deviation of above-roof mean wind speeds from the spatially-averaged profile ($\hat{U}$), for the three unsheltered blocks from Figure 2-5. It is apparent here that the magnitudes of these deviations depend strongly upon the height of the block, and are largest close to the leading edge. For example, above the leading edge of block C3, mean wind speeds are as much as 20% higher than that given by $\hat{U}$ at the same height. Above the higher blocks (A and B4) these deviations are slightly

smaller, reaching a maximum of 6 - 10%. It is important to bear in mind the potentially significant increases in available wind power that these wind speed deviations imply.

In real urban arrays, the extent by which above-roof mean wind speeds may deviate from the spatially-averaged profile will be highly dependent upon a number of factors, including the building's height, its angle with respect to the approaching wind, and the local surface

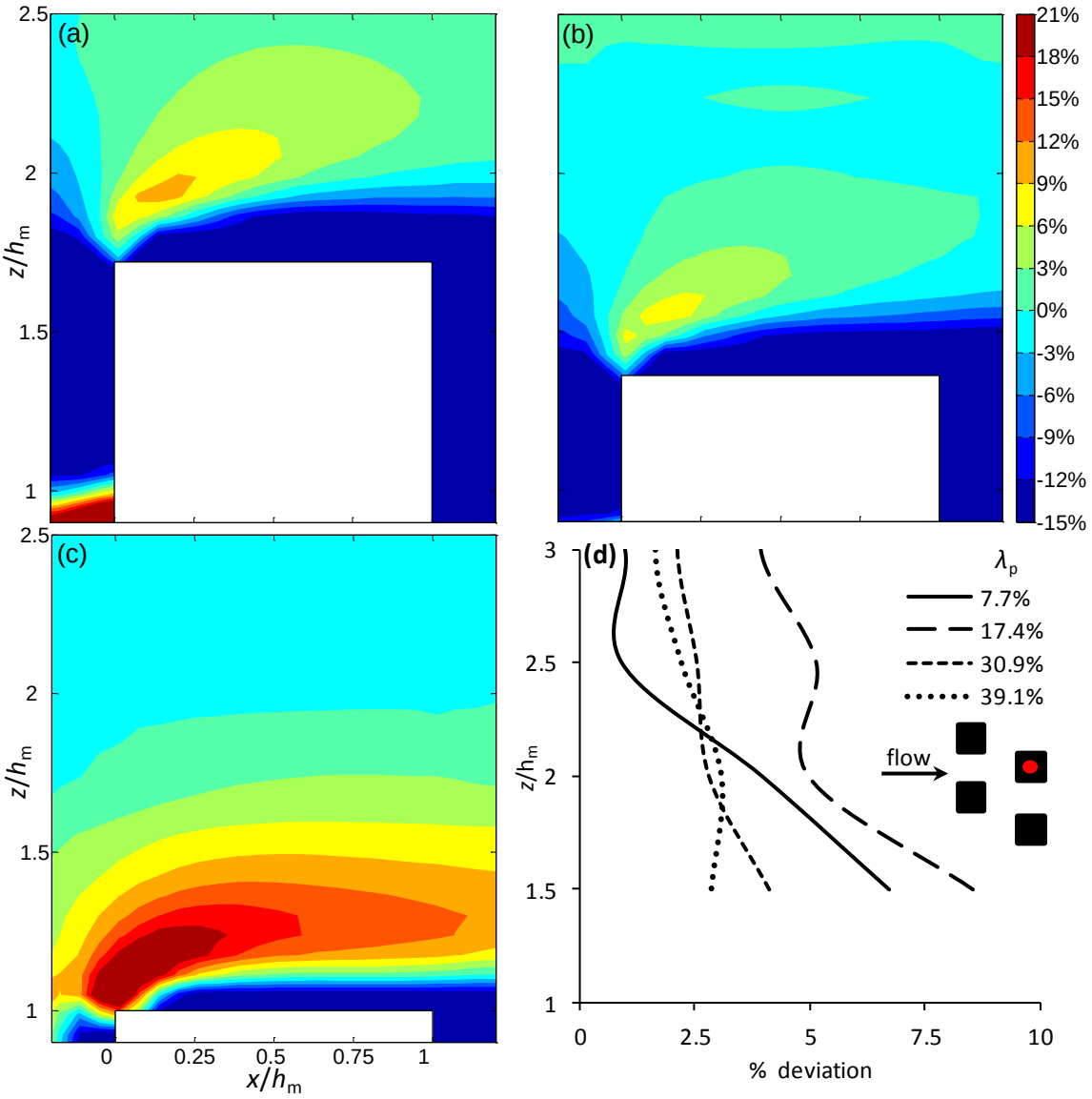

Figure 2-7: Contour plots showing the percentage deviation of the local mean wind speed from the spatially-averaged speed at the same height, for the RM10S array above (a) block A, (b) block B4, and (c) block C3. In (d), profiles are shown of the percentage deviation of the mean wind speed profiles directly above the cube centres (the white point on the figure inset) from the associated spatially-averaged profiles, for staggered uniform cube arrays of different packing densities. Wind tunnel data in (d) is from the experiments of Hagishima et al. (2009).

geometry. Furthermore, many buildings do not often have the simple sharp edged roofs as are represented by the blocks in this study, hence roof-top flow patterns may be far more complex. Consequently, without site specific computational modelling or on site measurements, these deviations would be difficult to assess accurately. By considering data from studies using different surface geometries however, it is possible to draw some qualitative conclusions.

In order to explore this point, the data of Hagishima et al. (2009) over staggered arrays of uniform cubes of various packing densities has been employed. In Figure 2-7 (d) the percentage deviation of the mean wind profile directly above the centre of a cube in each array, over the associated spatial-average is shown. It can be seen that up to a height of around $2h_m$, the wind resource above the centres of the cubes exceeds the spatial-average by a significantly larger amount for the lower packing densities of 7.7% and 17.4%, than for the higher packing densities of 30.9% and 39.1%. The reason for this is that for the lower packing densities, the flow is in the isolated, or wake interference regimes (Oke, 1988), and the flow over the buildings more closely resembles that over isolated buildings, hence it is slightly accelerated. For the higher packing densities, the flow is close to, or fully in the skimming flow regime, and consequently in both cases there is less spatial variability in the RSL flow as it skims over the tops of the blocks. This is most evident in the latter case of 39.1% packing density, where the unmodified spatial-average now offers a good estimate of the wind resource.

Overall these results suggest that a practical and reasonably accurate way to estimate wind resource over a neighbourhood region is to use a spatially-averaged wind profile, keeping in mind the influence that roof-top flow patterns may have. These can be summarised as follows:

- In urban areas, where building heights are heterogeneous, above any buildings that are unsheltered and greater than the local mean building height, the mean wind speeds may exceed those given by the spatially-averaged profile by up to about 20% (with favourable wind directions).
- In suburban areas of relatively low building density (λ_p < 20%), where building heights are similar, above-roof mean wind speeds may also exceed those given by the spatially-averaged profile.

- Conversely, in suburban areas of higher building density (λ_p > 20%) where a skimming flow regime is occurring, the horizontal variation in the RSL flow may be small, and hence above-roof mean wind speeds may be estimated well using the spatially-averaged profile.
- In all cases, if a turbine is placed too close to the roof and is affected by separated roof-top flow, then the available wind resource may be poor, and far lower than may be predicted using a spatially-averaged estimate.

A final point to make is in regards to the specific correction factors suggested by some previous authors to quantify the effects of roof-top flow patterns (e.g. Mertens, 2003; Heath et al., 2007; and Anderson et al., 2007). In practice, the suggested correction factors will be highly dependent upon many geometrical Influences, making it difficult to suggest values that are robust. In general, site specific computational modelling studies or onsite meteorological measurements are required to estimate roof-top flow patterns accurately.

For these reasons, the primary issue for wind atlas methodologies is now shifted onto how spatially-averaged wind profiles can be estimated given the available geometric information of a neighbourhood region.

2.4.3.2 Logarithmic profiles in the roughness and the inertial sublayers

A number of authors have suggested that it is appropriate to estimate the spatially-averaged wind profile throughout the RSL and ISL using a single logarithmic profile controlled by the aerodynamic parameters z_0 and d (as was discussed in Section 1.4). It was also described in Section 1.4 how the accuracy of the morphometric models that are typically used to estimate z_0 and d is often quite poor for real urban areas. However, there are two important questions that relate to using logarithmic profiles in the RSL above real urban areas, where building heights are heterogeneous, which have not yet been addressed:

(i) Can the spatially-averaged wind profile in the RSL above a building array of heterogeneous height still be assumed to be logarithmic, and if so, how far downwards can this profile be extrapolated?

(ii) How accurate are logarithmic profiles at describing near-roof wind profiles above heterogeneous arrays using z_0 and d values derived from currently available morphometric models?

These questions are important for wind resource prediction, and the answers have implications for how wind atlas methodologies may be applied in urban areas. In order to begin to answer them, the measured, spatially-averaged profiles above the RM10s and C20s arrays are considered.

These spatially-averaged profiles are shown in Figure 2-8 alongside the logarithmic profile predicted by the model of Raupach (1992; 1994; 1995), which is one of the more accurate morphometric models currently available (Grimmond and Oke, 1999). These aerodynamic parameters are recorded in Table 2-1. Note that the profile predicted by the Raupach model is the same for array RM10s and C20s, as both arrays have the same frontal and plan area densities. The flow above each however, is very different, and hence although Raupach's model gives a good approximation of the wind profile in both the RSL and ISL above array C20s, it significantly overestimates wind speeds in the RSL above the RM10s array. This is simply due to the fact that building height variation is not considered by the Raupach model, and for this reason the same conclusion applies to other available morphometric

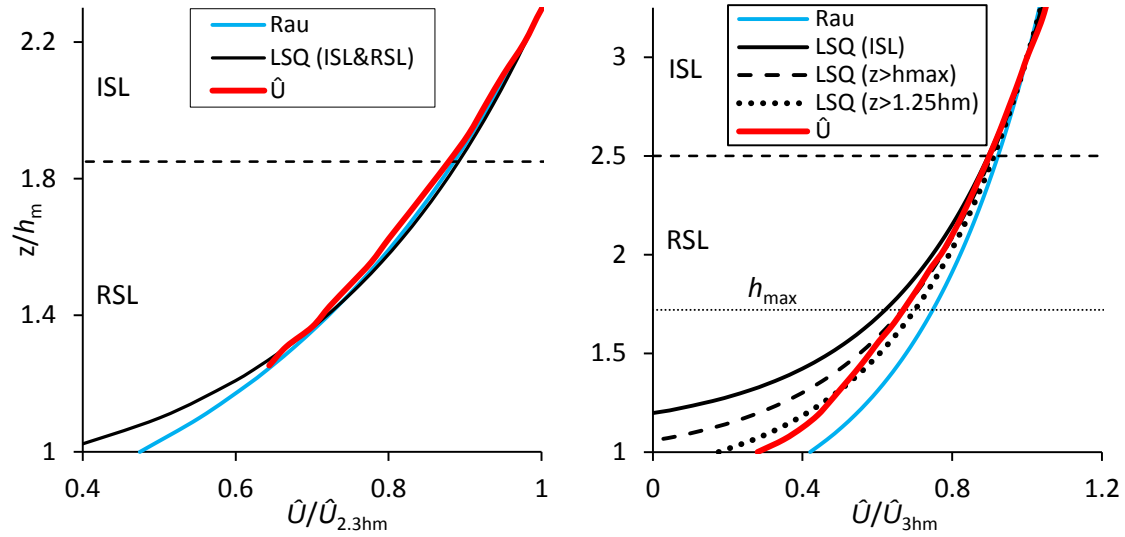

Figure 2-8: Measured wind profiles above the C20s array (left) and the RM10s array (right), of Cheng and Castro (2002b), normalised by the wind speed at the top of the ISL. The logarithmic profile predicted by Raupach (1992; 1994; 1995) is also shown. Statistically fit logarithmic profiles for different height intervals are also shown as LSQ(...), where the term in brackets refers to the height interval used for the fitting procedure.

models. Furthermore, it is important to mention that this factor could prove more significant in real cities, as the magnitude of height variation may be much greater than that of the RM10s array (Ratti et al., 2002).

Figure 2-8 also shows logarithmic profiles that are statistically best fit to each of the measured spatially-averaged profiles, within a specified height range. The fitting procedure involves using the friction velocity (u_*) obtained from the pressure drag of the surface, then performing a least squares fit of the logarithmic equation to $\hat{U}$ to give z_0 and d, as first discussed in Section 1.4.3.3 (Cheng et al., 2007). For the C20s array, the specified height range is the full depth of the roughness and inertial sublayers. For the RM10s array, three different height ranges are specified to obtain three different pairs of fitted aerodynamic parameters: throughout only the ISL, from h_{max} to the top of the ISL, and from $1.25h_m$ to the top of the ISL. Again, each pair of aerodynamic parameters is recorded in Table 2-1.

In Figure 2-8, the resulting logarithmic profile fitted to the measured profile above the C20s array can be seen to be very close to that estimated by the Raupach model. Above the RM10s array however, as expected, the fitted profiles are very different to that given by the Raupach model. When the fitting procedure is performed in just the ISL the resulting displacement height value is quite large ($1.1h_m$), and hence extrapolating this profile downwards into the RSL results in substantial underestimates of wind speeds. In contrast, the logarithmic profile which is best fit from $1.25h_m$ to the ISL top describes the profile above this array reasonably well. However, it can be seen that the measured profile is not perfectly logarithmic down to h_m, which can be attributed to the buildings taller than the average height.

Overall, these results offer some answers to the questions posed at the beginning of the section. They suggest that, above arrays of heterogeneous building heights, a logarithmic

Surface	Log profile	z_0/h_m	d/h_m
C20s	Rau	0.128	0.558
	LSQ (ISL&RSL)	0.052	0.822
RM10s	Rau	0.128	0.558
	LSQ (ISL)	0.099	1.1
	LSQ ($z>h_{max}$)	0.108	0.95
	LSQ ($z>1.25h_m$)	0.12	0.8

Table 2-1: The aerodynamic parameters used to determine the profiles plotted in Figure 2-8.

profile may be able to describe the wind profile in both the ISL and RSL reasonably well, although this approximation may begin to breakdown someway above the mean building height. Furthermore, currently available morphometric models do not appear to offer accurate descriptions of wind profiles above these types of arrays.

2.4.4 Relative uncertainties in predicting the urban wind resource

In this final section, a typical wind atlas methodology is followed for two illustrative case studies. These involve making wind speed predictions at a typical 'suburban' site and then a typical 'urban' site, using a wind atlas methodology that closely follows that of the Met Office (see Section 1.3). At each stage of the methodology, uncertainties in the input parameters (or data) are estimated, and by calculating the propagation of these uncertainties into the final wind speed predictions, their relative importance is assessed. The suburban and urban sites (and the built areas lying around them) are assumed to be of particular geometrical characteristics.

Firstly, the suburban site is assumed to lie a few km from the upwind edge of a city within a 'medium density' area of suburban properties, which have a mean height of 8 m. The fetch is assumed to consist of other low to medium density suburban areas with mean heights of 6 - 8m. This chosen range is reasonably consistent with those given in the tables of Grimmond and Oke (1999) for residential areas with buildings two to three stories in height, and close to the value of 6 m used by the Met Office for suburban areas (Best et al. 2008).

Secondly, the urban site is assumed to lie within a 'high rise area' in the city centre, where the mean building height is 15 m. For this site, the fetch is assumed to consist of a mixture of medium to high density inner city areas, with mean building heights in the range of 10 - 15 m. This range lies within that given by Grimmond and Oke (1999) for medium to high height and density residential areas and town centres. In addition, it is almost centred upon the value of 12 m used by the Met Office for urban areas (Best et al. 2008).

The first stage of the methodology involves scaling the regional wind climate wind speed (U_N) up to the top of the UBL (at height z_{UBL}). Here, the reference roughness length ($z_{0\text{-ref}}$) is set to a value of 0.03 m for both the suburban and urban predictions, but a thicker UBL is assumed for the urban prediction (400 m) than the suburban prediction (200 m). The uncertainties due to this up-scaling stage of the methodology depend partially upon the

regional wind climatology that is used. For the UK, the NOABL and NCIC databases are the main two available data sources, and the use of the more sophisticated NCIC database may minimise the errors at this stage. The Met Office note that, over urban areas, the NOABL database often contains wind speeds 10 – 30% higher than the NCIC database. There is also some uncertainty in the most appropriate value to use for $z_{0\text{-ref}}$ as a larger value of 0.14 m may also be appropriate, and this would increase the final wind speed estimates by just over 10%. Finally, although there is some uncertainty in the estimation of z_{UBL}, this typically has a negligible (less than 5%) effect on the final wind speed estimation (Best et al., 2008).

Methodology Stage	Equation used	Parameters (m)	Lower bound	Upper bound	Met Office	Maximum error associated with each stage
Suburban prediction						
1st up-scale ($U_N \rightarrow U_{UBL}$)	Equation 5	z_{0ref}	0.03	0.03	0.03	+ 30%
		z_{UBL}	200	200	200	
1st down-scale ($U_{UBL} \rightarrow U_{bl}$)	Equation 6	$z_{0\text{-fetch}}/h_{m\text{-fetch}}$	0.06	0.16	0.117	- 15% to + 10%
		$d_{fetch}/h_{m\text{-fetch}}$	0.35	0.7	0.525	
		$h_{m\text{-fetch}}$	6	8	6	
		z_{bl}	$2.5h_{local}$	$2.5h_{local}$	$2.5h_{local}$	
2nd down-scale ($U_{bl} \rightarrow U_{hub}$)	Equation 7	$z_{0\text{-local}}/h_{m\text{-local}}$	0.08	0.16	0.117	- 6% to + 2% & - 21% to + 5% @ $U_{hub} = 1.75h_m$ & $1.25h_m$
		$d_{local}/h_{m\text{-local}}$	0.55	0.7	0.525	
		$h_{m\text{-local}}$	8	8	8	
Roof-top flow variation	N/A	Site specfic considerations made				≈ + 20%
Urban prediction						
1st up-scale ($U_N \rightarrow U_{UBL}$)	Equation 5	z_{0ref}	0.03	0.03	0.03	+ 30%
		z_{UBL}	400	400	400	
1st down-scale ($U_{UBL} \rightarrow U_{bl}$)	Equation 6	$z_{0\text{-fetch}}/h_m$	0.07	0.16	0.133	- 14% to + 12%
		d_{fetch}/h_m	0.6	0.7	0.585	
		$h_{m\text{-fetch}}$	10	15	12	
		z_{bl}	$2.5h_{local}$	$2.5h_{local}$	$2.5h_{local}$	
2nd down-scale ($U_{bl} \rightarrow U_{hub}$)	Equation 7	$z_{0\text{-local}}/h_m$	0.1	0.2	0.133	- 7% to + 4% & - 24% to + 11% @ $U_{hub} = 1.75h_m$ & $1.25h_m$
		d_{local}/h_m	0.5	0.7	0.585	
		$h_{m\text{-local}}$	15	15	15	
Roof-top flow variation	N/A	Site specfic considerations made				≈ + 20%

Grimmond and Oke (1999): Low density | Medium density | High density | High rise

Table 2-2: The equations and aerodynamic parameters used in up/down-scaling stages from the methodology illustrated in Figure 1-4, for both the typical 'suburban' and 'urban' areas considered. 'LB' and 'UB' refer to aerodynamic parameters used for the lower and upper bounds, respectively, and 'CT' refers to those used by the Met Office (Best et al., 2008).

For the down-scaling stages of the methodology, upper and lower bounds on the input aerodynamic parameters are estimated, which indicate the maximum potential uncertainty on their values. These estimates are based upon the suggestions of Grimmond and Oke (1999) for different types of built-up area. Values chosen for other parameters (h_m, z_{UBL} and $z_{0\text{-ref}}$) are based upon values used in the sensitivity test in the Met Office report (Best et al., 2008), with the exception of z_{bl}, for which a value of 2.5 times the local mean building height is used (i.e. the value measured for the RM10s array). All these values are recorded in Table 2-2, along with central estimates of aerodynamic parameters that were used by the Met Office in the final implementation of their methodology.

Using the three sets of aerodynamic parameters in Table 2-2, the Met Office methodology is followed to obtain central, upper and lower wind speed estimates (normalised by U_N) at the suburban and urban example sites. These different estimates indicate the potential range of above-roof mean wind speed predictions due to uncertainties in surface aerodynamic parameters in urban areas. Figure 2-9 shows these potential errors and their increasing magnitude with decreasing above-ground height. They can be compared with errors

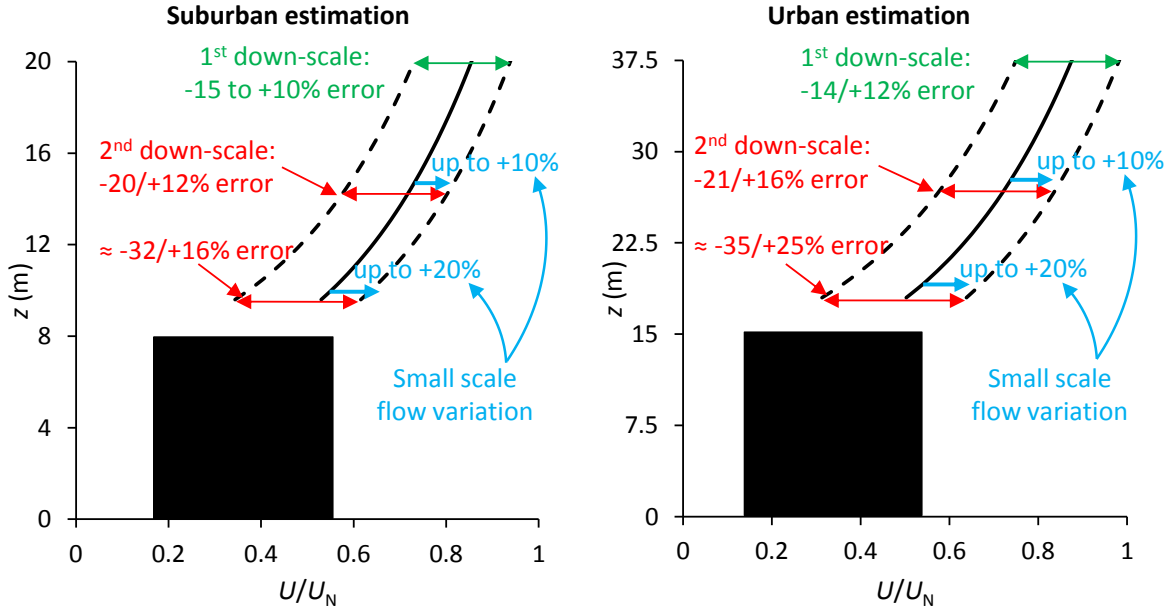

Figure 2-9: Estimations of mean wind speed profiles above the 'suburban' and 'urban' areas described in Section 2.4.4. The logarithmic profiles shown use the Met Office parameter estimates (solid black lines) and also the upper and lower bounds (dashed lines) recorded in Table 2-2. Uncertainties arising from the various scaling stages are also shown: percentages on the left arise due to errors in estimating the spatially-averaged profiles, and those on the right additional variability due to spatial location as described in Section 2.4.3.1.

occurring due to other uncertainties in the methodology, which are summarised in Table 2-2.

Accordingly, from Figure 2-9 and Table 2-2, it can be seen that these calculations suggest that the errors in current wind atlas methodologies when applied to urban areas are primarily due to uncertainties in estimating surface aerodynamic parameters. The associated errors may be as high as -35 to +25% in urban areas, and slightly less in suburban areas (-32 to +16%). Potentially, the input regional wind climatology may be an equally significant source of error (possibly contributing up to + 30%; Best et al. 2008), but this is difficult to assess fully without a large-scale comparison of different datasets, which is beyond the scope of this Thesis. In any case, the smaller-scale features that were explored in the Section 2.4.3 (i.e. the spatial variation in RSL flow and roof-top flow patterns) appear to be less important sources of error when making wind speed predictions at unsheltered locations (provided also that a turbine is not placed in separated roof-top flow). However, if these building-scale features are ignored significant underestimations of above-roof wind resource could potentially still be made.

In summary, these calculations suggest that for the accuracy of these types of wind atlas methodologies to improve, it may be of greater importance to improve methods of estimating spatially-averaged wind profiles above urban surfaces (i.e. estimates of z_0 and d), than to quantify smaller-scale flow variations within the RSL. This is provided however, that a turbine is mounted high enough above the roof so that it is clear of any separated flow, as this may substantially disrupt the wind resource.

Finally, to put Figure 2-9 into perspective, it is useful to note that the NOABL database typically gives wind speeds of about 5 ms^{-1} for U_N. This means that in the suburban and urban scenarios considered here the upper bounds of the estimated wind resource reach 5 ms^{-1} at above-ground heights of about 20 and 35 m, respectively.

2.5 Summary

In this Chapter, the spatial variation of the above-roof mean wind speeds in the roughness sublayer over a number of idealised urban arrays has been investigated. Particular attention was paid to the RSL flow above an array of heterogeneous height, which represents a

relatively complex urban area. The results were used to suggest guidelines for roof-top turbine siting in complex urban arrays. In order to investigate the RSL flow above typical residential areas, more simple arrays of cubes were then studied. Considering the spatial variation in the RSL flow, the potential uncertainty due to using spatially-averaged wind profiles to describe mean wind speeds in the RSL was then considered. These uncertainties were then compared to those occurring at the various other stages of a typical wind atlas methodology, and hence the relative contributions of the different uncertainties in determining the error in the final wind speed predictions were assessed.

Within the array of heterogeneous heights, the results show the existence of regions of accelerated flow above the roofs of the buildings which are greater or equal to the mean height, and unsheltered by taller buildings upwind. Below these accelerated regions of flow lie regions of flow separation within which wind speeds are low, and the flow highly turbulent. These flow patterns are more pronounced for the taller, more exposed blocks, where they resemble those observed over an isolated building. Consequently, the suggested siting guidelines are similar: in general, turbines should be mounted towards the leading edge of the roof with respect to the prevailing wind direction and above any separated flow. However, the 'leading edge' must not be overvalued as a mounting point, as the available resource from non-prevailing wind directions must also be considered.

For estimating the wind resource at the more suitable turbine locations (i.e. those greater or equal to the mean height, and unsheltered by taller buildings upwind), the spatially-averaged wind profile was found to be a suitable lower bound. The available mean wind speeds above these more viable rooftop turbine locations, were found to exceed this spatially-averaged profile by up to 20% (provided a turbine is clear of any separated roof-top flow). The magnitude of these deviations depended upon a multitude of factors, including the height of the installation building, the elevation of the turbine above this building, and the heights and density of the surrounding buildings. Thus, although some general guidelines were suggested for estimating the magnitude of these deviations based upon site-specific considerations, it is likely that computational modelling or onsite meteorological measurements would be required to quantify them precisely.

Potential methods of estimating spatially-averaged wind profiles above realistic urban surfaces were then discussed, and the accuracy of those available was assessed. The results

suggest that, above arrays of heterogeneous building heights, a logarithmic profile may be able to describe the wind profile in both the ISL and RSL reasonably well, although this approximation may begin to breakdown someway above the mean building height. However, currently available morphometric models (which relate z_0 and d to surface geometry) do not appear to offer accurate descriptions of wind profiles above these types of arrays.

Finally, a typical wind atlas methodology was followed for illustrative case studies in typical suburban and urban areas. The uncertainties present at each stage of the methodology were estimated, and by calculating the propagation of these uncertainties into the final wind speed predictions, their relative importance was assessed. The calculations suggested that the errors in current wind atlas methodologies when applied to urban areas are primarily due to uncertainties in estimating surface aerodynamic parameters (the input regional wind climatology may potentially be an equally significant source of error, but this is difficult to assess fully). Smaller-scale flow variations within the RSL appear to be less important sources of error, although if they are ignored significant underestimations of above-roof wind resource could potentially still be made. The calculations imply therefore, that it may be of greater importance to improve methods of estimating spatially-averaged wind profiles above urban surfaces (i.e. estimates of z_0 and d), than to quantify smaller-scale flow variations within the RSL. Thus this is the focus of the next Chapter of the Thesis.

3 Estimating Aerodynamic Parameters of Urban Like Surfaces with Heterogeneous Building Heights

3.1 Introduction and Objectives

In this Chapter a simplified morphometric model is developed to estimate z_0 and d based upon a number of geometric parameters. These include building height variability, which as yet has been omitted from previous models. The importance of this parameter in determining z_0 and d was highlighted in Chapter 1 (Sections 1.4.3.2 to 1.4.3.4). Values of z_0 and d output by the model can be used for estimating above-roof mean wind profiles, or alternatively they may be input into more complex models such as that of Di Sabatino et al. (2008).

In developing this model, the intention is that more accurate estimates of aerodynamic parameters can then be fed into wind atlas methodologies, thus improving the accuracy of mean wind speed predictions in urban areas. In addition, there are many other applications of such a model that are not investigated in this Thesis, for example in dispersion modelling, wind loading calculations, and numerical weather prediction.

The structure of the Chapter is as follows. In Section 3.2, a brief description of the modelling approach is given. In Section 3.3, a model for uniform building arrays is derived and validated that is strongly influenced by those of MacDonald et al. (1998), Bottema (1996, 1997) and Raupach (1992, 1994, 1995) (referred to throughout this Chapter as, Macdonald, Bottema and Raupach, respectively). In Section 3.4, this model is extended to arrays of heterogeneous heights and is validated against available wind tunnel and numerical data. Finally, in Section 3.5, the main conclusions of the Chapter are summarised.

3.2 Modelling Approach

The morphometric model that is developed achieves estimates of aerodynamic parameters via a quasi-empirical modelling approach, centred upon simplified drag balances on the urban surfaces and physical flow properties that have previously been observed in

experiments. Specifically, by considering the balance between the drag force of a surface (F_D) and the shear stress in the ISL, the dependence of roughness length upon surface geometry is estimated. Subsequently, to complete the model, zero-plane displacement is estimated by considering the vertical profile of the surface drag force. This is first done for uniform arrays (Section 3.3.3), and then similar ideas are extended to arrays of heterogeneous building heights (Section 3.4.2). The resulting relationship between aerodynamic parameters and building density can be understood by referring to the three flow regimes discussed in Section 1.4.3.1 (and illustrated in Figure 1-7).

3.3 Modelling Arrays of Uniform Height

3.3.1 The drag balance

By considering idealised, uniform arrays of square based blocks (now referred to simply as 'uniform arrays') and using drag balance principles, it is possible to capture the effects illustrated in Figure 1-7. This is achieved by following the method of Bottema and Macdonald. The symmetry of these types of arrays dictates that only one building need be considered, hence F_D is taken to be the drag on a single building. The balance (illustrated in Figure 3-1 (a)), simply reads:

$$\rho u_*^2 = F_D/A_T,$$

Equation 3-1

where A_T is the ground area associated with the building (as was illustrated in Figure 1-8).

Bottema and Macdonald make two assumptions, firstly that the drag is dominated by the pressure drag of the buildings, and secondly that the logarithmic profile of the ISL can be extended down to the mean building height. Therefore, any corrections to the RSL profile are assumed to be small enough to neglect. The former assumption was shown by Raupach (1992) to be true for surfaces denser than about λ_p = 0.05 to 0.1. Under these assumptions F_D can be written as follows:

$$F_D = 0.5\rho\, \hat{U}_{hm}^2\, C_D\, A_f^*$$

Equation 3-2

where $\hat{U}_{hm}$ is obtained from the standard logarithmic profile evaluated at h_m, C_D is the depth integrated drag coefficient, and A_f^* is the *unsheltered* frontal area of the building (illustrated

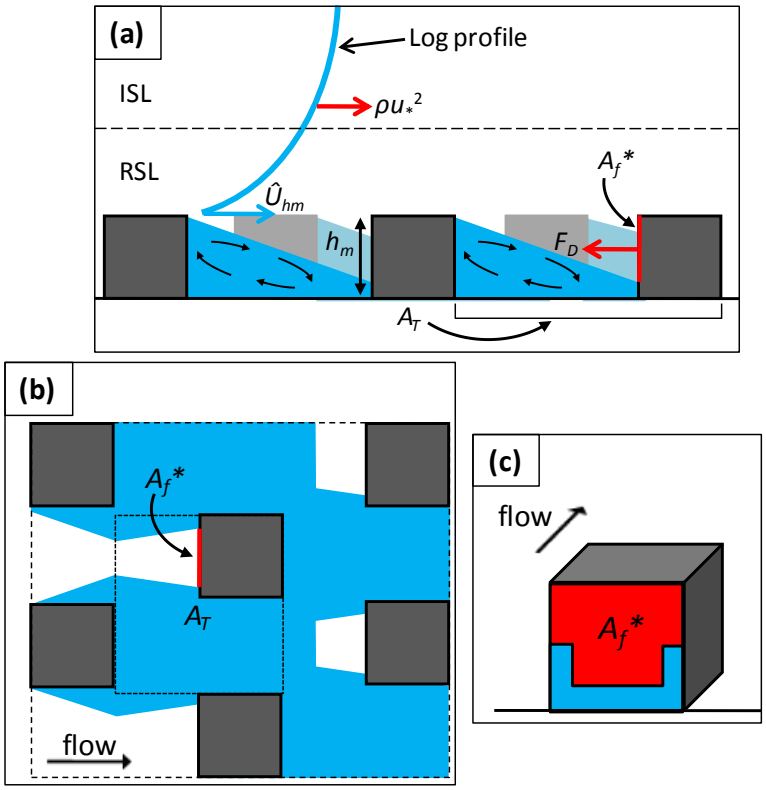

Figure 3-1: Illustration of the drag balance calculation for uniform arrays, and the mutual sheltering from the surrounding buildings. Blue areas indicate, approximately, the total sheltered region due to the combined sheltering of all the buildings, and red areas indicate the unsheltered frontal area of a single building in the array, A_f^*. (a) Side view; (b) top down view; (c) a single building from the array.

in Figure 3-1). The significance of A_f^* is that it is the area assumed to exert pressure drag on the flow. Clearly A_f^* decreases as the surface density increases. Therefore, this parameter is a useful, simplistic way in which to account for the mutual sheltering that occurs with increasing density, which avoids having to consider the complex flow patterns that occur within the obstacle arrays. At this point, the current approach and the methods of Bottema and Macdonald differ slightly, as they each employ different methods of estimating A_f^*. These differences are described in the following section.

By substituting Equation 3-2 and the standard logarithmic profile into Equation 3-1 and rearranging Equation 3-1, the following is obtained:

$$\frac{z_0}{h_m} = \left(1 - \frac{d}{h_m}\right) \exp\left[-\left(0.5 C_D \kappa^{-2} \frac{A_f^*}{A_T}\right)^{-0.5}\right].$$

Equation 3-3

Therefore, to estimate z_0 for a particular surface, and hence the curve of Figure 1-7, we must first estimate C_D, d and A_f^*/A_T.

Macdonald estimates C_D from the values given by the Engineering Services Data Unit (1980) for different building shapes, and the same approach is followed here. Strictly, these drag coefficients are defined by the height averaged mean square velocity. However, Macdonald discusses in his work the reasons for using these coefficients as nominal values with a reference velocity at roof level for this type of modelling application. He also makes the assumption that C_D is independent of the surface density (i.e. the shape of A_f^*). Under these assumptions he obtains satisfactory results, and hence we use these same assumptions here. For cubes a value for C_D of 1.2 is used. The methods employed in the current Chapter and by Macdonald and Bottema for estimating A_f^*/A_T and displacement height are discussed in Section 3.3.2 and 3.3.3, respectively.

3.3.2 Idealised descriptions of individual building wakes

In order to estimate A_f^*/A_T, Macdonald assumes that the drag below a height d is negligible. Thus, the shapes of the building wakes are not estimated in Macdonald's approach, and instead the following equation is obtained: $A_f^*/A_T = \lambda_f (1 - d/h_m)$. Alternatively, in order to estimate A_f^* more accurately, Bottema calculates the mutual sheltering due to all the buildings in an array by considering the specific shapes of building wakes. In this Chapter the approach of Bottema is taken, but a different parameterisation of wake shapes is employed. Therefore, in this subsection the current method of approximating the 'effective sheltered volume' of an isolated surface element due to its wake is described.

The effective sheltered volume is intended to enclose the separated regions of flow behind, and on the sides of the building. In reality flow patterns around isolated buildings are highly complex, and become even more so when a building is placed within an array. The volume we use here attempts to greatly simplify these effects. Once the shape and size of this volume has been estimated, it is assumed that a large number of surface elements and their effective sheltered volumes are distributed over a surface, as in the work of Bottema and Raupach. For uniform arrays it is then simple to estimate the sheltering of a single surface element in the array, and hence obtain an estimate of A_f^* (see Figure 3-1).

The surface elements considered in this work are square based, sharp edged blocks, lying normal to the flow, which are generally used in wind tunnel simulations of idealised urban areas. Many authors have described in detail the flow pattern that occurs around such an object (Castro and Robins, 1977, Hunt et al., 1978). In Figure 3-2 the idealised sheltered volume used in this Chapter to describe the sheltering due to this flow pattern is sketched. It can be seen that two parameters govern its shape, namely the rear reattachment length (L_R) and the spanwise extent of sheltering (L_W). Clearly, the most important of these parameters is L_R, and fortunately established formulae exist to describe this length in terms of the building height, width, and depth (H, b and l, respectively). Fackrell (1984) proposed the following empirical expression for L_R, after measuring the parameter for a large variety of different building shapes with b/H ranging from 0.5 to 0.5 and l/H ranging from 0.3 to 3:

$$\frac{L_R}{h} = \frac{1.8(b/H)}{(l/H)^{0.3}(1+0.24(b/H))}$$

Equation 3-4

where $l = b$ for the square based blocks considered here. This curve is plotted in Figure 3-3 (a). Although increasing turbulence and shear in the incoming flow are known to decrease the magnitude of L_R (Castro and Robins, 1977, Fackrell, 1984, Zhang et al., 1993), Equation 3-4 was found by Fackrell (1984) to be accurate to within less than ± 10% in simulated rural to urban-like boundary layers. Therefore, here it is assumed that L_R/H is dependent only upon the building dimensions.

The assumption of square based blocks has been made here since available data for arrays of variable height was for this type of geometry. This assumption would not hold if the

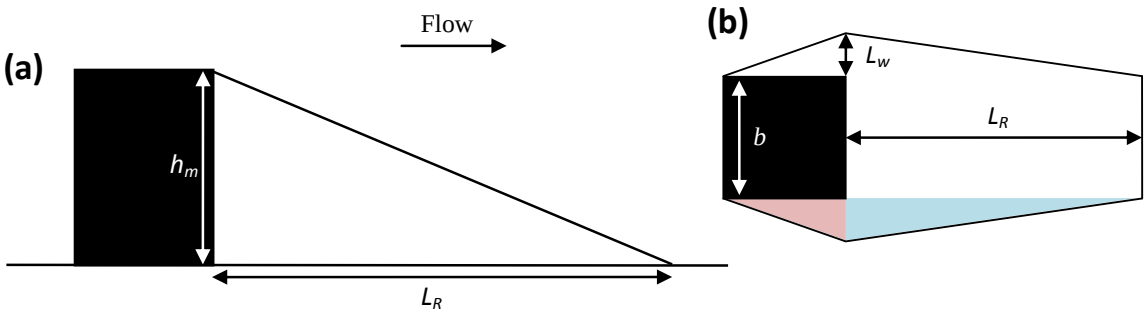

Figure 3-2: The shapes and dimensions of the idealised 'effective sheltered volumes' around isolated roughness elements that are used in this work, sketched from (a) above and (b) the side. (The blue and red shaded areas are described in the text).

model was applied to real urban areas, as typically these may have rows of elongated buildings forming street canyons. Equation 3-4 could be used to incorporate more complex building shapes since it was found to be valid for a wide variety of building dimensions (Fackrell 1984). However, the complex flow patterns found within urban street canyons such as helical flows (Dobre et al., 2005) cannot be explicitly captured with a simple modelling approach such as that used here. It may be interesting to assess the impact of street canyon type flows in future work, and as new data sets become available. However, our main focus here is to quantify the influence of height heterogeneity on aerodynamic parameters.

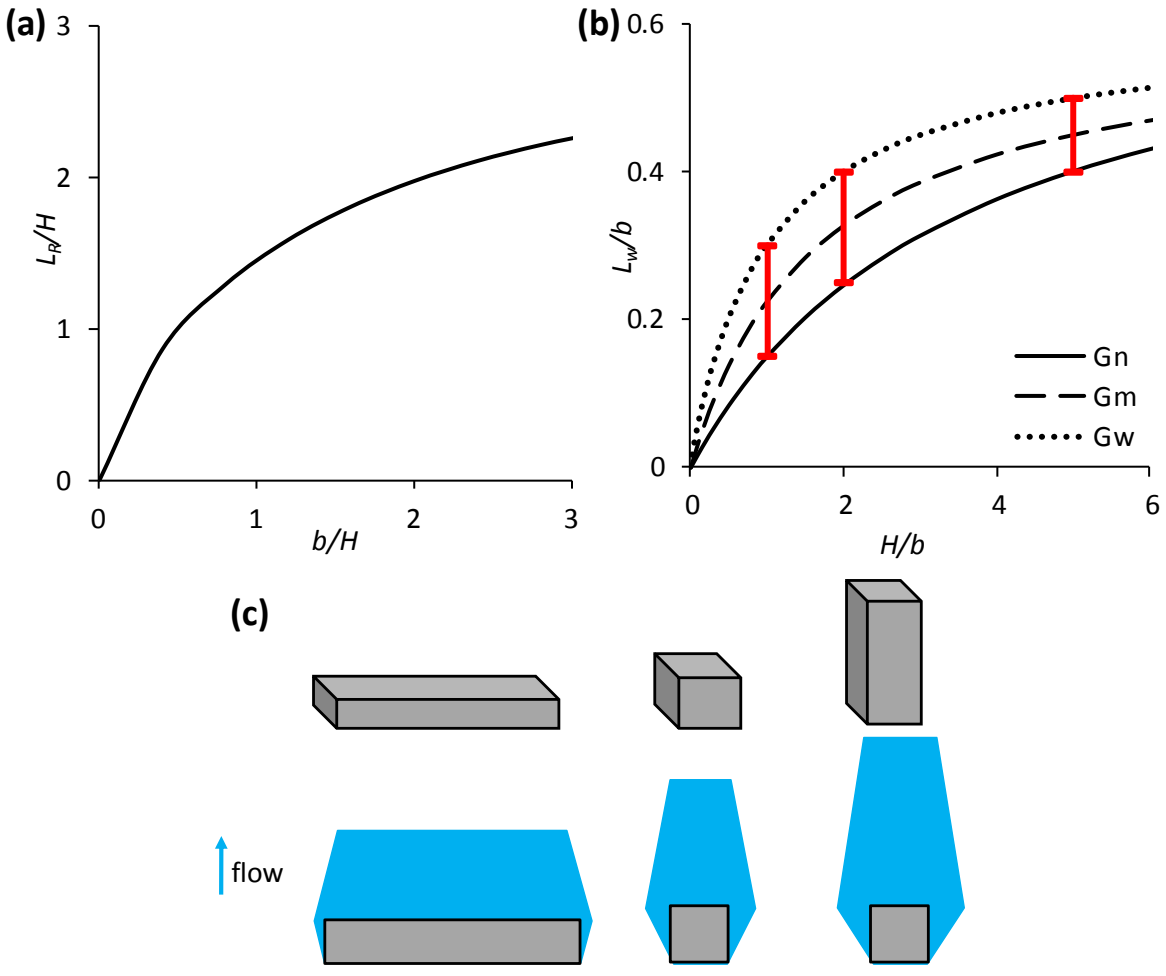

Figure 3-3: (a) The relationship between L_R/H and b/H for square based buildings given by Equation 3-4. (b) The relationship between L_W/b and H/b given by Equation 3-5. G_n, G_m, and G_w refer to the narrow, medium, and wide curves, respectively, that are used in the model of the current work (each given by Equation 3-5, with differing constants). The red bars are values estimated from experimental data. (c) Sketch of the sheltered volumes (in blue) behind buildings of three different shapes.

The second parameter governing the shape of the idealised shelter volume is L_W, which describes the lateral extent of the sheltering. Like L_R, this parameter can be related to the building dimensions, however it does not have as clear a criterion as that of L_R, and no standard formula exists to calculate it. Therefore, published data is now used to produce an empirical expression to estimate the dependence of L_W upon the building dimensions.

Intuitively, we would expect L_W to behave as sketched in Figure 3-3 (c). For a very low, wide building, most of the flow that impinges upon the upwind face will be forced over the roof rather than around the sides of the building. Consequently, there will be little lateral displacement of flow relative to the building width, and $L_W/b \approx 0$. As the building becomes taller and narrower, more of the flow becomes displaced around the sides, increasing the magnitude of L_W/b, until it asymptotes to a maximum value and increases no further with increasing building height. Therefore, the relationship between L_W/b and H/b is qualitatively the same as that between L_R/H and b/H, and hence an empirical formula similar to Equation 3-4 is used to describe the dependence of L_W/b upon H/b:

$$\frac{L_W}{b} = \frac{G_1(H/b)}{1+G_2(H/b)}$$

Equation 3-5

where the constants, G_1 and G_2, are chosen to fit published experimental data, which is described in the following paragraph.

Visualisation of the flow pattern around a cube in experiments such as that of Rodi (1997) show significant velocity deficits laterally either side of the object to about 15-30% of its width. This suggests that values of $L_W/b \approx 0.15$ - 0.3 are appropriate for cubes. Similar estimates can be made for taller buildings from other results. These suggest that for buildings with H/b of 2 (Tominag et al., 2008) and 5 (Song and He, 1993, Huang et al., 2007), reasonable values for L_W/b are about 0.25 - 0.4 and 0.4 - 0.5, respectively. These estimates are shown in Figure 3-3 (b) along with curves fitted centrally, and through the upper and lower limits of these estimates. All three curves use Equation 3-5 with differing constants. They are referred to as G_n, G_m, and G_w, which describe narrow, medium, and wide sheltered volumes, respectively. In this paper the central curve of G_m is used, where $G_1 = 0.36$ and $G_2 = 0.6$, and the crude choice and construction of this curve is justified by the fact that the

model has little sensitivity to the magnitude of L_W/b, provided it is a reasonable value. This is demonstrated in Section 3.3.4 using the alternative curves, G_n and G_w.

A final characteristic of the wake that must be described is in regard to the height of the volume of the wake that extends laterally either side of the building, one side of which is shaded in Figure 3-2 (b). Where the wake is alongside the building (the area shaded red) its height is assumed to be equal to that of the building, and where the wake is behind the building (the area shaded blue) its height is assumed to decrease at the same rate as the rest of the wake. Thus the wake is always assumed to be of an equal height over its full lateral width. This simplified assumption can again be justified by observing the low sensitivity to L_W/b in Section 3.3.4.

Using this method of describing the effective shelter volume behind a surface element, an estimate of A_f^* for use in Equation 3-3 can be made. Specifically, this estimate is made by first assuming that a particular density of surface elements and their effective sheltered volumes are distributed over a surface as in Figure 3-1 (a-b), then calculating the sheltering of a single surface element in the array to obtain an estimate of A_f^*.

3.3.3 Estimating zero-plane displacement

3.3.3.1 Existing methods:

The zero-plane displacement is the final parameter required to estimate z_0 from Equation 3-3. To estimate this parameter, each of the models developed by Macdonald, Bottema and Raupach, use different methods:

(i) Bottema estimates d from the ratio V/S, where V is the total volume of buildings and their front and rear recirculation zones, and S is the ground area associated with the buildings. During the current research this method was attempted using the parametrisation of sheltered volumes shown in Figure 3-2 and the inclusion of front recirculation zones following the method of Bottema. For densities below around $\lambda_p \approx 0.25$ the resulting values of d were found to be significantly lower than those reported from a number of relatively recent wind tunnel experiments and numerical studies (which are discussed below in due course), and consequently predicted values for z_0 were significantly higher. Increasing the size of the buildings' sheltered volumes to the upper limit of what could be considered reasonable did not change the agreement between predicted and

experimental vales of z_0 and d significantly. Therefore, a different approach was investigated, which is described in due course.

(ii) Macdonald used an empirical expression for d which was fitted to the experimental data of Hall et al. (1996):

$$\frac{d}{h_m} = 1 + A^{-\lambda_p}\left(\lambda_p - 1\right) .$$

Equation 3-6

For staggered and square arrays, values for the empirical constant, A, of 3.59 and 4.43, respectively, were suggested. However, concerns have been raised regarding the accuracy of the experimental data, primarily due to the relatively short fetch that was used in the wind tunnel and the lack of accurate shear stress measurements (Cheng et al. 2007; note that these two factors were disucssed in Section 1.4.3.3). Consequently, when compared to more recent experimental data, obtained in fully developed boundary layers using direct shear stress measurements, the equation performs less well, as will be shown later in this Chapter.

(iii) Raupach estimates d from the drag profile centroid (d_C), motivated by the theoretical arguments of (Jackson, 1981). Physically, d_C is the mean height at which the total surface drag force acts. Thus, for a particular surface, if the total magnitude of wind induced forces can be calculated along with the total moment of these forces, then d_C can be obtained by dividing the latter value by the former value. The values obtained by Raupach from this method were suggested by Grimmond and Oke (1999) to be reasonable, although relatively low at higher surface densities.

Overall, these different approaches highlight the uncertainty surrounding the physical meaning and calculation of d. However, the theoretical arguments of Jackson (1981) offer an intuitive explanation for d, giving a physical basis to the parameter. Although his theory has not yet been tested over a wide variety of urban like arrays, in this work we continue under the assumption that the theory is valid. Therefore, we now attempt to determine d by estimating the height of the drag profile centroid.

3.3.3.2 Current method:

For uniform surfaces, d_C can be estimated from the following equation:

$$V_{Dc}h_m + \int_0^{h_m} z dF_D = d_C \left[V_{Dc} + V_{Dg} + \int_0^{h_m} dF_D \right]$$

Equation 3-7

where dF_D is the differential pressure drag force on a surface element at height z, and V_{Dc} and V_{Dg} are viscous drag terms due to the rooftop (i.e. crest) and ground friction, respectively. Physically, the terms on the left of Equation 3-7 represent the total moment of the forces on the surface, and those on the right represent the total magnitude of forces on the surface multiplied by d_c. A very similar equation is given in Leonardi and Castro (2010), the only difference being that here, the friction on the building sides is not included. This is because the experiments of Leonardi and Castro (2010) showed its contribution to be relatively insignificant.

The calculation of dF_D is similar to that of F_D, hence Equation 3-2 can be re-written in terms of the 'sectional drag coefficient' (C'_D), which is typically assumed constant with height in flow models (Macdonald 2000; Coceal and Belcher 2004):

$$dF_D = 0.5\rho\, \hat{U}(z)^2\, C'_D\, (A_f/h_m)\, dz.$$

Equation 3-8

To calculate dF_D an estimate of the $\hat{U}$ profile below the height of the surface elements must be made (i.e. within the canopy layer). Here the profile can be well approximated as exponential, although this may break down for surfaces above $\lambda_p \approx 0.3$ (Macdonald 2000):

$$\hat{U}(z) = \hat{U}_{hm} \exp\left[a\left(z/h_m - 1\right)\right]$$

Equation 3-9

where a is the attenuation coefficient, which Macdonald (2000) found empirically to be $\approx 9.6\lambda_p$ or $9.6\lambda_f$.

For surfaces denser than $\lambda_p = 0.1$, surface drag is dominated by the pressure drag of the buildings (Leonardi and Castro 2010), and hence the viscous terms, V_{Dc} and V_{Dg}, can be

ignored. Therefore, on substituting Equation 3-8 and Equation 3-9 into Equation 3-7 and solving, we obtain:

$$\frac{d_C}{h_m} = \frac{19.2\lambda_p - 1 + \exp\left(-19.2\lambda_p\right)}{19.2\lambda_p\left[1 - \exp\left(-19.2\lambda_p\right)\right]}.$$

Equation 3-10

For $\lambda_p \geq 0.1$, this equation offers an approximation for d which compares well with various recent experimental datasets. This is demonstrated in Figure 3-4 (a) where predictions using Equation 3-10 are plotted in red alongside wind tunnel (Hagishima et al. 2009; Cheng et al. 2007) and numerical data (Jiang et al. 2008; Leonardi and Castro 2010) for uniform arrays. The experimental data is for staggered, square and aligned arrays (st, sq and al, respectively), each of which are illustrated in Figure 3-4 (e). Also the curves from the model of Macdonald and the more recent model of Kastner-Klein and Rotach (2004) are shown in blue. It can be seen that these models' estimates of d are generally much lower than recent experimental data suggests, although the predictions of Kastner-Klein and Rotach (2004) become increasingly more consistent with this experimental data as the area density increases. It is also important to comment on the large scatter that is present in these datasets, particularly at low densities. This highlights the uncertainties in experimentally derived aerodynamic parameters even over relatively simple arrays, as was discussed in Section 1.4.3.3. In particular, for the experimental data included here, the majority of the scatter appears to come from the differing height intervals in which aerodynamic parameters were obtained by Hagishima et al. (2009), i.e. they were not always obtained from the ISL where they are theoretically valid. It is also clear from Figure 3-4 (a) that an issue with Equation 3-10 is that for $\lambda_p < 0.1$ it overestimates d and does not tend to the correct limit of $d = 0$ at $\lambda_p = 0$. This is now corrected by estimating the viscous terms in Equation 3-7, V_{Dc} and V_{Dg}, for uniform cube arrays, as these forces become important at these lower building densities.

At low densities, within an isolated roughness flow regime, the drag force on each building is likely to remain approximately constant and V_{Dg} is expected to be proportional to the unsheltered ground area. From Equation 3-4 and Equation 3-5, the dimensionless, sheltered ground area, due to both the sheltered volume and footprint of a single cube, is $3H^2/A_T$ or

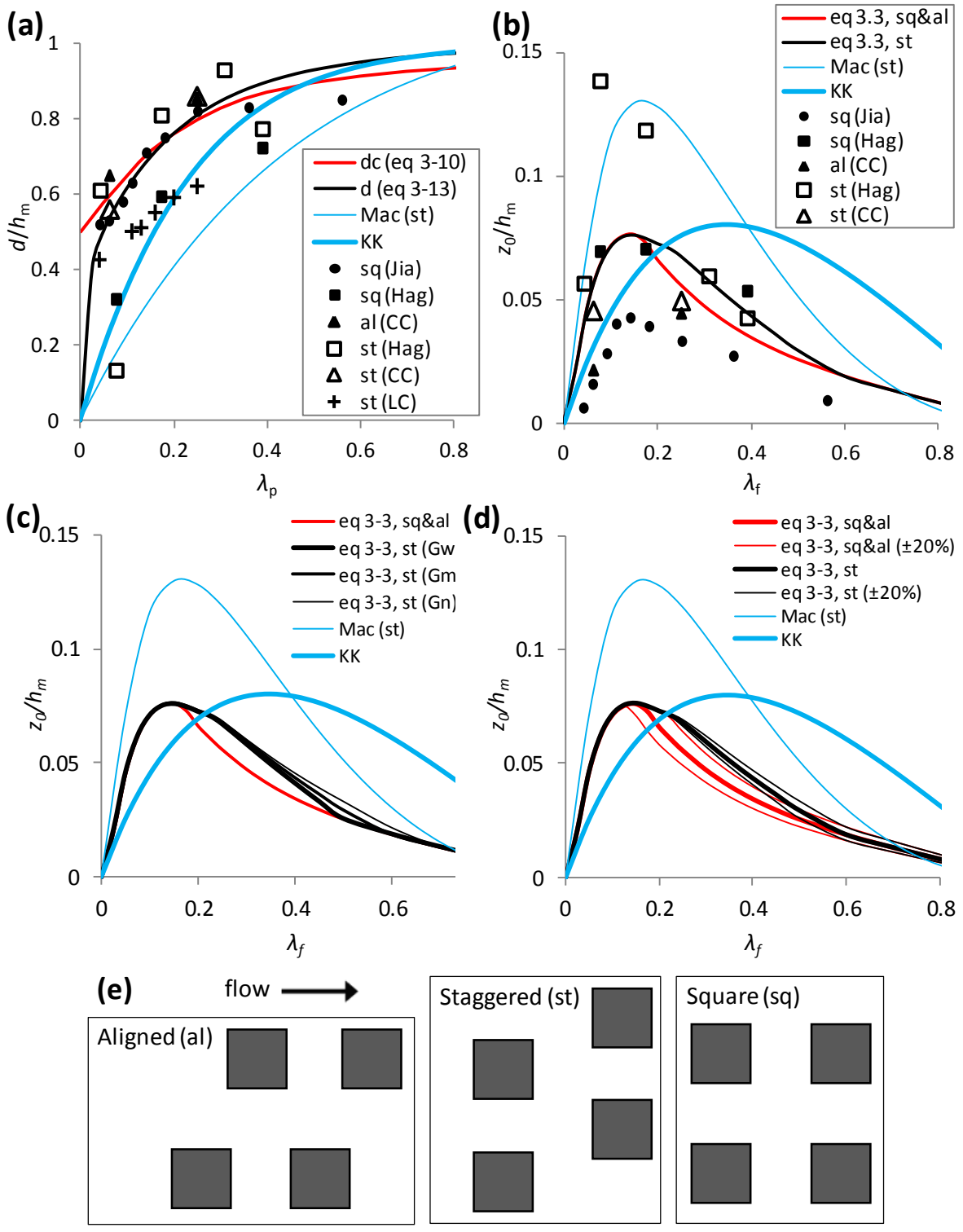

Figure 3-4: Estimates of (a) d given by Equation 3-10 and Equation 3-13, and (b) z_0 given by Equation 3-3. The sensitivity of the z_0 predictions to the width of the sheltered volume (c), and the length of the sheltered volume (d), are also shown. On (a)-(d) the models of Macdonald et al. (1998; Mac) and Kastner-Klein and Rotach (2004; KK) are also shown. (e) Shows sketches of square, staggered, and inline arrays of cubes. Experimental data from Cheng et al. (2007), Jiang et al. (2008), Hagishima et al. (2009) and Leonardi and Castro (2010), is referred to as CC, Jia, Hag and LC, respectively.

$3\lambda_p$. Hence, if V_{Dg} is proportional to the unsheltered ground area it follows that $V_{Dg}/F_D \propto (1-3\lambda_p)/\lambda_p$. Leonardi and Castro (2010) found in their numerical experiments that at $\lambda_p = 0.1$, $V_{Dg} \approx 0.06F_D$, and here this observation is used to calculate the constant of proportionality. Therefore, with F_D given by the integral of dF_D over the height interval $0 < z < h_m$, we obtain:

$$V_{Dg} = \frac{\rho C_D' A_f \hat{U}_{hm}{}^2 \left[1-\exp\left(-19.2\lambda_p\right)\right]}{4480\lambda_p}\left(\frac{1-3\lambda_p}{\lambda_p}\right).$$

Equation 3-11

Estimating V_{Dc} is less intuitive as it is strongly dependent upon the rooftop flow pattern as well as the roof shape. However, the results of Leonardi and Castro (2010) show that $V_{Dc}/F_D \propto \lambda_p{}^2$ is a good approximation for $\lambda_p < 0.2$. When fitting this relationship to their dataset, a constant of proportionality of approximately 1.6 is obtained using the method of least squares. Therefore, with F_D again given by the integral of dF_D over the building height, we obtain:

$$V_{Dc} = \frac{\rho C_D' A_f \hat{U}_{hm}{}^2 \left[1-\exp\left(-19.2\lambda_p\right)\right]}{24}\lambda_p.$$

Equation 3-12

On substituting Equation 3-8 and Equation 3-9 along with the viscous drag terms of Equation 3-11 and Equation 3-12 into Equation 3-7 and solving we obtain:

$$\frac{d_C}{h_m} = \frac{117\lambda_p + \left(187.2\lambda_p{}^3 - 6.1\right)\left[1-\exp\left(-19.2\lambda_p\right)\right]}{\left(1+114\lambda_p+187\lambda_p{}^3\right)\left[1-\exp\left(-19.2\lambda_p\right)\right]}.$$

Equation 3-13

In Figure 3-4 (a) it can be seen that at low densities this equation predicts the expected behaviour of d, and predictions also compare well with recent experimental data. At $\lambda_p = 0.1$, both Equation 3-10 and Equation 3-13 predict very similar zero-plane displacements, but the curves only intercept at $\lambda_p \approx 0.19$.

Therefore, in the current work d for uniform arrays is estimated as follows:

$$\frac{d}{h_m} = \mathrm{f}_d(\lambda_{pi}) = \begin{cases} \dfrac{19.2\lambda_p - 1 + \exp\left(-19.2\lambda_p\right)}{19.2\lambda_p\left[1-\exp\left(-19.2\lambda_p\right)\right]} & \left(\text{for } \lambda_\mathrm{p} \geq 0.19\right) \\ \dfrac{117\lambda_p + \left(187.2{\lambda_p}^3 - 6.1\right)\left[1-\exp\left(-19.2\lambda_p\right)\right]}{\left(1+114\lambda_p + 187{\lambda_p}^3\right)\left[1-\exp\left(-19.2\lambda_p\right)\right]} & \left(\text{for } \lambda_\mathrm{p} < 0.19\right) \end{cases}.$$

Equation 3-14

This equation is assumed to be independent of the different layouts of surface elements sketched in Figure 3-4 (d), as Cheng et al. (2007) found the centroid of the drag profile to be independent of the building layout.

It is important to comment on any limitations arising from the derivation of Equation 3-14. Firstly, it should be highlighted that in Figure 3-4 (a) the only experimental data for *d* derived specifically from the drag centroid is that of Leonardi and Castro (2010). The rest was obtained by traditional best fitting methods, as were described in Section 1.4.3.3. For low densities the agreement between their experimental data and the model predictions is good, but for medium densities their experimental data lies around 20% below the current model predictions. The most likely reason for this is the current model's assumption that C'_D is constant with height. It can be seen in the results of Leonardi and Castro (2010) that this assumption becomes less accurate with increasing area density. However, as yet there are no established methods of estimating the profile of C'_D and its dependence upon surface geometry. Furthermore, as mentioned previously, the current model predictions of *d* agree well with the other sources of experimental data.

A second important discussion regarding the model's derivation is the parametrisation of the attenuation coefficient. The value of $a \approx 9.6\lambda_p$ suggested by Macdonald (2000) was based upon experiments over square and staggered cube arrays of various densities. However it is possible that *a* is also influenced by building shape, and hence for arrays of non-cubical buildings that are short and squat, or elongated, more complex parametrisations of *a* may be required to model *d* more accurately. Currently however there is little data available regarding the dependence of *a* upon surface geometry, although if this data were to become available it could be incorporated into the current model with relative ease.

Finally, the method by which viscous forces are incorporated into the model deserves further discussion. Clearly the modelling of these effects is relatively simple, and the empirical observations are from a single experiment. However, overall the surface parameters predicted by the model are only influenced by these simplifications for low densities. Furthermore, for low densities of practical use (about $0.03 < \lambda_p < 0.1$), the predictions are relatively insensitive to the treatment of viscous drag. Taking all of these issues into account we proceed with using Equation 3-14 to estimate d, but the limitations and potential improvements to this method should be kept in mind.

3.3.4 Validating the roughness length predictions of uniform arrays

In Figure 3-4 (b) model predictions for z_0 from Equation 3-3 are shown, where d has been estimated from Equation 3-14. Predictions for staggered, square and aligned arrays are shown, alongside wind tunnel (Hagishima et al. 2009; Cheng et al. 2007) and numerical data (Jiang et al. 2008). (Note: For square and aligned arrays the predictions are identical). Predictions of z_0 are slightly towards the higher end of the experimental data, however considering the scatter it can be concluded that the model performs well, and the peak roughness occurs at the density the experiments suggest. Compared to the model of Macdonald, present model predictions for d and z_0 are far more consistent with recent experimental data, most likely due to issues with model calibration as mentioned in the previous section. Agreement between the model of Kastner-Klein and Rotach (2004) and this experimental data is quite poor. However, Kastner-Klein and Rotach (2004) calibrated their model using experimental data obtained from a wind tunnel study of a scale model of a single European city centre. The height variation that was present may explain the shifted peak in z_0 with respect to the experimental data shown here. Due to this calibration, they specifically warn against applying the model to other urban sites without further considerations.

In Figure 3-4 (c), the model's sensitivity to the width of the sheltered volume is shown using values for L_W of $0.15b$, $0.225b$ and $0.3b$, which correspond to the curves G_N, G_M, and G_W shown in Figure 3-3 (b), respectively. It is clear that the model has little sensitivity to this length-scale for staggered arrays, and is completely unaffected for square/aligned arrays. Similarly, to assess the sensitivity of the model to changes in the description of the length of the sheltered volume, in Figure 3-4 (d) model predictions are shown with L_R varied by ± 20%.

A variation of 20% represents about twice the uncertainty Fackrell (1984) found when using Equation 3-4 to estimate L_R and should therefore be a conservative estimate. Clearly the model is more sensitive to L_R than it is to L_W. However, the change in the predictions is still relatively small considering the scatter in the experimental data in Figure 3-4 (b).

3.4 Modelling Arrays of Heterogeneous Height

3.4.1 Modifying the drag balance

As the model described in Section 3.3 was found to give good predictions of d and z_0 for uniform arrays, similar techniques are now used to adapt it to consider arrays of heterogeneous heights. Again, the model is centred upon the balance between the drag force on a surface and the shear stress in the ISL, however there are two important differences. Firstly, clearly every building in the array must be involved in the calculation. Secondly, it is no longer reasonable to assume that the logarithmic profile of the ISL can be extended into the RSL to estimate the profile of $\hat{U}$ down to a height h_m. Therefore, an 'effective mean building height' ($h_{m\text{-}eff}$), which is greater than h_m, is chosen to be the lower limit of the logarithmic profile extension.

The calculation of $h_{m\text{-}eff}$ is detailed in Section 3.4.3, but an important point to make is that it is such that the taller buildings in a heterogeneous array will extend above this height (as illustrated in Figure 3-5). Consequently, the surface drag force is comprised of a contribution below $h_{m\text{-}eff}$, and a contribution above, referred to as F_{D1} and F_{D2}, respectively. The balance from Equation 3-1 now reads:

$$\rho u_*^2 = F_D/A_T = (F_{D1} + F_{D2}) / A_T.$$

Equation 3-15

Below $h_{m\text{-}eff}$, the drag contribution is estimated by the same method as was used for uniform arrays:

$$F_{D1} = 0.5\rho\, \hat{U}_{hm\text{-}eff}^2\, C_D\, A_f^*(z<h_{m\text{-}eff})$$

Equation 3-16

where $\hat{U}_{hm\text{-}eff}$ is the reference wind speed at $h_{m\text{-}eff}$ from the logarithmic profile, and $A_f^*(z<h_{m\text{-}eff})$ the unsheltered frontal area of the blocks below $h_{m\text{-}eff}$. Strictly, as the buildings below $h_{m\text{-}eff}$ are of different heights, different drag coefficients should be used for each of them.

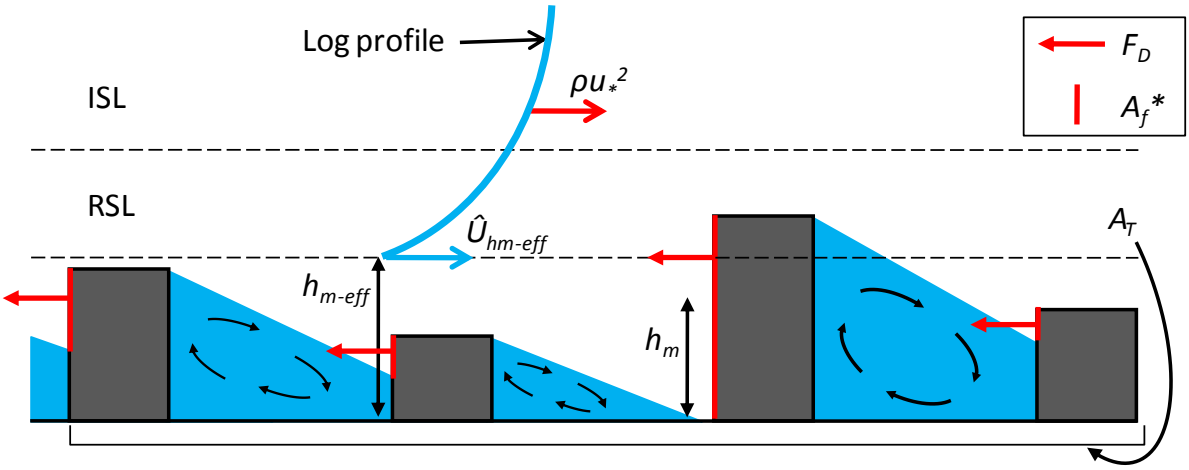

Figure 3-5: Sketch of the drag balance for heterogeneous arrays and the mutual sheltering of the buildings. Blue areas indicate, approximately, the sheltered regions behind the buildings, and red indicate the unsheltered frontal area of the buildings, which when summed give A_f^*.

However, for simplicity, in Equation 3-16 a single value of C_D is chosen that is appropriate for the average building shape. Therefore, for heterogeneous geometries, where the average building shape is a cuboid (i.e. $\lambda_p = \lambda_f$), C_D is chosen to be the same as that used for uniform cube arrays, i.e. $C_D = 1.2$.

Above $h_{m\text{-}eff}$, the drag force can be evaluated by integrating the differential drag force between $h_{m\text{-}eff}$ and the maximum building height (h_{max}):

$$F_{D2} = \int_{h_{m-eff}}^{h_{max}} 0.5\rho C'_D \hat{U}(z)^2 \, dA_f^*$$

Equation 3-17

where $\hat{U}(z)$ is now the standard logarithmic profile, and again C'_D is the 'sectional drag coefficient'. In the current work, a value for C'_D of 2 is chosen which, for simplicity, remains constant with surface density, as used by Coceal and Belcher (2004). It is well known that C'_D is a difficult parameter to estimate, however the model is not too sensitive to its value. For example, for the arrays studied later in this paper, predicted z_0 values are still in good agreement with the experimental data even when C'_D is increased to 3 (typically z_0 only changes by about 5%).

To obtain an equation that can be used to estimate the roughness length of a heterogeneous array, the logarithmic profile, Equation 3-16 and Equation 3-17, can be

substituted into the drag balance of Equation 3-15 and rearranged as follows:

$$2A_T\kappa^2 = C_D\left[\ln\left(\frac{h_{m-eff}-d}{z_0}\right)\right]^2 A_f^*(z<h_{m-eff}) + \int_{h_{m-eff}}^{h_{max}} C_D'\left[\ln\left(\frac{z-d}{z_0}\right)\right]^2 dA_f^* .$$

Equation 3-18

Similarly to Equation 3-3, Equation 3-18 can be used to estimate the roughness length of a heterogeneous array, provided the parameters $A_f^*(z<h_{m\text{-}eff})$, $h_{m\text{-}eff}$ and d, are estimated (although the integral requires that the equation is solved iteratively).

The geometric parameter, $A_f^*(z<h_{m\text{-}eff})$, is estimated by considering the mutual sheltering of the individual buildings' sheltered volumes (as sketched in Figure 3-5), in exactly the same way in which A_f* was previously calculated for uniform arrays. Methods for estimating d and $h_{m\text{-}eff}$ are now described in Sections 3.4.2 and 3.4.3, respectively.

3.4.2 The zero-plane displacement of heterogeneous arrays

An estimate of the zero-plane displacement of heterogeneous arrays cannot easily be made by estimating the drag profile centroid as before. This is due to the fact that the $\hat{U}$ profile from the ground up to the maximum building height is difficult to estimate. Therefore, a different approach is taken, which is now described by considering the simple heterogeneous array sketched in Figure 3-6 (a).

Primarily, the zero-plane displacement of a surface is dictated by the flow pattern which occurs within the CL, as different flow patterns raise the height at which the mean drag acts. For the simple heterogeneous array sketched in Figure 3-6 (a), it would be reasonable to suggest that there are effectively two different flow patterns occurring simultaneously. Isolated vortices, characteristic of a SF regime, may be present within the dense lower canopy, while the flow pattern around the sparser tops of the larger blocks may be better described as being in the WIF regime. Accordingly, the canopy may be split into two distinct, uniform vertical layers (as illustrated). Based upon the density of these layers, Equation 3-14 may be used to calculate the zero-plane displacement of each layer, d_1 and d_2, were they to be in isolation. This is done by calculating the height normalised zero-plane displacement for each layer and multiplying each value by the thickness of the layer, i.e. $d_1 = h_1\, f_d(\lambda_{p1})$ and $d_2 = h_2\, f_d(\lambda_{p2})$. Furthermore, it may be assumed that when these layers are stacked vertically to

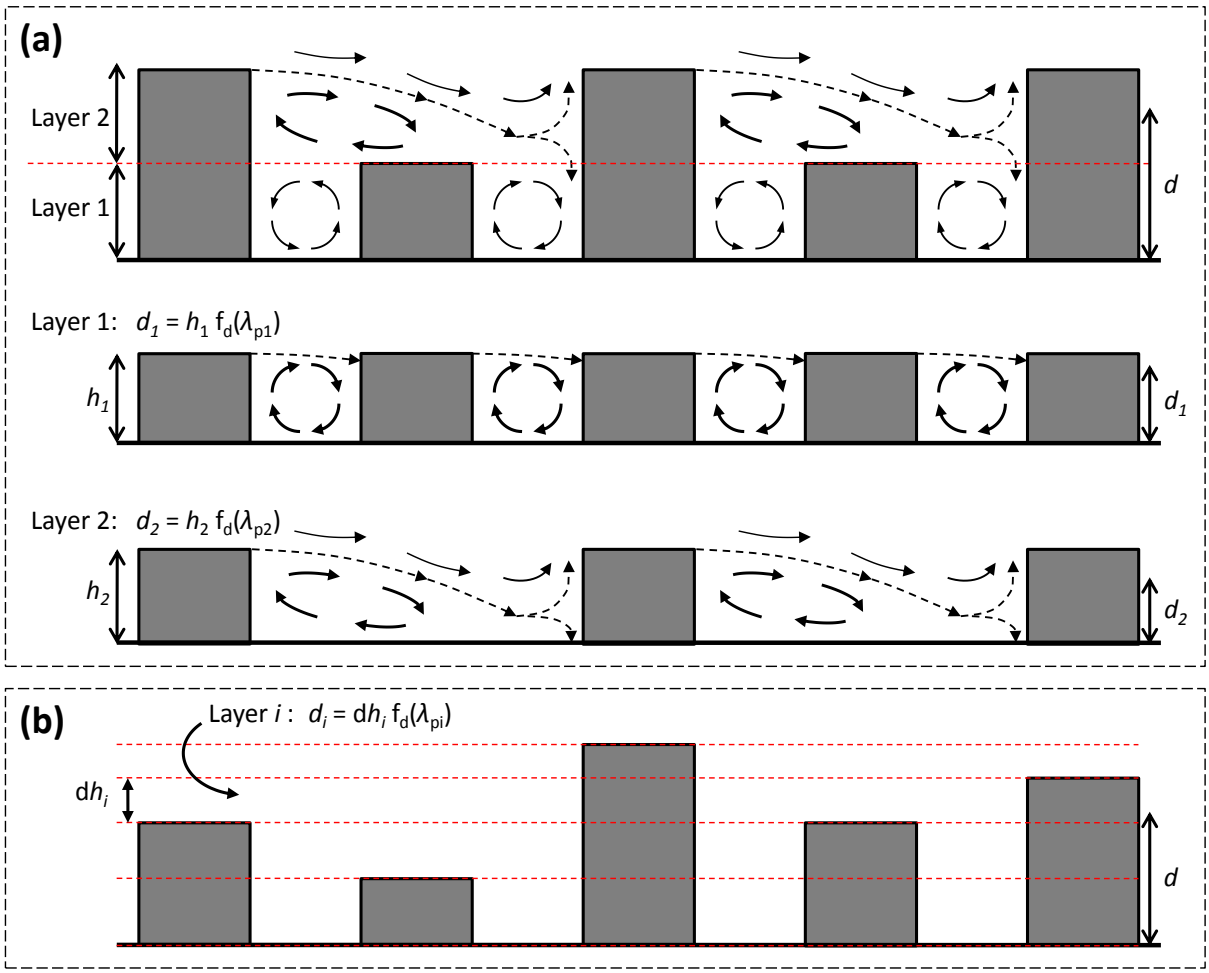

Figure 3-6: Illustration of the current method of calculating d for heterogeneous arrays by dividing the canopy into horizontal slices for (a) a simple, repeating heterogeneous array, and (b) any complex heterogeneous array.

obtain the original array, the zero-plane displacement is simply the sum of the values calculated for each layer; $d = d_1 + d_2$.

It is simple to extend this approach to any heterogeneous array by dividing the canopy into sufficiently many distinct, horizontal layers, n, so that each layer is of uniform height, as in Figure 3-6 (b). As these layers have now become quite thin, it is unreasonable to suggest that a different flow pattern occurs within each layer as in Figure 3-6 (a). However, it still seems reasonable to assume that when these layers are stacked vertically to obtain the original heterogeneous array, d can be approximated by taking the height normalised zero-plane displacement of each layer multiplied by the layers thickness; $d_i = dh_i f_d(\lambda_{pi})$, and summing over all the layers:

$$d = \sum_{i=1}^{n} \mathrm{d}h_i \, \mathrm{f}_d(\lambda_{pi}) \, .$$

Equation 3-19

Figure 3-7 (a-b) show the zero-plane displacement heights calculated by this method for four heterogeneous surfaces, which are each illustrated in Figure 3-7 (c). ST1.5-st is the two-height surface from the wind tunnel studies of Hagishima et al. (2009), of area densities; 0.077, 0.174, 0.309 and 0.391. R1.5 is the complex urban-like surface from the wind tunnel experiments of Zaki et al. (2011), of area densities; 0.077, 0.174, 0.309, 0.391 and 0.481. RM10s is the random height surface of λ_p = 0.25 from the wind tunnel studies of Cheng and Castro (2002). R1, from the numerical studies of Jiang et al. (2008), is a two height surface of λ_p = 0.11, with the normalised standard deviation of the building heights (σ_h/h_m) set to the following values; 0.17, 0.33, 0.5, 0.67 and 0.83, by making the high and low blocks in Figure 3-7 (c) gradually higher and lower, respectively. Average height to width ratios of the blocks in arrays ST1.5-st, R1.5, RM10s and R1, are 1.5, 1.5, 1 and 1, respectively.

It is clear from figures Figure 3-7 (a-b) that zero-plane displacement heights predicted by Equation 3-19 are in very good agreement with the experimental data over the heterogeneous arrays ST1.5-st, RM10s and R1, but over array R1.5 there are significant differences. However, considering the uncertainties that can occur when obtaining z_0 and d from experimental data using the statistical methods described in Section 1.4.3.3, the latter disagreement is not unexpected for such a complex array. Importantly, for all the arrays, Equation 3-19 predicts the characteristic that for heterogeneous arrays the magnitude of d can significantly exceed h_m.

3.4.3 The effective mean building height

Within a complex heterogeneous array, it is inaccurate to assume that the $\hat{U}$ profile can be estimated as logarithmic down to h_m. Therefore, $h_{m\text{-}eff}$ is chosen to be the lower limit of the logarithmic profile. To estimate this height, the concept of 'effective plan area density' ($\lambda_{p\text{-}eff}$) is introduced, which is simply the plan area density of a heterogeneous surface *discounting* the sheltered blocks in the array.

The justification for this parameter is that if a particular heterogeneous array contains low buildings that lie sheltered by larger, upstream buildings, then these have a negligible effect

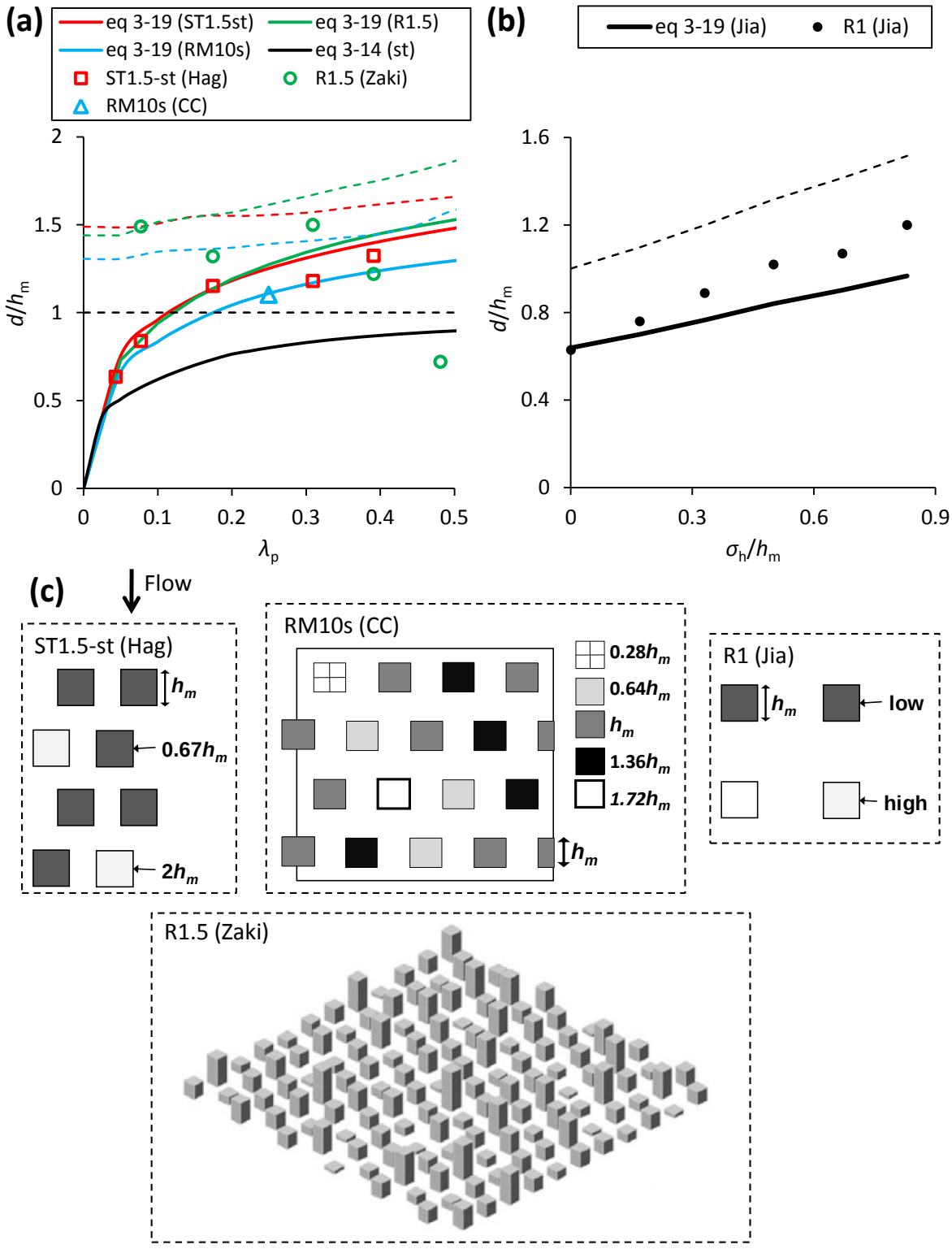

Figure 3-7: (a)-(b) Estimates of d given by Equation 3-19 and the corresponding experimental results for the arrays illustrated in (c). In (a)-(b) the dashed lines indicate calculated values of $h_{m\text{-}eff}$ for each array using appropriate colour coding. Experimental data from Cheng et al. (2002), Jiang et al. (2008), Hagishima et al. (2009) and Zaki et al. (2011), is referred to as CC, Jia, Hag and Zaki, respectively. The illustration in (c) for array R1.5 is from Zaki et al. (2011).

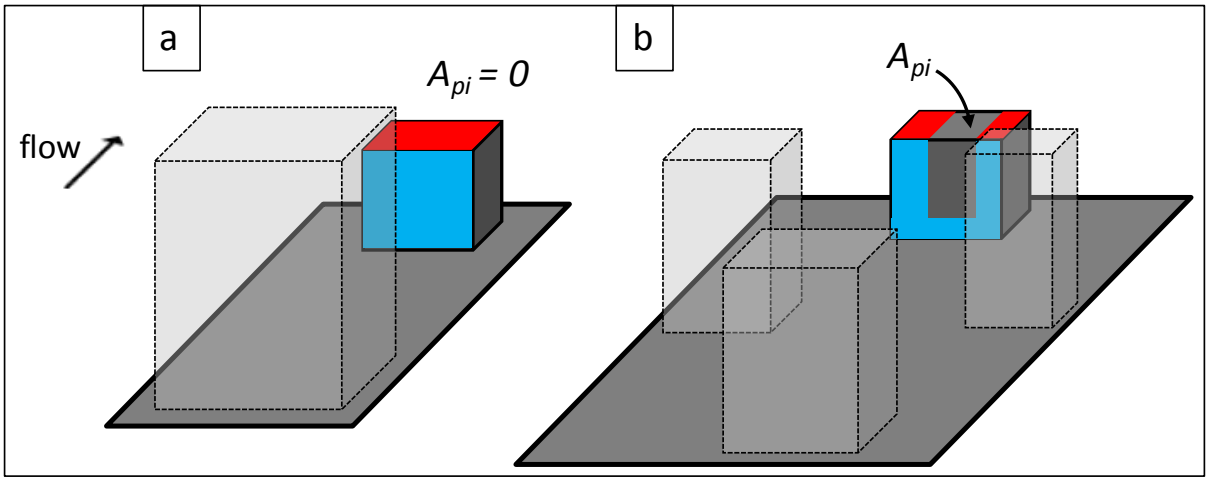

Figure 3-8: Examples of individual plan area contributions (A_{pi}) of two sheltered blocks to the 'effective plan area density' ($\lambda_{p\text{-}eff}$) of a heterogeneous array. Blue areas indicate the sheltering of the block windward faces by upstream blocks, red indicate the plan area *not* contributing to $\lambda_{p\text{-}eff}$, and the transparent blocks are those lying upstream.

on the above roof flow. Therefore, it may be more appropriate when modelling the above roof profile to ignore any sheltered blocks when calculating the plan area density, and hence we assign the surface a $\lambda_{p\text{-}eff}$ value. For example, if a particular block lays entirely within the wake shed from a large upstream building so that its windward face is fully sheltered (as in Figure 3-8 (a)) then the block is considered to contribute no area to the calculation of $\lambda_{p\text{-}eff}$, as A_{pi} would be zero. Similarly, any block that has its leading edge sheltered (as in Figure 3-8 (b), where the leading edge is sheltered by buildings laying upstream and laterally) has its plan area contribution reduced in proportion to this sheltering, as it is the top of the building's upwind face that exerts the most drag and influences the above roof flow most strongly.

To obtain $h_{m\text{-}eff}$ for a particular heterogeneous surface, d and $\lambda_{p\text{-}eff}$ are calculated first via Equation 3-19 and the method described in the previous paragraph, respectively. Subsequently, $h_{m\text{-}eff}$ is defined to be the mean building height of the uniform surface of plan area density $\lambda_{p\text{-}eff}$ that would have a zero-plane displacement equal to that of the heterogeneous surface. Hence, since for uniform arrays the logarithmic profile is assumed to be valid down to the mean building height, it is reasonable to consider $h_{m\text{-}eff}$ to be the lowest possible height a logarithmic profile could be extended down to in a heterogeneous array. To obtain $h_{m\text{-}eff}$, therefore, d and $\lambda_{p\text{-}eff}$ are substituted into a rearranged version of Equation 3-14:

$$h_{m-eff} = \begin{cases} d\dfrac{19.2\lambda_{p-eff}\left[1-\exp\left(-19.2\lambda_{p-eff}\right)\right]}{19.2\lambda_{p-eff}-1+\exp\left(-19.2\lambda_{p-eff}\right)} & \left(\text{for } \lambda_{\text{p-eff}} \geq 0.19\right) \\ d\dfrac{\left(1+114\lambda_{p-eff}+187\lambda_{p-eff}{}^{3}\right)\left[1-\exp\left(-19.2\lambda_{p-eff}\right)\right]}{117\lambda_{p-eff}+\left(187.2\lambda_{p-eff}{}^{3}-6.1\right)\left[1-\exp\left(-19.2\lambda_{p-eff}\right)\right]} & \left(\text{for } \lambda_{\text{p-eff}} < 0.19\right) \end{cases}.$$

Equation 3-20

3.4.4 Validation of the model for heterogeneous arrays

Methods of estimating all of the parameters required to estimate z_0 from Equation 3-18 have now been discussed. Hence it is possible to follow these steps and assess the ability of the model to predict z_0 for the arrays sketched in Figure 3-7 (c). A comparison of the model predictions and experimental data for z_0 is shown in Figure 3-9 (a-b). Model predictions of z_0 for staggered cube arrays are also shown (using Equation 3-3) to highlight the significantly larger roughness of arrays of random heights compared to arrays of uniform height.

It can be seen that for arrays ST1.5-st and RM10s, the model predictions are in very good agreement with the experimental data. Compared to uniform arrays, a softer peak in roughness with respect to plan area density is predicted for these heterogeneous arrays.

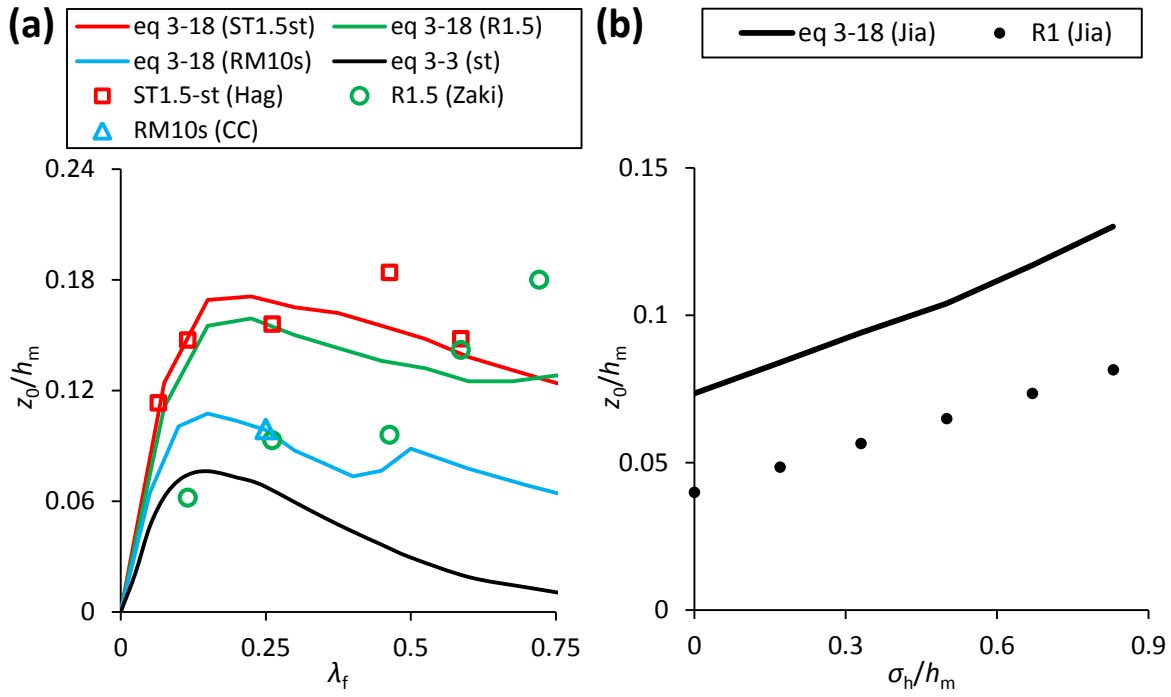

Figure 3-9: Estimates of z_0 from Equation 3-18 for the arrays illustrated in Figure 3-7 (c) and the corresponding experimental results. Experimental data from Cheng et al. (2002), Jiang et al. (2008), Hagishima et al. (2009) and Zaki et al. (2011), is referred to as CC, Jia, Hag and Zaki, respectively.

The dip in the z_0 curve for array RM10s at $\lambda_p \approx 0.4$ is simply due to the method of defining $h_{m\text{-}eff}$, as there is a small, but rapid increase in $h_{m\text{-}eff}$ at this density (see Figure 3-7 (a)).

For the array R1, the experimental data is significantly lower than the model z_0 predictions. However, the numerical data of Jiang et al. (2008) for uniform, square arrays is also significantly lower than the wind tunnel experiments (see Figure 3-4 b). Furthermore, the linear rate of increase of z_0 with increasing building height variation predicted by the model is in very good agreement with the experimental data. For the R1.5 array, the model predictions are also significantly different to the experimental data for z_0. This could potentially be due to the uncertainties in obtaining z_0 and d from experimental profiles, as was previously suggested for the d predictions for this array. Specifically, the method used by Zaki et al. (2011) allows for the height interval within which the log profile is best fit to obtain z_0 and d to vary with area density. This means that for higher area densities, z_0 and d may have been obtained from the RSL and ISL profiles, while for lower densities they may have been obtained, correctly, from the ISL profile only. This may possibly explain the reduction in d they found with increasing λ_p, which contradicts the generally accepted view that d increases monotonically with λ_p. Furthermore, these low d estimates at higher area densities would result in estimates of z_0 being biased towards higher values.

It is useful to also compare the $\hat{U}$ profiles measured in these experiments with the logarithmic profiles predicted by the model (although it should be emphasised here that various pairs of z_0 and d can give quite similar wind profiles). A number of comparisons are shown in Figure 3-10, for arrays ST1.5-st, RM10s, R1 and R1.5. Profiles plotted using the parameters of the model of Macdonald are also shown for comparison as, although there were potentially some issues with the model's calibration, it gives reasonably accurate estimates of wind profiles above uniform cube arrays.

From Figure 3-10 (a-b) it is apparent that, down to a height of $h_{m\text{-}eff}$ as intended, the predicted logarithmic $\hat{U}$ profiles and the measured $\hat{U}$ profiles are in excellent agreement for array ST1.5-st and RM10s. Furthermore, the inflection points in the profiles from the experimental data are at almost the same height as the values of $h_{m\text{-}eff}$ predicted by the model, suggesting that it is reasonable to consider $h_{m\text{-}eff}$ as the lower limit of the validity of the logarithmic profile. In Figure 3-10 (c) it can be seen that for array R1, the predicted and measured $\hat{U}$ profiles diverge slightly as σ_h increases. However, the agreement is still good for

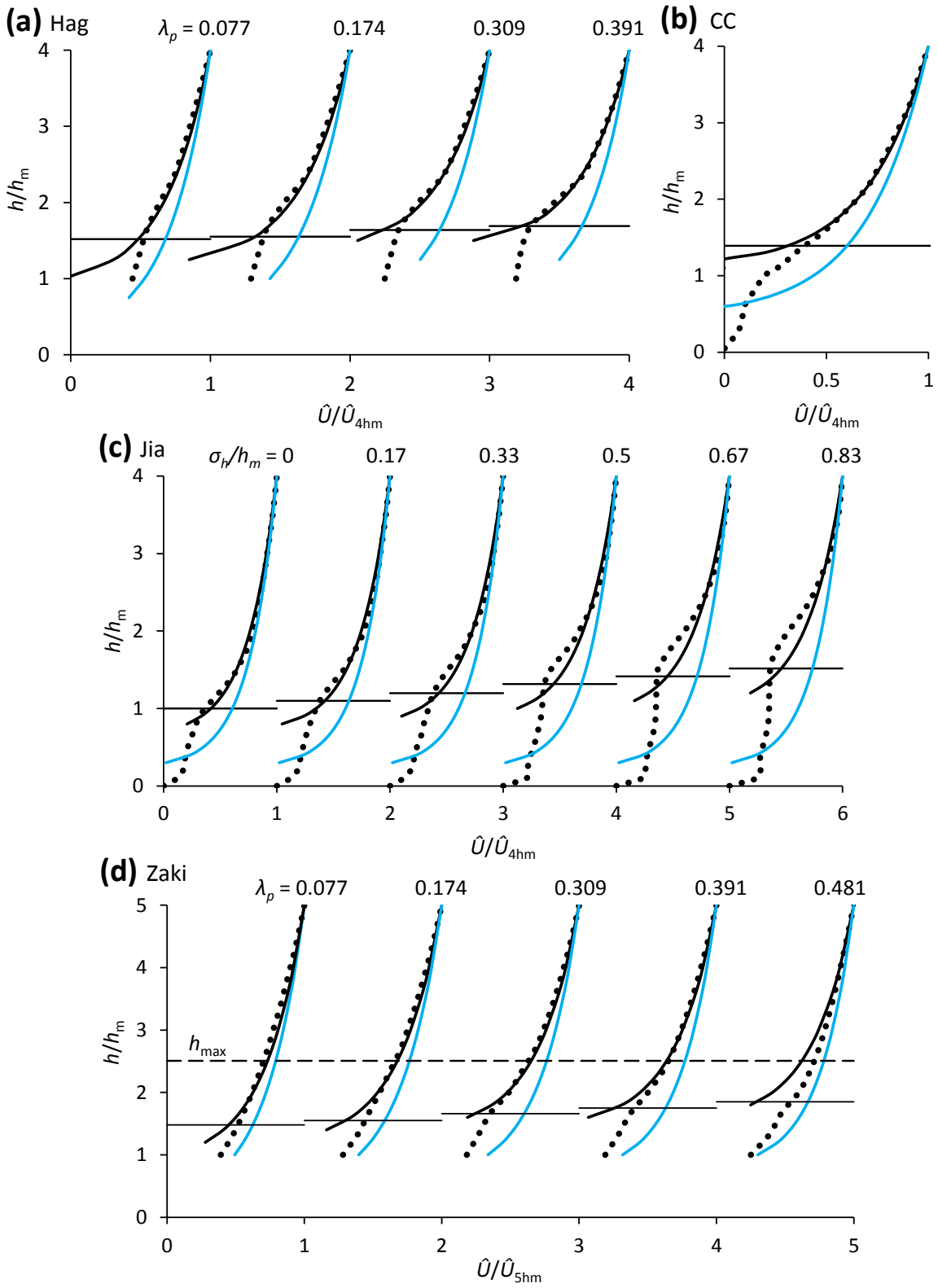

Figure 3-10: Logarithmic $\hat{U}$ profiles predicted by the model (sold lines) over arrays (a) ST1.5-st, (b) RM10s, (c) R1 and (d) R1.5. Shown for comparison are the $\hat{U}$ profiles (dotted lines) from the experiments, and the predictions of the model of Macdonald et al. (1998) (blue lines). The solid horizontal lines indicate $h_{m\text{-}eff}$. In (a-c) profiles are normalised by $\hat{U}$ at $4h_m$, and in (d) by $\hat{U}$ at $5h_m$. Profiles are offset 1 unit for clarity of presentation.

σ_h/h_m = 0.5, which is the greatest magnitude of height variability found in many major cities (Ratti et al. 2002). Furthermore, again the inflection points in the profiles from the experimental data are at a similar height as the values of $h_{m\text{-}eff}$ predicted by the model. Over array R1.5, the predicted and measured $\hat{U}$ profiles are in excellent agreement, down to a height just above $h_{m\text{-}eff}$. This is despite the fact that the predictions of z_0 and d differ significantly from the experimental values. The exception is for the highest density surface, $\lambda_p \approx 0.48$, where the model predictions of the measured $\hat{U}$ profile become less accurate. This perhaps highlights a level of density and height heterogeneity at which it is no longer reasonable to describe the $\hat{U}$ profile in the RSL by a downwards extension of the ISL logarithmic law. It is likely as well that at this point some of the model's assumptions break down, such as the description of the idealised shelter volumes and the chosen drag coefficients. It is also clear from Figure 3-10 that Macdonald's model significantly overestimates wind profiles above these heterogeneous arrays. This highlights the large inaccuracies that could occur when a model that has not been developed to consider height variation, is incorrectly used to estimate wind profiles above these types of surfaces.

3.5 Summary

In this Chapter, a model has been developed to produce a first estimate of the simultaneous effects of building height variability and surface area density upon the aerodynamic parameters of surfaces, in order to estimate the profile of spatially averaged, horizontal mean wind speed ($\hat{U}$) throughout the RSL and ISL, using a logarithmic profile. The model is influenced strongly by those of Macdonald et al. (1998), Raupach (1992, 1994, 1995) and Bottema (1996, 1997). It has built upon their work to include the influences of building height variability, which is one of the most significant geometric factors influencing surface parameters.

Firstly, a model was developed for uniform arrays which predicted the aerodynamic parameters suggested by recent experiments reasonably well, with the peak roughness occurring at the correct density. Subsequently, the model was extended to arrays of heterogeneous building heights and, over a number of heterogeneous arrays, the predicted aerodynamic parameters compared well with wind tunnel and numerical data. Specifically, two important characteristics were captured. Firstly the peak z_0 with respect to surface

density for heterogeneous arrays becomes softer when compared to uniform arrays. Secondly d can exceed the mean building height significantly for heterogeneous arrays. Furthermore, the logarithmic profiles predicted by the model were generally in good agreement with the profiles of $\hat{U}$ from the experimental data down to the 'effective mean building height' ($h_{m\text{-}eff}$), which is a model output.

Overall, the model offers good estimates of z_0 and d, and hence $\hat{U}$ profiles above heterogeneous surfaces, particularly when compared to previous models that do not consider height variability. However, the validation has also shown that the predicted wind profiles can become less accurate for surfaces that are either too highly heterogeneous, or too dense. There may also be other limitations of the model that affect its accuracy due to some of the assumptions made in its derivation, as the validation in this Chapter has been restricted to arrays of square based blocks. It would be informative to extend the model validation in the future to arrays with both variable height and building shape. However, producing the experimental data that may be used to extent the model validation is a substantial task, and hence it is beyond the scope of this Thesis. Therefore, the model will be used in its current form throughout the remainder of this Thesis.

4 Aerodynamic Parameters of a UK City Derived from Morphological Data

4.1 Introduction and Objectives

In this Chapter, a methodology is developed for applying the new morphometric model developed in Chapter 3 to complex urban environments, using the UK city of Leeds as a case study. Following the development of the methodology, the estimations of aerodynamic parameters are compared with other reported values from the literature to ensure they are realistic, and then relationships between the predictions and various geometric parameters describing the urban morphology are investigated. This methodology is the crucial first step in the wind atlas methodologies that are implemented in the following Chapters to estimate urban wind resource.

An overview of the methodology is given in Figure 4-1, in which the differences between this and previous approaches can be observed. The initial stage of the current methodology involves using detailed morphological data for Leeds to determine neighbourhood regions that consist of relatively homogeneous surface geometry (i.e. the average height and density of the buildings is similar throughout the region). Subsequently, a number of important geometric parameters are calculated for each neighbourhood region. Finally, these parameters are incorporated into the morphometric model developed in Chapter 3 in order to estimate values of z_0 and d. The main advantages of this approach over previous methods are that (i) the neighbourhood regions considered are more appropriate for the application of a morphometric model than those that would result from using a uniform grid, and (ii) the morphometric model used considers the influence of height variability, which is shown to be significant.

The structure of the Chapter is as follows: (i) Section 4.2 describes the development and calculation process of the methodology, (ii) In Section 4.3, the predictions are compared to the ranges given by the widely used roughness tables of Grimmond and Oke (1999) and the relative sensitivity of the predictions to building footprint shape and height variation is explored. Recommendations are then made for the level of geometric detail that should be

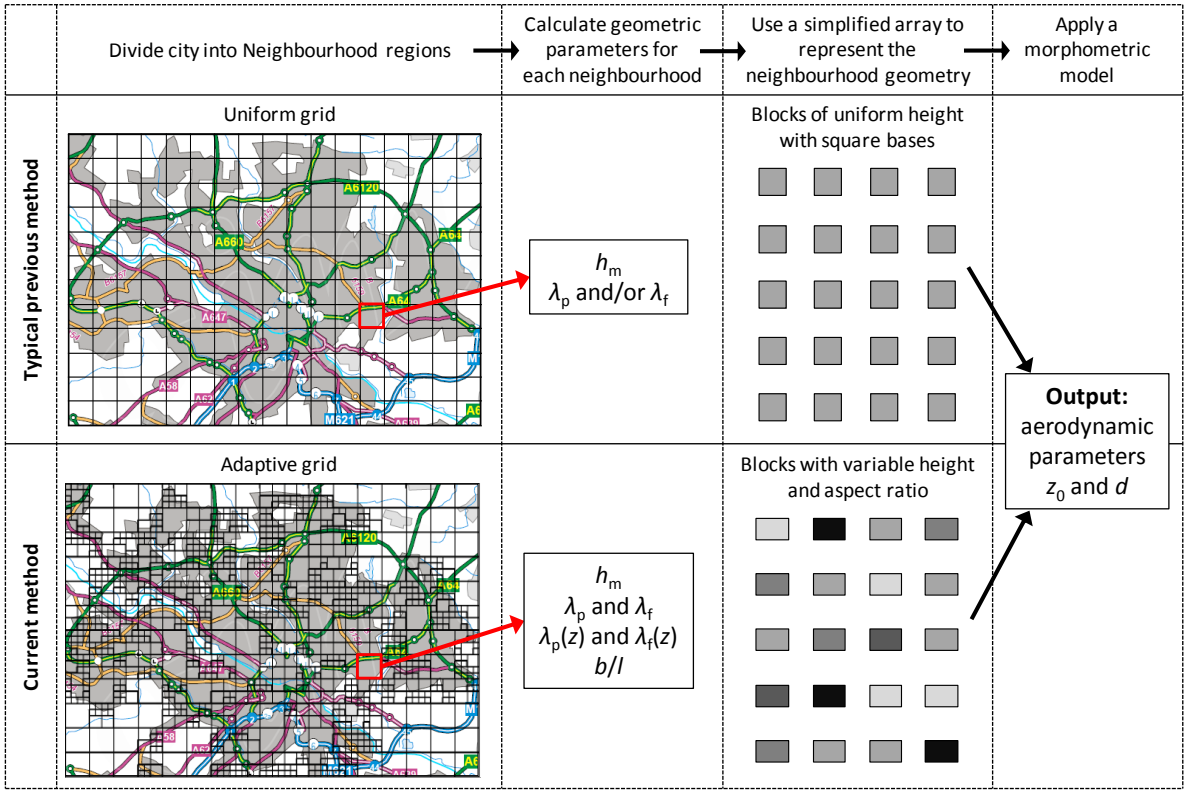

Figure 4-1: An overview of the methodology used in this Chapter to estimate surface aerodynamic parameters (bottom row) shown in comparison with typical previous methods (top row). Differences in the gridding method that is used and the level of complexity of the urban geometry that is considered are evident. The current method of dividing the city into neighbourhood regions is described in Section 4.2.2, the geometric parameters calculated are introduced in Section 4.2.3.2, and the method of producing simplified arrays to use in a morphometric model to estimate aerodynamic parameters is described in Section 4.2.3.3.

considered when estimating values of z_0 and d in urban areas. (iii) Finally, in Section 4.4 the important findings of the Chapter are summarised.

4.2 Developing the Methodology

4.2.1 The morphological dataset

The city of Leeds that this Chapter is focused upon is a large urban area with a population of nearly 0.75 million, located in the North of England. The region of investigation is a rectangular area of 204 km^2 (12 × 17 km) as shown in Figure 4-2. This region contains a broad range of land use types, including the heterogeneous high rise city centre, and a wide variety of industrial and residential areas. These cover the majority of land use types likely to be found in most UK cities.

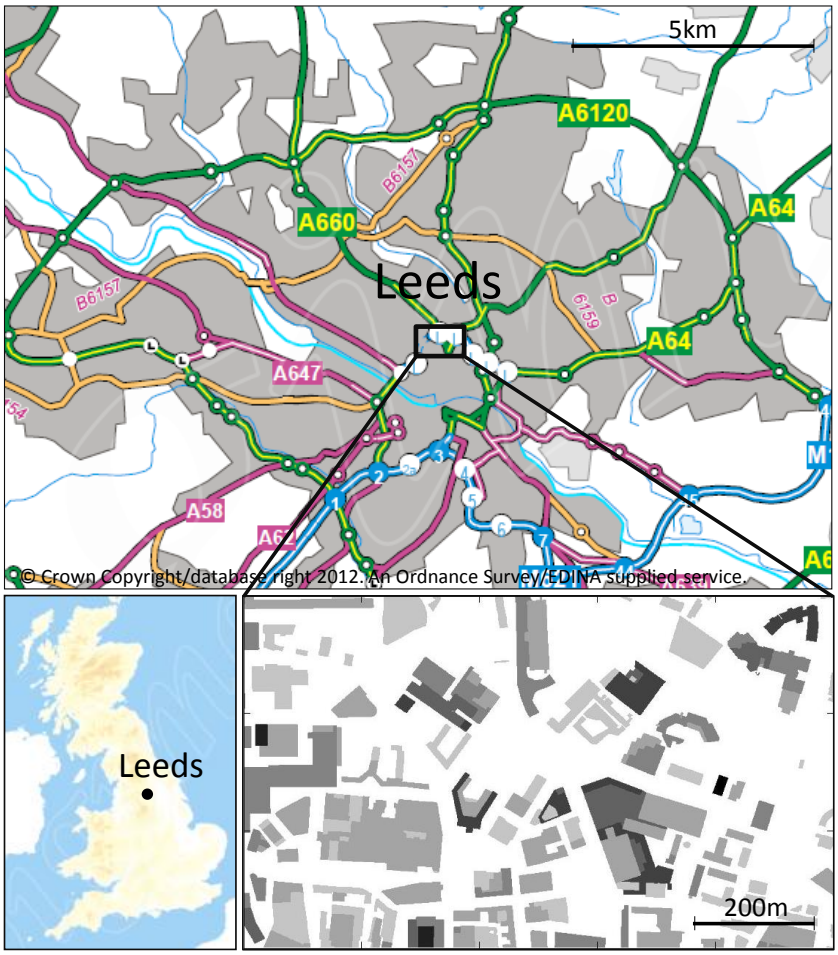

Figure 4-2: The study area of Leeds (top), its location in the UK (bottom left), and a sample of the building data (bottom right) which is available at: www.landmap.ac.uk (Cities Revealed © The GeoInformation Group 2008).

The morphological data used are available to the UK academic community and can be obtained online from Landmap (www.landmap.ac.uk) through the 'Cities Revealed' agreement (Cities Revealed © The GeoInformation Group 2008). Various types of data are available, but this Chapter focuses only upon data from the 'building heights' feature collection. These data were derived by Landmap from LiDAR surveys (with ± 0.15 m vertical accuracy) and high resolution aerial photography, which were processed to give simple information on the heights and footprints of the ground features (or roughness elements). Each feature (which includes manmade structures as well as woodland areas) is given in vector format, which specifies its footprint and its height above the ground to an accuracy of ± 0.5 m (horizontally and vertically).

Before any geometrical analysis is carried out, the data is converted into a digital elevation model (DEM), in raster form. This data format is generally used when analyzing urban areas

with respect to air flow (Ratti et al., 2002, Ratti and Richens, 2004, Ratti et al., 2006, Di Sabatino et al., 2010). The raster is simply a pixelated, top-down image of the urban area, where the value of each pixel refers to the height of the roughness element above the ground. Therefore, it gives a full, three-dimensional description of the urban area. During this conversion process the pixel resolution must be chosen, and this is important in determining how accurately the geometry is represented (Di Sabatino et al., 2010). Ideally, the resolution should be chosen to be as fine as possible, however in this work, due to the large size of the study area, computational restraints limit the resolution of the DEM to 1 m in both the horizontal and vertical directions. This resolution is likely to slightly reduce the accuracy of the current predictions, but it is expected to be sufficient for the purposes of this work.

4.2.2 Dividing the city into neighbourhood regions

Before the aerodynamic properties of Leeds are estimated, the city is divided into distinct neighbourhood regions whose aerodynamics can be assessed using the model of Chapter 3. As discussed in Section 1.4.3.5, it is difficult to choose an appropriate size for these neighbourhood regions as both fine and coarse grids have advantages and drawbacks. For example, in areas of Leeds containing long, wide buildings, large neighbourhoods may be required to encompass enough buildings for aerodynamic parameters, and hence the logarithmic profile, to be applicable. Conversely, in regions of rapidly varying surface cover, smaller neighbourhoods may be required so that distinctly different surfaces can be considered separately. This suggests that ideally the grid size and alignment should be allowed to vary to adapt to the local morphology.

With this in mind, an adaptive, non-uniform square grid of three grid sizes (0.25, 0.5 and 1 km) is used to divide the city into neighbourhood regions. This is in contrast to previous methods which generally use uniform grids, as indicated in Figure 4-1. These sizes are chosen for the grid squares so that a tessellation of the full domain can always be found. Neighbourhoods are selected so that within each neighbourhood the variations in mean building height and plan area density are minimised, but in such a way that small neighbourhoods are not chosen where large surface elements may be present. The programming environment, Matlab© is used to implement the methodology, which is now described.

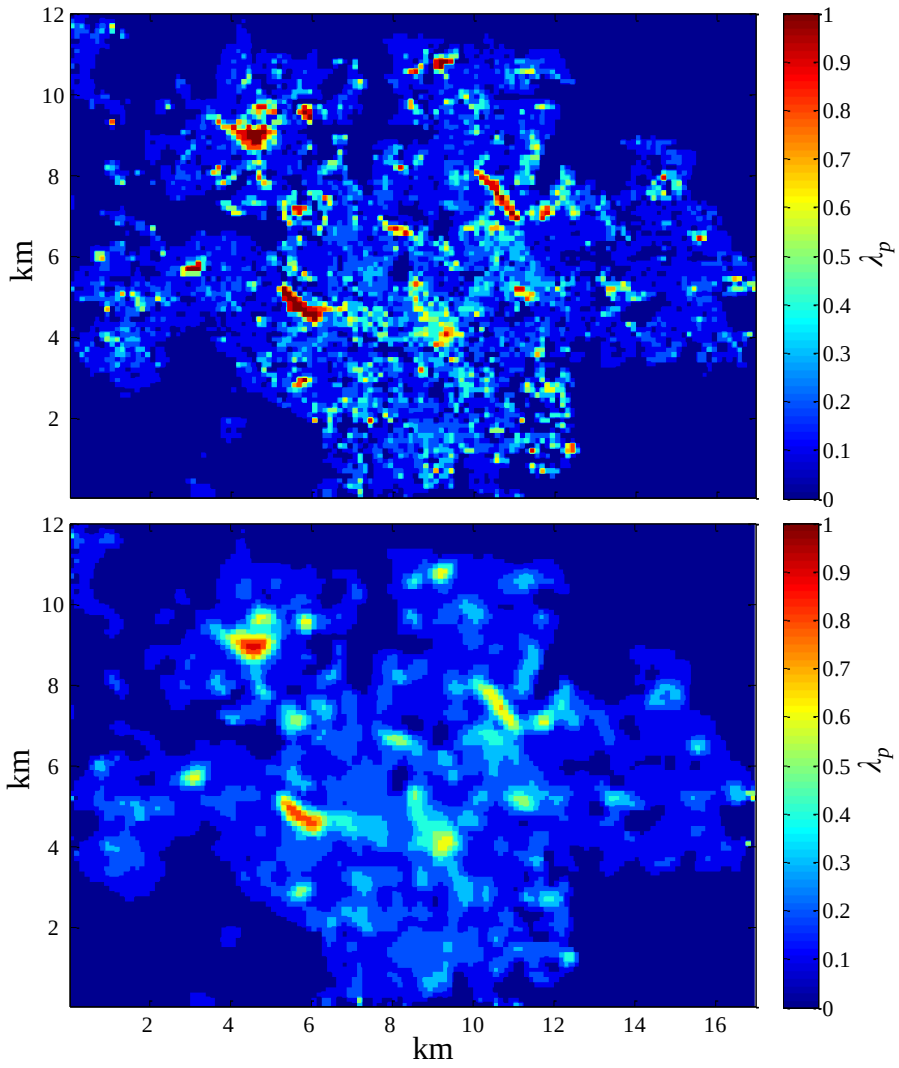

Figure 4-3: Unfiltered (top) and filtered (bottom) maps of plan area density over the city of Leeds at a 125 m resolution.

First, the city is divided into a 125 m grid (i.e. half of the smallest neighbourhood size) and the plan area density and mean building height are calculated for each cell. Subsequently, in order to smooth out any street scale variations in these parameters, the maps are filtered using a Gaussian image processing filter, 5 × 5 cells in size (i.e. two cells in each direction). These filtered maps are then used as an aid to determine approximately homogeneous neighbourhood regions. To illustrate this step, the 125 m resolution map of plan area density is shown before and after filtering in Figure 4-3.

Second, the city is divided into a uniform, 1 km grid. If the variation in mean building height or plan area density within any 1 km cell based on the filtered data is too large, then it is broken down into four smaller, 500 m cells. The variation is considered too large if either:

$$\sqrt{\overline{\left(\lambda_{pi}-\overline{\lambda_{pi}}\right)^2}}\Big/\overline{\lambda_{pi}}>0.25$$

Equation 4-1

or

$$\sqrt{\overline{\left(h_{mi}-\overline{h_{mi}}\right)^2}}\Big/\overline{h_{mi}}>0.25\,,$$

Equation 4-2

where λ_{pi} and h_{mi} are the plan area density and mean building height, respectively, of the ith filtered cell laying within a 1 km cell. This same process is then used to break down 500 m cells into four 250 m cells, if they are determined to be too heterogeneous by Equation 4-1 or Equation 4-2.

Finally, this process is reversed, and hence 250 m and 500 m cells are merged into 500 m or 1 km cells, provided the larger cell does not break either equality in Equation 4-1 or Equation 4-2. Therefore, 1 km cells can potentially be formed that are not aligned with the original 1 km grid. The grid resulting from this process is shown in Figure 4-4, and the neighbourhoods used in this Chapter are specified by this grid.

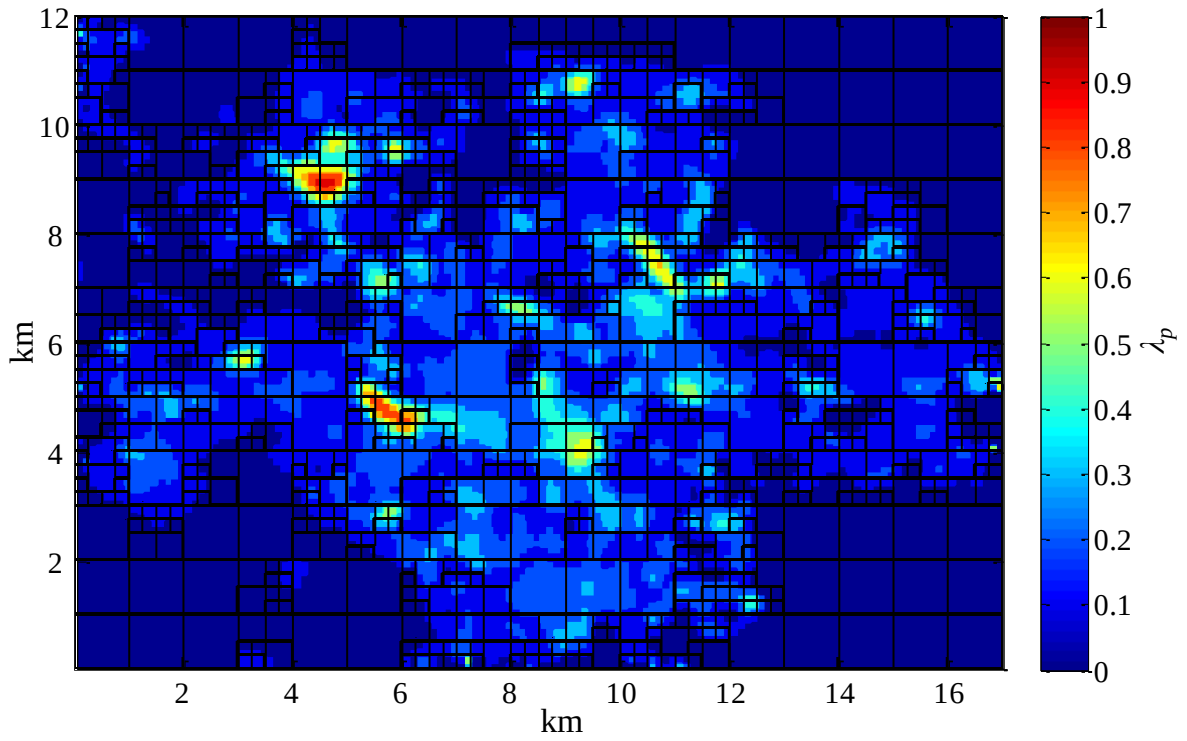

Figure 4-4: The adaptive grid used to determine neighbourhood regions in this paper overlaid on-top of the filtered plan area density map from Figure 4-3 (bottom).

Improvements to the method:

The method described above offers a first attempt at choosing neighbourhood regions appropriate for applying morphometric models to estimate aerodynamic parameters. However, the choice of 0.25 in Equation 4-1 and Equation 4-2 is quite arbitrary. Other values besides 0.25 were tested, but when lower values were used the grid failed to detect the city's edge in some regions, and when higher values were used the number of small neighbourhoods produced appeared to be excessive. However, in any case, neighbourhoods determined by this method are expected to be more homogeneous than those that would result from employing a uniform grid. For example, when the city is divided into a uniform 1 km grid, the values calculated from the left hand side of Equation 4-1 and Equation 4-2 are on average around 1, i.e. four times greater than the threshold used to determine the adaptive grid cells. Furthermore, if an aggregated model (such as those discussed in Section 1.4.4.1) was applied using the aerodynamic parameters on this grid to estimate 'effective' aerodynamic parameters on a coarser grid (e.g. as input into a mesoscale model), then any sensitivity to small changes in the grid should be substantially lower.

In future it would be beneficial to develop a mathematical process to determine the most appropriate values to use in Equation 4-1 and Equation 4-2, but in this Thesis no further attempt is made to optimise these values.

4.2.3 Mapping aerodynamic parameters

4.2.3.1 Applying morphometric models

In order to estimate z_0 and d for a neighbourhood using measured building data and a morphometric model (such as that of Chapter 3), it is necessary to use the building data to calculate the set of geometric input parameters that the model requires. It is important to recognise that by using these geometric parameters, morphometric models do not consider urban geometries in their exact form – rather, there is an implicit assumption that the real urban surface has the same aerodynamic parameters as an idealised array with the same geometrical parameters. Clearly this assumption becomes more reasonable the greater the range of geometric parameters the morphometric model can accept. Examples of these idealised arrays for the current method (and previous methods) are illustrated in Figure 4-1, along with the geometric parameters they require.

The model of Chapter 3 is similar to other morphometric models in that it was developed for idealised arrays of regularly spaced blocks with identical plan area footprints, however the inclusion of height variability is a significant improvement in representing the complexities of real urban geometries.

4.2.3.2 Calculating geometric parameters

The following geometric parameters are accepted as inputs by the model of Chapter 3: h_m, λ_p, λ_f, b/l, D_y/D_x, and the distribution of building heights in the neighbourhood. Here, b/l is the average breadth over length ratio of the buildings in the array (with respect to the incoming wind direction), and D_y/D_x is the average breadth over length ratio of the ground area associated with each building (illustrated in Figure 4-5; bottom). The height distribution of the buildings can be well represented by the vertical profile of the frontal or plan area density, $\lambda_f(z)$ or $\lambda_p(z)$, respectively. Together, these inputs can be used to produce a horizontally homogeneous, but vertically heterogeneous, array with geometric parameters equal to those of the original neighbourhood region.

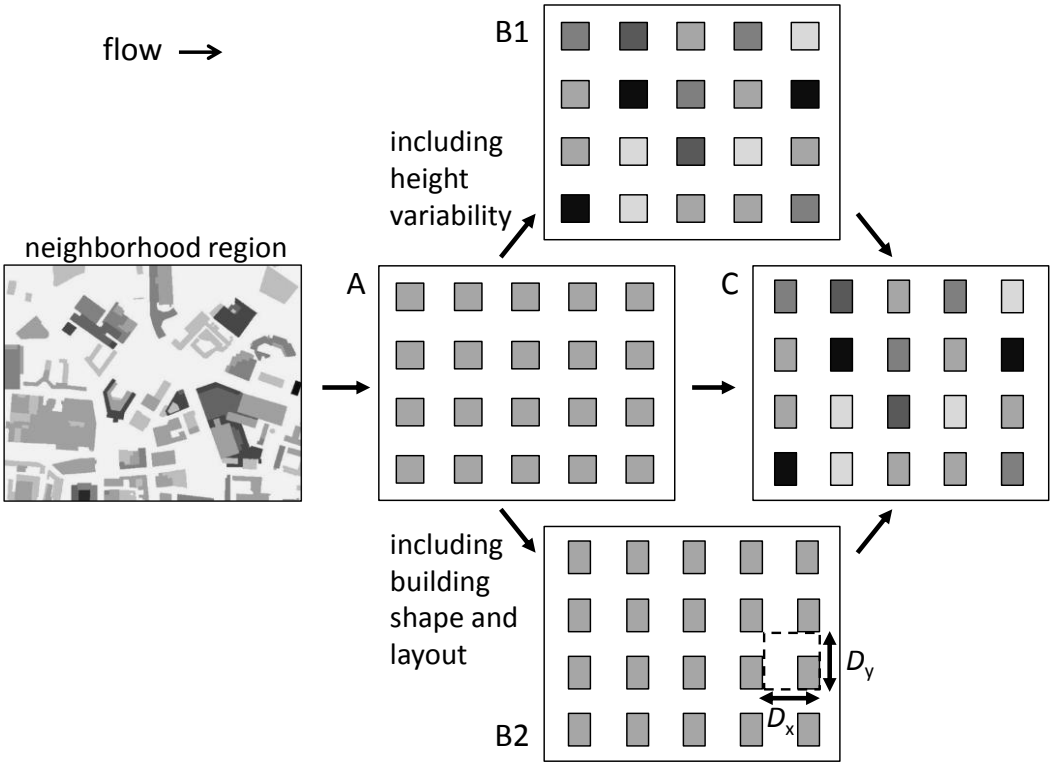

Figure 4-5: A sample of a neighbourhood region in Leeds and schematic diagrams of various simplified arrays that can be used to represent its geometry by using different combinations of geometric parameters. The morphometric model of Chapter 3 can be applied to these simplified arrays to estimate aerodynamic parameters. Different levels of shading on the diagrams indicate differences in building height.

As a final input, the model allows the layout of this array to be specified as staggered or square. For simplicity this is restricted to square, since streets and buildings are frequently aligned. However, whether a neighbourhood should be categorised as either square or staggered is generally quite ambiguous for complex city geometries.

Each geometric parameter can be calculated directly from the DEM, with a varying degree of difficulty. Most simple is the calculation of λ_p, which is simply the ratio of the number of non-zero pixels in a neighbourhood to the total number of pixels. Similar calculations can be used to obtain $\lambda_p(z)$. When calculating h_m each building height is weighted by its plan area, and hence h_m simply becomes the mean height of the non-zero pixels in a neighbourhood. Similarly, also calculated is the standard deviation of height of the non-zero pixels in each neighbourhood (σ_h), which is not a model input but becomes useful later in the Chapter.

The calculation of λ_f is slightly more involved. Furthermore, this parameter is a function of the incoming wind direction (although in this Chapter only winds from the North are considered as an illustrative example of the approach). Firstly, the building faces opposing the direction of the flow must be detected and their areas projected onto the vertical plane lying normal to the incoming flow. Summing the projected frontal areas in a neighbourhood and dividing by the total ground area gives λ_f. A similar calculation process yields $\lambda_f(z)$. Calculating a good average value of b/l is difficult as the breadth and length of a building of a complex shape can be quite ambiguous, and again this parameter is a function of wind direction. However, for each neighbourhood b/l can be estimated by considering λ_f values calculated for the neighbourhood for different wind directions. Specifically, b/l can be estimated by taking the ratio of λ_f in the wind direction of interest to the average λ_f in the perpendicular directions. Therefore in the case of Northerly winds, b/l is estimated from the λ_f values calculated for North, East and West:

$$b/l_N = 2\lambda_{f\text{-N}} / (\lambda_{f\text{-E}} + \lambda_{f\text{-W}}),$$

Equation 4-3

where subscripts N, E and W, refer to the wind directions from. This crude estimate of b/l is justified in Section 4.3.3 where it is shown that the model is not highly sensitive to this parameter. Finally, D_y/D_x is assumed to be unity, as the subjectivity in determining the ground area associated with each building from the DEM could make any attempt to estimate this parameter highly uncertain.

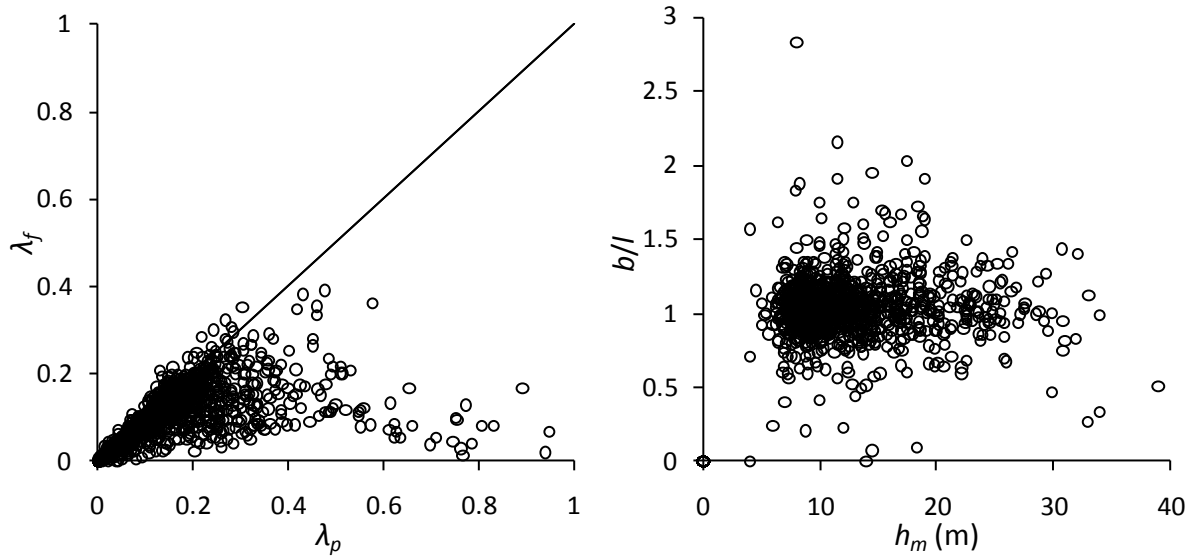

Figure 4-6: Values of λ_f vs. λ_p (left) and b/l vs. h_m (right) for each neighbourhood region in Leeds.

As can be seen in Figure 4-6, for the neighbourhoods of Leeds h_m is generally between 5 and 25 m, reaching a maximum of 39 m, while λ_p is mostly below 0.4. Generally, the neighbourhoods have larger values of λ_p than of λ_f, suggesting that the buildings are typically low and long, or low and wide. The average aspect ratios (b/l) are almost exclusively in between 0.25 and 2, implying that, on average, the buildings' footprints can be significantly rectangular.

4.2.3.3 Calculating aerodynamic parameters

The geometric parameters discussed in the previous section can be input into the model of Chapter 3 in order to estimate aerodynamic parameters over Leeds. The model achieves estimates of aerodynamic parameters by producing idealised arrays such as that illustrated in Figure 4-5 with the same geometric parameters of each neighbourhood region, and then estimating the aerodynamic parameters of these arrays.

Although the model can accept each of the geometric parameters discussed in Section 4.2.3.2 as inputs, they do not necessarily all have to be specified. If less of the input parameters are specified then simpler arrays are assumed to represent the geometries of each neighbourhood, as illustrated in Figure 4-5. Most simply, if only parameters h_m, λ_p and λ_f were specified then an idealised array similar to that in Figure 4-5 (A) would be assumed to represent each neighbourhood. More thoroughly, the full range of geometric parameters could be specified (h_m, λ_p, λ_f, b/l, D_y/D_x, and the building height distribution) and hence an

idealised array similar to that in Figure 4-5 (C) would be assumed to represent each neighbourhood. The variation in aerodynamic parameters predicted by the model when varying the level of simplification of the urban geometry is discussed in Section 4.3.3.

In order to consider height variation when estimating aerodynamic parameters, the model of Chapter 3 requires the heights of the buildings in the simplified array to be specified via a matrix. Perhaps the most appropriate parameter to use to produce this matrix is $\lambda_f(z)$, as it is considered to be powerful for capturing height variability when modelling urban flows (Di Sabatino et al. 2008). A natural way of utilizing this parameter is to set the heights in the matrix such that there is only a negligible difference between the $\lambda_f(z)$ profiles of the idealised array and the neighbourhood region. In order for these $\lambda_f(z)$ profiles to be closely matched, the idealised array must contain a sufficient number of buildings, and in this work arrays of 20 × 20 buildings are found to be adequate. The appropriate matrix is easily obtained by making the frequency of buildings of height H in the array proportional to $\lambda_f(H) - \lambda_f(H + dz)$.

It should be noted that the specific arrangement of the building heights in the matrix is random, and different permutations result in slightly different estimations of aerodynamic parameters. However, these differences are found to be insignificant, in agreement with the work of Zaki et al. (2011) who came to a similar conclusion in their wind tunnel studies.

It has been described above how an idealised array is produced to represent a neighbourhood region's geometry in order to then estimate its aerodynamic parameters. However, the model of Chapter 3 can estimate d directly from the $\lambda_p(z)$ profile of the neighbourhood. This is done using the integral form of Equation 3-19:

$$d = \int_0^{h_{\max}} \mathrm{f}_d\left(\lambda_p(z)\right) dz \quad ,$$

Equation 4-4

where, h_{max} is the maximum building height and f_d is the function used to estimate d/h_m for uniform height arrays from Chapter 3 (i.e. Equation 3-14).

Using this estimate of d and the simplified array representing the neighbourhood region, the model of Chapter 3 can be implemented to calculate z_0, via the use of Equation 3-18. This is the approach taken throughout this Thesis.

4.2.4 Model evaluation

Previous model evaluation in Chapter 3 found predictions of z_0 and d, as well as the profiles of U, to be in generally good agreement with the experimental data for a number of arrays of heterogeneous height. However, the comparison suggested model predictions may become inaccurate for surfaces that are either too heterogeneous in height, or too dense. Furthermore, the model's derivation makes it unsuitable for surfaces with very low densities. Accordingly, in this Chapter the model is applied only to neighbourhoods with $\lambda_p >$ 0.03, and the results for $\lambda_p > 0.5$ should be treated with caution.

Unfortunately, there is insufficient meteorological data available to evaluate the current predictions for z_0 and d over a single city such as Leeds. In fact, there are many practical difficulties in accurately estimating z_0 and d based on measurements in urban areas, due in large part to the elevation required to reach the inertial sublayer (Grimmond et al., 1998) – which may not even exist above complex urban areas (Cheng and Castro, 2002b). This highlights the potential value of further wind tunnel studies over city-like heterogeneous arrays for the evaluation of morphometric models. Furthermore, even if appropriate measurements were available, because of the frequent variations in surface geometry the air flow is rarely in equilibrium with the underlying urban surface (Cheng and Castro, 2002a), and hence aggregate values for aerodynamic parameters typically have to be calculated to describe surface layer wind profiles (see Section 1.4.4). This makes any direct validation of morphometric models problematic.

For these reasons, and due to the promising model evaluation of the previous Chapter, we proceed here under the assumption that the current predictions are reasonable. The wind atlas methodology used later in this Thesis focuses on predicting above roof wind speeds, and the comparison of these against available measurements from several cities allows a wider evaluation of the methodology of this Chapter.

4.3 Results and Discussion

4.3.1 General variation of aerodynamic parameters over Leeds

Maps of aerodynamic parameters for the neighbourhoods of Leeds, calculated using the method outlined in Section 4.2, are shown in Figure 4-7 (d and d/h_m) and Figure 4-8 (z_0 and

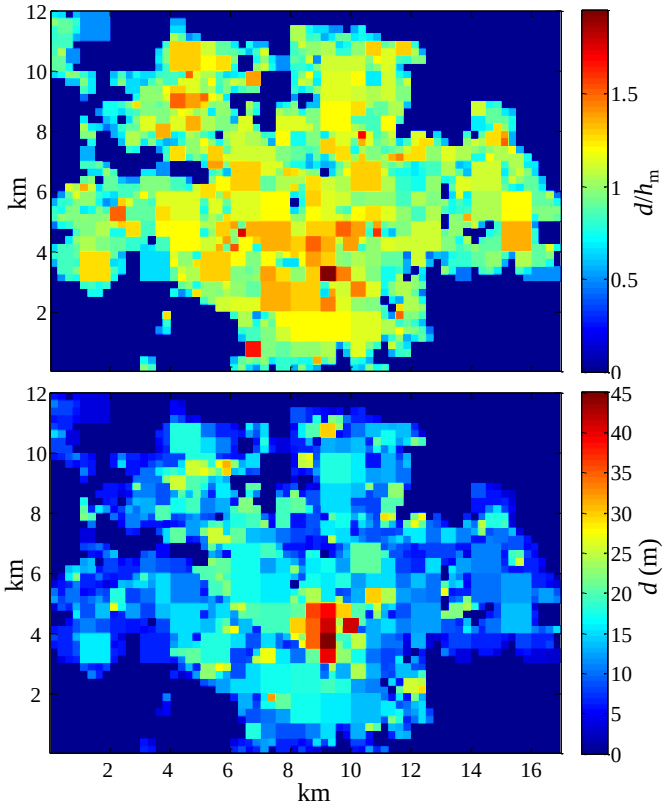

Figure 4-7: Maps of predicted normalised (top; normalised using the mean building height) and absolute (bottom; m) displacement heights for the neighbourhoods of Leeds.

z_0/h_m). For built areas, values of d generally range between about 3 and 25 m, but in the city centre they can be as high as 45 m. The associated normalised values (d/h_m) are generally between 0.5 and 1.5, with maximum values of about 2. In comparison, the variation in predicted values of z_0 and z_0/h_m is slightly greater: z_0 is generally less than about 2.5 m, reaching a maximum value of about 4.5 m, while z_0/h_m is generally less than about 0.15, reaching a maximum of about 0.25. Overall the predictions appear to be realistic and within the range of values reported for other European cities (Bottema and Mestayer, 1998, Ratti et al., 2002, Di Sabatino et al., 2010).

4.3.2 Comparing predictions with roughness tables

Due to the difficulties in accurately predicting aerodynamic parameters of urban surfaces that were discussed in Section 1.4.3, roughness tables are sometimes used as a convenient method of making first estimates of z_0 and d. Most commonly used are the tables given by Grimmond and Oke (1999) that were suggested after their extensive review of field and scale model data over various types of urban areas. They suggest ranges for the expected

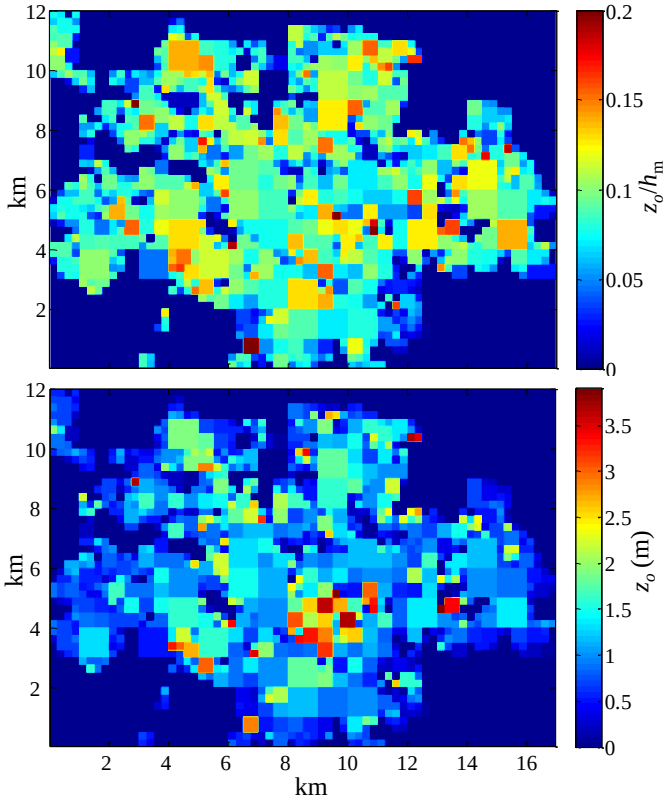

Figure 4-8: Maps of predicted normalised (top) and absolute (bottom; m) roughness lengths for the neighbourhoods of Leeds. Normalization is by the mean building height.

values of z_0 and d for four types of urban area: low, medium and high density, and high rise (these tables were referred to earlier in this Thesis in the sensitivity test of Chapter 2, Section 2.4.4). Two forms of the tables are given, one primarily using mean height to estimate aerodynamic parameters (Table 6 in their paper), and the other using aerial photographs to visually categorise neighbourhood regions by their plan area density (Table 7 in their paper).

For comparison, in Figure 4-9, the predicted aerodynamic parameters for all the neighbourhoods of Leeds are plotted against λ_p (top) and h_m (bottom), along with the ranges suggested by the tables of Grimmond and Oke (1999). Perhaps the most important observation to be gained from Figure 4-9 (a-b) is that the scatter in the predictions of both d/h_m and z_0/h_m is substantial, even for the same plan area density. For d/h_m, this scatter is entirely due to variations in the building height distributions of each neighbourhood. For z_0/h_m, varying frontal area density and building footprint shape further amplify this scatter, predominantly the former. This highlights the limitations of any model that estimates aerodynamic parameters based upon only h_m and λ_p. Figure 4-9 (a) also shows that the

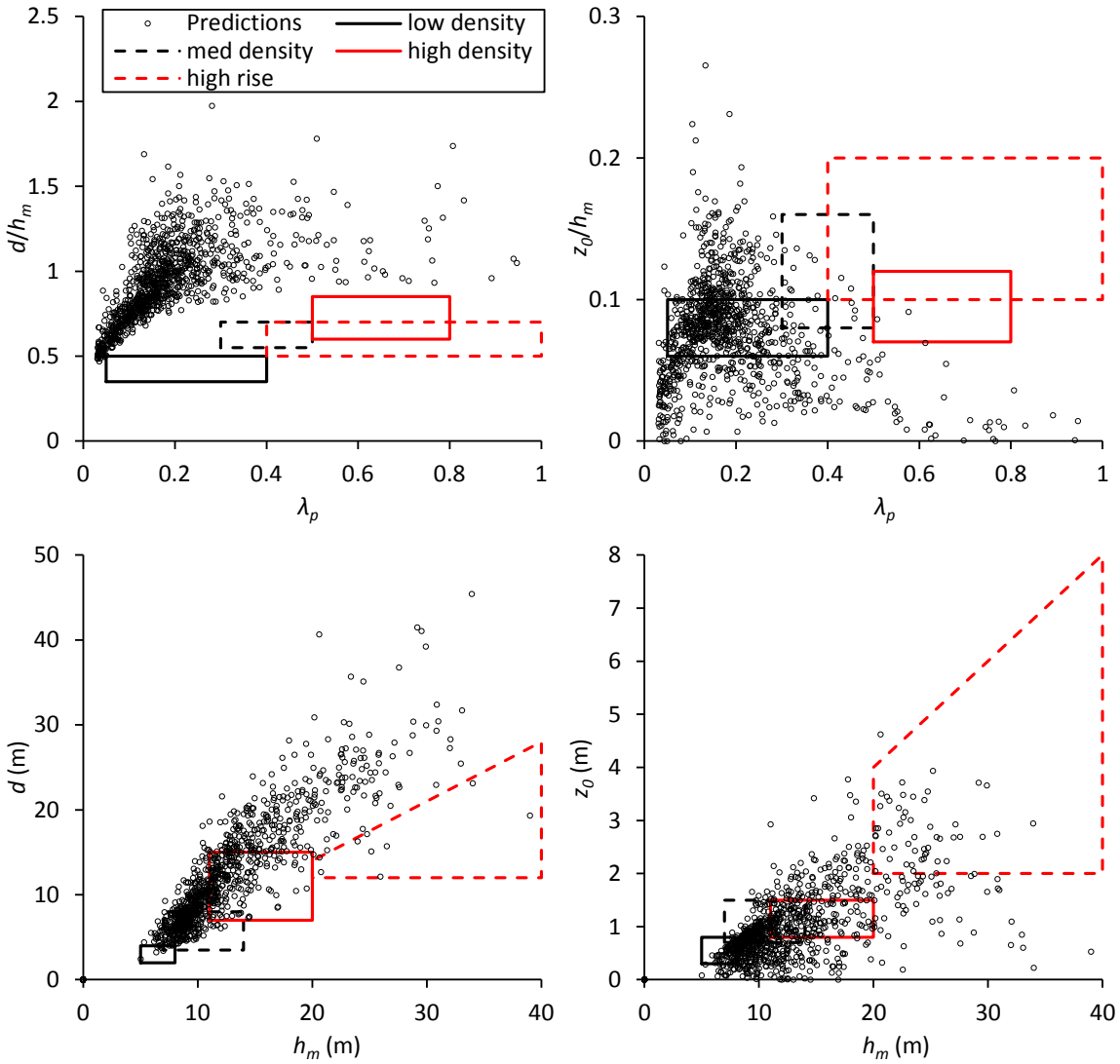

Figure 4-9: Plots of predicted (a) d/h_m, (b) z_0/h_m, (c) d, and (d) z_0 for the neighbourhoods of Leeds. Boxes indicate the ranges suggested in the tables of Grimmond and Oke (1999) for four different categories of urban area, which can be determined based upon plan area density (top; their table 7) or mean building height (bottom; their table 6).

predicted values of d/h_m are significantly higher than those given in the tables. This is because the model of Chapter 3 allows d to become larger than h_m for surfaces of heterogeneous height, which is consistent with experimental data, as discussed in Section 1.4.3.4.

It is evident from Figure 4-9 (c-d) that the current predictions compare better with the height based tables of aerodynamic parameters, suggesting these may be more appropriate for UK cities. This may be because the ranges in the λ_p based table are unsuitable for UK cities – for example in Leeds the vast majority of the neighbourhoods have a λ_p value that

places them in the 'low density' category. Clearly however, even when using the height based table some significant discrepancies remain – predictions of d are still generally greater than values from the table, and although many of the predicted values of z_0 fall into the ranges given in the table the scatter results in many also laying far outside.

Overall this comparison demonstrates that there is a wide range of geometric parameters that greatly influence the aerodynamics of urban areas and that the most significant of these must be accounted for if reasonably accurate estimates of aerodynamic parameters are to be made.

4.3.3 The relative importance of geometric details

In this section, an investigation is made into the relative importance of the different geometric parameters in predicting aerodynamic parameters for Leeds. This is achieved by systematically excluding different geometric parameters from the morphometric models inputs, and hence the sensitivity of the predictions to the level of simplification of the urban geometry is examined. Specifically, the various simplified arrays illustrated in Figure 4-5 are used to represent neighbourhood regions. Although essentially this investigation is considering the sensitivity of the morphometric model to geometric details, as the predictions have been validated over a variety of different arrays this is likely to be informative of real aerodynamic processes.

In this remainder of this Chapter, aerodynamic parameters predicted for Leeds that ignore height variability will include 'u' in the subscript, to indicate a uniform height array. Predictions that are made assuming square based blocks (i.e. ignoring building footprint shape) will include 'sq' in the subscript. For example, 'z_{0usq}' indicates roughness length predictions for arrays of square based blocks of uniform height (Figure 4-5 (a)), while 'z_0' continues to indicate predictions including the full range of model inputs (Figure 4-5 (c)).

Figure 4-10 (a) shows predictions of displacement height for Leeds with and without the inclusion of height variability. Note that, from Equation 3-14 and Equation 4-4, predictions of displacement height are not dependent upon building footprint shape, and hence $d_{usq} = d_u$ and $d_{sq} = d$. This assumption was necessary in the derivation of the model, although in reality there may be some dependence of displacement height upon building shape. In any

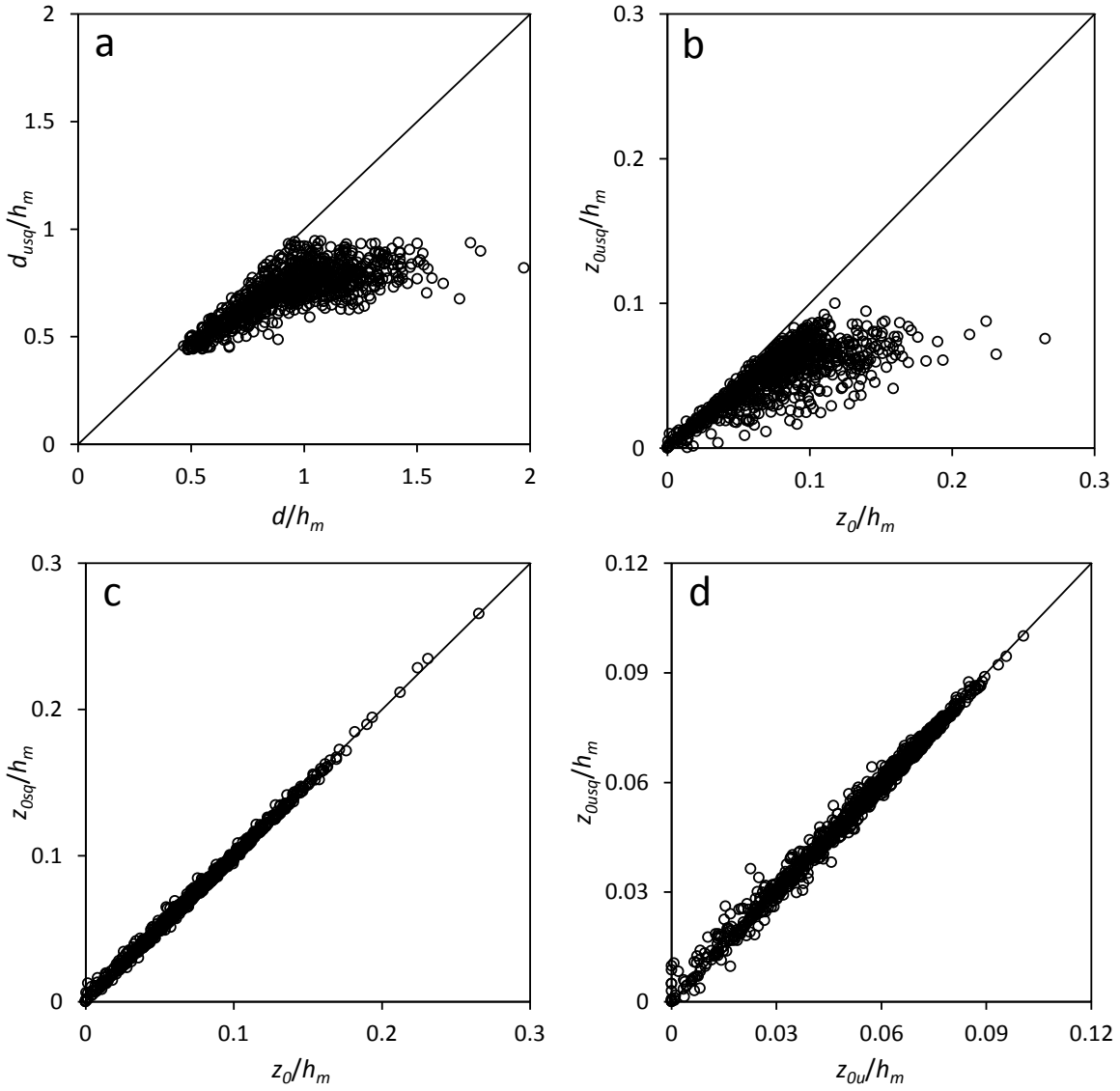

Figure 4-10: A comparison of displacement heights (a) and roughness lengths (b, c and d) predicted for the neighbourhoods of Leeds by considering different combinations of geometric parameters. The solid line indicates a one-to-one relationship.

case, it is clear from Figure 4-10 (a) that when height variability is not taken into account, the predicted displacement heights can be significantly lower.

In Figure 4-10 (b), it is apparent that predicted roughness lengths are also typically much lower when building height variability and footprint shape are not considered (z_{0usq}). However, when height variability is considered the predictions appear to have little sensitivity to building footprint shape (Figure 4-10 (c)). Bou-Zeid et al. (2009) came to a relevant conclusion after performing Large Eddy Simulations over a built-up area using three different, increasingly more detailed representations of the buildings. Each representation had the same value of λ_f and the same variation in building heights. They found a negligible

difference between the aerodynamic parameters of each representation, and concluded that it should be possible for urban canopy models based on density parameters to yield acceptable results. However, they did not explicitly emphasise that the models must consider the correct level of height variability, as this was constant in their three simulations.

Another interesting observation can be made from Figure 4-10 (d), which compares roughness length predictions for uniform height arrays with and without considering building footprint shape. The scatter in Figure 4-10 (d) is significantly larger than in Figure 4-10 (c). This implies that roughness length predictions are significantly more sensitive to building footprint shape for arrays of uniform height. A rational explanation for this follows from considering the well known skimming flow regime (Oke, 1988) described in Section 1.4.3.1. For uniform height arrays, the onset of skimming flow occurs when each building's wake begins to almost fully shelter the downstream building. As the building density increases further, there is a sharp decrease in roughness length. Consequently, the particular density at which this peak roughness occurs is highly sensitive to the particular building layout and the footprint shape (the latter is significant because the wake length is a function of all three dimensions of a building; Fackrell, 1984). Conversely, for arrays of heterogeneous height, the majority of the surface drag comes from the upper portions of the tallest buildings (Xie et al., 2008). The sheltering of these buildings is minimal and is not significantly influenced by variations in building shape or layout. Consequently, neither are the aerodynamic parameters of these types of array.

Overall, these results suggest that to accurately predict aerodynamic parameters of urban areas building height variability must be considered. Building layout and footprint shape may be relatively insignificant for areas which are reasonably heterogeneous in height, which is typically the case in real cities. In such areas it may be possible to make simple assumptions about building layout and footprint shape without significantly impacting on the accuracy of predicted aerodynamic parameters. This is a useful finding as even the most sophisticated morphometric models typically accept only average building aspect ratios and building spacing as inputs. Determining these averages for real urban environments can be problematic and potentially subjective. An additional implication of this is that it may be beneficial for future experimental work to place more emphasis on exploring the influence

of height variation upon surface aerodynamics than on that of building spacing, footprint shape and layout.

4.3.4 A simplified statistical model to quantify the influence of height variability on aerodynamic parameters

The implication of the previous section is that, along with the commonly used parameters λ_p and λ_f, urban aerodynamic parameters are potentially most sensitive to height variation. This was suggested to be the case in Section 1.4.3.4, and also Di Sabatino et al. (2008). However, in both this Thesis and Di Sabatino et al. (2008), height variation is parameterised using $\lambda_f(z)$, which is a relatively complex parameter to obtain for real city geometries and also quite involving to incorporate into flow models (although it has the benefit of offering a full description of the building height distribution). It would be more convenient if the influence of height variation upon aerodynamic parameters could be quantified via a simple parameter, such as the standard deviation of the building heights (σ_h), as this would allow the simplification of the current methodology. Therefore, in this section the relationship between the aerodynamic parameters predicted for Leeds and the geometric parameters λ_p, λ_f and σ_h is explored.

The differences between aerodynamic parameters predicted with and without considering height variation, $(d - d_u) / h_m$ and $(z_0 - z_{0u}) / h_m$, are shown scaled with σ_h in Figure 4-11. The data are separated into three different ranges of λ_p and λ_f, to demonstrate the dependence of the relationships upon building density. Significant scatter can be seen in the model predictions, even when building density and σ_h are fixed, which is primarily due to variations in the shape of the building height distributions. In addition, for z_0, this scatter is amplified because the influence of height variation depends upon the ratio, λ_p/λ_f as well as λ_f. However, for simplicity the influence of this ratio is ignored in the relationships formed later in this section.

Figure 4-11 shows that the influence of σ_h upon z_0 and d is predicted to increase with increasing building density. For z_0 this agrees with the findings of other authors (Kanda 2006; Zaki et al. 2011). However, for d it has been suggested that the influence of σ_h upon d decreases with increasing building density (Zaki et al. 2011). Figure 4-11 also shows that d increases slightly non-linearly with σ_h, although a linear approximation is reasonably

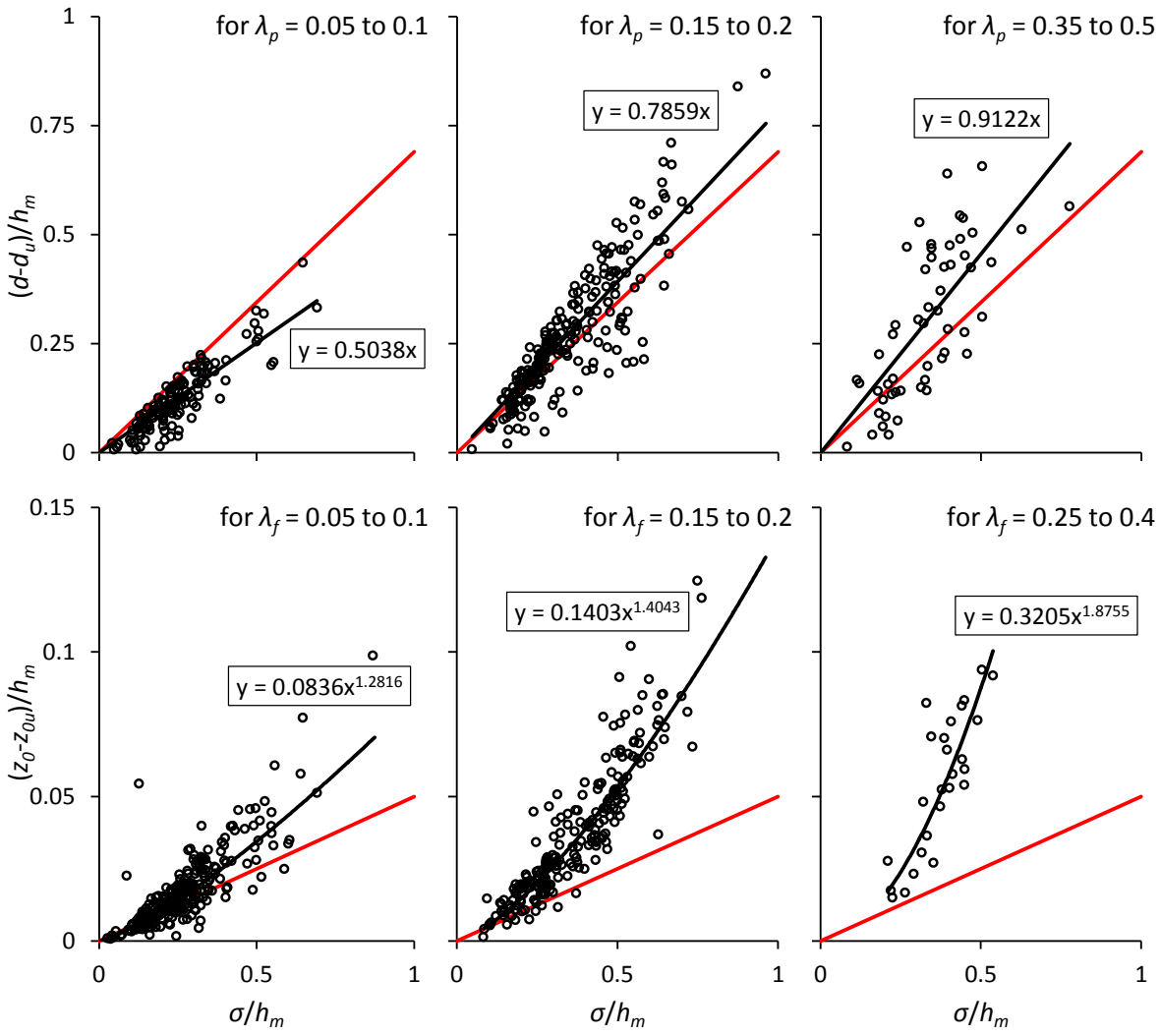

Figure 4-11: The relationship between standard deviation of building heights (σ_h) and predicted displacement heights (top), and roughness lengths (bottom). Data are separated into the ranges of plan area density (top) and frontal area density (bottom) shown in the legends. Equations shown are for the solid black regression lines, while the solid red lines are the relationships suggested by Jiang et al. (2008).

accurate, which is consistent with the findings of Jiang et al. (2008). Their particular relationship is also plotted, and it can be seen to be generally higher than the current predictions at low building densities, and lower at high building densities. In contrast, the non-linearity in the relationship between σ_h and z_0 is non-negligible. Therefore, the current predictions differ significantly from the relationship presented by Jiang et al. (2008).

A potential explanation for this nonlinearity is that the building height distributions of the neighbourhoods of Leeds generally become increasingly right-skewed as σ_h increases. The skewness, γ_1, can be calculated from:

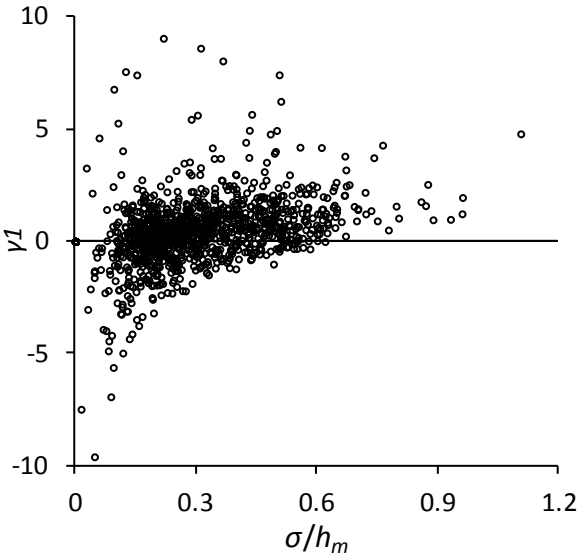

Figure 4-12: The 'skewness' of the building height distributions for the neighbourhoods of Leeds, plotted against the standard deviation of building heights.

$$\gamma_1 = \overline{\left(H_{pi} - \overline{H_{pi}}\right)^3} \Big/ \sigma_h^{\,3}$$

Equation 4-5

where H_{pi} is the height of each non-zero pixel in the neighbourhood region. As shown in Figure 4-12, γ_1 is found to have a significant, positive correlation with σ_h, implying that neighbourhoods with greater height variability typically have disproportionally many taller buildings. Consequently, as higher buildings dominate surface drag and significantly increase roughness, for real urban areas z_0 is observed to increase nonlinearly with increasing σ_h.

The analysis suggests that the following statistical equations are most appropriate to quantify the influence of σ_h upon z_0 and d:

$$\frac{d}{h_m} = \frac{d_u}{h_m} + F(\lambda_p)\frac{\sigma_h}{h_m}$$

Equation 4-6

and

$$\frac{z_0}{h_m} = \frac{z_{0u}}{h_m} + G(\lambda_f)\left(\frac{\sigma_h}{h_m}\right)^{H(\lambda_f)},$$

Equation 4-7

where F, G, and H, are functions of a density parameter, λ_p or λ_f. If the aerodynamic parameters of a neighbourhood region are estimated without considering height variation

(d_u and z_{0u}), then these simplified equations could potentially be used to correct for the influence of height variation using only σ_h.

Using a non-linear least squares method, Equation 4-6 and Equation 4-7 were fitted to the predicted aerodynamic parameters for all the neighbourhoods of Leeds for which $0.03 < \lambda_p < 0.5$. This density range is chosen as it is the range within which the model results are expected to be most reliable. A variety of suitable forms of the functions F, G, and H were investigated. These are shown in Table 4-1, along with values for the coefficients, *A*, *B* and *C*, resulting from a least squares fit. The final column gives the root mean squared relative error for each fit, multiplied by 100 to convert to percent, rmse (%).

It is evident from Table 4-1 that simplified predictions of z_0 and d using Equation 4-6 and Equation 4-7 are less accurate if the influence of height variation is considered to be independent of building density. This is particularly significant for z_0, for which the simplified predictions that assume G and H are constant, are about 6% less accurate overall than those that assume that G and H are functions of λ_f. Table 4-1 suggests that the most suitable, simplified equations to account for height variability when estimating aerodynamic parameters are:

$$\frac{d_{\mathrm{stat}}}{h_{\mathrm{m}}} = \frac{d_{\mathrm{u}}}{h_{\mathrm{m}}} + \left(0.2375\ln\left(\lambda_{\mathrm{p}}\right)+1.1738\right)\frac{\sigma_{\mathrm{h}}}{h_{\mathrm{m}}},$$

Equation 4-8

function form/s	*A*	*B*	*C*	rmse (%)
d				
F = A	0.7451	-	-	10.05
F = $A \ln(\lambda_p) + B$	0.2375	1.1738	-	9.00
F = $A\lambda_p^{\,B}$	1.298	0.3143	-	9.06
z_0				
G = A, H = B	0.1425	1.5353	-	17.37
G = $\exp(A\lambda_f) - 1$, H = $\exp(B\lambda_f)$	0.8867	2.3271	-	11.56
G = $A\lambda_f^{\,B}$, H = $\exp(C\lambda_f)$	0.7668	0.9065	2.0487	11.67

Table 4-1: The different forms of the functions F, G and H, used in Equation 4-6 and Equation 4-7 to attempt to simply estimate the influence of height variation upon aerodynamic parameters. The coefficients resulting from the best fit (*A*, *B* and *C*), and the overall error (rmse, %) are shown.

$$\frac{z_{0\mathrm{stat}}}{h_{\mathrm{m}}} = \frac{z_{0\mathrm{u}}}{h_{\mathrm{m}}} + \left(\exp\left(0.8867\lambda_{\mathrm{f}}\right) - 1\right)\left(\frac{\sigma_{\mathrm{h}}}{h_{\mathrm{m}}}\right)^{\exp\left(2.3271\lambda_{\mathrm{f}}\right)},$$

Equation 4-9

based upon the aerodynamic parameters predicted for the neighbourhoods of Leeds using the model developed in Chapter 3.

Figure 4-13 shows simplified predictions of aerodynamic parameters using Equation 4-8 and Equation 4-9 (d_{stat} and z_{0stat}), plotted against the predictions of the model of Chapter 3 obtained by using the height distributions from the building data. These equations appear to perform reasonably well considering the simplistic nature of the parameter, σ_{h}, which they rely upon. Therefore, they may be suitable for estimating aerodynamic parameters of vertically heterogeneous surfaces when a high degree of accuracy is not required. However, Figure 4-13 suggests that to estimate urban aerodynamic parameters accurately, it is necessary to use more comprehensive descriptors of height variability than σ_{h}, such as $\lambda_f(z)$.

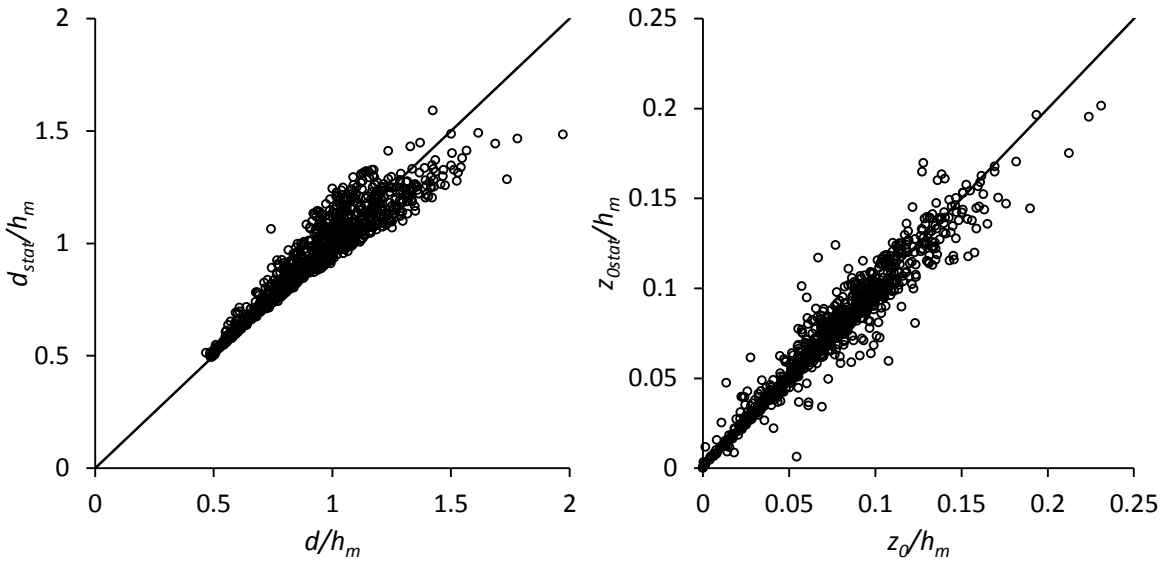

Figure 4-13: Simplified predictions of displacement height and roughness length using Equation 4-8 and Equation 4-9 (d_{stat} and z_{0stat}) compared with the predictions using the model developed in Chapter 3. The solid line indicates a one-to-one relationship.

4.4 Summary

In this Chapter, detailed 3-dimensional building data along with the morphometric model developed in Chapter 3 have been used to estimate the aerodynamic parameters of the city of Leeds. Firstly, a method was developed to divide the city domain into a heterogeneous

grid of neighbourhood regions, for the reasons discussed in Section 1.4.3.5. These regions were chosen to be of a relatively consistent geometry throughout in order for them to be appropriate for applying a morphometric model. The geometric parameters required by the morphometric model were then calculated from the building data for each neighbourhood.

The predicted aerodynamic parameters were compared with estimations made using standard tables of aerodynamic parameters (Grimmond and Oke, 1999). Considering the current predictions, as well as recent experimental work on variable height arrays, the values of displacement height reported in the tables appeared to be quite low. The current predictions compared better with the values in the height-based tables of aerodynamic parameters (Grimmond and Oke, 1999; their table 6) rather than those based on plan area density (their table 7), and hence those based on height may be more accurate for UK cities. However, overall the comparisons suggested that a wide range of geometric parameters must be considered if reasonably accurate estimates of aerodynamic parameters are to be made.

The importance of geometric details in determining aerodynamic parameters was then explored. The predicted displacement heights and roughness lengths were found to be substantially lower when building height variability was ignored from the analysis, highlighting the importance of this geometric characteristic in determining aerodynamic parameters. However, interestingly, building footprint shape only had a significant influence upon the predictions when height variability was not considered.

Finally, simple equations were developed to quantify the influence of height variation upon aerodynamic parameters via a simple description of the height variability, namely the standard deviation of building heights (σ_h). The equations appeared to perform reasonably well considering the simplistic nature of the parameter σ_h. However the differences between these predictions and those of the more complex approach highlighted the importance of considering the specific shape of the building height distributions.

Collectively, these results suggest that to accurately predict aerodynamic parameters of real urban areas their height variability must be considered in detail, but it may be possible to make simple assumptions about building layout and footprint shape without significantly impacting on the accuracy of the predictions. An additional implication of this is that it may be beneficial for future experimental work to place more emphasis on exploring the

influence of height variation upon surface aerodynamics than on that of building spacing, footprint shape and layout.

Although no formal validation of the methodology developed in this Chapter has been attempted, the validation of the wind atlas methodology developed in the following Chapters will allow for a wider evaluation of its accuracy.

5 Mapping the Wind Resource over UK Cities

5.1 Introduction and Objectives

In this Chapter, the model developed in the previous two Chapters is integrated into a Wind Atlas Methodology in order to estimate mean wind speeds (as a function of height) over a number of UK cities. The methodology builds upon that developed by the UK Met Office that was described in Chapter 1.

In order to explore the gains in predictive accuracy that may be made by considering the urban surface and boundary layer flow in greater detail, three different wind atlas methodologies are tested in the various cities. The most simple of these methods is the Met Office methodology (described in Section 1.3.3) and in addition two more complex methods are developed. These latter methods utilise maps of aerodynamic parameters derived from the modelling methods developed in Chapter 4, and they also consider wind directional effects. The predictions of each model are compared to measured meteorological data from a number of locations within each city in order to assess the predictive accuracy.

The structure of the Chapter is as follows: (i) First, in Section 5.2, the three different wind methodologies are described in detail, (ii) subsequently the data used to evaluate the models is described in Section 5.3, including details of the site locations, (iii) results are then presented in Section 5.4 in order to compare the accuracy of each of the models and explore the source of model errors, (iv) and finally the most important findings of the Chapter are summarised in Section 5.5.

5.2 Wind Atlas Methodologies

5.2.1 The UK Met Office methodology

The first methodology used in this Chapter is that of the UK Met Office that formed the bases of the Carbon Trust Wind Estimator (Section 1.3.3; Figure 1-4), and hence this is refered to as ‘model CT’ throughout the Chapter. As described previously, this model obtains estimates of wind speeds by scaling unadjusted wind speeds from a regional wind climate (the NCIC database) up to a height at which the frictional effect of the surface is

negligible, then scaling back down accounting for the effect of the surface roughness upon the wind profile. This process is achieved via three scaling stages using Equation 1-5, Equation 1-6 and Equation 1-7.

One additional aspect of the model that was not discussed in Section 1.3.3 is the issue of predicting wind speeds in the canopy layer. Within this layer the flow is highly complex and spatially variable, and the logarithmic profile is not appropriate for describing wind speeds (as was described in Section 1.4.2.2). Wind speeds here are generally be too low for turbines to operate, however an approximation of the canopy layer wind profile can be made using an exponential function (Macdonald, 1998), namely:

$$U_{\mathrm{hub}} = U_{\mathrm{hm\text{-}local}} \exp\left[9.6\lambda_{\mathrm{f}}\left(z_{\mathrm{hub}}/h_{\mathrm{m\text{-}local}} - 1\right)\right],$$

Equation 5-1

where $U_{\mathrm{hm\text{-}local}}$ is the wind speed at the local mean building height ($h_{\mathrm{m\text{-}local}}$), obtained using the logarithmic profile, and λ_{f} is the fontal area density of the local area. Here, the Carbon Trust tool assumes values for λ_{f} of 0.2 and 0.3 for suburban and urban local terrain types, respectively. This exponential profile is illustrated in Figure 5-1 (top).

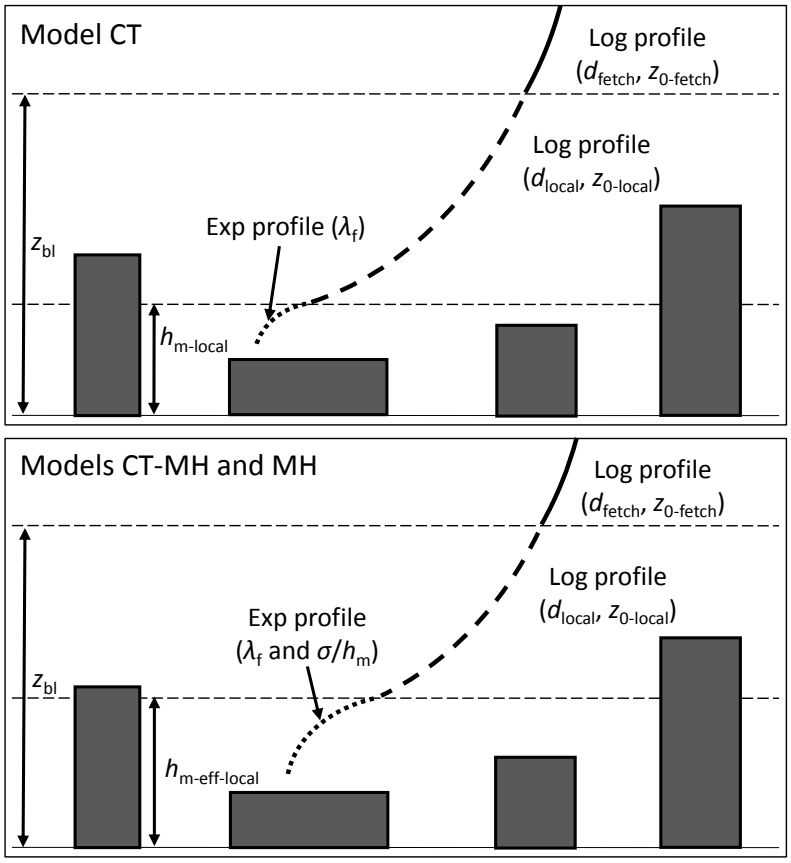

Figure 5-1: Illustration of the down-scaling process used by the methodologies to hub heights below the canopy top. Parameters controlling the profiles are given in brackets.

5.2.2 Improving estimates of surface aerodynamic parameters

5.2.2.1 Estimating roughness length and displacement height using detailed building data

The second methodology investigated (referred to as model CT-MH in this Chapter) uses the same process as model CT in order to correct a regional wind atlas for the effects of the surface roughness upon the wind profile. However, the roughness lengths and displacement heights input into model CT-MH are estimated using the method developed in Chapter 4, utilising the Landmap 'building heights' dataset. The method of the previous Chapter is used to calculate these maps of aerodynamic parameters for each of the cities on two different grids: a fine uniform grid (of 250 m resolution) and a coarse uniform grid (of 1 km resolution). These maps of aerodynamic parameters are then used to represent the *local* and *regional* scale aerodynamic parameters, respectively. This means that parameters from these 250 m resolution maps are used in Equation 1-7 for $z_{0\text{-local}}$ and d_{local}, and parameters from the 1 km resolution maps are used in Equation 1-6 for $z_{0\text{-fetch}}$ and d_{fetch}. Note that the reason these uniform grids are used, rather than Chapter 4's adaptive grid, is so that method CT-MH remains consistent with that of the Met Office.

In order to implement this model the method of Chapter 4 must be extend slightly, as it is not appropriate for estimating the aerodynamic parameters of neighbourhoods with either very low or very high densities of buildings. This makes it necessary to estimate the aerodynamic parameters of these regions via other means in order to give a complete parameterisation of the cities' aerodynamics. Consequently, for neighbourhoods with $0.03 < \lambda_p < 0.75$, the method of Chapter 4 is used, while for low or high density regions we assume the following values of z_0 and d:

(i) when $0.01 < \lambda_p < 0.03$, the neighbourhood is considered to be a 'low density urban' area, and hence we assume: $d/h_m = 0.35$ and $z_0/h_m = 0.06$, based on the recommendations in Grimmond and Oke (1999),

(ii) when $\lambda_p < 0.01$, the number of buildings in the neighbourhood is assumed to be negligible, and hence we assume aerodynamic parameters appropriate for open terrain: $d = 0$ and $z_0 = 0.14$ m (Best et al., 2008),

(iii) when $0.75 < \lambda_p < 1$, we assume the neighbourhood consists mostly of woodland, as built areas very rarely become this densely packed, and hence we assign aerodynamic

parameters: $d/h_m = 0.67$ and $z_0 = 1$ m, based on the values in Best et al. (2008) and Wieringa (1993).

There is of course a significant degree of uncertainty in these chosen values, and there are potentially other factors that could be considered to gain more accurate parameter estimates, such as the specific land use within areas for which $\lambda_p < 0.03$. However, this could require a detailed inspection of the neighbourhood regions on a case-by-case basis, which is impractical to carry out for multiple cities. Fortunately, the uncertainties in these assumptions are likely to have only a small influence upon the overall wind resource assessment, as for well over 90% of the neighbourhood regions in the cities studied here, $0.03 < \lambda_p < 0.75$.

It is also important to highlight that when the method of Chapter 4 is used to estimate aerodynamic parameters, the surface roughness becomes a function of the incoming wind direction. Moreover, the sensitivity of surface roughness to wind direction in real urban areas can be significant (Barlow et al., 2008). The reason for this can be understood by considering a region of terraced housing: when the wind blows parallel to the buildings the flow may channel down the streets, and hence the surface may appear less rough to the wind flow than it would if the wind direction were perpendicular to the buildings, as in this case the blockage to the flow may be greater.

Consequently, when using model CT-MH, wind speed predictions for eight compass wind directions are made: N, NE, E, SE, S, SW, W and NW. In order to then obtain the final averaged wind speed predictions, a weighted average of these directionally dependent predictions is calculated, with the weighting based upon the temporal frequency of the wind from each of the eight compass directions as recorded at a nearby reference station. These stations are described in Section 5.3.

5.2.2.2 Other modifications to the UK Met Office methodology

There are a number of other aspects of model CT-MH that differentiate it from model CT. The first of these relates to the regional wind climate, for which the freely available NOABL database (www.bwea.com/noabl) is used in model CT-MH, rather than the commercially licensed NCIC database. Secondly, the blending height is set to twice the *local* mean building height in model CT-MH, rather than the maximum height on a regional scale as in model CT.

This is potentially a more appropriate blending height than that used in model CT, as the near surface flow over urban areas may adapt to the local underlying geometry over a relatively short distance, similar to the 250 m length-scale of the local neighbourhood regions used here (see Section 1.4.4). The two final differences, described below, are relevant only to wind speed predictions made close to, or below the top of the building canopy.

In the second stage of downscaling using model CT-MH the logarithmic profile is only used down to the local 'effective mean building height' ($h_{\text{m-eff}}$), rather than the local mean building height as in model CT. This is illustrated in Figure 5-1 (bottom). This height, $h_{\text{m-eff}}$, was introduced in Section 3.4.3 as a method of modifying the normal mean building height to account for the disproportionate effect of tall buildings upon the wind flow in areas where buildings are of heterogeneous height. It is predicted alongside z_0 and d by the method of Chapter 4.

Below $h_{\text{m-eff}}$ an exponential profile is used to describe the canopy layer wind profile, as in model CT. However, a slight modification is made to Equation 5-1 to account for the influence of height variation upon the wind profile (Jiang et al., 2008):

$$U_{\text{hub}} = U_{\text{hm-eff-local}} \exp\left[9.6\lambda_{\text{f}}\left(1-\sigma_h/h_{\text{m-local}}\right)\left(z_{\text{hub}}/h_{\text{hm-eff-local}}-1\right)\right].$$

Equation 5-2

Here, $U_{\text{hm-eff-local}}$ is the wind speed at $h_{\text{m-eff-local}}$ obtained from the log profile, and σ_{h} is the standard deviation of the building heights in the local neighbourhood. Both σ_{h} and λ_{f} are easily obtained directly from the building data using the methodology of Chapter 5.

5.2.3 Incorporating the influence of changing wind direction

The most detailed wind atlas methodology implemented (referred to as 'model MH') is the same as model CT-MH except for two significant modifications. These are made to account for the influence of incoming wind direction upon the wind profile. An illustration of the model is shown in Figure 5-2.

Firstly, model MH accounts for the influence of incoming wind direction by describing the height of the UBL as a function of the distance from the upwind edge of the city (X; as illustrated in Fig. 1), rather than setting it to a constant as in models CT and CT-MH. This

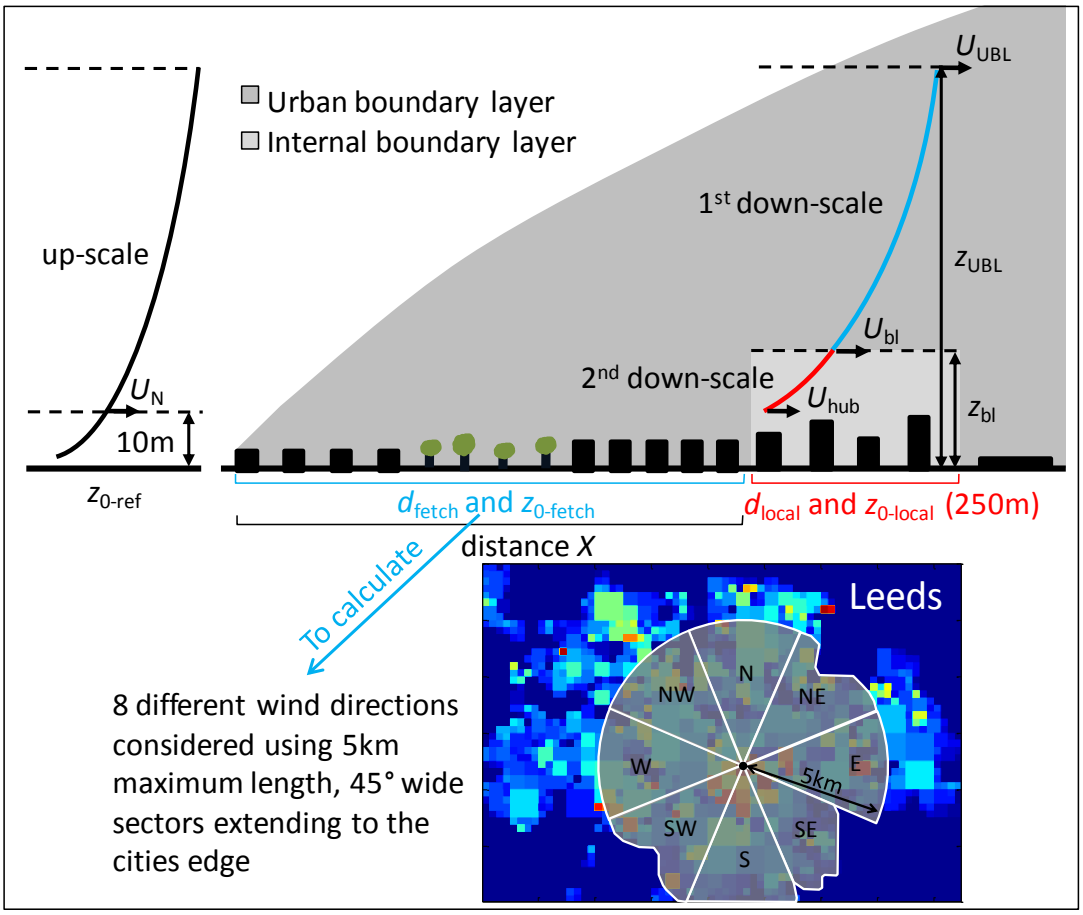

Figure 5-2: Schematic diagram of the wind atlas methodology referred to as model MH.

reflects the physical process of boundary layer growth, which occurs due to the fact that as the flow travels further into the city, vertical turbulent mixing leads to the frictional influence of the surface roughness extending upwards (Best et al., 2008). The estimation of this height is made using the formula of Elliot (1958) for boundary layer growth, limited to a realistic, maximum height of 500 m (Britter and Hanna, 2003; Best et al., 2008):

$$z_{UBL} = \min\left\{ z_{0-fetch}\left[0.65 - 0.03\ln\left(z_{0-fetch}/z_{0-ref}\right)\right]\left[\frac{X}{z_{0-fetch}}\right]^{0.8}, \quad 500 \right\}.$$

Equation 5-3

Here, $z_{0\text{-ref}}$ and $z_{0\text{-fetch}}$ are included in the formula of Elliot (1958) as they are the appropriate values for the roughness lengths 'upwind' and 'downwind', respectively, of the roughness change, which is the edge of the city. Additionally, the constant of 0.65 has been modified slightly from its original value of 0.75, as recommended by the Met Office (Best et al., 2008). It should be noted that determining the exact edge of a city, and hence *X*, can be quite

subjective. However, the predicted wind speeds have a very low sensitivity to *X*, with the exception of those within a few hundred metres from the upwind city edge.

Secondly, model MH accounts for the influence of the incoming wind direction in the calculation of the aerodynamic parameters $z_{0\text{-fetch}}$ and d_{fetch} that are used in Equation 1-6. These parameters are calculated by considering the aerodynamics of the upwind urban surface, rather than using regional (1 km scale) values as in models CT and CT-MH. The extent of the upwind area that is considered in the calculation is a 45° wide sector extending either to the city's edge or a maximum length of 5 km, as illustrated in Figure 5-2. The 5 km maximum sector length is chosen as Equation 5-3 suggests this is about the distance required for a fully developed UBL to develop (500 m deep) after a typical rural ($z_0 \approx 0.14$ m) to urban ($z_0 \approx 1$ m) surface cover change. Varying this maximum length between 4 km and 7 km had a negligible influence upon the results.

For each wind direction, $z_{0\text{-fetch}}$ is calculated from the values of roughness length lying within the upwind sector by applying a blending method to estimate the average, area-weighted frictional effect of the surface in that sector (Bou-Zeid et al., 2007). The roughness lengths input into the blending method are derived from building data using the same method that was used for model CT-MH (i.e. that of Chapter 4). However, they are now calculated for neighbourhood regions determined by an *adaptive* grid as described in Chapter 4, rather

		Method		
		CT	**CT-MH**	**MH**
Parameters	U_N	NCIC	NOABL	NOABL
	$z_{0\text{-ref}}$	0.14 m	0.14 m	0.14 m
	z_{UBL}	200 m	200 m	calculated from Eq. 5.3
	d_{fetch} and $z_{0\text{-fetch}}$	from the 1 km resolution aerodynamic parameter map	from the 1km resolution aerodynamic parameter map	calculated for eight different wind directions from the aerodynamic parameters lying within each sector
	z_{bl}	twice the maximum canopy height in the 1km neighbourhood	$2h_m$ (from the 250m resolution map)	$2h_m$ (from the 250m resolution map)
	d_{local} and $z_{0\text{-local}}$	based upon local terrain type	from the 250 m resolution aerodynamic parameter map	from the 250 m resolution aerodynamic parameter map

Table 5-1: Summary of the input parameters used in each methodology.

than a uniform grid. Unfortunately, there are no equivalent blending methods available to calculate an appropriate displacement height for use as d_{fetch}. Therefore, for each wind direction, d_{fetch} is simply calculated as the arithmetic mean of the displacement height values from the adaptive grid lying within the upwind sector. A summary of the differences in the input parameters used in each of the three models is given in Table 5-1.

5.2.4 Comparisons with the model of Drew et al. (2013)

It is useful to now discuss the methodology of Drew et al. (2013) alongside that of the Met Office and the current Chapter. With respect to model CT of the Met Office, Drew et al. (2013) make a number of improvements, such as incorporating the influence of wind direction, using detailed building data to derive aerodynamic parameters (as opposed to land use data), and accounting for the effect of the upwind fetch upon the wind profile rather than basing estimations of wind profiles upon only the local 1 km area. These particular three factors are also incorporated into model MH.

However, in contrast to models CT, CT-MH and MH, Drew et al. (2013) use a single downscaling profile, rather than considering two separate layers of flow affected in turn by the regional and local areas. There are also a number of other factors treated in a more detailed manner by model MH, with respect to Drew et al. (2013). For example, Model MH considers both building height variation and vegetation when estimating surface aerodynamic parameters, and the resolution of model MH is slightly higher as it uses 250 m scale neighbourhoods in the second downscaling stage (shown in Figure 5-2). This approach, however, means the model of Drew et al. (2013) could be applied to other cities more easily and quickly than model MH.

5.3 Validation Datasets

5.3.1 Site locations

To evaluate the accuracy of the three models to be tested, measured wind speed data from a number of UK cities is used, namely Edinburgh, Leeds, Manchester, Nottingham, and Warwick/Leamington Spa. The locations of the cities range from the Midlands of England to the East coast of Scotland, as shown in Figure 5-3, and their sizes range from around 25 km^2 (Warwick) to over 500 km^2 (Manchester). These cities were chosen partially as they span a

Figure 5-3: Locations of the UK study sites of the current work. Map courtesy of Digimap (©Crown Copyright/database right 2012. An Ordnance Survey/EDINA supplied service).

broad range of UK city types but also due to the availability of appropriate meteorological data to evaluate the methodologies.

The data used for the model evaluation were obtained from various measurement campaigns, including the Warwick Wind Trials (Encraft, 2009) and several University and Met Office (MIDAS) weather stations (including the Edinburgh School of GeoSciences

Weather Station, www.geos.ed.ac.uk and the Whitworth Meteorological Observatory, www.cas.manchester.ac.uk). Once these data were collated, mean wind speeds measured at 21 anemometers spread over the 5 cities were available to evaluate the models. Each site was at an independent geographical location, with the exception of those at Leeds University and Leeds City Council (two anemometers at different heights) and those at Eden, Southern and Aston Court (two anemometers at different locations).The sites cover a range of building types, from two-story suburban properties to medium-rise city-centre buildings and high-rise blocks of flats, and they lie within local areas that can broadly be categorised as residential, industrial, university campus or city centre. Basic information on each of the sites is given in Table 5-2.

Site name	Location	Local area	Used for	Measurement period (yrs)	% Data capture	Original source
UofL (8m)	Leeds	University	Validation	1.92	86	University of Leeds
UofL (12m)	Leeds	University	Validation	1.92	86	University of Leeds
LCC (12m)	Leeds	Industrial	Validation	2.33	98	Leeds City Council
LCC (32m)	Leeds	Industrial	Validation	2.33	98	Leeds City Council
Church Fenton	20km E of Leeds	Airport	Reference	5	99	MIDAS site 533
Lillington Road	Leamington Spa	Residential	Validation	0.95	100	Warwick wind trials
Hill Close Gardens	Warwick	Residential	Validation	0.98	100	Warwick wind trials
Princess Drive	Leamington Spa	Industrial	Validation	0.67	93	Warwick wind trials
Eden Court 1	Leamington Spa	Residential	Validation	0.88	89	Warwick wind trials
Eden Court 2	Leamington Spa	Residential	Validation	0.88	89	Warwick wind trials
Southorn Court 1	Leamington Spa	Residential	Validation	0.96	100	Warwick wind trials
Southorn Court 2	Leamington Spa	Residential	Validation	0.96	92	Warwick wind trials
Ashton Court 1	Leamington Spa	Residential	Validation	0.78	100	Warwick wind trials
Ashton Court 2	Leamington Spa	Residential	Validation	0.84	91	Warwick wind trials
Coventry	12km N of Warwick	Residential	Reference	5	99	MIDAS site 24102
EdiWeaSta	Edinburgh	University	Val & Ref	5	98	University of Edinburgh
Napier	Edinburgh	University	Validation	0.89	95	Warwick wind trials
Holme Library	Manchester	City centre	Val & Ref	5	100	MIDAS site 18904
Whitworth	Manchester	University	Validation	0.79	99	University of Manchester
Sacksville St.	Manchester	City centre	Validation	1	100	University of Manchester
Watnall	Nottingham	Residential	Val & Ref	5	100	MIDAS site 556
University	Nottingham	University	Validation	1	100	Warwick wind trials
Delta Court	Nottingham	Residential	Validation	0.68	91	Warwick wind trials

Table 5-2: Basic information on the measurement locations used as validation and/or a reference sites. UofL and LCC refer to the University of Leeds and the Leeds City Council, respectively.

5.3.2 Measurement details

The time period over which measurements were made at each site varied, as did the data coverage within each period. However, the measurement periods all lay within the five year period from 01/08/06 - 01/08/11. In order for each of the measured wind speeds (U_{msr}) to correspond to a consistent time period each was extrapolated to be representative of this five year period (U_{5yr}) by using a simple correction factor accounting for the seasonal and annual variation in wind speed at a local reference site. This factor was calculated by taking the reference site's measured, five-year mean wind speed and dividing this by the mean wind speed measured at the reference site within the time period corresponding to the measurements taken at the validation site. For Edinburgh, Manchester and Nottingham, there were validation sites which had over 99% data coverage for the five year period, and hence these were appropriate to also be used as reference sites. For Leeds and Warwick, Met Office weather stations which were located a short distance outside each city and had continuous data coverage over the five years were chosen as reference sites. Further details on these reference sites are recorded in Table 5-2 alongside the information on the validation sites.

Details of the local geometry at each site are recorded in Table 5-3, including the anemometer mast height (H_{mast}), the building height (H), the local mean building height ($h_{m\text{-}local}$), and the local effective mean building height ($h_{m\text{-}eff\text{-}local}$). These values of H, $h_{m\text{-}local}$ and $h_{m\text{-}eff\text{-}local}$ were calculated from the same Landmap sourced building data that is used to derive the aerodynamic parameters. It can be seen that the effective mean building height is always greater than the mean building height.

For the majority of the validation sites the above ground measurement height (z_{hub}) is simply taken to be the sum of the anemometer mast height (H_{mast}) and the building height (H). For the remaining sites, as the masts were not located on the highest part of the building roofs, z_{hub} is set to be the sum of H and the height that the anemometer mast protrudes above the roof. Based upon the local geometrical details in Table 5-3, sites are then classified as '*sheltered*' if the measurement height is lower than the local mean building height ($z_{hub} - h_{m\text{-}local} < 0$) or if the measurement height is within 2 m of the building's height ($z_{hub} - H < 2$). Any site not classified as sheltered is classified as '*exposed*'. The 2 m threshold mast height could be considered a slightly ambiguous choice, but it is difficult to determine this value by an objective criteria. However, it is useful to note that if the threshold were raised to 3 m or reduced to 1.5 m, then only 1 or 2 sites, respectively, would be classified differently.

Site name	Heights (m)			
	H	H_{mast}	$h_{m\text{-}local}$	$h_{m\text{-}eff\text{-}local}$
UofL (8m)	23	6	23.6	28.3
UofL (12m)	23	10	23.6	28.3
LCC (12m)	-	16.5	13.8	17.8
LCC (32m)	-	32	13.8	17.8
Lillington Road	8.1	1.5	7.6	10.8
Hill Close Gardens	-	4	7.7	10.4
Princess Drive	8.5	1.5	6.7	10.9
Eden Court 1	30.7	5	11.3	19.8
Eden Court 2				
Southorn Court 1	8.8	5	11.3	19.8
Southorn Court 2				
Ashton Court 1	10.8	5	6.4	9.1
Ashton Court 2				
EdiWeaSta	33	1.2	23.3	29.3
Napier	32	2	22.8	33.8
Holme Library	19	3.1	11.8	15.6
Whitworth	42	5	17.5	22.6
Sacksville St.	45	2.6	33.7	48.2
Watnall	-	10	9.7	12.0
University	14	3	22.6	31.8
Delta Court	16	3	12.8	20.2

Table 5-3: Geometric characteristics at the validation sites. Italics indicate sheltered sites.

5.3.3 Implementing the models

To test the accuracy of each of the three models, wind speed predictions are made at the above ground measurement height, z_{hub}, for each of the validation sites in Table 5-2.

To obtain predictions using model CT it was necessary to specify the inputs of 'local terrain type' and 'canopy height' in the online user interface, in addition to the sites location and the above ground height. In order to choose the most appropriate local terrain type for each site from the available categories, aerial photography from Google Earth© is used to visually assess the local urban geometry. The local canopy height was then specified in two different ways: (i) using the default canopy height given by the tool for the particular local terrain type selected, and (ii) using the local mean building height ($h_{m\text{-}local}$) calculated from the Landmap building data. In the remainder of this Chapter these predictions are referred to as 'CT_{dft}' and 'CT_{hm}', respectively.

In order to make predictions with models CT-MH and MH, the methodologies are implemented using Matlab© to give mean wind speed predictions as a function of height for each city on a square, 250 m resolution grid. The mean wind speeds predicted for each validation site are easily obtained from these maps by determining which grid square each site lies within and then extracting the predicted wind speed at the corresponding measurement height.

5.4 Results and Discussion

5.4.1 Model evaluation

To evaluate the accuracy of each methodology, Figure 5-4 shows scatter plots of the predicted (U_{pre}) vs measured (U_{5yr}) wind speeds from all the validation sites. The figure suggests that the wind speed predictions for these sites generally become more accurate when more complex methodologies are implemented. This is particularly evident for the exposed sites. To test this conclusion the mean percentage errors are calculated:

$$\%\text{Error} = 100 \times \frac{1}{n} \sum \frac{\left| U_{pre} - U_{5yr} \right|}{U_{5yr}}$$

Equation 5-4

and the mean absolute error:

$$\mathrm{MAE} = \frac{1}{\mathrm{n}}\sum\left|U_{\mathrm{pre}} - U_{5\mathrm{yr}}\right|$$

Equation 5-5

where n is the number of sites. To calculate these errors the summations are made over all sites, and also for the exposed and sheltered sites separately, with the results summarised in Figure 5-5. Two different metrics are considered as each provides different sensitivities (Weekes and Tomlin, 2013), and therefore it is useful to compare multiple metrics to test the robustness of the conclusions. For example, the %Error is more sensitive to errors at lower wind speed sites than the MAE.

Figure 5-5 confirms that the accuracy of the predictions increases with the level of detail included in the methodologies. The figure shows that for the chosen validation sites the predictions of the Carbon Trust Tool can be improved significantly (by about 8% and 0.2 ms^{-1} in %Error and MAE, respectively) by overriding the default canopy height with the local

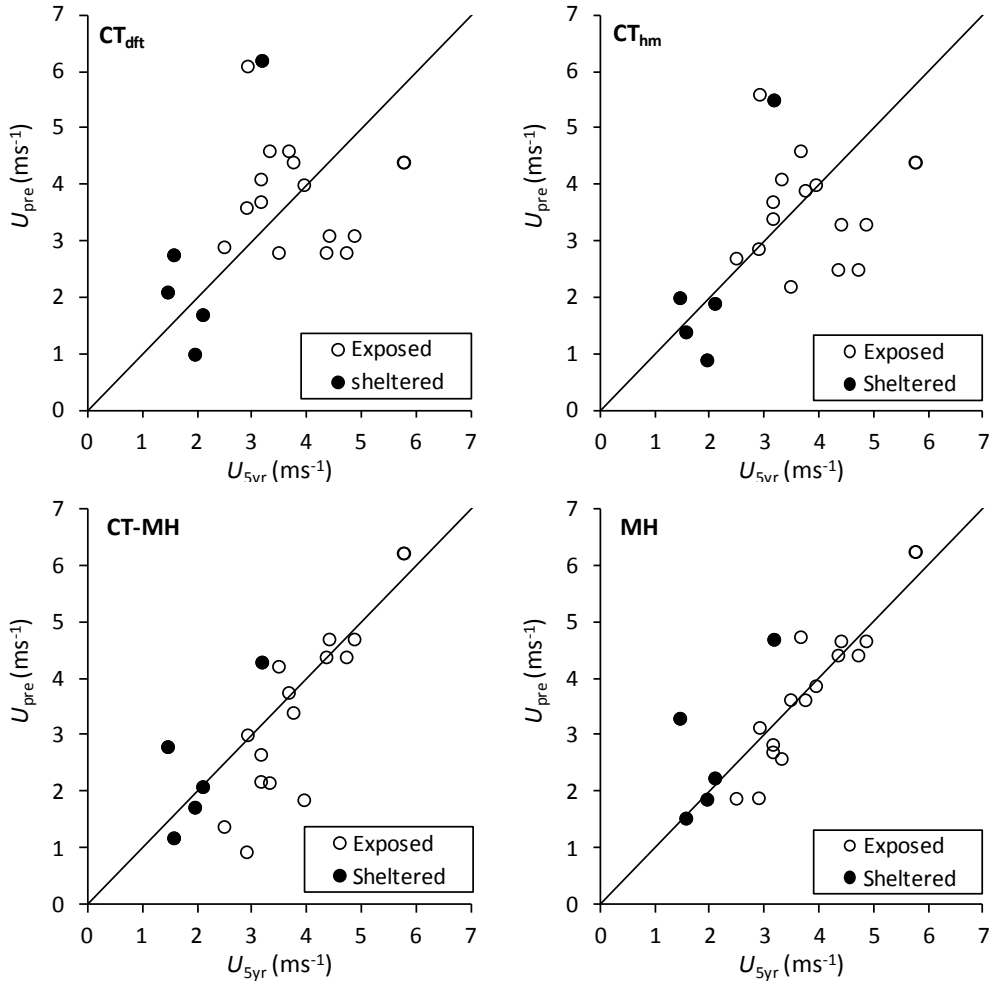

Figure 5-4: Comparisons of predicted (U_{pre}) and measured, 5 year corrected ($U_{5\mathrm{yr}}$) wind speeds for each methodology.

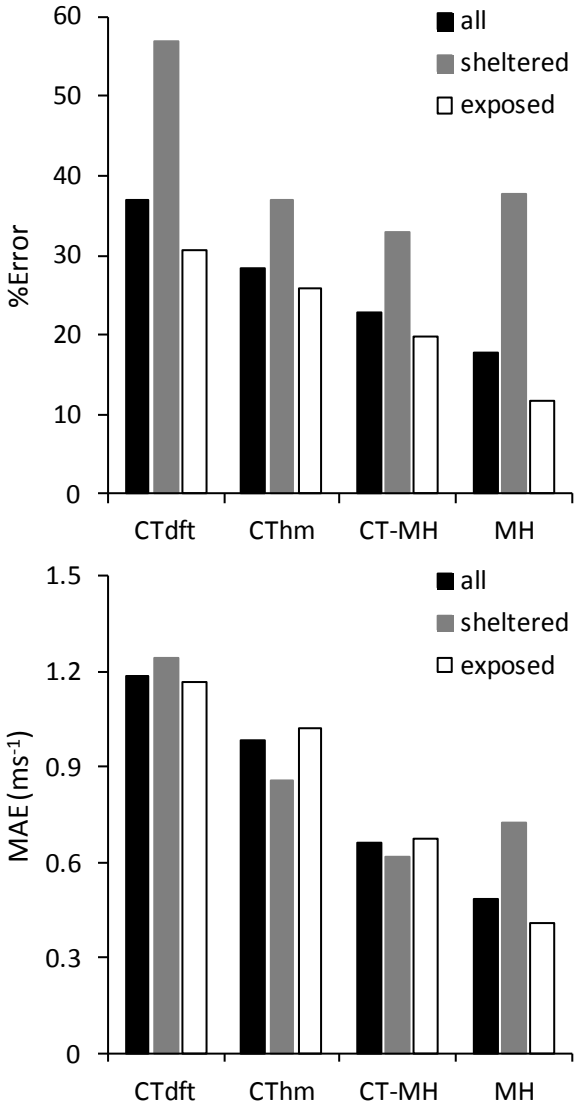

Figure 5-5: Average percentage errors (top) and mean absolute errors (bottom) calculated using each methodology over all the validation sites and also the sheltered and exposed sites separately.

mean building height calculated from the building data. When model CT-MH is used there is a further reduction in overall errors of about 5% and 0.3 ms^{-1}, which can be attributed to the more detailed manner in which surface aerodynamic characteristics are calculated i.e. through the use of detailed building data as opposed to land use data. An additional reduction in errors of about 5% and 0.2 ms^{-1} is achieved when model MH is used, which highlights the advantages of thoroughly considering the influence of wind direction upon wind profiles in a prediction methodology. However, it is clear from Figure 5-4 that even when using model MH the maximum and minimum errors are still significant.

Weekes and Tomlin (2013) also considered the accuracy of the Carbon Trust tool in predicting mean wind speeds relevant to small-scale wind turbines. They also concluded that the accuracy of wind speed predictions can be increased significantly by considering a larger surrounding area in the calculation of aerodynamic parameters and accounting for the frequency of winds occurring from each direction.

It is important to also consider the variation in the performance of the models between the sheltered and exposed sites. It is evident from Figure 5-5 that the methodologies generally perform better at the exposed sites, which is entirely as expected as the sheltered sites lie in complex regions of flow where wind speeds are influenced strongly by individual buildings. Local effects such as these are difficult to quantify without complex fluid dynamics (CFD) modelling (as concluded in Chapter 2), and hence the current methodologies are only expected to predict wind speeds at exposed sites with good accuracy. A useful observation is that if the accuracy of each methodology at just the exposed sites is considered, then the enhanced performance of model MH is more pronounced. Specifically, for the exposed sites the %ERROR and MAE using model MH are 11.7% and 0.41 ms^{-1}, respectively, while the errors resulting from the use of model CT_{dft} are 30.7% and 1.17 ms^{-1}.

To determine if any bias exists in the predictions of each model, box plots are shown in Figure 5-6 of the residual errors, defined as U_{5yr} - U_{pre}. These show that the predictions of

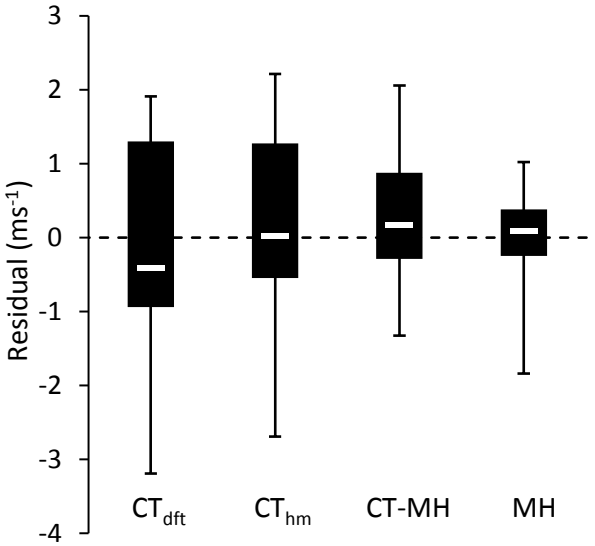

Figure 5-6: Box plots of residual errors (ms^{-1}) calculated over all the validation sites. These show the inter-quartile range (black boxes), the median (white horizontal dashes) and the maximum and minimum errors (error bars).

models CT_{hm} and MH are relatively unbiased, but model CT_{dft} has a tendency towards overestimations and CT-MH towards underestimations. The bias in model CT_{dft} is most likely due to the fact that the default local mean building heights given by the tool are generally lower than those calculated from the building data. Consequently the local roughness length and displacement height used in the model can potentially be quite low compared to those used in the other methodologies. For model CT-MH the underestimates are likely to occur because only a 1 km surrounding area is considered in the calculation of $z_{0\text{-fetch}}$. This means that in complex urban areas of high surface roughness, the values calculated for $z_{0\text{-fetch}}$ can be quite high relative to those that would be obtained if a larger, more realistic fetch was used, as this could encompass areas of lower roughness such as suburbs and parkland.

5.4.2 Sources of model error

5.4.2.1 Uncertainties in the modelling approach

The previous section has shown that when using model MH it is possible to obtain reasonably accurate mean wind speed predictions for a variety of urban sites. However, significant errors could remain due to a number of uncertainties within the modelling approach. These include the following issues:

(i) It has been suggested that the NOABL database may slightly over-predict the wind climatology in urban areas (Best et al., 2008). The 1 km resolution NCIC database may provide more accurate input data although unfortunately it is not freely available.

(ii) The effect of local rooftop flow patterns upon the wind resource (as described in Section 1.4.5) is not accounted for in such neighbourhood average approaches. Detailed CFD studies would be required in order to obtain detailed flow information around individual rooftops (although, it is expected that model MH may provide useful boundary conditions for such studies).

(iii) Uncertainties also occur when estimating aerodynamic parameters of real urban surfaces, even when using a relatively sophisticated morphometric model such as that developed in Chapter 3.

(iv) In addition, the Landmap building data that is used to derive the aerodynamic parameters also has a property which may amplify these errors.

This final point regarding the Landmap building data will now be discussed in more detail.

5.4.2.2 Uncertainties in the input building data

Within the Landmap building heights data set used in this work, each building is assigned only a single, above ground height. This means that assumptions have to be made for buildings with complex or pitched roofs and those located upon sloping ground. Consequently, the heights given in the data actually refer to the *highest* part of the roof above ground level, as noted in Chapter 4. This can give rise to two issues: (i) it can significantly increase estimates of any 'height parameters' input into the model, such as mean building heights, effective mean building heights and displacement heights, and (ii) there can be discrepancies between the height of a building measured onsite and its height as obtained from the building data. In the current work, the latter issue has been minimised by taking the anemometer heights to be the mast height plus the building height contained in the building database. However, the former issue may explain some of the error in the model's predictions.

For this reason, in Figure 5-7 we consider the effect of a small reduction in the three height parameters on the predicted wind speeds. This is done by recalculating the predictions for all the sites, using model MH, with the height parameters reduced by 10%. A value of 10% is chosen as the mean height a typical two story UK house with a 25° pitched roof (Anderson et al., 2007) is about 90% of its maximum height. Clearly however, the difference between a building's maximum and mean roof height will vary dramatically depending upon the

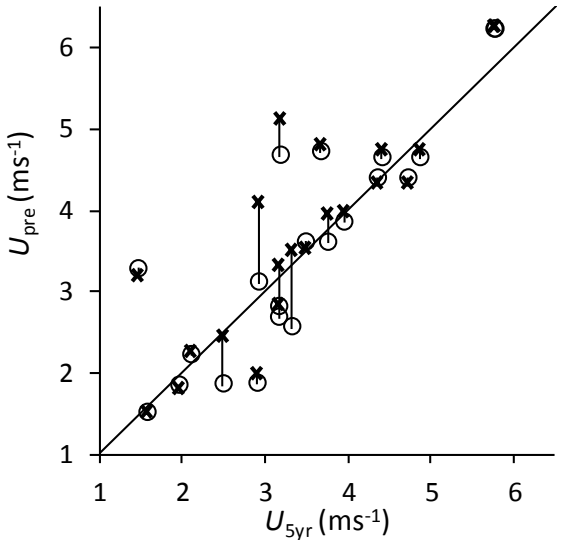

Figure 5-7: Sensitivity of the predictions of model MH to the 'height parameters'. The original wind speed predictions (circles) and those with the height parameters reduced by 10% (crosses) are plotted against the measured, onsite wind speeds.

building type, and hence this sensitivity test can offer only limited information on the potential for more detailed building data to improve the accuracy of model predictions. Figure 5-7 shows the new predicted wind speeds plotted alongside the original predictions for comparison. It is clear that the sensitivity of the predictions to the height parameters varies substantially between sites. This is because in general, small changes in the height parameters only significantly impact upon the wind speeds close to the local effective mean building height, as it is here where the change in wind speed with height is the greatest (see Figure 5-1). Six of the validation sites lie close to this height, and at four of these the predictions are significantly improved, while at the remaining two the accuracy is reduced. Consequently, the overall accuracy of the predictions improves only modestly: by about 1% and 0.03 ms^{-1} in %Error and MAE, respectively at the exposed sites.

Overall, this sensitivity test demonstrates that wind speed predictions near to the top of the building canopy are highly sensitive to the local canopy height. This implies that to maximise the accuracy of wind speed predictions it is crucial that height based inputs (i.e. h_m, $h_{m\text{-}eff}$ and d) are estimated as accurately as possible, and additionally the heights of potential turbine installations must be estimated consistently with respect to morphological input data. In practice this may require a detailed description of the shapes of the local building roofs, in addition to their heights.

This sensitivity test indicates that using more detailed input building data may potentially improve the model predictions, and hence exploring how this can be achieved will be a primary focus of Chapter 6.

5.5 Summary

In this Chapter, three different analytical methodologies for predicting mean wind speeds have been compared for various urban areas within the UK, using measurements from 21 different sites. The character of these sites ranged from two-story suburban properties to medium-rise city-centre buildings and high-rise blocks of flats.

The methodologies generally became more accurate as more complexity was incorporated into the approach, particularly for sites which were not significantly sheltered by surrounding buildings, and were therefore well exposed to the wind. Significant

improvements in accuracy were observed when aerodynamic parameters were derived from detailed building data, as opposed to land use data, and also when the influence of wind direction upon the wind profile was considered in detail. Both of these more detailed modelling approaches also led to a reduction in the bias of the predictions (when measured as the average residual error). Using the most detailed methodology at the well exposed sites, average percentage errors and mean absolute errors of 11.7% and 0.41 ms^{-1}, respectively, were achieved for mean wind speed predictions. The corresponding average residual error was small at 0.07 ms^{-1}, indicating that the predictions were relatively unbiased with a very weak tendency towards underestimating measurements. Considering the complexity of the underlying urban surface, this is a reasonable level of accuracy for locations that could be considered as viable sites for the siting of small-scale turbines. However, even when the most complex methodology was used, significant predictive errors were still observed at some of the validation sites.

It was suggested that uncertainties within the building height data may have contributed to prediction errors. This is particularly the case for sites which are near to the top of the building canopy, where predicted wind speeds are highly sensitive to small changes in the local building data. This suggests that to maximise the accuracy of wind speed predictions it is crucial that height based inputs, such as average building heights and displacement heights, are estimated with a high degree of accuracy. In practice this may require a detailed description of both the shapes and heights of the local building roofs. Therefore, these results suggest that using more detailed input building data may improve the model's predictions, and this will be the aim of Chapter 6.

6 Assessing the Potential of Urban Wind Energy in a Major UK City

6.1 Introduction

An implication of the model evaluation of the previous Chapter is that the average accuracy of the predicted wind speeds (made using model MH) is reasonably good, although some significant uncertainties remain. Potentially these uncertainties may be reduced further via the use of more accurate geometrical data. Therefore, in this Chapter detailed LiDAR (light detection and ranging) data is integrated into model MH, which describes buildings and vegetation throughout the study areas. Model predictions are then re-evaluated with respect to the accuracy of the predictions of the previous Chapter.

Following this model validation, the available wind resource is considered at the city-scale, using the UK City of Leeds as a case study. Two separate investigations are made:

(i) First, a preliminary evaluation of the cumulative potential for generating wind energy in Leeds is made. This is achieved by estimating the total number of viable roof-top wind turbine locations in the city, based upon them receiving a sufficiently high mean wind speed.

(ii) Subsequently, an investigation is made into where, in general, these viable roof-top turbine locations may be found.

Specifically, the structure of the Chapter is as follows: (i) Firstly, in Section 6.2, improvements that are made to the model of MH are described, primarily the processing and integration of the LiDAR data, (ii) secondly, in Section 6.3, the updated predictions are again compared with measured data to assess the model's accuracy, before they are then used to explore the potential for generating wind energy in Leeds.

6.2 Enhancing the Methodology

6.2.1 Modifying the geometric input data

6.2.1.1 Previous data

The most important modification made to model MH in this Chapter is the use of more detailed geometric datasets than were used in the previous Chapter. For this purpose LiDAR data is used, which is again sourced from www.landmap.ac.uk.

Recall that in Chapters 4 and 5, the geometric data used to derive aerodynamic parameters of the urban areas studied was the 'building heights' feature collection from Landmap. The main issue with these data with regard to estimating surface aerodynamic parameters is that buildings and areas of vegetation are each assigned only a single, above ground height (as described in Section 5.4.2.2). These heights were originally obtained by Landmap via the use of LiDAR data, although as this data was used only to obtain single heights for each surface feature much geometric detail was lost. Thus, by relying instead upon the original LiDAR data for input into model MH, these geometric details are recaptured.

6.2.1.2 Integrating LiDAR data

The LiDAR data are provided by Landmap in raster format DSM's (digital surface model) with a 2 m horizontal and 0.1 m vertical resolution. These are measured by survey aircraft using remote sensing equipment to accurately detect the elevation of any obstructions above sea level. This method of data collection does not allow for different types of surface elements (e.g. buildings, bridges, trees, etc.) to be distinguished, and furthermore, erroneous heights can occasionally be registered (e.g. rooftop aerials or birds). Therefore, before the LiDAR DSM's can be used to derive estimates of aerodynamic parameters, it is necessary for them to undergo some processing.

The first stage of processing simply involves subtracting from each DSM the height of the underlying terrain (typically referred to as a DTM, or digital terrain model; also available from Landmap). This gives DEMs indicating the above-ground heights of the surface elements, which is the appropriate geometric data for estimating surface aerodynamic parameters.

In the second stage of processing, any surface elements which either do not affect the aerodynamic parameters of urban areas significantly, or which may reduce the accuracy of

the parameter estimations, are removed from the DEMs. This is done with the use of Ordinance Survey MasterMap© data (EDINA, 2012), which describes the footprints of all fixed ground features greater than a few meters in length or width, such as buildings, roads, woodlands and water features (in shape-file format). For each city, the footprints of all buildings and woodland areas are extracted from the MasterMap data, as it is primarily these surface elements that contribute to surface drag, and hence determine aerodynamic parameters. Subsequently, these footprints are overlaid onto the DEMs, and everything outside the footprints is set to zero. In addition, any height values that refer to woodlands are reduced in magnitude by 20%, as the porosity of trees means they affect aerodynamic parameters less strongly than buildings of the same height (Holland et al., 2008).

For the third and final stage of processing, the DEMs are passed through a simple image processing filter in order to remove erroneous height measurements as well as any minor gaps (less than ≈ 2 m) in between buildings or within tree canopies. The filter is designed to be minimally invasive – in others words it only filters values in the DEMs which appear to be an unrealistic height relative to the surrounding pixels. Without this filtering, these features can lead to overestimates of the blockage on the flow induced by the surface elements, and hence roughness lengths can be overestimated.

The filtering is accomplished by considering each block of 3 × 3 pixels in the DEM and calculating the height of the central pixel relative to those within the four adjoining 2 × 2 clusters (i = 1 to 4, as illustrated in Figure 6-2; top). For each cluster, the maximum difference between the height of the central pixel and those three adjoining it (j = 1 to 3) is calculated. If this maximum value is lower than a chosen tolerance value for at least one of the four clusters (i.e. if the following equation is satisfied) then the central pixel is left unchanged:

$$\min_{\mathrm{i}}\left\{\max_{\mathrm{j}}\left\{h_{ij}-h_c\right\}\right\} < \text{tolerence}\,,$$

Equation 6-1

If this equation is not satisfied this suggests that the central pixel is not part of a surrounding surface obstruction, and hence its height may be an anomaly. In this case, the value of the central pixel is reset to be equal to the mean of the three values in the adjoining cluster that has both the highest mean height as well as a range of pixel values less than the tolerance value, thus:

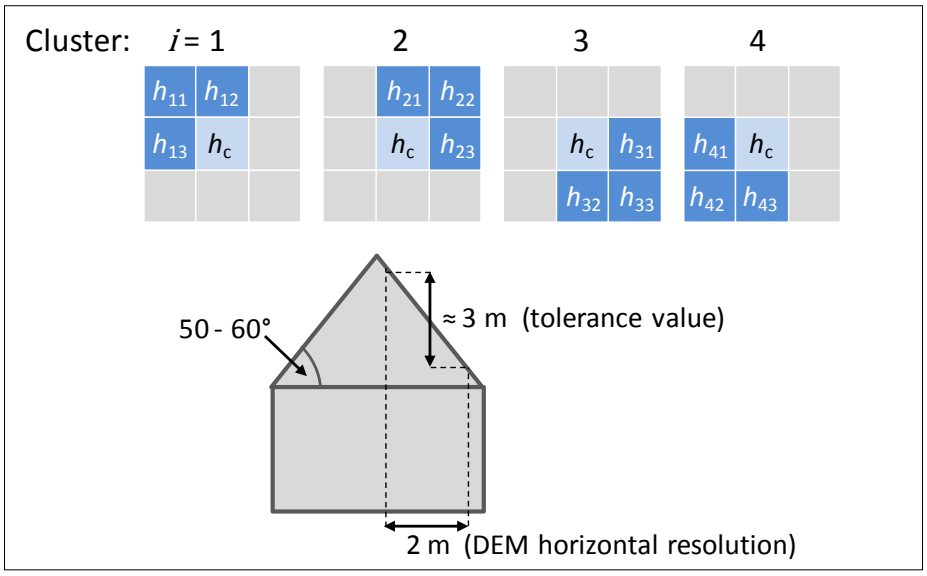

Figure 6-1: Diagrams illustrating the process of filtering the LiDAR DEM.

$$h_c = \max_i \left(\text{mean}_j \left(h_{ij} \right) \right)$$

Equation 6-2

provided:

$$\text{range}_j \left(h_{ij} \right) < \text{tolerence} \, .$$

Equation 6-3

The tolerance value is chosen based upon the height difference that a steeply pitched roof (50 to 60°) would give rise to over a distance corresponding to the horizontal resolution of the DEM. Thus, when the resolution is 2 m the tolerance is set to 3 m (see Figure 6-1; bottom).

6.2.1.3 Differences in the geometric datasets

A sample of the resulting LiDAR based DEM is shown in Figure 6-2, alongside the building-heights data used in the Chapters 4 and 5. It can be seen in this figure that, although the horizontal resolution of the LiDAR data is quite coarse, it captures the complexity of building roofs far more accurately than the building-heights data. Furthermore, small clusters of trees which are absent in the building-heights data are well captured in the LiDAR data. This enhanced level of geometric detail indicates that aerodynamic parameters may be estimated more accurately from these LiDAR based DEMs.

To indicate the magnitude of the differences that can be found between both geometric and aerodynamic parameters when the LiDAR data is used as opposed to the building-heights

data, Figure 6-3 shows scatter plots of the mean heights (left) and roughness lengths (right) calculated for the neighbourhoods of Leeds (on a uniform, 250 m grid). The figure shows that there is a large discrepancy in the calculated mean heights, and that for the majority of neighbourhoods they are significantly lower when the LiDAR data is used. This is the expected tendency, but the significant magnitudes that these differences reach is perhaps larger than may have been expected. Differences between the roughness lengths calculated using the different geometric data are less dramatic, but still very significant – again, the predicted values are generally lower when the LiDAR data is used, but this tendency is now weak.

Overall, the figure indicates the shortcoming of assigning buildings (or areas of vegetation) that are of a complex geometry with a single height. Furthermore, the maximum height (as used for the building-heights data in this case) appears to be quite an unreliable measure.

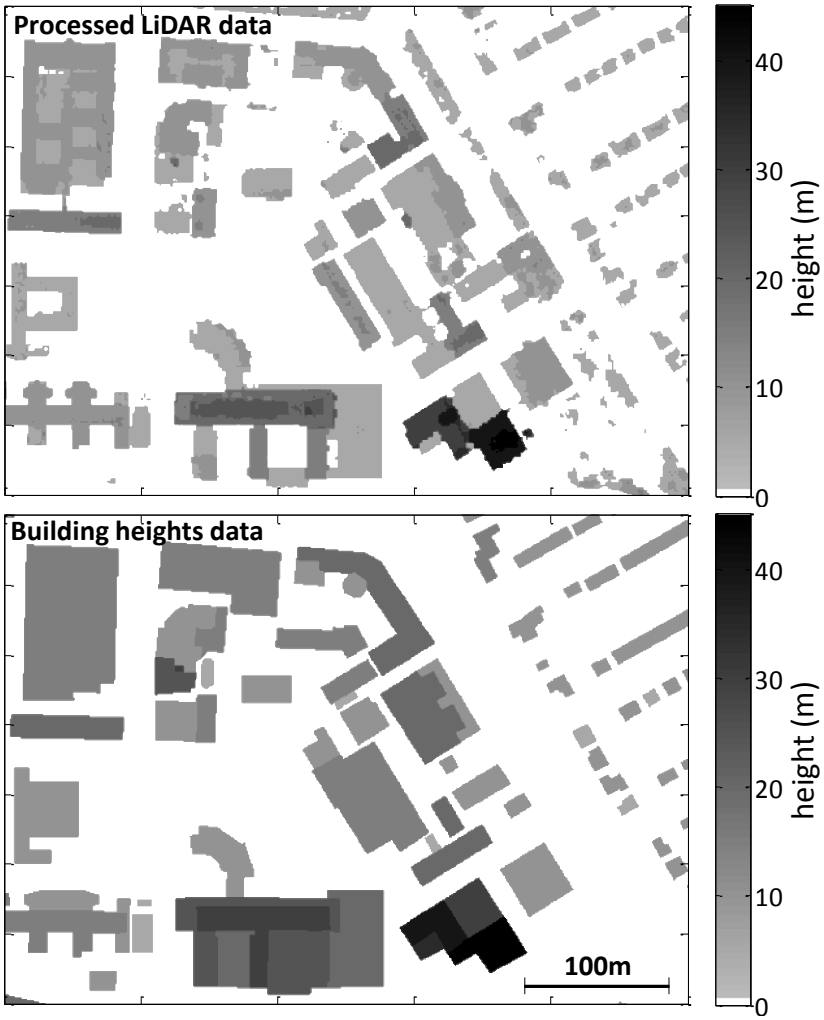

Figure 6-2: Examples of the two sets of geometric data for a sample area of Edinburgh.

6.2.2 Other modifications to the methodology

The wind atlas methodology used in Chapter 5 remains unchanged in the current work, with the exception of the LiDAR geometric data described in the previous section, the regional wind climate, and also the value used for the blending height.

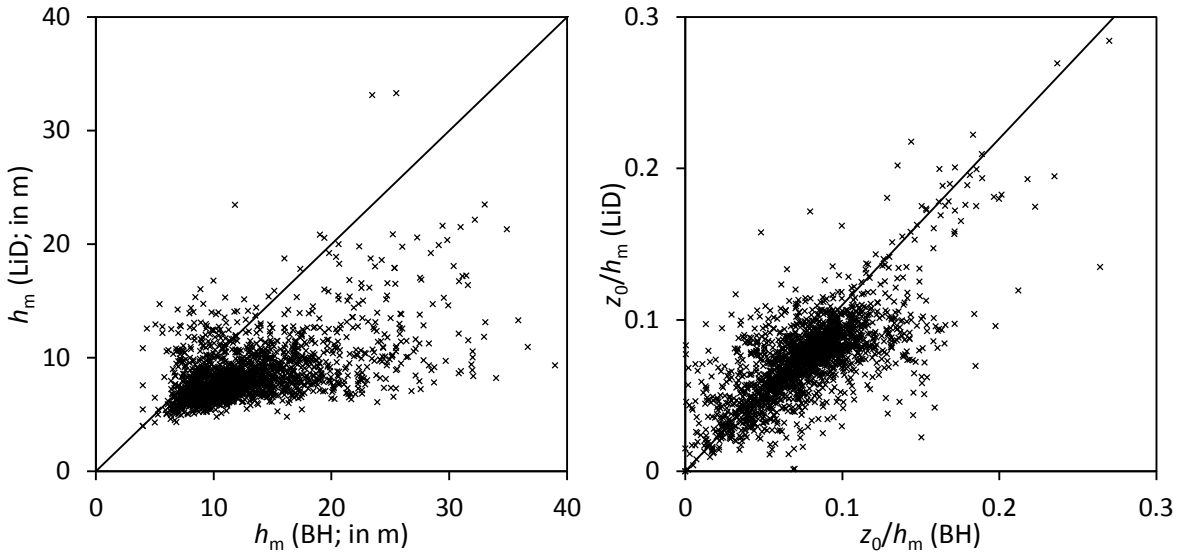

Figure 6-3: Mean heights (left) and roughness lengths (right) calculated for Leeds using the LiDAR (vertical axis) and building-heights data (horizontal axis). Calculations are made on a uniform, 250 m grid.

6.2.2.1 The regional wind climate

At this stage of the research, wind speed values from the NCIC database were obtained for the validation sites described in Section 5.3. This database is used by the Met Office methodology as a more accurate input than the NOABL database, as discussed in Section 1.3 (differences between the two datasets are described by the Met Office in an online report: www.metoffice.gov.uk/renewables/wind-map). Therefore, this data is used in the remainder of the Thesis in order to reduce the sources of error in model MH. The only potential disadvantage from sourcing this data is that its use would add a significant financial cost to any practical wind resource assessment, given that in contrast the NOABL database is freely available.

6.2.2.2 The blending height

The significance of the blending height (z_{bl}, see Figure 5-1) is that it is considered to be the top of the 'roughness sublayer', below which the wind profile is assumed to be determined by the local geometry. In Chapter 5, when using the Building Heights data as input for model

MH, z_{bl} was set to twice the local mean building height (h_m) so as to be consistent with the original methodology of the UK Met Office (Best et al., 2008). Generally, however, the urban roughness sublayer extends to 2 - 5h_m above the ground depending upon the surface geometry (Raupach, 1991), and experimental results show that it is thicker above arrays of buildings of heterogeneous heights (Cheng and Castro, 2002a).

The implication of this is that a multiple of the 'effective mean building height' may be a more appropriate for estimating z_{bl}, as a characteristic of $h_{m\text{-}eff}$ is that it increases with increasing building height variation (see Chapter 3). Given that in general, for the four study cities in this work $h_m < h_{m\text{-}eff} < 2.5h_m$, it is appropriate to set $z_{bl} = 2h_{m\text{-}eff}$, as this makes the depth of the roughness sub-layer consistent with the accepted range of 2 - 5h_m noted above. Therefore, in this Chapter, when using both the Landmap building-heights data and the LiDAR data as input, a blending height of $2h_{m\text{-}eff}$ is used in making predictions with model MH.

Although not shown, an important point to make is that when using LiDAR data, setting $z_{bl} = 2h_{m\text{-}eff}$ led to a significant increase in overall predictive accuracy relative to predictions made using $z_{bl} = 2h_m$ (with respect to the measured data we consider in the model evaluation). In contrast, when using the Landmap building-heights data, the predictive accuracy of model MH was unchanged whether $z_{bl} = 2h_{m\text{-}eff}$ or $z_{bl} = 2h_m$ was used. It should be noted however, that the predictions for individual sites demonstrate a relatively high sensitivity to the blending height, with both sets of the geometric data.

6.3 Results and Discussion

6.3.1 Re-evaluating the accuracy of the predictions

In order to re-evaluate the accuracy of the predictions with the improved input data, Figure 6-4 (left) shows the predicted (U_{pre}) vs. measured (corrected) wind speeds (U_{5yr}) at each validation site. Predictions at the exposed sites and the sheltered sites are distinguishable in the figure. Note that the study area of Warwick had to be discounted from the analysis in this Chapter, due to the lack of available LiDAR data. It is also important to note that the predictions made with the building heights data are different to those made in Chapter 5, due to the fact that the NCIC database is now used and z_{bl} is set $2h_{m\text{-}eff}$.

It can be observed from these plots that there is a significant improvement in accuracy when the LiDAR data is used rather than the building-heights data. Moreover, because the rest of the input data remains unchanged for all the predictions in the figure (e.g. the NCIC database and the blending height), it can be concluded that the use of the LiDAR data is solely responsible for this increase in predictive accuracy. Considering the predictions site-by-site, the use of LiDAR data either improves the predicted wind speed or has little difference to its accuracy.

More general trends in the accuracy of the predictions are illustrated by the box plots of residual errors, defined as U_{mes} - U_{pre}, which are shown in Figure 6-4 (right). Although the maximum and minimum residuals are significant, irrespective of which geometric data is used, the median is brought much closer to zero when using the LiDAR data. In addition, the inter-quartile range of the residuals is much narrower when using the LiDAR data.

This improvement in predictive accuracy is also evident in the mean absolute error (MAE; ms^{-1}) calculated for the sites (from Equation 5-5). When this error metric is calculated over all the sites, for the predictions based upon the building-heights data is it 0.7 ms^{-1} while for the LiDAR based predictions it is slightly lower at 0.41 ms^{-1}. However, this metric is amplified

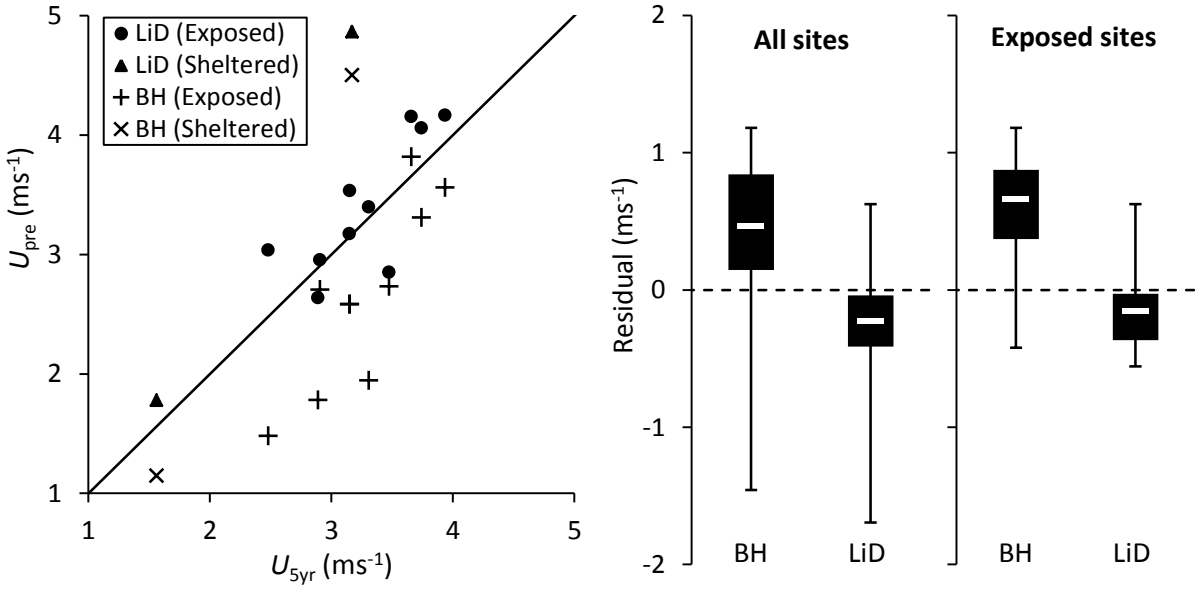

Figure 6-4: Shown on the left, comparisons of predicted (U_{pre}) and measured, 5 year corrected (U_{5yr}) wind speeds for at the validation locations using both the LiDAR (LiD) and building heights (BH) geometric input data. Shown on the right, box plots of the residual errors (ms^{-1}) indicating their inter-quartile range (black boxes), median (white horizontal dashes) and maximums and minimums (error bars) when using each set of input data.

by the sheltered site with the largest error. Consequently, when the error metric is calculated over just the exposed sites, it is 0.67 ms^{-1} for the building-heights based predictions, and significantly lower at 0.3 ms^{-1} for LiDAR data based predictions.

Some important conclusions can be drawn from considering the bias in the predictions. When using the LiDAR data, the predictions are very slightly biased towards over-predictions, whereas with the building-heights data there is a large bias towards under-predictions (see Figure 6-4; right). However, the latter under-predictions were not evident in Chapter 5. This can be explained as a cancellation of the errors inherent in the input data; namely the building-heights data itself and the NOABL wind speeds used to obtain the results of Chapter 5. Specifically, the NOABL database is known to overestimate wind speeds in built areas (Best et al. 2008), while in contrast, in Chapter 5, overestimations of surface aerodynamic parameters (and hence underestimates of predicted wind speeds) were suggested to arise from the use of the building-heights data. Consequently, as the NCIC database is used as input data in the current Chapter, this error cancellation no longer occurs.

The reasons for the tendency towards over-predictions when using the LiDAR data are not so clear. Potentially, this is due to the fact that, in practice, even those sites classified here as 'exposed' may suffer from sheltering effects due to roof-top flow patterns, and these effects are not accounted for in the current spatially-averaged modelling approach (see Section 2.4.3.1). However, there are also uncertainties in the estimations of the spatially-averaged wind profiles themselves, which can occur even when using fully accurate geometric information (as was evident in Section 3.4.4). In any case, as the medium residual error of the LiDAR based predictions is only -0.2 ms^{-1}, it appears to be small enough to be considered negligible, and hence we proceed with the city-scale resource assessment.

6.3.2 Evaluating the cumulative potential for urban wind energy in Leeds

6.3.2.1 The scope of the investigation

In this section a preliminary evaluation of the cumulative, city-scale potential for generating wind energy in urban areas is made, using the UK City of Leeds as a case study. The assessment involves estimating the total number of suitable roof-top turbines locations that exist in the city based upon the available wind resource (i.e. limitations due to structural and planning constraints are not considered).

McIntyre et al. (2010) also assessed the cumulative potential for wind energy generation in the City of Guelph in Canada. The approach used in their work was considerably less detailed than the current work with respect to the modelling of wind flow and identifying suitable turbine locations based upon building data. However, they went on to estimate the cumulative energy generating potential of the turbine installations and made comparisons with the City of Guelph energy usage, and hence the scope of their investigation was much broader in this respect. Although it is beyond the scope of this Thesis, future work is planned which will make similar energy yield calculations for the City of Leeds.

6.3.2.2 Approach and assumptions

Two different approaches are used to estimate the number of viable roof-top locations that may exist in Leeds, each of which involves making several assumptions. Note that during this assessment, when using geometric datasets to indentify potential roof-top turbine locations, care must be taken not to include vegetation or other inappropriate data entries. To ensure that these errors are not made, Ordinance Survey MasterMap© data (EDINA, 2012) can be used to distinguish buildings from other features within the geometric data set. A further important point to make is that the NCIC database was not avaliable over the whole of Leeds for the current work. At the validation sites for which it was avaliable, the wind speeds were 6 - 9% lower than those in the NOABL database. Therefore, for the assessment in this section the NOABL database is used as a model input, but with the wind speeds reduced uniformly over the city by 7.5%. The map published by the Met Office indicating the differences between the NCIC and NOABL databases suggests this is a reasonable assumption (www.metoffice.gov.uk/renewables/wind-map).

The first method (referred to simply as 'method I') is carried out in Matlab© using maps of predicted mean wind speeds calculated over Leeds above each building's roof in conjunction with DEMs of either the building-heights or LiDAR data. Simple calculations, assuming a fixed mast height, lead to an estimate of the total roof area in the city which receives a particular wind speed. These calculations can be carried out over a range of predicted wind speeds to obtain Figure 6-5 (left), where a mast height of 3m has been assumed.

The second method (method II) involves assuming one turbine is installed upon each building upon the highest part of the roof, and then calculating the number of turbines that

would access a particular wind speed (as shown in Figure 6-5; right). Although this is an intrinsically simple approach, it is not possible to perform the calculations using the raster format DEMs, as these do not distinguish between different buildings. Therefore, the original shape-file format of the Landmap building heights data and the Mastermap data must be used (in the latter case, the height of each building is obtained from the LiDAR DEM), as in this format separate buildings can easily be identified. The shape-file format makes it convenient to carry out these calculations using ArcGIS© software. An advantage of method II over method I is that it allows different mast heights to be assumed for different size buildings, as the roof area of each building is easily calculated in ArcGIS©. Therefore, for buildings that are most probably residential properties (horizontal roof area < 150 m^2) we assume a 2 m mast height, while for larger buildings we assume a 5 m mast height. It should be noted here that a 2 m mast height is generally not large enough for turbines to escape roof-top flow patterns, and these may be detrimental to their performance. However this mast height is typical of current installations (Encraft, 2009).

In order to directly compare the results of methods I and II, for method I an additional assumption is made that one turbine is installed every 100 m^2 of roof area, which is assumed to be that of a typical, two-story UK house (Anderson et al., 2007). Thus, the

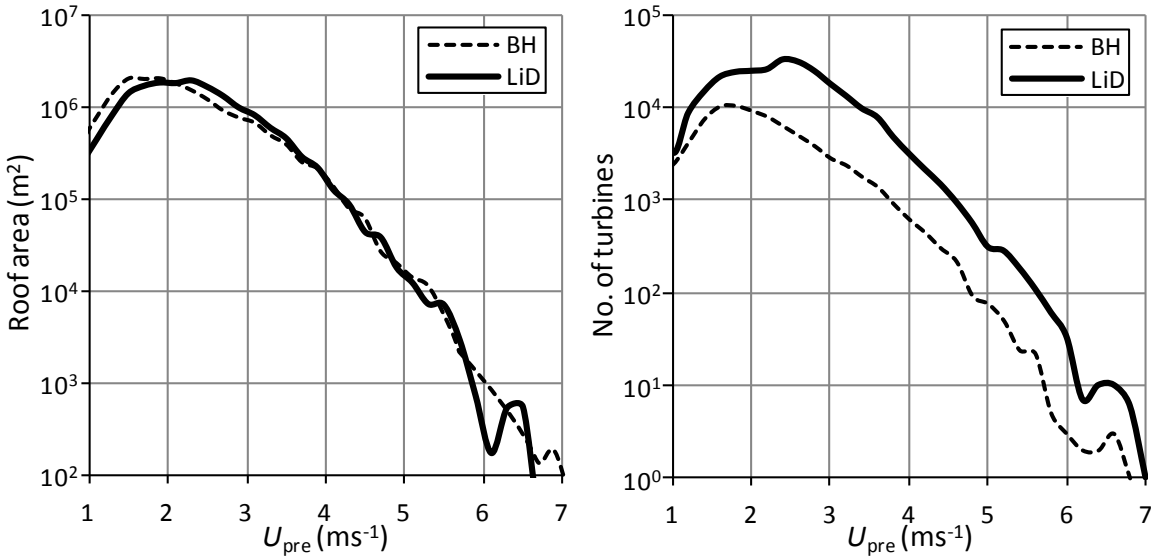

Figure 6-5: The total roof area in Leeds (left) estimated to receive each of the wind speeds recorded on the x-axis, assuming a 3 m mast height. The number of roof-top turbine locations in Leeds (right) estimated to receive each of the wind speeds recorded on the x-axis, assuming one turbine is installed per building roof with a mast height of 2 m for small buildings (horizontal roof area < 150 m^2) and 5 m for larger buildings.

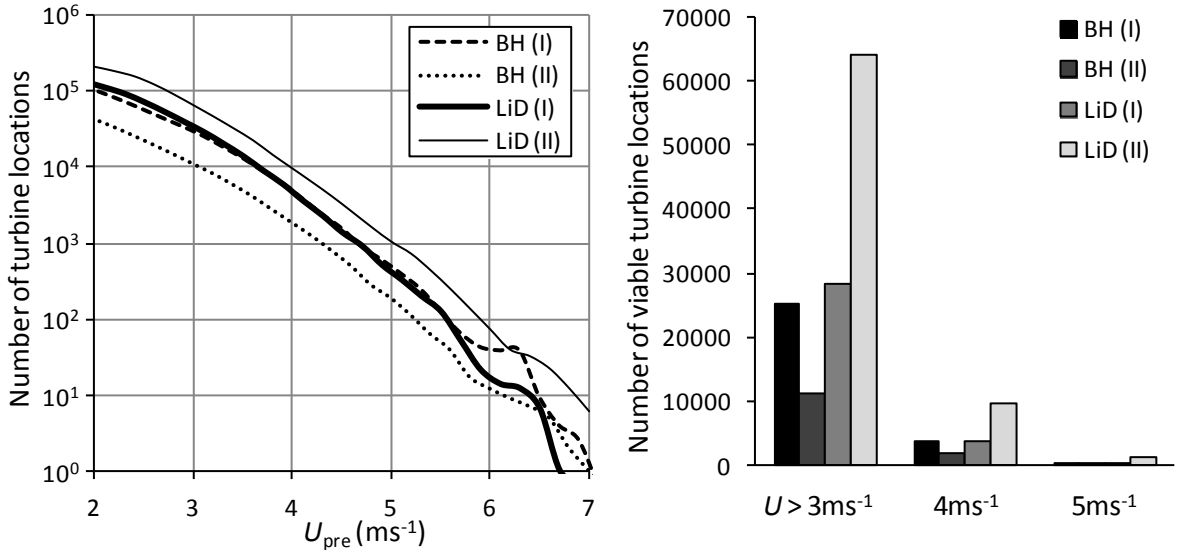

Figure 6-6: The number of roof-top turbine locations in Leeds estimated to receive the minimum wind speeds recorded on the horizontal axis (left). The number of viable roof-top turbine locations estimated to exist in Leeds (right). The estimates shown are made using methods I and II in combination with each set of geometric input data.

number of turbine locations that potentially access a particular minimum mean wind speed is obtained (see Figure 6-6, left). The calculations for method II from Figure 6-5 (right) can easily be translated to so as to also describe the number of turbine locations (and therefore individual roofs) accessing a particular minimum mean wind speed (again see Figure 6-6, left).

6.3.2.3 How many viable wind turbine locations exist in Leeds?

Figure 6-6 (left) indicates that the four calculations (two different methods and sets of input geometric data) give reasonably consistent results. The different estimates for the number of turbine locations with access to a particular minimum mean wind speed are each within the same order of magnitude. Considering the differences in the four approaches, this is as close an agreement as could be expected. The range of these estimates provides an indication of the uncertainty within the predictions.

To suggest an estimated value for the number of viable wind turbine locations that may exist in Leeds, it is necessary to make a final assumption regarding the minimum on-site mean wind speed that's required. In reality, this value will depend on many factors such as the particular turbine design (which impacts on its power curve), the long-term wind speed distribution, and financial and environmental considerations such as overall installation

costs vs. income generated. Financial incentives such as Feed in Tariff framework present in the UK (James et al., 2010) can have a particularly significant influence upon the wind resource required for financial payback to be achieved (as discussed in Section 1.2.2).

In order to make an appropriate estimate of this minimum wind speed required, energy production data obtained from the Warwick Wind Trials (Encraft, 2009) is considered (for currently available small-scale, horizontal-axis wind turbines). Four different types of site are chosen ranging from rural to high rise urban locations, and the measured monthly capacity factors for the turbines at these sites are shown in Figure 6-7. The figure indicates that when mean wind speeds are less than 4 ms^{-1}, turbine performance is generally quite poor and difficult to predict. However, for wind speeds just over 3.5 ms^{-1} capacity factors of around 6% appear to be attainable, and this may be sufficient performance for financial payback to be achieved in the UK (although it should be noted that this depends upon a number of economic factors; James et al., 2010). At higher wind speeds the measured capacity factors start to become much better correlated with wind speed, and at about 4.5 ms^{-1} capacity factors reach the commonly quoted manufacturer's value (for building mounted installations) of 10% (Energy Savings Trust; 2009).

For these reasons, we choose a minimum viable wind speed of 4ms^{-1} for this assessment, but we test the sensitivity to this choice by also considering wind speeds of 3 ms^{-1} and of 5

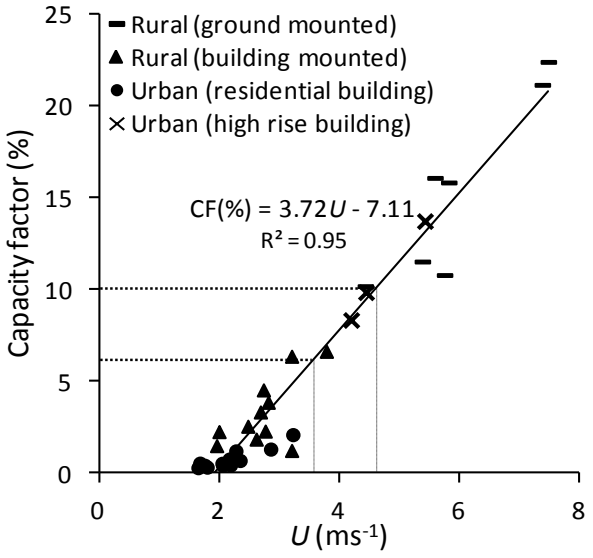

Figure 6-7: The relationship between turbine capacity factor and mean wind speed (both measured monthly) for small-scale, horizontal-axis wind turbines installed at a variety of sites during the Warwick Wind Trials (Encraft, 2009).

ms^{-1}. Respectively, these alternative wind speeds could be considered to represent scenarios where more advanced low wind speed turbines become available, or there are significant reductions in financial subsidies.

The results in Figure 6-6 (right) indicate that the number of viable turbine locations in Leeds is estimated to be within the region of 2000 to 9500 assuming a minimum viable wind speed of 4 ms^{-1}. The variation in these estimations is due to differences in the method and geometric data used, but the values appear to be more sensitive to the minimum wind speed chosen. Specifically, when a value of 3 ms^{-1} (or 5 ms^{-1}) is chosen, then the estimates increase (or decrease) by a factor of ≈ 7 (or ≈ 10), to in between 11000 and 64000 (or between 200 and 1000) viable turbine sites.

In summary, considering that there are currently only a handful of roof-top turbines installed within Leeds (see www.ref.org.uk and www.aeat.com/microgenerationindex), these results highlight the potential for small scale wind technology to be far more widely deployed than has currently been achieved, provided care is taken when assessing site suitability. In addition, they demonstrate the high sensitivity of the technology's potential to the minimum wind resource required to make an installation viable, which in turn may be strongly influenced by technological progress and levels of financial support.

6.3.3 Variation in the available wind resource across the city

Finally, it is important to discuss where, in general, viable roof-top turbine locations may be found. Figure 6-8 (top) shows the long-term predicted mean wind speeds over Leeds (LiDAR based) at 10m above the mean building height in each 250m resolution grid square. It suggests that the wind speeds at this height are highest around the city's edge, and that as the city centre is approached they decrease consistently. This pattern arises as the surface roughness in the city centre is typically much higher —and the urban boundary layer thicker— than in the outskirts of the city. Considering the magnitude of these wind speeds, the installation of wind turbines within 10m of the local mean building height can only be recommended for locations on the outskirts of Leeds, where the predictions are typically above 4ms^{-1}. In the city centre, predicted wind speeds at this height are much lower than required for a turbine installation to be worthwhile. This conclusion is consistent with that of Drew et al. (2013) for the City of London.

When the predicted wind speeds 3 m above the highest building within each grid square are considered (Figure 6-8, bottom), a different pattern emerges to that found in Figure 6-8 (top). It is clear from this figure that throughout much of the city there are tall buildings with access to significant mean wind speeds (frequently over 5ms^{-1}). Furthermore, as well as on the outer edges of Leeds, the highest wind speeds are now found in the city centre where there are many tall, exposed buildings with access to relatively undisturbed winds, despite the high roughness of the surrounding area. This is illustrated more clearly in Figure 6-9 (right), which shows the predicted wind speeds above each building roof in an area of the city centre. In actual fact, the potential for wind energy generation above these tall buildings is likely to be significantly greater than is indicated in Figure 6-8 & Figure 6-9 (top & right), as upon larger buildings' roofs mast heights as tall as 10 m may be feasible. In contrast to this, buildings within residential areas are often all of a similar height (e.g. Figure 6-9, left), and hence above the majority of these properties, wind speeds may be too low for turbine installation to be worthwhile.

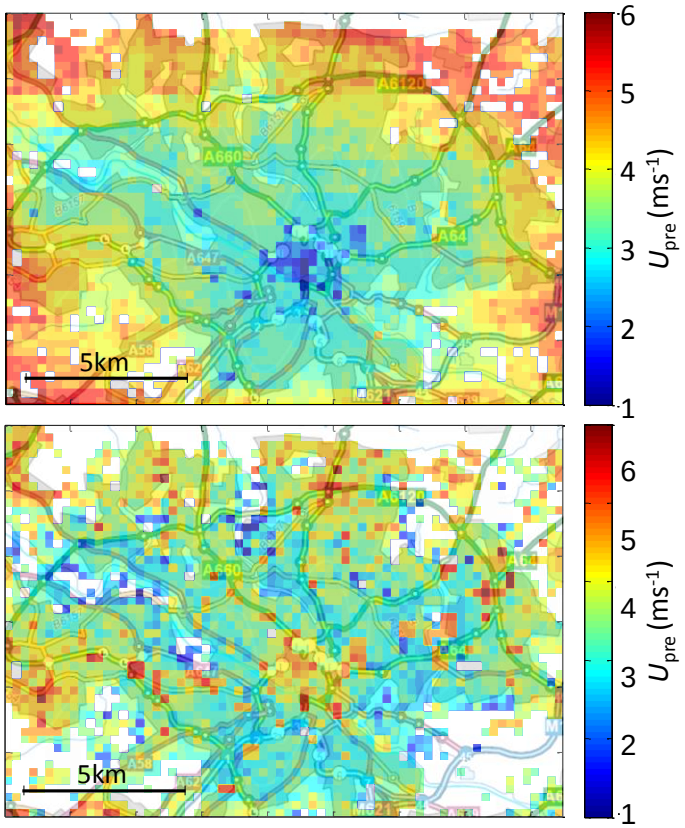

Figure 6-8: Maps of predicted, long-term mean wind speeds over the Leeds at a resolution of 250 m, made using the LiDAR data. The predictions are made at a height of 10 m above the mean building height in each 250 m grid square (top) and at a 3 m mast height above the maximum building height in each 250 m grid square (bottom).

When these taller buildings are considered the current results differ from those of Drew et al. (2013), who suggested that the wind resource available in the centre of the City of London was generally quite poor. These differences occur simply due to the fact that Drew et al. (2013) considered the wind resource available at 5 m above the mean building height across the city. Consequently, if high rise buildings are taken into account, there may be significant potential for urban wind energy in the City of London, even in the city centre.

Overall these results indicate that, although there are many buildings for which the installation of a rooftop turbine should not be recommended (particularly residential properties), there are many tall buildings upon which the installation of a rooftop turbine with a reasonably tall mast is likely to be a worthy investment. Furthermore, above the roof of exposed buildings which are significantly taller than those in the local area (such as blocks of flats and high-rise city centre buildings), the wind resource may be very favourable and comparable with well exposed rural sites (Energy Savings Trust; 2009).

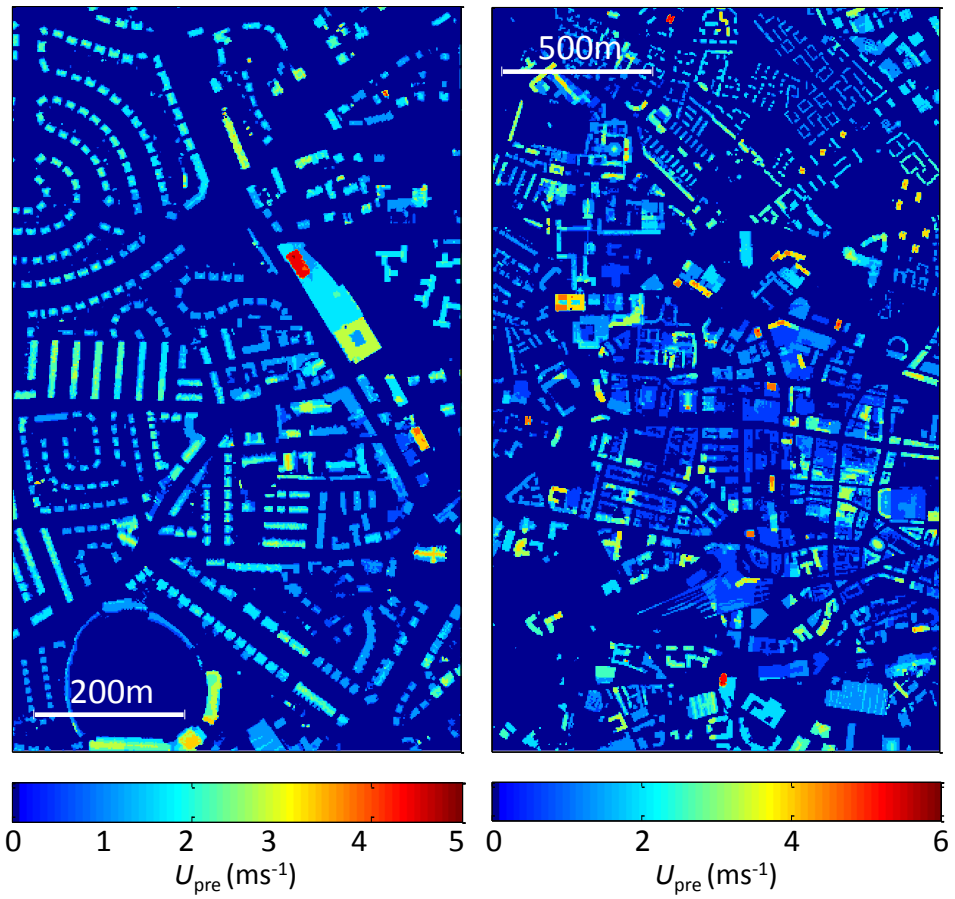

Figure 6-9: Maps of a sample residential area (left) and the city centre (right) of Leeds, indicating the predicted wind speeds above each building roof. Mast heights of 2 m (left) and 5 m (right) are assumed. Note the colour-bars differ between the two figures.

6.4 Summary

In this Chapter, the most sophisticated of the three analytical models tested in Chapter 5 (model MH) has been used to map wind speeds over four different UK cities. The initial objective of the work was to improve the accuracy of model MH, relative to the model evaluation in Chapter 5, by using more detailed input data. This was achieved by using LiDAR geometric data for model input (which describes building roof shapes in addition to their heights) to estimate surface aerodynamic parameters. In addition, a more sophisticated regional wind climate was used for model input, namely the NCIC database.

When these updated predictions were re-evaluated against measured mean wind speeds (from 12 anemometers spread over four cities) the use of LiDAR data was shown to improve model accuracy significantly. At the sites which were well exposed to the wind, the mean absolute error in the predictions was reduced from 0.67 ms^{-1} to 0.3 ms^{-1} when LiDAR data was used, with respect to the predictions made using the building-heights data from Chapters 4 and 5. The results also suggested that the accuracy of the predictions in Chapter 5 had benefited from error cancellation, as sensitivities to uncertainties in the building-heights data had worked in opposition to those in the regional wind climate (i.e. the NOABL database).

Wind speed predictions made with this more detailed input data were then used to fulfil the second objective, namely, to make a preliminary evaluation of the cumulative, city-scale potential for generating wind energy, using the UK City of Leeds as a case study. The assessment involved estimating the total number of viable roof-top wind turbine locations in the city, based upon them receiving a sufficiently high mean wind speed. The results depended upon the method and building data used in the calculations, but more strongly upon the required minimum mean wind speed that is assumed. Potentially, this highlights the sensitivity of this technology's potential to financial support and technological progress. When a minimum value of 4 ms^{-1} is assumed, the results suggest 2000 to 9500 viable building-mounted wind turbine locations exist in Leeds, and hence there appears to be huge scope for the technology to be more widely deployed.

Finally, it was investigated where, in general, viable roof-top turbine locations may be found. The results suggested that there are many viable sites (typically tall unsheltered

buildings) that are distributed throughout the city, including within the complex city centre. At the most suitable sites predicted above-roof mean wind speeds are comparable to those observed at well exposed rural sites. However, in residential areas that consist of buildings of a similar height, it is likely that the majority of properties will experience wind speeds that are too low for turbine installation to be worthwhile.

The wind maps and methodology developed in this Chapter may be utilised by turbine suppliers and customers for assessing the viability of potential sites, as well as being instructive for policymakers developing subsidies for small-scale renewable energy projects. For this reason, future work will be undertaken to integrate these maps into user friendly online tools, to be made easily and freely accessible to interested parties and individuals.

7 Final Discussion and Conclusions

7.1 Research summary

The research described in this Thesis has addressed the challenge of predicting the wind resource available to roof-mounted wind turbines in urban areas. In order to explore the predictability of this resource and investigate how accurate predictions may be achieved, a number of experimental datasets have been analysed and new models have been developed utilising techniques based upon boundary layer meteorology.

Initially, in Chapter 2, an evaluation of currently available wind atlas methodologies for predicting mean wind speeds in urban areas was undertaken, and the relative contributions of various sources of model error was estimated. The investigation indicated that a major source of model error arises due to uncertainties in estimating aerodynamic parameters of urban surfaces. In order to address this issue, in Chapters 3 and 4, a new morphometric model was developed and then validated using experimental data from a variety of sources. Subsequently, in Chapter 5, this morphometric model was integrated into a wind atlas methodology, which was then optimised for use in urban areas. An evaluation of the wind speed predictions of this methodology suggested that there was further room for improvement in predictive accuracy, and hence in Chapter 6, the necessary steps were taken towards this. Also in Chapter 6, a preliminary evaluation of the cumulative potential for generating wind energy in cities was made, using the City of Leeds as a case study.

7.2 Results and Implications

In Chapter 2, an analysis of experimental data obtained over idealised urban arrays shows that the spatially-averaged vertical wind profile may act as a lower bound for the mean wind speed received at unsheltered roof-top locations. These unsheltered sites were considered to be those located such that they did not suffer from significant sheltering, either due to the wakes behind upwind buildings or separated roof-top flow. Above-roof wind speeds at these preferable locations exceeded the spatial-average by up to 20%. However, the exact magnitudes of these building-scale flow variations are likely to be difficult to predict accurately without detailed site specific assessment.

It was also observed that the standard logarithmic profile can describe spatially-averaged wind profiles some distance down into the roughness sublayer, even above complex arrays with height variation. However, currently available morphometric models appear to be unable to accurately predict the aerodynamic parameters of these more complex arrays. It is likely therefore, that errors in estimating z_0 and d make a substantial contribution to the overall uncertainties in current urban wind atlas methodologies.

The implications of these results are that when predicting wind speeds at unsheltered locations, it may be acceptable to overlook building-scale flow features and obtain reasonably accurate estimates of wind speeds using spatially-averaged wind profiles. Therefore, the accuracy of urban wind atlas methodologies could potentially be improved significantly via the use of improved morphometric models that can help estimate these profiles more accurately. Thus, the focus of the following two Chapters was upon the development of such a model.

In Chapters 3 and 4 a new morphometric model was developed, designed primarily to account for the influence of building height variability upon surface aerodynamic parameters. Height variation was chosen because the literature review of Chapter 1 suggested that this is potentially the most important geometric complexity of those omitted from previous morphometric models.

By accounting for the influence of height variability, the model predicted a much softer peak roughness length (with respect to surface density) relative to uniform height arrays, and in addition, the predicted displacement heights often exceeded the mean building height significantly. Both of these characteristics are qualitatively consistent with experimental data (as discussed in Section 1.4.3.5). Furthermore, an evaluation of the model's predictions of both the aerodynamic parameters and wind profiles found the results to be reasonably accurate in a quantitative sense. However, the morphometric models that have been developed for uniform height arrays were shown to give generally incorrect predictions for these types of geometries.

Overall, height variability appeared to be a crucial factor in estimating z_0 and d (and also wind profiles), and hence it should not be omitted when modelling flow in the lower urban boundary layer. In contrast, variations in building layout and footprint shape appeared to be insignificant in determining z_0 and d when height variation was present. Furthermore, the

results suggested that it is important to consider the specific shape of building height distributions, rather than simple parametrisations such as the standard deviation of building heights (σ_h). Therefore, it can be recommended that a significant proportion of future experimental investigations should be focused upon exploring the influence of height variation upon wind flow.

In Chapter 5, an urban wind atlas methodology was developed that incorporated the morphometric model developed in the previous two Chapters. When the model's predictions were evaluated, using measured meteorological data from a variety of sites, significant improvements in predictive accuracy were observed relative to currently available methods. These gains in accuracy were attributed to the use of detailed building data and the new morphometric model, as well as the inclusion of wind directional effects.

Despite this improvement in predictive accuracy, significant uncertainties remained in the method for a number of reasons. One such reason was the building-scale variability in the flow that was highlighted in Chapter 2, and hence the predictions at the sheltered validation sites were significantly less accurate. Other uncertainties were suggested to occur due to issues with the building data and the input regional wind climatology. Therefore, Chapter 6 aimed to reduce the impact of these sources of error.

In Chapter 6, the final improvements made to the urban wind atlas methodology primarily involved the use of LiDAR geometric data. In addition, a more sophisticated regional wind climate was used, and the value of the blending height was optimised. These changes were found to improve the model's predictive accuracy further, although some uncertainties still remained.

It can be deduced from the predicted wind speeds that to maximise the predictive accuracy of these kinds of models, both high detail geometric data and sophisticated input wind data are needed. However, it should be noted that both the geometric data and regional wind climate used in Chapter 6 would incur a significant financial cost if the model predictions were used on a commercial basis. In addition, due to the remaining uncertainties in the predictions, such models may be best suited to preliminary site evaluations or city-scale assessments – onsite measurements may be needed to confirm the available wind resource at a potential turbine location. This confirmation is particularly important when installing turbines upon residential properties, where the surrounding buildings are of a similar

height. The wind flow at these locations often suffers from sheltering effects due to adjacent buildings (such as those described in Chapter 2), and in addition mast heights can be constrained to within a couple of meters above the roof for structural reasons.

Finally, an evaluation of the cumulative potential for generating wind energy in the City of Leeds was undertaken, and this highlighted a largely untapped wind resource that is available in the city. Thus, there appears to be great scope for the expansion of urban wind energy in the City of Leeds, and this is likely to be the situation for many other large cities throughout the UK. However, the magnitude of the technology's deployment potential was shown to be highly sensitive to the minimum mean wind speed selected for a site to be considered viable. In turn, this minimum wind speed depends heavily upon levels of available financial support and technological progress.

7.3 Limitations and Future Work

While undertaking the research reported in this Thesis, various limitations were encountered in the analysis. Generally, this occurred either due to practical reasons, such as a lack of availability of experimental data, or as a result of pre-decided boundaries of the research project, which were chosen so as to remain within the time constraints of the project.

In Chapter 2, the limitations of the analysis were determined primarily by the available experimental data. Specifically, the data considered was obtained above arrays of cubic blocks, aligned normally with the flow, and hence there was no analysis of flow patterns occurring above complex roofs, or buildings aligned obliquely to the incoming wind. In addition, the roof-mounting guidelines that were suggested were made based upon a single, prevailing wind direction.

An additional, but perhaps less significant limitation, was due to the fact that the experimental data was obtained in fully developed boundary layers, which might not often be found in urban areas. It may be that the wind profiles above urban areas with frequently varying surface cover rarely follow those estimated by morphological models, even in the roughness sublayer. In addition, roof-top flow patterns above buildings laying on the edge

of parkland or other open areas within cities may more closely resemble those found above isolated buildings, despite their urban locations.

In the future, further investigation of the flow found around more complex (and oblique) roof-tops could prove beneficial. Although there have been a number of such studies reported previously (see Section 1.4.5), there are many types of geometry that remain to be explored. However, due to the diversity of roof shapes found in urban areas in conjunction with the infinitely variable geometry of the surrounding buildings, it can be difficult to obtain guidelines that are widely applicable.

In Chapters 3 and 4, the main limitation of the research that was undertaken involved the evaluation of the model's predictions and the data that was used. In Chapter 3 for example, although the model was evaluated for arrays with various levels of height variation and a wide range of building densities, each of the arrays shared the geometric characteristic of being comprised entirely of square based blocks. In fact, no data for arrays of blocks of variable height with non-square bases could be found in the literature, and hence this potentially presents an opportunity for future research. In Chapter 4, there was no evaluation of the predictions for the City of Leeds, as no suitable measured data was available in the area. Therefore, it may be beneficial for the model to be validated with such datasets if they become available in the future. However, there are a number of practical difficulties with validating wind profiles in real urban areas, as were noted in Section 4.2.4.

The other notable limitation found in Chapter 3 was the particular physical limitations of the morphometric model, i.e. the fact that its predictions appeared to become less accurate for surfaces that were either too highly heterogeneous in height, or of a very high packing density. Therefore, it was suggested that caution should be taken when applying the model to highly complex geometries.

An additional limitation of Chapter 4 occurred when estimating building layout and footprint shape from the geometric data – average parameters were difficult to determine objectively. However, the results obtained did suggest that variations in these geometric factors may be insignificant in determining the flow above arrays of heterogeneous height.

In Chapters 5 and 6, there were a number of limitations associated with the urban wind atlas methodology that was developed, due to simplifications that inevitably have to be made with such a modelling approach.

Two of the most obvious of these limitations occur because the effects of building-scale flow features and local topography are omitted from the model – clearly these represent sources of uncertainty in the predictions. In the future, simple correction factors to account for these effects could be included. Other uncertainties can arise from the method of matching logarithmic and exponential profiles (see Figure 1-6), rather than considering the roughness sublayer flow in more detail. This could be improved by using a more detailed flow model (locally) to estimate the wind profile below the blending height (z_{bl}), such as the model of Di Sabatino (2008). However, this might prove impractical for mapping wind resource over entire cities, due to the greater complexity of implementing the model and handling the output data, relative to using a morphometric model and a simple logarithmic profile.

Another important limitation of the urban wind atlas methodology (in its current form) is its treatment of areas outside of the city and beyond the boundaries of the study areas. Effectively, the surface cover of these areas was assumed to be open terrain, and hence only the effect of the particular study city upon the wind profile was considered. To improve upon this assumption, the methodology could be unified with that of the Met Office by utilising the latter methodologies treatment of areas outside of cities. More specifically, this would involve using land use data (indicating areas of grassland, shrubs, water etc; Best et al., 2008) to estimate the aerodynamic parameters of non-urban surfaces.

A further limitation of the wind atlas methodology is the fact that as the geometry of cities changes over time, the wind maps will become outdated. The importance of this is difficult to quantify as these changes will of course be highly spatially variable. For example, a single new skyscraper is likely to have an immediate and significantly detrimental effect upon the wind resource received by the local buildings. In contrast, it may take many large new buildings to alter the large-scale roughness characteristics of a city, and hence affect the wind resource more generally. Routinely revising the wind maps using up-to-date geometric data would be the only way to thoroughly address this issue.

The final limitations to be discussed are relevant only to Chapter 6, and the city-scale assessment of wind energy potential in the City of Leeds. These limitations originate for two

related reasons: firstly, the mean wind speed was the only factor considered in the assessment of viable sites, and secondly, there was significant uncertainty in choosing a suitable viable minimum mean wind speed. Specifically, there are various technological, economic, and social factors that were not taken into account in the assessment (many of which were mentioned in Section 6.3.2).

One of the most obvious improvements that could be made to address these limitations would be to choose viable turbine sites based upon the energy available in the wind, rather than just the mean wind speed. This would involve estimating a suitable wind speed distribution, by using both the predicted wind speed and an assumed distribution shape. The issue that would then be encountered would be how to choose a suitable minimum quantity for the available wind energy required for a site to be considered viable (equivalent to the issue of choosing a viable minimum mean wind speed in Chapter 6). Varying degrees of complexity could be considered when making this choice, including paying attention to specific turbine models and their associated power curves, and estimating environmental and financial payback times (the latter being dependent upon available financial subsidies). Finally, structural considerations could be made in order to determine the feasibility of different building roofs for siting turbines, and any limitations as to the size, elevation and number of turbines that a roof may accommodate.

By including all these additional complexities, future investigations into wind energy generation in cities could make more accurate estimations of deployment potential. In addition, estimates of expected cumulative energy generation could be made, which could potentially be a more instructive measure than the estimated number of viable locations presented in Chapter 6.

7.4 Research Impacts

7.4.1 Impacts in the field of urban meteorology

It is expected that the findings of this research will have impacts in the field of urban meteorology, as well as in its primary area of focus which is that of urban wind energy.

The most significant findings for urban meteorology are those of Chapters 3 and 4. This is because aerodynamic parameters of urban areas are frequently required for types of urban

wind modelling work other than estimating wind resource in cities, such as the modelling of pollution dispersion, estimating wind loads on buildings, and accounting for the effects of urban areas in numerical weather prediction models. Thus, the model of Chapters 3 and 4 could be used to estimate urban aerodynamic parameters for these types of applications. The model could also be used to estimate displacement height for urban flow models that require this single parameter as an input boundary condition (e.g. Di Sabatino et al., 2008), or for field studies that require displacement height as a fitting parameter to obtain roughness length estimates (Barlow et al., 2008).

It is useful to note that it is not just the morphometric model of Chapters 3 and 4 that has these potential uses. The method that was developed for choosing geometrically homogeneous neighbourhood regions could also prove valuable in the areas of research noted above. In fact, this method could be used in conjunction with other morphometric models aside from that developed in Chapter 3. The reason for this is that when any morphometric model is applied to an urban neighbourhood, in order for its application to be theoretically sound, the neighbourhood must be reasonably consistent geometrically throughout (as discussed in Section 1.4.3.5).

Finally, for some applications in the areas of research noted above, the wind atlas methodology of Chapters 5 and 6 could be utilised in full. For example, computational fluid dynamical studies modelling pollution dispersion, such as that of Xie and Castro (2009), require the specification of the vertical wind profile over the inlet of the computational domain. This could easily be obtained via the wind atlas methodology.

7.4.2 Impacts in the field of urban wind energy

The primary goal of this research was to develop models to assist in the development of urban wind energy by increasing the understanding of the urban wind resource and its predictability. Accordingly, in Chapters 5 and 6, the work of Chapters 1 to 4 was brought together in the development of the urban wind atlas methodology. It is the information that this methodology can provide that is expected to be the most valuable output of this research.

In order to maximise the impact of the research, it is perhaps most important that the wind maps over the various study areas are made available so that they can be easily accessed by

interested parties and individuals. A free, user friendly tool, similar to that of the Carbon Trust Tool (as discussed in Section 5.3.3), would be the ideal way to maximise the benefits and exposure of this information. However, there are technical issues and data licensing restrictions that must be addressed for this to be achieved, as the geometric building data from Landmap is currently only freely available for academic use.

In addition to the specific wind speed predictions, the estimated deployment potential of urban wind energy highlighted in Chapter 6 has practical value for turbine manufactures and urban planners alike. The results may prove even more valuable if the current models are expanded in order to estimate the potential, cumulative energy yields of small-wind deployment scenarios in major cities.

It could be argued that before any such online tool is created, attempts should be made to continue the development of the methodology in order to further reduce uncertainties (i.e. by addressing the limitations outlined in the Section 7.3). However, on the other hand, considering current predictions (and observations) with regards to anthropogenic climate change, there is a pressing need to lower global emissions of greenhouse gases. The urgency of the situation is underlined by the recent World Bank Report (2012; 'Turn Down the Heat'), which emphasises the dangers of a 4°C warmer world, and points out that even including mitigation efforts since 2009, warming of 3°C by 2100 is likely. To put this into perspective, there is a global recognition that temperature rise should be kept below 2°C to avoid the most dangerous impacts of climate change.

Given these circumstances, it appears to be crucial that carbon reduction and renewable energy targets in the UK and elsewhere are met. In the UK these include the government's carbon budgets that run up to 2027, and the target of supplying 15% of the UK energy demand with renewable technologies by 2020. From this perspective, if the wind maps in their current form could encourage the deployment of urban wind energy at locations where any useful carbon savings can be made, then it would be advantageous for them to be made available as soon as possible.

7.4.3 Renewable energy: one piece of the puzzle

It is appropriate to make some final comments regarding the role of renewable energy technologies, such as small-scale wind energy, in addressing anthropogenic contributions to climate change and other environmental issues.

Clearly no single renewable energy technology can solve the climate change problem alone, but there is much evidence to suggest that even a full mobilisation of sustainable and energy efficient technologies will not prevent a dangerous level of climate change from occurring (Kramer and Haigh, 2009, Kerr, 2010, Davis et al., 2010, Moriarty and Honnery, 2012). Underlying this conclusion are a number of practical, political and social factors, including limitations upon the speed of deployment and development of new technologies (Kramer and Haigh, 2009, Kerr, 2010), and also the availability of raw materials for renewable energy generating systems, such as solar PV (Feltrin and Freundlich, 2008). These factors become serious issues when considering the question of meeting the gigantic, and still rapidly rising global demand for energy (IEA, 2012). Consequently, it appears that reducing consumption via behavioural change must also play a crucial role in reducing carbon emissions to safe levels.

Of course, it is not the duty of renewable energy engineers to suggest in detail what form these behavioural changes should take and how they should be achieved (this is far beyond the scope of the current work). However, in work such as this Thesis it is useful to emphasise that these technologies are only a partial solution for reducing carbon emissions to safe levels, as this may help to minimise the possibility that societal changes to reduce consumption are neglected.

It could in fact be considered to be a responsibility of engineers to explicitly state these technological limitations, given that the Royal Academy of Engineering's Statement of Ethical Principles include: "*Actively promoting public awareness and understanding of the impacts and benefits of engineering achievements*", "*Taking due account of the limited availability of natural and human resources*", *and* "*Not knowingly misleading or allowing others to be misled about engineering matters*". To abide by these principles would require that where possible, engineers do not allow the capability of sustainable technologies to be overstated with regard to avoiding dangerous levels of climate change in case this leads to the neglect of other vital measures.

Some simple numbers can be used to show the importance of each of these different approaches for achieving emissions reductions. Firstly, using the results of the Met Office (Best et al., 2008), the Carbon Trust (2008b) estimate that the installation of a small-wind turbine at each property in the UK could achieve an annual saving of 17.8 Mt CO_2e, which compares to the 6.8 Mt CO_2e that is saved per year by the full ensemble of offshore and onshore currently installed in the UK in 2013 (www.renewableuk.com/en/renewable-energy/wind-energy). (It should be noted that the former estimate is overly optimistic due to the unsuitability of many UK properties for small-scale wind turbines, while the latter figure is expected to rise significantly with the new wave of offshore wind farms planned). For comparison, an energy efficiency measure such as turning all UK building thermostats down by 1°C could reduce emissions by 5.5 Mt CO_2e per year (UK Committee on Climate Change, 2008). In addition, a lifestyle shift such as UK citizens taking one meat free day a week could save an estimated 13 Mt of CO_2e per year (Beukering et al., 2008).

In summary, small-wind energy (including applications in urban areas) can make valuable carbon reductions along with other renewable energy technologies, such as solar and hydro energy generating systems. However, it is crucial that substantial reductions in consumption through behavioural change and energy efficiency are also made if carbon emissions are to be reduced to safe levels. The good news is that if large reductions in consumption can be achieved, it is likely that the resulting energy demand can be met using renewable and sustainable technologies exclusively (Kemp and Wexler, 2010).

8 List of References

AGREN, O., BERG, M. & LEIJON, M. 2005. A time-dependent potential flow theory for the aerodynamics of vertical axis wind turbines. *Journal of Applied Physics,* 97.

ALLEN, S. R. & HAMMOND, G. P. 2010. Thermodynamic and carbon analyses of micro-generators for UK households. *Energy,* 35**,** 2223-2234.

ALLEN, S. R., HAMMOND, G. P. & MCMANUS, M. C. 2008. Energy analysis and environmental life cycle assessment of a micro-wind turbine. *Proceedings of the Institution of Mechanical Engineers Part a-Journal of Power and Energy,* 222**,** 669-684.

ANDERSON, J., PHILLIPS, R., BLACKMORE, P., CLIFT, M., AGUILO-RULLAN, A. & PESTER, S. 2007. *Micro-wind turbines in urban environments: an assessment,* Watford, UK, BRE Trust.

ASHIE, Y. & KONO, T. 2011. Urban-scale CFD analysis in support of a climate-sensitive design for the Tokyo Bay area. International Journal of Climatology, 31, 174-188.

AYHAN, D. & SAĞLAM, Ş. 2012. A technical review of building-mounted wind power systems and a sample simulation model. *Renewable and Sustainable Energy Reviews,* 16**,** 1040-1049.

BAHAJ, A. S., MYERS, L. & JAMES, P. A. B. 2007. Urban energy generation: Influence of micro-wind turbine output on electricity consumption in buildings. *Energy and Buildings,* 39**,** 154-165.

BALDUZZI, F., BIANCHINI, A. & FERRARI, L. 2012. Microeolic turbines in the built environment: Influence of the installation site on the potential energy yield. *Renewable Energy,* 45**,** 163-174.

BARLOW, J. F., ROONEY, G. G., VON HUENERBEIN, S. & BRADLEY, S. G. 2008. Relating urban surface-layer structure to upwind terrain for the salford experiment (Salfex). *Boundary-Layer Meteorology,* 127**,** 173-191.

BECKER, S., LIENHART, H. & DURST, F. 2002. Flow around three-dimensional obstacles in boundary layers. *Journal of Wind Engineering and Industrial Aerodynamics,* 90**,** 265-279.

BEST, M., BROWN, A., CLARK, P., HOLLIS, D., MIDDLETON, D., ROONEY, G., THOMSON, D. & WILSON, C. 2008. *Small-scale wind energy Technical Report*, UK Met Office, *www.carbontrust.co.uk/emerging-technologies*

BEUKERING, P. V., LEEUW, K. V. D., IMMERZEEL, D. & AIKING, H. 2008. Meat the Truth: The contribution of meat consumption in the UK to climate change. The Netherlands: Institute for Environmental Studies, Vrije Universiteit.

BOTTEMA, M. 1996. Roughness parameters over regular rough surfaces: Experimental requirements and model validation. *Journal of Wind Engineering and Industrial Aerodynamics,* 64**,** 249-265.

BOTTEMA, M. 1997. Urban roughness modelling in relation to pollutant dispersion. *Atmospheric Environment,* 31**,** 3059-3075.

BOTTEMA, M. & MESTAYER, P. G. 1998. Urban roughness mapping - validation techniques and some first results. *Journal of Wind Engineering and Industrial Aerodynamics,* 74-76**,** 163-173.

BOU-ZEID, E., MENEVEAU, C. & PARLANGE, M. B. 2004. Large-eddy simulation of neutral atmospheric boundary layer flow over heterogeneous surfaces:

Blending height and effective surface roughness. *Water Resources Research,* 40**,** -.

BOU-ZEID, E., OVERNEY, J., ROGERS, B. D. & PARLANGE, M. B. 2009. The Effects of Building Representation and Clustering in Large-Eddy Simulations of Flows in Urban Canopies. *Boundary-Layer Meteorology,* 132**,** 415-436.

BOU-ZEID, E., PARLANGE, M. B. & MENEVEAU, C. 2007. On the parameterization of surface roughness at regional scales. *Journal of the Atmospheric Sciences,* 64**,** 216-227.

BRITTER, R. E. & HANNA, S. R. 2003. Flow and dispersion in urban areas. *Annual Review of Fluid Mechanics,* 35**,** 469-496.

BURTON, T. 2001. *Wind Energy Handbook*, John Wiley & Sons.

CARBON TRUST. *Small-scale wind energy, Policy insights and practical guidance*. 2008

CASTRO, I. P. & ROBINS, A. G. 1977. Flow around a Surface-Mounted Cube in Uniform and Turbulent Streams. *Journal of Fluid Mechanics,* 79**,** 307-335.

CELIK, A. N., MUNEER, T. & CLARKE, P. 2007. An investigation into micro wind energy systems for their utilization in urban areas and their life cycle assessment. *Proceedings of the Institution of Mechanical Engineers Part a-Journal of Power and Energy,* 221**,** 1107-1117.

CHENG, H. & CASTRO, I. P. 2002a. Near-wall flow development after a step change in surface roughness. *Boundary-Layer Meteorology,* 105**,** 411-432.

CHENG, H. & CASTRO, I. P. 2002b. Near wall flow over urban-like roughness. *Boundary-Layer Meteorology,* 104**,** 229-259.

CHENG, H., HAYDEN, P., ROBINS, A. G. & CASTRO, I. P. 2007. Flow over cube arrays of different packing densities. *Journal of Wind Engineering and Industrial Aerodynamics,* 95**,** 715-740.

CHENG, Y., LIEN, F. S., YEE, E. & SINCLAIR, R. 2003. A comparison of large Eddy simulations with a standard k–e Reynolds-averaged Navier–Stokes model for the prediction of a fully developed turbulent flowover a matrix of cubes. *Journal of Wind Engineering and Industrial Aerodynamics,* 91**,** 1301-1328.

COCEAL, O. & BELCHER, S. E. 2004. A canopy model of mean winds through urban areas. *Quarterly Journal of the Royal Meteorological Society,* 130**,** 1349-1372.

COCEAL, O. & BELCHER, S. E. 2005. Mean winds through an inhomogeneous urban canopy. *Boundary-Layer Meteorology,* 115**,** 47-68.

COCEAL, O., THOMAS, T. G., CASTRO, I. P. & BELCHER, S. E. 2006. Mean flow and turbulence statistics over groups of urban-like cubical obstacles. *Boundary Layer Meteorology,* 121**,** 491-519.

COMMITTEE ON CLIMATE CHANGE. *Building a low-carbon economy – The UK's contribution to tackling climate change*. 2008.

DAVIDSON, P. A. 2004. *Turbulence: An introduction for Scientists and Engineers*, Oxford University Press.

DAVIS, S. J., CALDEIRA, K. & MATTHEWS, H. D. 2010. Future CO2 Emissions and Climate Change from Existing Energy Infrastructure. *Science,* 329**,** 1330-1333.

DI SABATINO, S., LEO, L. S., CATALDO, R., RATTI, C. & BRITTER, R. E. 2010. Construction of Digital Elevation Models for a Southern European City and a Comparative Morphological Analysis with Respect to Northern European and North American Cities. *Journal of Applied Meteorology and Climatology,* 49**,** 1377-1396.

DI SABATINO, S., SOLAZZO, E., PARADISI, P. & BRITTER, R. 2008. A simple model for spatially-averaged wind profiles within and above an urban canopy. *Boundary-Layer Meteorology,* 127**,** 131-151.

DOBRE, A., ARNOLD, S. J., SMALLEY, R. J., BODDY, J. W. D., BARLOW, J. F., TOMLIN, A. S. & BELCHER, S. E. 2005. Flow field measurements in the proximity of an urban intersection in London, UK. *Atmospheric Environment,* 39**,** 4647-4657.

DREW, D. R., BARLOW, J. F. & COCKERILL, T. T. 2013. Estimating the potential yield of small wind turbines in urban areas: A case study for Greater London, UK. *Journal of Wind Engineering and Industrial Aerodynamics,* 115**,** 104-111.

EDINA 2012. OS MasterMap Topography Layer [GML geospatial data], Using: EDINA Digimap Ordnance Survey Service, http://edina.ac.uk/digimap/.

ELLIOT, W. P. 1958. The Growth of the Atmospheric Internal Boundary Layer. *Trans. Amer. Geophy. Union,,* 39**,** 1048-1054.

ENERGY SAVINGS TRUST, Feed in Tariff scheme. *www.energysavingtrust.org.uk*

ENERGY SAVINGS TRUST. 2009*. Location, location, location: Domestic small-scale wind field trial report*. *www.energysavingtrust.org.uk*

ENCRAFT 2009. Warwick Wind Trials Final Report, avaliable at http://www.warwickwindtrials.org.uk/ (accessed 06/01/2012).

ERIKSSON, S., BERNHOFF, H. & LEIJON, M. 2008. Evaluation of different turbine concepts for wind power. *Renewable & Sustainable Energy Reviews,* 12**,** 1419-1434.

ESDU 1980. Mean fluid forces and moments on rectangular prisms: surface-mounted structures in turbulent shear flow. Engineering Sciences Data Unit Item Number 80003.

FACKRELL, J. E. 1984. Parameters characterising dispersion in the near wake of buildings. *Journal of Wind Engineering and Industrial Aerodynamics,* 16**,** 97-118.

FELTRIN, A. & FREUNDLICH, A. 2008. Material considerations for terawatt level deployment of photovoltaics. *Renewable Energy,* 33**,** 180-185.

GARRATT, J. R. 1990. The Internal Boundary-Layer - a Review. *Boundary-Layer Meteorology,* 50**,** 171-203.

GIPE, P. 2004. *Wind Power,* London, UK, James and James ltd.

GLASS, A. & LEVERMORE, G. 2011. Micro wind turbine performance under real weather conditions in urban environment. *Building Services Engineering Research & Technology,* 32**,** 245-262.

GOODE, K. & BELCHER, S. E. 1999. On the parameterisation of the effective roughness length for momentum transfer over heterogeneous terrain. *Boundary-Layer Meteorology,* 93**,** 133-154.

GRIMMOND, C. S. B., KING, T. S., ROTH, M. & OKE, T. R. 1998. Aerodynamic roughness of urban areas derived from wind observations. *Boundary-Layer Meteorology,* 89**,** 1-24.

GRIMMOND, C. S. B. & OKE, T. R. 1999. Aerodynamic properties of urban areas derived, from analysis of surface form. *Journal of Applied Meteorology,* 38**,** 1262-1292.

HAGISHIMA, A. & TANIMOTO, J. 2005. Investigations of urban surface conditions for urban canopy model. *Building and Environment,* 40**,** 1638-1650.

HAGISHIMA, A., TANIMOTO, J., NAGAYAMA, K. & MENO, S. 2009. Aerodynamic Parameters of Regular Arrays of Rectangular Blocks with Various Geometries. *Boundary-Layer Meteorology,* 132**,** 315-337.

HALL, D. J., MACDONALD, R., WALKER, S. & SPANTON, A. M. 1996. Measurements of dispersion within simulated urban arrays—a small scale wind tunnel study. BRE Client Report, CR178/96.

HANG, J., SANDBERG, M., LI, Y. & CLAESSON, L. 2009. Pollutant dispersion in idealized city models with different urban morphologies. Atmospheric Environment, 43, 6011-6025.

HANSEN, J., SATO, M. & RUEDY, R. 2012. Perception of climate change. *Proceedings of the National Academy of Sciences*.

HEATH, M. A., WALSHE, J. D. & WATSON, S. J. 2007. Estimating the Potential Yield of Small Building-mounted Wind Turbines. *Wind Energy,* 10**,** 271-287.

HILL, N., DOMINY, R., INGRAM, G. & DOMINY, J. 2009. Darrieus turbines: the physics of self-starting. *Proceedings of the Institution of Mechanical Engineers Part a-Journal of Power and Energy,* 223**,** 21-29.

HOLLAND, D. E., BERGLUND, J. A., SPRUCE, J. P. & MCKELLIP, R. D. 2008. Derivation of Effective Aerodynamic Surface Roughness in Urban Areas from Airborne Lidar Terrain Data. *Journal of Applied Meteorology and Climatology,* 47**,** 2614-2626.

HOSKER, R. P. 1984. *Flow and Diffusion Near Obstacles*, Edited by D. Randerson, Atmospheric Science and Power Production, US Dept of Energy.

HUANG, S., LI, Q. S. & XU, S. 2007. Numerical evaluation of wind effects on a tall steel building by CFD. *Journal of Constructional Steel Research,* 63**,** 612-627.

HUNT, J. C. R., ABELL, C. J., PETERKA, J. A. & WOO, H. 1978. Kinematical studies of the flows around free or surface-mounted obstacles; applying topology to flow visualization. *Journal of Fluid Mechanics,* 86**,** 179-200.

HUSSAIN, M. & LEE, B. E. 1980. A Wind-Tunnel Study of the Mean Pressure Forces Acting on Large Groups of Low-Rise Buildings. *Journal of Wind Engineering and Industrial Aerodynamics,* 6**,** 207-225.

IEA 2012. World Energy Outlook 2012.

INTERGOVERNMENTAL PANEL ON CLIMATE CHANGE. *Climate Change 2007 - The Physical Science Basis.* 2007.

JACKSON, P. S. 1981. On the Displacement Height in the Logarithmic Velocity Profile. *Journal of Fluid Mechanics,* 111**,** 15-25.

JAMES, P. A. B., SISSONS, M. F., BRADFORD, J., MYERS, L. E., BAHAJ, A. S., ANWAR, A. & GREEN, S. 2010. Implications of the UK field trial of building mounted horizontal axis micro-wind turbines. *Energy Policy,* 38**,** 6130-6144.

JIANG, D. H., JIANG, W. M., LIU, H. N. & SUN, J. N. 2008. Systematic influence of different building spacing, height and layout on mean wind and turbulent characteristics within and over urban building arrays. *Wind and Structures,* 11**,** 275-289.

JOHNSON, K. E., FINGERSH, L. J., BALAS, M. J. & PAO, L. Y. 2004. Methods for increasing region 2 power capture on a variable-speed wind turbine. *Journal of Solar Energy Engineering-Transactions of the Asme,* 126**,** 1092-1100.

KANDA, M. 2006. Large-eddy simulations on the effects of surface geometry of building arrays on turbulent organized structures. *Boundary-Layer Meteorology,* 118**,** 151-168.

KASTNER-KLEIN, P. & ROTACH, M. W. 2004. Mean flow and turbulence characteristics in an urban roughness sublayer. *Boundary-Layer Meteorology,* 111**,** 55-84.

KEMP, M. & WEXLER, J. 2010. Zero Carbon Britain 2030: A New Energy Strategy. Centre for Alternative Technology.

KERR, R. A. 2010. Do We Have the Energy for the Next Transition? *Science,* 329**,** 780-781.

KRAMER, G. J. & HAIGH, M. 2009. No quick switch to low-carbon energy. *Nature,* 462**,** 568-569.

KURITA, S. & KANDA, M. 2009. Characteristics of Boundary Layer over a Sequence of Small Localized Urban Canopies with Various Heights Obtained by Wind-Tunnel Experiment. *Journal of the Meteorological Society of Japan,* 87**,** 705-719.

LANDBERG, L., MYLLERUP, L., RATHMANN, O., PETERSEN, E. L., JØRGENSEN, B. H., BADGER, J. & MORTENSEN, N. G. 2003. Wind Resource Estimation—An Overview. *Wind Energy,* 6**,** 261-271.

LEDO, L., KOSASIH, P. B. & COOPER, P. 2010. Roof mounting site analysis for micro-wind turbines. *Renewable Energy,* 36**,** 1379-1391.

LEONARDI, S. & CASTRO, I. P. 2010. Channel flow over large cube roughness: a direct numerical simulation study. *J. Fluid Mech.,* 651**,** 519-539.

LIU, Y. S., CUI, G. X., WANG, Z. S. & ZHANG, Z. S. 2011. Large eddy simulation of wind field and pollutant dispersion in downtown Macao. Atmospheric Environment, 45, 2849-2859.

LU, L. & IP, K. Y. 2009. Investigation on the feasibility and enhancement methods of wind power utilization in high-rise buildings of Hong Kong. *Renewable and Sustainable Energy Reviews,* 13**,** 450-461.

MACDONALD, R. W. 2000. Modelling the mean velocity profile in the urban canopy layer. *Boundary-Layer Meteorology,* 97**,** 25-45.

MACDONALD, R. W., GRIFFITHS, R. F. & HALL, D. J. 1998. An improved method for the estimation of surface roughness of obstacle arrays. *Atmospheric Environment,* 32**,** 1857-1864.

MAHRT, L. 1996. The bulk aerodynamic formulation over heterogeneous surfaces. *Boundary-Layer Meteorology,* 78**,** 87-119.

MALLA, G. 2008. Climate Change and Its Impact on Nepalese Agriculture. *The Journal of Agriculture and Environment,* 9**,** 62-71.

MANWELL, J. F., MCGOWAN, J. G. & ROGERS, A. L. 2002. *Wind energy explained,* Amherst, USA, Wiley.

MARSH, G. 2008. *No child's play? Making small wind pay, www.renewableenergyfocus.com/ (03/09/2012)* [Online].

MASON, P. J. 1988. The Formation of Areally-Averaged Roughness Lengths. *Quarterly Journal of the Royal Meteorological Society,* 114**,** 399-420.

MCINTOSH, S. C., BABINSKY, H. & BERTENYI, T. 2007. Optimizing the Energy Output of Vertical Axis Wind Turbines for Fluctuating Wind Conditions. *45th AIAA Aerospace Sciences Meeting and Exhibit.* Reno, Nevada.

MCINTYRE, J. H., LUBITZ, W. D. & STIVER, W. H. 2010. Local wind-energy potential for the city of Guelph, Ontario (Canada). *Renewable Energy,* 36**,** 1437-1446.

MERTENS, S. 2003. The energy yield of roof mounted wind turbines *Wind Engineering,* 27**,** 507-518.

MERTENS, S., VAN KUIK, G. & VAN BUSSEL, G. 2003. Performance of an H-Darrieus in the skewed flow on a roof. *Journal of Solar Energy Engineering-Transactions of the Asme,* 125**,** 433-440.

MORIARTY, P. & HONNERY, D. 2012. What is the global potential for renewable energy? *Renewable and Sustainable Energy Reviews,* 16**,** 244-252.

MORTENSEN, N. G., HEATHFIELD, D. N., MYLLERUP, L., LANDBERG, L. & RATHMANN, O. 2003. Getting Started with WAsP. Roskilide: Risø National Laboratory.

NEOPHYTOU, M., GOWARDHAN, A. & BROWN, M. 2011. An inter-comparison of three urban wind models using Oklahoma City Joint Urban 2003 wind field measurements. Journal of Wind Engineering and Industrial Aerodynamics, 99, 357-368.

OKE, T. R. 1988. Street Design and Urban Canopy Layer Climate. *Energy and Buildings,* 11**,** 103-113.

PEACOCK, A. D., JENKINS, D., AHADZI, M., BERRY, A. & TURAN, S. 2008. Micro wind turbines in the UK domestic sector. *Energy and Buildings,* 40**,** 1324-1333.

PETERKA, J. A., MERONEY, R. N. & KOTHARI, K. M. 1985. Wind flow patterns about buildings. *Journal of Wind Engineering and Industrial Aerodynamics,* 21**,** 21-38.

PETERSEN, E. L. & TROEN, I. The UK wind resource and the European wind atlas. *Proceedings of the 12th BWEA Wind Energy Conference*, 1990. 129-135.

RAFAILIDAS, S. 1997. Influence of Building Areal Density and Roof Shape on the Wind Characteristics Above a Town. *Boundary-Layer Meteorology,* 85**,** 255–271.

RAHMSTORF, S. & COUMOU, D. 2011. Increase of extreme events in a warming world. *Proceedings of the National Academy of Sciences*.

RANKINE, R. K., CHICK, J. P. & HARRISON, G. P. 2006. Energy and carbon audit of a rooftop wind turbine. *Proceedings of the Institution of Mechanical Engineers Part a-Journal of Power and Energy,* 220**,** 643-654.

RATTI, C., DI SABATINO, S. & BRITTER, R. 2006. Urban texture analysis with image processing techniques: winds and dispersion. *Theoretical and Applied Climatology,* 84**,** 77-90.

RATTI, C., DI SABATINO, S., BRITTER, R., BROWN, M., CATON, F. & BURIAN, S. 2002. Analysis of 3-D urban databases with respect to pollution dispersion for a number of European and American cities. *Water Soil Air Poll Focus,* 2**,** 459-469.

RATTI, C. & RICHENS, P. 2004. Raster analysis of urban form. *Environment and Planning B-Planning & Design,* 31**,** 297-309.

RAUPACH, M. R. 1992. Drag and Drag Partition on Rough Surfaces. *Boundary-Layer Meteorology,* 60**,** 375-395.

RAUPACH, M. R. 1994. Simplified Expressions for Vegetation Roughness Length and Zero-Plane Displacement as Functions of Canopy Height and Area Index. *Boundary-Layer Meteorology,* 71**,** 211-216.

RAUPACH, M. R. 1995. Corrigenda. *Boundary-Layer Meteorology,* 76**,** 303-304.

RODI, W. 1997. Comparison of LES and RANS calculations of the flow around bluff bodies. *Journal of Wind Engineering and Industrial Aerodynamics,* 71**,** 55-75.

ROONEY, G. G. 2001. Comparison of upwind land use and roughness length measured in the urban boundary layer. *Boundary-Layer Meteorology,* 100**,** 469-486.

ROSEN, A. & SHEINMAN, Y. 1994. The Average Output Power of a Wind Turbine in a Turbulent Wind. *Journal of Wind Engineering and Industrial Aerodynamics,* 51**,** 287-302.

ROTH, M. 2000. Review of atmospheric turbulence over cities. *Quarterly Journal of the Royal Meteorological Society,* 126**,** 941-990.

SONG, C. C. S. & HE, J. 1993. Computation of wind flow around a tall building and the large-scale vortex structure. *Journal of Wind Engineering and Industrial Aerodynamics,* 46-47**,** 219-228.

STANKOVIC, S., CAMPBELL, N. & HARRIES, A. 2009. *Urban Wind Energy*, Earthscan, London (p41).

TAYLOR, P. A. 1987. Comments and further analysis on effective roughness lengths for use in numerical three-dimensional models. *Boundary-Layer Meteorology,* 39**,** 403-418.

THE DEPARTMENT OF ENERGY AND CLIMATE CHANGE. 2009. *The UK Renewable Energy Strategy*.

THE WORLD BANK. 2012. *Turn Down the Heat.*

TOMINAG, Y., MOCHIDA, A., MURAKAMI, S. & SAWAKI, S. 2008. Comparison of various revised k–e models and LES applied to flow around a high-rise building model with 1:1:2 shape placed within the surface boundary layer. *Journal of Wind Engineering and Industrial Aerodynamics,* 96**,** 389-411.

WALKER, S. L. 2011. Building mounted wind turbines and their suitability for the urban scale—A review of methods of estimating urban wind resource. *Energy and Buildings,* 43**,** 1852-1862.

WEEKES, S. M. & TOMLIN, A. S. 2013. Evaluation of a semi-empirical model for predicting the wind energy resource relevant to small-scale wind turbines. *Renewable Energy,* 50**,** 280-288.

WIERINGA, J. 1993. Representative Roughness Parameters for Homogeneous Terrain. *Boundary-Layer Meteorology,* 63**,** 323-363.

XIE, Z. & CASTRO, I. P. 2009. Large-eddy simulation for flow and dispersion in urban streets. *Atmospheric Environment,* 43**,** 2174-2185.

XIE, Z. T. & CASTRO, I. P. 2006. LES and RANS for turbulent flow over arrays of wall-mounted obstacles. *Flow Turbulence and Combustion,* 76**,** 291-312.

XIE, Z. T., COCEAL, O. & CASTRO, I. P. 2008. Large-Eddy Simulation of Flows over Random Urban-like Obstacles. *Boundary-Layer Meteorology,* 129**,** 1-23.

YANG, L. & LI, Y. 2011. Thermal conditions and ventilation in an ideal city model of Hong Kong. Energy and Buildings, 43, 1139-1148.

ZAKI, S., HAGISHIMA, A., TANIMOTO, J. & IKEGAYA, N. 2011. Aerodynamic Parameters of Urban Building Arrays with Random Geometries. *Boundary-Layer Meteorology,* 138**,** 99-120.

ZHANG, Y. Q., HUBER, A. H., ARYA, S. P. S. & SNYDER, W. H. 1993. Numerical simulation to determine the effects of incident wind shear and turbulence level on the flow around a building. *Journal of Wind Engineering and Industrial Aerodynamics,* 46-47**,** 129-134.